

Electronic Thesis and Dissertation Repository

3-27-2014 12:00 AM

Distinct roles of BMP and LKB1/AMPK signalling impacting ovarian cancer spheroid biology

Teresa M. Peart, *The University of Western Ontario*

Supervisor: Dr. Trevor Shepherd, *The University of Western Ontario*

Joint Supervisor: Dr. Gabriel DiMattia, *The University of Western Ontario*

A thesis submitted in partial fulfillment of the requirements for the Doctor of Philosophy degree in Anatomy and Cell Biology

© Teresa M. Peart 2014

Follow this and additional works at: <https://ir.lib.uwo.ca/etd>



Part of the [Cancer Biology Commons](#), and the [Cell Biology Commons](#)

Recommended Citation

Peart, Teresa M., "Distinct roles of BMP and LKB1/AMPK signalling impacting ovarian cancer spheroid biology" (2014). *Electronic Thesis and Dissertation Repository*. 1993.
<https://ir.lib.uwo.ca/etd/1993>

This Dissertation/Thesis is brought to you for free and open access by Scholarship@Western. It has been accepted for inclusion in Electronic Thesis and Dissertation Repository by an authorized administrator of Scholarship@Western. For more information, please contact wlsadmin@uwo.ca.

DISTINCT ROLES OF BONE MORPHOGENETIC PROTEIN AND LIVER KINASE
B1/AMP-ACTIVATED PROTEIN KINASE SIGNALLING IMPACTING OVARIAN
CANCER SPHEROID BIOLOGY

(Thesis format: Integrated Article)

by

Teresa Marie Peart

Graduate Program in Anatomy and Cell Biology

A thesis submitted in partial fulfillment
of the requirements for the degree of
Doctor of Philosophy

The School of Graduate and Postdoctoral Studies
The University of Western Ontario
London, Ontario, Canada

© Teresa Marie Peart 2014

Abstract

High-grade serous (HGS) carcinoma, the most prevalent and most deadly subtype of epithelial ovarian cancer (EOC), presents unique therapeutic challenges since the majority of cases are diagnosed at advanced, metastatic stage. At this point widespread intraperitoneal metastatic lesions are numerous, which is why models that recapitulate disease dissemination are critical to uncover novel therapeutic targets. One of the initiating events in ovarian cancer metastasis is shedding from the primary tumour into the peritoneal cavity where cells must survive in suspension in order to seed secondary tumours. This non-adherent population of cells exists as multicellular aggregates, or spheroids; data from our lab has demonstrated that cells within spheroids are dormant, yet are readily alter their phenotype upon reattachment to an adherent substratum. To further explore the pathobiology of ovarian cancer spheroids, my thesis work describes the functional characterization of two different signalling pathways—bone morphogenetic protein (BMP), and the liver kinase B1 (LKB1)/AMP-activated protein kinase (AMPK)—which mediate distinct and important aspects of spheroid formation and reattachment. Activated BMP signalling resulted in smaller, loosely-aggregated spheroids, which were more readily able to reattach and disperse. These phenotypic alterations observed as a result of active BMP signalling were mediated, at least in part, by cooperation with the AKT signalling pathway. These studies implicate inhibition of BMP and AKT signalling as potential strategies for therapeutic targeting of reattaching spheroids, which is critical for the formation of secondary metastatic lesions. Other work in our lab implicated the downregulation of AKT signalling in spheroid formation-induced dormancy. In an attempt to uncover additional pathways promoting the dormant phenotype of ovarian cancer spheroids, I investigated the LKB1/AMPK signalling cascade given its ability to alter cellular metabolism in response to nutrient and energy availability. Despite a dramatic enhancement in AMPK activity observed in ovarian cancer spheroids, targeted knockdown had no effect on viability of cells in this context. However, knockdown of its upstream kinase, LKB1, revealed a dramatic decrease in ovarian cancer spheroid viability, suggesting a role for this kinase in mediating anoikis-resistance in an AMPK-independent manner. Taken together, my results have uncovered two distinct and important signalling pathways that regulate unique aspects of spheroid formation, cell survival, and reattachment. By understanding the molecular mechanisms used by ovarian cancer spheroids to survive during dissemination and promote

secondary metastasis, my work has uncovered additional therapeutic targets for the potential treatment of advanced-stage ovarian cancer.

Keywords

Ovarian cancer, high-grade serous ovarian carcinoma, patient samples, spheroids, BMP,
LKB1, AMPK

Co-Authorship Statement

All chapters were written by Teresa Peart and edited by Dr. Trevor Shepherd and Dr. Gabriel DiMattia.

The data presented in Chapter 2 appeared in the published manuscript “BMP signalling controls the malignant potential of ascites-derived human epithelial ovarian cancer spheroids via AKT kinase activation.” Teresa Peart, Rohann Correa, Yudith Ramos-Valdes, Gabriel DiMattia, Trevor Shepherd. *Clin Exp Metastasis*. 2012. 29: 293-313. YRV and RC contributed to flow cytometry and reattachment assays respectively. All other data was generated and analyzed by TP. The manuscript was written by TP and edited by TS and GD.

In Chapter 3 analysis of TCGA dataset was performed by RC, immunofluorescence staining was performed by Dr. Elena Fazio, and the immunoblot in Figure 3.7 was performed by YRV. All other data appearing in this Chapter was generated and analyzed by TP.

Acknowledgments

The completion of this thesis would not be possible without the help and support of a number of different people. First, I'd like to thank my supervisor Dr. Trevor Shepherd for his continued support and guidance. Your mentorship has helped me to become more confident in my scientific abilities and to grow not only as a scientist, but also as a person. I would also like to thank my co-supervisor Dr. Gabriel DiMattia whose mentorship has been invaluable throughout this project. You have shown me what it means to be a truly dedicated scientist and I will continue to look up to you throughout my scientific career. Additionally, I would like to thank my advisory committee: Dr. Christopher Pin, Dr. Lynne Postovit and Dr. Alison Allan for sharing with me their knowledge and providing me guidance throughout this project.

Next I would like to thank the members of the Translational Ovarian Cancer Research laboratory, past and present, for making coming into work fun and for putting up with me all these years! Specifically, I would like to thank Yudith Ramos-Valdes who is not only a technician but also a dear friend.

I would also like to acknowledge the gynaecologic oncology surgeons Drs. Michel Préfontaine, Monique Bertrand, Jacob McGee, and Akira Sugimoto for providing us with patient specimens as well as insight into the clinical aspects of ovarian cancer. Carrie Thornton, Christine Gawlik and Kay Faroni have also been a tremendous help in collecting patient information for clinical specimens. Additionally, I would like to acknowledge all the women with ovarian cancer who participated in our study.

Finally, I would like to thank my entire family for their love and support throughout this process. I would not have been able to do it without you. Specifically, I would like to thank my parents, Robert and Kathy Peart. I could have not asked for more supportive, caring parents. Thank you for giving me the freedom to follow my dreams and helping me to grow into the person I am today. I love you more than you'll ever know.

Table of Contents

| | |
|--|------|
| Abstract..... | ii |
| Keywords..... | iv |
| Co-Authorship Statement..... | v |
| Acknowledgments..... | vi |
| Table of Contents..... | vii |
| List of Abbreviations..... | xi |
| List of Tables..... | xiv |
| List of Figures..... | xv |
| List of Appendices..... | xvii |
| Chapter 1..... | 1 |
| 1 Introduction..... | 1 |
| 1.1 Overview of Chapter 1..... | 1 |
| 1.2 Ovarian Cancer..... | 1 |
| 1.2.1 Ovarian Cancer Classification and Genetics..... | 1 |
| 1.2.2 Origins of Ovarian Cancer..... | 4 |
| 1.2.3 Ovarian cancer treatment and prognosis..... | 5 |
| 1.2.4 Ovarian cancer metastasis..... | 6 |
| 1.3 Multicellular spheroids..... | 6 |
| 1.3.1 Spheroids as an <i>in vitro</i> model of metastasis..... | 6 |
| 1.3.2 Multicellular spheroids in ovarian cancer..... | 9 |
| 1.4 BMP/TGF- β signalling..... | 12 |
| 1.4.1 Overview..... | 12 |
| 1.4.2 Pathway activation..... | 12 |
| 1.4.3 Pathway attenuation..... | 17 |

| | | |
|-----------|--|----|
| 1.4.4 | Smad-independent signalling | 19 |
| 1.4.5 | BMP signalling in cancer | 20 |
| 1.4.6 | BMP signalling in ovarian cancer | 21 |
| 1.5 | LKB1/AMPK signalling..... | 22 |
| 1.5.1 | Overview | 22 |
| 1.5.2 | Pathway activation and attenuation | 23 |
| 1.5.3 | LKB1/AMPK signalling in cancer | 30 |
| 1.5.4 | LKB1/AMPK signalling in ovarian cancer | 34 |
| 1.5.5 | Summary..... | 35 |
| 1.6 | Scope of Thesis..... | 35 |
| 1.7 | References | 37 |
| Chapter 2 | | 59 |
| 2 | BMP signalling controls the malignant potential of ascites-derived human epithelial ovarian cancer spheroids via AKT kinase activation | 59 |
| 2.1 | Introduction | 59 |
| 2.2 | Materials and Methods | 60 |
| 2.2.1 | Cell culture | 60 |
| 2.2.2 | Adenovirus vectors and cell transduction..... | 61 |
| 2.2.3 | RNA expression analysis..... | 61 |
| 2.2.4 | Real-time quantitative RT-PCR | 62 |
| 2.2.5 | Cell number a viability assays..... | 62 |
| 2.2.6 | Spheroid formation and reattachment assays | 63 |
| 2.2.7 | Spheroid disaggregation assay | 63 |
| 2.2.8 | Flow cytometry..... | 64 |
| 2.2.9 | BrdU cytochemistry..... | 64 |
| 2.2.10 | Western blotting | 64 |

| | | |
|-----------|---|-----|
| 2.2.11 | Antibodies and other reagents | 65 |
| 2.2.12 | Statistical analysis..... | 66 |
| 2.3 | Results | 66 |
| 2.3.1 | Reduced BMP signalling activity in primary human EOC spheroids | 66 |
| 2.3.2 | Forced BMP activity in EOC spheroids alters cell adhesion | 70 |
| 2.3.3 | Inhibition of endogenous BMP signalling affects EOC spheroid adhesion | 74 |
| 2.3.4 | BMP signalling activates the AKT pathway in EOC cells & spheroids .. | 78 |
| 2.4 | Discussion..... | 88 |
| 2.5 | References | 94 |
| Chapter 3 | | 127 |
| 3 | LKB1 signalling protects dormant ovarian cancer spheroids from cell death in an AMPK-independent manner | 127 |
| 3.1 | Introduction | 127 |
| 3.2 | Materials and Methods | 129 |
| 3.2.1 | Culture of cell lines, ascites-derived cells and isolation of native ascites spheroids..... | 129 |
| 3.2.2 | TCGA Analysis | 129 |
| 3.2.3 | Immunoblotting and Immunofluorescence..... | 130 |
| 3.2.4 | Cell Viability and ATP assays..... | 130 |
| 3.2.5 | siRNA transfections..... | 131 |
| 3.2.6 | Graphing and Statistical Analysis | 131 |
| 3.3 | Results | 132 |
| 3.3.1 | AMPK α 1 is expressed in metastatic ovarian tumour samples and is associated with a high frequency of copy-number gains and amplifications. | 132 |
| 3.3.2 | Multicellular aggregates filtered from patient ascites fluid exhibit enhanced AMPK activity. | 134 |

| | | |
|---|---|-----|
| 3.3.3 | Ovarian cancer cell lines and ascites-derived cells in suspension exhibit decreased levels of ATP and enhanced AMPK activity..... | 134 |
| 3.3.4 | LKB1 protein is expressed in metastatic ovarian tumour samples..... | 137 |
| 3.3.5 | Suspension-induced activation of AMPK signalling is accompanied by enhanced LKB1 signalling and inhibition of mTORC1..... | 137 |
| 3.3.6 | Spheroids are much less sensitive to further activation of the AMPK pathway than adherent ovarian cancer cells. | 138 |
| 3.3.7 | LKB1, but not AMPK, is required for ovarian cancer cell survival in suspension..... | 142 |
| 3.4 | Discussion..... | 146 |
| 3.5 | References | 150 |
| Chapter 4 | | 157 |
| 4 | Discussion..... | 157 |
| 4.1 | Summary of findings | 157 |
| 4.2 | BMP signalling plays context-specific roles during ovarian cancer spheroid formation and reattachment..... | 158 |
| 4.3 | LKB1 has AMPK-independent effects on cellular viability in ovarian cancer spheroids..... | 162 |
| 4.4 | BMP and LKB1 signalling: Is there a connection? | 166 |
| 4.5 | Synthesis..... | 168 |
| 4.6 | References | 168 |
| Appendix A: Additional Figures | | 171 |
| Appendix B: Ethics Approval | | 172 |
| Appendix C: Summary of Clinical Data for EOCs | | 174 |
| Appendix D: Copyright Permissions..... | | 175 |
| Curriculum Vitae | | 176 |

List of Abbreviations

| | |
|---------------|--|
| ACC | Acetyl-CoA carboxylase |
| ADP | Adenosine diphosphate |
| AICAR | 5-Aminoimidazole-4-carboxamide ribonucleotide |
| Alk | Activin receptor-like kinases |
| AMPK | Adenosine monophosphate-activated protein kinase |
| ARID1A | AT-rich interactive domain-containing protein 1A |
| ARKs | AMPK-related kinases |
| ATG 13 | autophagy-related 13 |
| ATP | Adenosine triphosphate |
| BAMBI | BMP and activin membrane-bound inhibitor |
| BMP | Bone morphogenetic protein |
| BRAF | v-Raf murine sarcoma viral oncogene homolog B1 |
| CAMKK β | Calmodulin-dependent protein kinase kinase β |
| CICs | Cortical inclusion cysts |
| CtBP | C-terminal binding protein |
| CTNNB1 | catenin (cadherin-associated protein), beta 1 |
| Dan | Differential screening-selected gene aberrative in neuroblastoma |
| E-Cadherin | Epithelial Cadherin |
| ECM | Extracellular matrix |
| EMT | Epithelial-to-mesenchymal transition |

| | |
|------------|---|
| EOC | Epithelial Ovarian Cancer |
| GS domain | Glycine and serine rich domain |
| HGSCs | High-grade serous carcinomas |
| HMGR | 3-hydroxy-3-methylglutaryl-CoA reductase |
| KRAS | v-Ki-ras2 Kirsten rat sarcoma viral oncogene homolog |
| LKB1 | Liver kinase B1 |
| MAPK | Mitogen-activated protein kinase |
| MARK4 | microtubule affinity-regulating kinase 4 |
| MEK | MAPK and ERK kinase |
| MO25 | Mouse protein 25 |
| mTORC1 | mechanistic Target of Rapamycin 1 |
| N-cadherin | Neural cadherin |
| NLS | Nuclear localization signal |
| NSCLC | Non-small-cell lung carcinoma |
| OSE | Ovarian surface epithelium |
| P-cadherin | Placental cadherin |
| PERK | protein kinase (PKR)-like endoplasmic reticulum kinase |
| PIK3CA | Phosphatidylinositol-4,5-bisphosphate 3-kinase, catalytic subunit alpha |
| PJS | Peutz-Jeghers syndrome |
| PKA | Protein kinase A |

| | |
|--------------|---|
| PTEN | Phosphatase and tensin homolog |
| RAPTOR | regulatory-associated protein of mTOR |
| RSK | p90 ribosomal S6 protein kinase |
| Smurf | Smad ubiquitination regulatory factors |
| STICs | Serous tubal intraepithelial carcinomas |
| STK11 | Serine threonine kinase 11 |
| STRAD | STE20-related adaptor |
| TCGA | The cancer genome atlas |
| TGF- β | Transforming growth factor beta |
| TP53 | Tumour protein 53 |
| TSC2 | Tuberous sclerosis complex 2 |
| ULK1 | Unc-51 like autophagy activating kinase 1 |
| UPR | Unfolded protein response |
| VEGF | Vascular endothelial growth factor |

List of Tables

| | |
|---|-----|
| Table 1.1: Classification of type I and type II ovarian carcinomas..... | 3 |
| Table 1.2: Type I BMP receptors. | 16 |
| Table 1.3: Knockout mouse models of BMP ligands and antagonists. | 18 |
| Table 2.1: Up-regulated genes in response to Alk3QD expression and common between adherent and spheroid EOC cells. | 79 |
| Table 2.2: Down-regulated genes in response to Alk3QD expression common between adherent and spheroid EOC cells. | 82 |
| Table S2.1: Genes with increased expression due to Alk3QD in adherent EOC cells..... | 100 |
| Table S2.2: Genes with increased expression due to Alk3QD in EOC spheroids. | 105 |
| Table S2.3: Genes with decreased expression due to Alk3QD in adherent EOC cells..... | 113 |
| Table S2.4: Genes with decreased expression due to Alk3QD in EOC spheroids..... | 120 |

List of Figures

| | |
|--|----|
| Figure 1.1: Mechanism of high-grade serous ovarian cancer metastasis. | 11 |
| Figure 1.2: Activation of Bone Morphogenetic Protein (BMP) signalling. | 13 |
| Figure 1.3: Activation of the LKB1/AMPK signalling cascade..... | 25 |
| Figure 1.4: LKB1 is a master kinase, phosphorylating a number of AMPK-related kinases (ARKs). | 29 |
| Figure 2.1: BMP signalling is decreased during EOC spheroid formation. | 67 |
| Figure 2.2: TGF- β signalling is not altered during EOC spheroid formation. | 69 |
| Figure 2.3: Activated BMP signalling results in smaller EOC spheroids that are more loosely aggregated..... | 71 |
| Figure 2.4: EMT is induced during EOC spheroid formation..... | 73 |
| Figure 2.5: Alk3 ^{QD} expression enhances the movement of EOC cells from spheroids after reattachment. | 75 |
| Figure 2.6: Inhibition of BMP signalling enhances EOC spheroid formation and decreases reattachment. | 77 |
| Figure 2.7: The PI3K-AKT-mTOR pathway is activated by BMP signalling in EOC cells and spheroids..... | 85 |
| Figure 2.8: BMP-enhanced spheroid reattachment is partially mediated by AKT signalling. | 87 |
| Figure 2.9: Proposed model of BMP signalling in EOC metastasis..... | 93 |
| Figure S2.1: Validation of microarray results by quantitative RT-PCR analysis of specific up-regulated genes. | 98 |
| Figure S2.2: Inhibition of PI3K-mTOR signalling reduces EOC cell dispersion upon spheroid reattachment. | 99 |

| | |
|--|-----|
| Figure 3.1: The AMPK pathway is active in metastatic ovarian tumour samples. | 133 |
| Figure 3.2: Native ascites spheroids have enhanced AMPK activity compared to adherent cells..... | 135 |
| Figure 3.3: Spheroids formed from EOC cell lines and ascites-derived cells have decreased levels of ATP and corresponding increases in AMPK activity. | 136 |
| Figure 3.4: Despite heterozygous deletion, LKB1 protein is expressed in metastatic ovarian tumour samples..... | 139 |
| Figure 3.5: Spheroids formed from EOC cell lines and ascites-derived cells express LKB1 protein and have decreased levels of mTORC1 signalling. | 140 |
| Figure 3.6: AICAR treatment of EOC cell lines and ascites-derived cells decreases cell viability in adherent and spheroid cells. | 141 |
| Figure 3.7: Allosteric AMPK activator A-769662 decreases viability of EOC cells in a context-dependent manner..... | 144 |
| Figure 3.8: siRNA-mediated knockdown of <i>STK11</i> but not <i>PRKAA1</i> results in a decrease in viability of ovarian cancer spheroids..... | 145 |
| Figure S3.1: LKB1 is located in the cytoplasm in adherent and spheroid EOC cells..... | 154 |
| Figure S3.2: AICAR and A-769662 have different effects on cell cycle progression and apoptosis in adherent ovarian cancer cells. | 155 |
| Figure S3.3: LKB1 and AMPK are expressed in EOC cell lines under adherent conditions but activity is low. | 156 |
| Figure 4.1: Contribution of BMP and LKB1/AMPK signalling pathways to ovarian cancer metastasis..... | 163 |
| Figure 4.2: Proposed mechanisms of dormancy induction in ovarian cancer spheroids..... | 165 |

List of Appendices

| | |
|---|-----|
| Appendix A: Additional Figures | 171 |
| Appendix B: Ethics Approval | 172 |
| Appendix C: Summary of Clinical Data for EOCs | 174 |
| Appendix D: Copyright Permissions..... | 175 |

Chapter 1

1 Introduction

1.1 Overview of Chapter 1

This thesis focuses on examining signalling pathways, which we believe mediate important aspects of ovarian cancer spheroid formation and survival. This chapter begins with a description of ovarian cancer (Section 1.2) specifically focusing on the origins, classification, and mortality associated with this very complex disease. The next section (Section 1.3) focuses on the multicellular spheroid as an *in vitro* model of ovarian cancer metastasis and the unique properties that spheroid cells acquire to avoid anoikis, including induction of cellular quiescence, altered cellular metabolism, and altered adhesion characteristics. The bone morphogenetic (BMP) (Section 1.4) and adenosine monophosphate-activated protein kinase (AMPK) (Section 1.5) signalling pathways will be described, and their relevance to ovarian cancer given my data in Chapters 2 and 3 showing that these pathways are important to the formation and survival of ovarian cancer spheroids. The final section provides rationale for our studies (Section 1.6) and outlines the studies presented in this thesis.

1.2 Ovarian Cancer

1.2.1 Ovarian Cancer Classification and Genetics

Ovarian cancers can be broadly characterized as epithelial and non-epithelial. Non-epithelial ovarian cancers, which are not the subject of my research, include granulosa cell tumours, fibrothecomas, teratomas and yolk sac tumours¹. The most common form of ovarian cancer however is epithelial, comprising over 90% of cases².

Epithelial Ovarian Cancer (EOC) is not a single entity but rather consists of several subtypes that are distinguishable by unique histology and molecular aberrations^{3,4}. The four main subtypes of ovarian cancer (mucinous, endometrioid, clear-cell and serous) can be further characterized as benign, malignant or borderline and classified as low or high-grade⁵. Each of these histologic subtypes has distinct clinical

characteristics and rates of occurrence. Serous carcinomas are the most common subtype and are typically high-grade neoplasms, which initially respond well to treatment with platinum/taxane-based chemotherapy but recur in the majority of cases^{6,7}. Endometrioid and mucinous carcinomas are much less common (10% and 3-4% respectively) and are typically low-grade lesions with a relatively indolent course of progression, allowing them to be diagnosed at early stage^{8,9}. Clear-cell carcinomas account for 10% of all cases of ovarian cancer and typically do not respond to conventional chemotherapeutics, resulting in a poor outcome for most patients^{10,11}.

In 2004, a dualistic model for the classification of ovarian cancer was proposed, which incorporated histopathological discoveries, clinical and molecular genetic findings¹². In this model, the various types of ovarian cancer are broadly separated into two categories. Type I tumours include all of the major histotypes (serous, endometrioid, mucinous and clear-cell) but are low-grade and typically slow growing^{10,13}. These tumours are associated with mutations in v-Ki-ras2 Kirsten rat sarcoma viral oncogene homolog (KRAS), v-Raf murine sarcoma viral oncogene homolog B1 (BRAF), phosphatase and tensin homolog (PTEN), phosphatidylinositol-4,5-bisphosphate 3-kinase, catalytic subunit alpha (PIK3CA), catenin (cadherin-associated protein), beta 1 (CTNNB1), and AT-rich interactive domain-containing protein 1A (ARID1A)^{12,14}. Type II tumours, on the other hand, are comprised almost exclusively of high-grade serous carcinomas but also include high-grade endometrioid, undifferentiated carcinomas and carcinosarcomas¹³. These tumours are aggressive in nature and often present at an advanced, metastatic stage, owing to their relatively poor prognosis¹⁵. Type II tumours display a high degree of chromosomal aberrations and genomic instability unlike type I tumours which are relatively genetically stable¹³. An overwhelming proportion of these type II tumours (~95%) have mutated TP53¹⁶⁻¹⁹ (Table 1.1). This new classification takes into account the idea that low and high-grade ovarian tumours of the same subtype are not a spectrum of disease, but rather, two distinct entities with different origins, mutations and clinical course^{1,20,21}.

Table 1.1: Classification of type I and type II ovarian carcinomas

| | Subtype | Precursor | Frequent Mutation(s) | Level of genomic instability |
|---------|-------------------------|---|-------------------------------|------------------------------|
| Type I | Low-grade serous | Serous borderline tumour | <i>KRAS, BRAF</i> | low |
| | Low-grade endometrioid | Endometriosis | <i>CTNNB1, PTEN, ARID1A</i> | low |
| | Clear-cell | Endometriosis | <i>PIK3CA, ARID1A, FBXW74</i> | low |
| | Mucinous | Mucinous borderline tumour (Gastrointestinal) | <i>KRAS</i> | low |
| Type II | High-grade serous | Fallopian tube | <i>TP53, BRCA1/2</i> | High |
| | High-grade endometrioid | Unknown | <i>TP53</i> | High |
| | Undifferentiated | Unknown | Unknown | Unknown |
| | Carcinosarcoma | Unknown | <i>TP53</i> | Unknown |

*adapted from Nik et. al. (2013) and references therein

1.2.2 Origins of Ovarian Cancer

Many epithelial malignancies have well-defined precursor lesions and cells of origin¹. This is not the case for EOC where until recently the origin and pathogenesis of this disease remained elusive¹³. The traditional view assumed that all ovarian cancer subtypes share a common site of origin within the ovarian surface epithelium (OSE). This is interesting, given the fact that the OSE is not a well-differentiated epithelium, but rather a mesothelial layer that originates embryonically from the mesodermally-derived coelomic epithelium². This theory postulates that the process of damage and repair of the ovarian surface that occurs as a result of multiple ovulations throughout a woman's reproductive life increases the susceptibility of the OSE to transformation. In addition, multiple invaginations of the ovarian surface are also common as women age. These invaginations can pinch off over time and become entrapped within the ovarian stroma where they form cortical inclusion cysts (CICs). It is hypothesized that the epithelial cells lining these cysts undergo metaplasia in response to the hormone-rich environment within the ovary, differentiating into a Müllerian-like epithelium that eventually becomes dysplastic leading to ovarian carcinoma^{2,5}. Although this model is consistent with epidemiologic evidence demonstrating that decreased ovulation is significantly correlated with a decreased risk of developing ovarian cancer, it does have many limitations²². One of the major drawbacks to this model is it does not address the significantly divergent phenotypes and genotypes that exist between tumour subtypes⁵.

As technology has improved, so has our understanding of ovarian cancer where it is now established that it is a complex and heterogeneous disease without a single cell of origin¹. Many studies have provided strong evidence indicating that endometriosis is the precursor lesion for clear-cell and endometrioid carcinomas²³⁻³⁰. Additionally, mucinous carcinomas have been shown to originate from appendiceal and other gastrointestinal origins¹. In the late 1990s to early 2000s, pathologists identified occult non-invasive and invasive carcinomas in the fimbria of fallopian tubes collected from prophylactic salpingo-oophorectomy specimens in *BRCAl/2* mutation carriers³¹⁻³⁶. Based on this, Piek and colleagues³⁷ proposed a model whereby occult tubal carcinomas shed malignant cells that implant and grow on the ovary, mimicking primary ovarian cancer. The hypothesis

that the fallopian tube is the primary site of high-grade serous carcinomas has since been supported by multiple studies³⁸⁻⁴¹. In 2007, for example, a study performed on women with high-grade serous carcinomas (HGSCs) who did not harbor a *BRCA* mutation reported the presence of serous tubal intraepithelial carcinomas (STICs) in 48% of patients⁴¹. Additionally, studies matching STICs and HGSCs from the same patient not only reveal TP53 mutations in 92% of STICs but also show that these mutations match the mutation found in the ovarian carcinoma¹³. Most recently, the Drapkin and Dinulescu labs reported the development of an HGSC murine tumour model emanating specifically from the murine fallopian tube (oviduct) even after hysterectomy and oophorectomy⁴². This study provides additional support for the fallopian tube and STICs as the origin of HGSC. This new model defining the origin of high-grade serous ovarian cancer will open up new avenues for early detection and intervention as we gain a better understanding of STICs and their role in carcinogenesis. In fact, it may no longer be appropriate to categorize HGSCs as ‘ovarian cancer’ since it seems as though the ovary is simply a favourable microenvironment for these cancer cells to spread and grow.

1.2.3 Ovarian cancer treatment and prognosis

Ovarian cancer is the most lethal gynecologic malignancy in the western world, the overall survival of which has remained unchanged for more than 50 years^{13,43}. Ovarian cancers that are diagnosed at an early-stage, before they have spread beyond the ovary (stage I) have a 90% cure rate through surgical resection. Unfortunately, the majority of cases (>75%) are diagnosed once the disease has metastasized to the pelvic organs, abdomen (stage III) or to distant sites (stage IV), at which point the chance of cure decreases substantially⁴⁴.

The high mortality rate associated with this disease is not only due to the lack of screening methods for early detection but also to the lack of effective therapies for advanced stage disease. Despite the high degree of heterogeneity associated with ovarian tumours, the majority of ovarian cancer patients are treated with cytoreductive surgery followed by platinum and taxane-based chemotherapy⁵. Although most tumours initially respond to chemotherapeutics, approximately 70% will develop platinum resistance and succumb to recurrent disease⁴⁵. This results in a dismal five-year survival rate for

advanced-stage ovarian cancer patients of only 30%⁴⁶. It is becoming obvious as we gain a better understanding of the molecular underpinnings of this complex disease that a “blanket approach” to treatment is not going to be enough. Rather, we must use our knowledge of the molecular genetic characteristics of individual tumours to focus our efforts into developing more targeted therapeutics⁵.

1.2.4 Ovarian cancer metastasis

Ovarian cancer metastasis is unique in that it rarely occurs through the bloodstream as is common for other solid tumours³. Instead, single cells or small clusters of cells are shed into the peritoneal cavity where they subsequently adhere to mesothelial cells of various abdominal organs to establish secondary lesions⁴⁷⁻⁴⁹. Since there is no anatomical barrier to prevent metastasis, tumour implants become widespread, blocking lymphatic vessels, and allowing ascites fluid to accumulate from leaky vasculature⁴⁴. This peritoneal ascites fluid is a relatively unique environment in which tumour cells must survive in suspension⁴. The composition of ascites fluid from ovarian cancer patients has been shown to vary considerably; in fact, one study showed higher proportions of red blood cells when the fluid had rapidly accumulated⁵⁰. A typical distribution of the cellular components of ascites fluid consists of 37% lymphocytes, 29% mesothelial cells, 32% macrophages, and <0.1% adenocarcinoma cells⁵¹. This fluid is a convenient source of tumour cells because it is routinely removed by paracentesis and is often of high volume facilitating isolation of tumour cells for study into the unique biological characteristics of cancer cells from different patients.

1.3 Multicellular spheroids

1.3.1 Spheroids as an *in vitro* model of metastasis

Multicellular spheroids have been recognized as a valuable tool in the fields of cell and developmental biology for over 50 years⁵²⁻⁵⁵. It wasn't until the 1970s, however, that Sutherland and colleagues established multicellular spheroids as a valuable *in vitro* model with which to study tumour biology⁵⁶⁻⁵⁸. Since then, tumour spheroids have been widely used to recapitulate the functional and microenvironmental features of human tumour tissue in order to study biological processes such as proliferation, metabolism,

differentiation, cell death, invasion, angiogenesis and immune response in an *in vitro* setting⁵⁹⁻⁶⁶. Spheroids exhibit many histologic similarities to their solid tumour counterparts including areas of necrosis as well as expression of ECM components⁶⁷.

1.3.1.1 *ECM and cell adhesion*

The ECM is a complex network made up of several proteins and polysaccharides such as fibronectin, collagen, laminin, hyaluronate, heparin sulfate, and elastin. These components are produced and secreted by cells, the combination of which depends on the functional requirements of a particular tissue⁶⁸.

The link between cell survival and adhesion to the extracellular matrix (ECM) has been well-established in the literature⁶⁹⁻⁷². Anoikis, from the Greek word meaning “homelessness”, refers to apoptosis induced by loss of cell adhesion to ECM⁷³. This is an important physiological process as it prevents cells from reattaching to new matrices and growing in a dysplastic manner⁷⁴. The ability to overcome anoikis has important implications for metastatic cancer. In fact, cancer cell lines are significantly less sensitive to anoikis than normal epithelial cells and in many cases have developed anchorage-independence, meaning they are able to survive and proliferate without attachment to ECM⁷⁵⁻⁷⁸. Integrins are important mediators of anchorage-independent survival that through their interaction with the ECM, stimulate numerous signalling pathways capable of modulating organization of the cytoskeleton, cell motility, and cell growth⁷⁹⁻⁸¹. In addition to integrin-associated signalling molecules, many cancer cells also have alterations in cell-cell adhesion molecules, protein kinases, and cell cycle regulators. This also contributes to anoikis-resistance, allowing these cells to disseminate and become metastatic^{77,78,82-84}. Epithelial cadherin (E-Cadherin), for example, has been shown to be a crucial mediator of cell-cell adhesion in multicellular spheroids. Oral squamous carcinoma cells, as well as mammary and prostate epithelial cells require E-cadherin in order to avoid anoikis in suspension^{85,86}. These studies as well as others have shown that part of the pro-survival function of E-cadherin involves the induction of quiescence, or reversible exit from the cell cycle. When E-cadherin is overexpressed in the EMT/6 breast cancer cell line, which lacks endogenous E-cadherin expression, cells form

compact spheroids and the proportion of dividing cells is greatly reduced. This exit from the cell cycle is mediated by induction of p27^{Kip1} activity in E-cadherin expressing cells⁸⁷.

Many tumour cells are not able to survive under anchorage-independent conditions if they remain as single cells. Rather, single cells must aggregate in order to avoid anoikis. In this context, survival signals arising from cell-cell contact substitute signals that normally come from matrix adhesion. Understanding the complex relationship between ECM components and cell-cell contact in multicellular spheroids is relevant in the field of tumour biology as they may more closely recapitulate the *in vivo* situation when tumour cells are detached from their tissue of origin⁶⁸. In fact, the ECM profile and organization of glioma, osteosarcoma and melanoma spheroids have been shown to more closely resemble *in vivo* tumours than that of conventional monolayer cultures⁸⁸⁻⁹⁰. Additional studies in human epidermoid and colorectal carcinoma spheroids revealed a similar pattern with respect to integrin expression, whereby the expression pattern of various integrins observed in multicellular spheroids closely resembled that of solid tumours^{91,92}. These results provide support for the use of multicellular spheroids as *in vitro* models with which to study the contribution of cell-matrix and cell-cell contacts in anoikis resistance.

1.3.1.2 *Response to cytotoxic drugs*

Many studies on multicellular spheroids have focused on the response of these structures to various tumour therapies⁹³⁻¹⁰⁸. The most extensively studied phenomenon is the response of spheroids to ionizing radiation. One of the most interesting findings from these studies was the observation that cells within multicellular spheroids are more resistant to ionizing radiation than monolayer cultures¹⁰⁹⁻¹¹¹. This was some of the first evidence to support the idea that spheroids mimic the *in vivo* response of cancer cells to treatment more closely than conventional monolayer cell cultures⁶⁷.

Multicellular spheroids remain an attractive model with which to examine the role of the tumour microenvironment on response to various therapeutic strategies. These structures maintain many of the metabolic and proliferative gradients that occur as a result of cellular interactions in a 3D context¹¹². In fact, spatial variations in cellular

proliferation are quite common in solid tumours, where cellular proliferation is highest in areas adjacent to microvessels¹¹³⁻¹¹⁶. Decreased proliferation in areas with lower oxygen and nutrient concentrations is often associated with quiescence, reversible exit from the cell cycle^{114,117}. These proliferation gradients common to solid tumours have not been demonstrated in monolayer cultures, but have been well-documented in multicellular spheroids^{67,118}. In fact, cells toward the center of the spheroid exhibit prolonged cell-cycle times and often enter a non-proliferating or quiescent state¹¹⁹. Given the fact that the vast majority of therapeutics aimed at cancer cells target rapidly dividing cells, it is not surprising that multicellular spheroids are generally more resistant to cytotoxic drugs than the same cells in monolayer culture^{58,120}.

1.3.2 Multicellular spheroids in ovarian cancer

Multicellular spheroids are valuable tools for the study of ovarian cancer because, as described above, they more closely mimic the characteristics of solid tumours, but also because of the unique way ovarian cancer metastasizes. One of the early events in ovarian cancer metastasis is the proteinase-mediated shedding of cells from the primary tumour into the peritoneal cavity, which has now been elegantly demonstrated in a murine model of HGSC^{4,42,121-123}. It is here, suspended within peritoneal ascites fluid, that this unique non-adherent population of ovarian cancer cells must respond to a series of unique environmental cues in order to survive and metastasize⁴. It is believed that in order to maintain cell-cell contact and avoid anoikis, cells under these conditions aggregate to form multicellular spheroids¹²⁴ (Figure 1.1). When forced into suspension, cells spontaneously aggregate as part of their natural survival response. Spheroid compaction is mediated by the interaction of key cell adhesion molecules such as integrins and cadherins¹²⁴. E-cadherin expression, for example, has been shown to be lower in cells suspended within ascites fluid as compared to the primary tumour¹²⁵. This loss of E-cadherin is part of a global “cadherin switch” whereby Neural Cadherin (N-Cadherin) and Placental cadherin (P-cadherin) are upregulated to compensate^{121,126}. This switch in cadherin expression is indicative of an epithelial-to-mesenchymal transition (EMT), which has been shown to allow cells to survive under hypoxic conditions when cells are crowded together¹²⁷. Integrins have also been shown to be important mediators

of survival when cells are in suspension. Ovarian cancer spheroid formation is greatly inhibited, for example, when cells are treated with a blocking antibody against $\beta 1$ integrin¹²⁸. Another important attribute of ovarian cancer spheroids is their ability to implant on mesothelial-lined peritoneal surfaces such as the peritoneum, omentum and pleural surface⁴⁹. Skubitz and colleagues were the first to model this *in vitro*, demonstrating that ovarian cancer spheroids had the ability to reattach and invade live mesothelial cell monolayers⁴⁸. More recently, the Brugge lab has shown that ovarian cancer spheroids use myosin-generated force in order to displace the mesothelial layer of cells and gain access to the underlying ECM to promote invasion¹²⁹.

These studies have taken the first steps towards gaining a better understanding of ovarian cancer spheroid biology, however, the stresses associated with ECM-detachment puts cells under a significant selection pressure. The cells that are able to survive within the peritoneal cavity and subsequently metastasize have likely altered many key signalling pathways. We have just begun to scratch the surface when it comes to understanding the adaptations of cells in this unique environment where they must exist in suspension. Since ovarian cancer mortality can be directly attributed to disseminated peritoneal metastasis, it is critical that we identify signalling pathways which are important for spheroid formation, survival and reattachment⁴

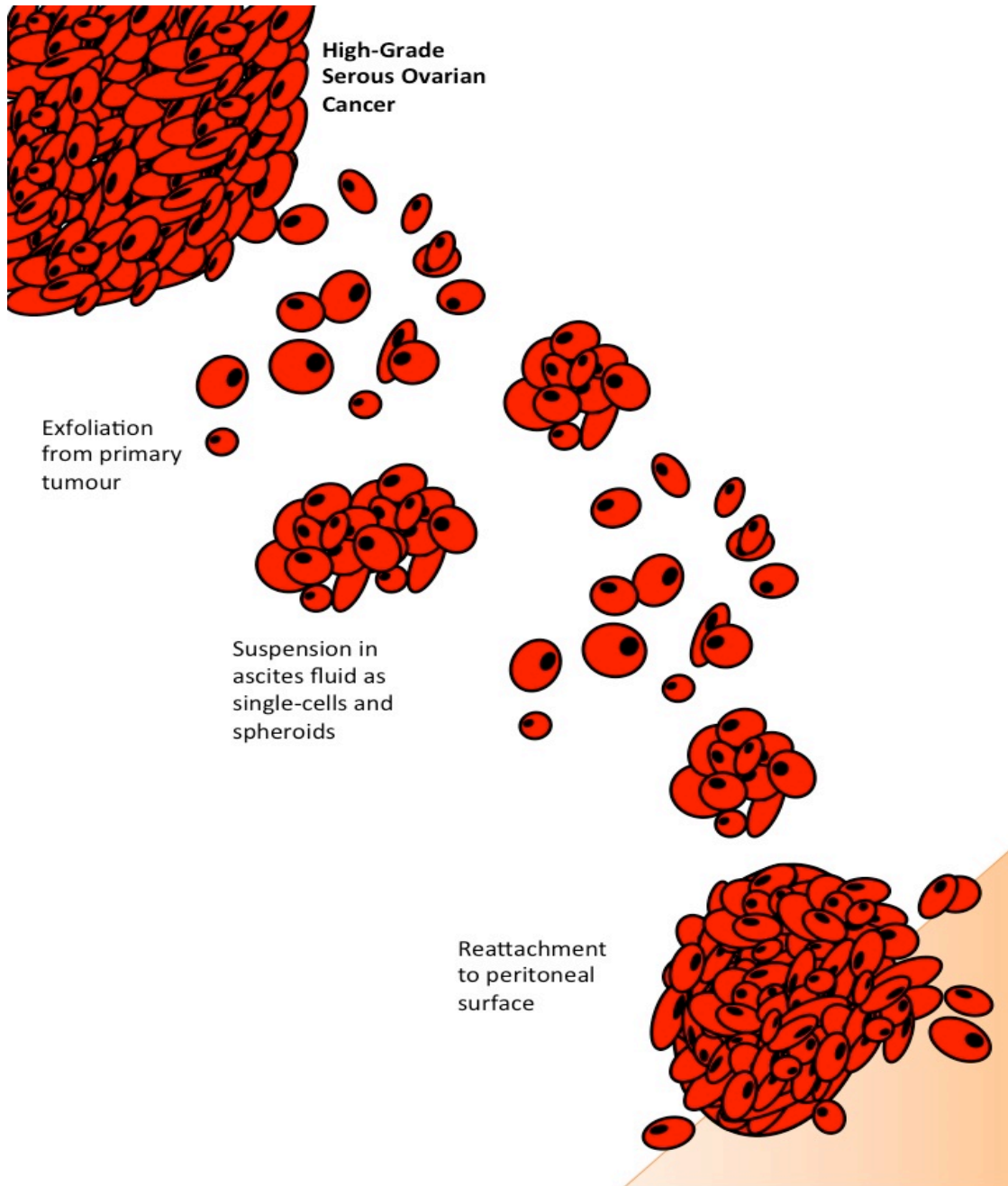


Figure 1.1: Mechanism of high-grade serous ovarian cancer metastasis.

During the process of ovarian cancer metastasis, malignant cells are shed from the primary tumour into the peritoneal cavity. It is here, suspended within ascites fluid, that single-cells and multicellular aggregates (spheroids) disperse throughout the peritoneal cavity. Widespread secondary metastatic lesions are formed when cells re-attach to mesothelial surfaces throughout the peritoneal cavity.

1.4 BMP/TGF- β signalling

1.4.1 Overview

Bone morphogenetic proteins (BMPs) belong to the transforming growth factor- β (TGF- β) superfamily and, as their name suggests, were originally identified based on their ability to induce bone and cartilage formation at extraskeletal sites¹³⁰⁻¹³². These powerful cytokines have since become recognized for their role in other cellular processes such as, differentiation, apoptosis and migration¹³³⁻¹⁸⁰. Given the importance of BMP signalling in controlling proliferation and differentiation during development and in maintaining and regenerating tissue during adulthood, it is not surprising that this pathway has also been shown to play an important role in many types of cancer^{157,180-187}. This section will discuss TGF- β /BMP signal transduction, how this pathway is regulated as well as its role in various different cancers, including ovarian cancer.

1.4.2 Pathway activation

BMP dimers are secreted to the extracellular environment, where they initiate signalling by cooperatively binding to two types of serine/threonine kinase receptors (type I and type II)^{188,189}. These receptors are separated in the plasma membrane until a ligand binds and increases oligomerization, essentially acting as a bridge between the two receptors. Both types of receptors are structurally similar consisting of an extracellular domain, a single transmembrane-spanning domain, and an intracellular domain with serine/threonine kinase activity¹⁹⁰. The type II receptors are constitutively active and are responsible for transphosphorylating the type I receptors when a signal is present¹⁹¹. This phosphorylation occurs on the GS domain (glycine and serine rich domain) which is located N-terminal to the serine/threonine kinase domain on the type I receptor (Figure 1.2). The activated type I receptor is responsible for binding and activating the downstream signalling mediators for this pathway, the Smads^{190,191}.

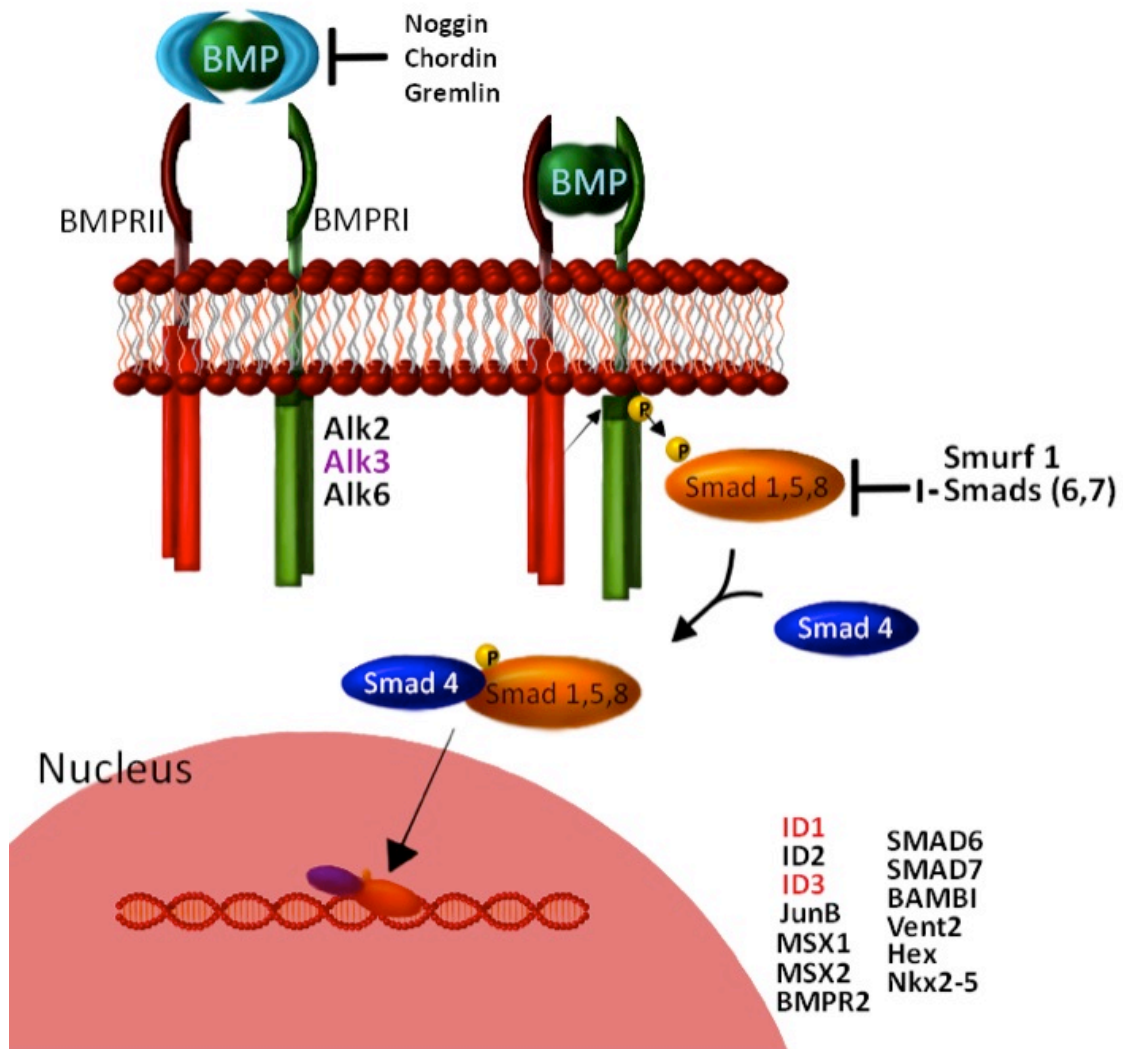


Figure 1.2: Activation of Bone Morphogenetic Protein (BMP) signalling.

Dimeric BMP ligands transduce their signal through a heterotetrameric complex composed of type I and type II transmembrane receptors. Following phosphorylation by the type II receptor, the type I receptor phosphorylates and activates Smads 1,5,8, allowing them to complex with Smad 4 and translocate to the nucleus to regulate target gene expression. Negative regulation of this pathway can occur through extracellular antagonists as well as intracellular inhibitory Smads.

1.4.2.1 *Smad protein family*

Eight different Smad proteins have been identified in mammals, each of which can be separated into three categories: Receptor-regulated Smads (R-Smads), Common-mediator Smad, or Inhibitory Smads (I-Smads)¹⁹²⁻¹⁹⁴.

The Receptor-regulated Smads or R-Smads are those that interact with the type I receptor and are activated by phosphorylation. This interaction with the receptor is transient and once phosphorylation occurs, the R-Smad is released to the cytoplasm where it is free to form a complex with co-Smad¹⁹⁰. The particular Smad that interacts with the receptor depends on the type of receptor as well as the ligand that triggers the signal. Smad2 and Smad3 transmit the signal from TGF- β , Nodal and activin ligands^{195,196}, whereas Smad1, 5 and 8 transduce the signal from BMP ligands¹⁹⁷⁻¹⁹⁹.

The common-mediator Smad, of which there is only one, Smad4, has the ability to interact with any R-Smad, forming a heteromeric complex that can translocate to the nucleus to affect the expression of target genes¹⁹¹. This complex can be composed of one R-Smad bound to Smad4 or two R-Smads, depending on the target gene²⁰⁰.

The third group of Smads, the inhibitory Smads (I-Smads), is comprised of Smad6 and Smad7. These Smads have the ability to modulate signalling by competing with R-Smads for binding to either the receptor or Smad4^{201,202}.

1.4.2.2. *TGF- β /BMP receptors*

Seven different type I receptors for the TGF- β family have been identified in mammals (activin receptor-like kinases 1-7; Alk 1-7). Of these, type I BMP receptors BMPR1A (Alk3) and BMPR1B (Alk6), as well as, type I activin receptor Acvr1 (Alk2) activate Smad 1,5, and 8 in response to BMP ligands. The remaining type I receptors activate Smad 2 or 3 and are responsible for transducing signal from TGF- β , Activin, or Nodal ligands¹⁹⁰. Table 1.2 describes the various type I receptors and summarizes their expression patterns, their ligand-affinity and downstream signalling targets.

The binding preferences of a particular ligand for a type I receptor is determined by the presence of the type II receptor²⁰³. There are three type II receptors used by BMPs in mammals. BMPR-II is specific for BMPs, whereas, ActR-II and ActR-IIB are also used by activins and myostatin¹⁹⁰.

Table 1.2: Type I BMP receptors.

| Receptors | Cell type | Ligands | Smads | References |
|---------------------------------------|---------------------------------|----------------------|--------------|--|
| BMPR-1A (Alk-3) | Ubiquitously expressed | BMP2,4 | 1,5,8 | (ten Dijke, Yamashita et al. 1994; Dewulf, Verschuere et al. 1995; Miyazono, Kamiya et al. 2010) |
| BMPR-1B (Alk-6) | Brain | BMP2,4,6,7 | 1,5,8 | (ten Dijke, Yamashita et al. 1994; Dewulf, Verschuere et al. 1995; Miyazono, Kamiya et al. 2010) |
| Alk-1 | Endothelial cells, chondrocytes | TGF- β , BMP9 | 2,3 1,5,8 | (Goumans and Mummery 2000; Oh, Seki et al. 2000; Seki, Hong et al. 2006; Finnson, Parker et al. 2008; Luo, Tang et al. 2010; Miyazono, Kamiya et al. 2010) |
| Alk-2 | Ubiquitously expressed | BMP6,7,9 | 1,5,8 | (Zhang, Schwarz et al. 2003; Luo, Tang et al. 2010; Miyazono, Kamiya et al. 2010) |
| ActR-1B (Alk-4) | Blood | TGF- β , Nodal | 2,3 | (Reissmann, Jornvall et al. 2001; Bianco, Adkins et al. 2002; Miyazono, Kamiya et al. 2010) |
| TβR-I (Alk-5) | Endothelial cells, chondrocytes | TGF- β | 2,3 | (Seki, Hong et al. 2006; Finnson, Parker et al. 2008; Miyazono, Kamiya et al. 2010) |
| ActR-1C (Alk-7) | Adipose tissue | Nodal | 2,3 | (Carlsson, Jacobson et al. 2009; Miyazono, Kamiya et al. 2010) |

1.4.3 Pathway attenuation

Both BMP and TGF- β signalling are modulated at many different levels: outside the cell, inside the cell as well as at the membrane. In many instances, the expression of these inhibitory signals is controlled by the TGF- β /BMP signalling cascade, which creates a negative-feedback loop²⁰⁴.

1.4.3.1 *Extracellular modulation*

At the extracellular level, secreted antagonists are capable of sequestering BMP ligands and preventing them from binding to the receptor. In vertebrates, more than seven of these antagonists have been identified^{191,204}. These proteins are not redundant inhibitory signals as each antagonist displays a unique affinity for different ligands. Table 1.3 describes a number of BMP ligands and their antagonists in addition to knockout mouse models demonstrating their important embryonic functions.

Table 1.3: Knockout mouse models of BMP ligands and antagonists.

| | Gene | Embryonic lethal? | Phenotype | Reference(s) |
|---|------------------------|---|---|--|
| BMP ligands | <i>BMP2</i> | Yes | Amnion/chorion malformation Defects in cardiac development | (Zhang and Bradley 1996) |
| | <i>BMP3</i> | No | Increased trabecular bone density | (Daluisi, Engstrand et al. 2001) |
| | <i>BMP4</i> | Yes | Defects in extraembryonic and posterior/ventral mesoderm formation | (Winnier, Blessing et al. 1995) |
| | <i>BMP5</i> | No | Abnormal skull and axial part of skeleton | (Green 1958; Kingsley, Bland et al. 1992) |
| | <i>BMP6</i> | No | Mild delay of sternum ossification in late gestation | (Solloway, Dudley et al. 1998) |
| | <i>BMP7</i> | Postnatal lethal | Holes in the basisphenoid bone and the xyphoid cartilage, retarded ossification of bones, fused ribs and vertebrae, underdeveloped neural arches of the lumbar and sacral vertebrae | (Jena, Martin-Seisdedos et al. 1997) |
| | BMP Antagonists | <i>Noggin</i> (highest affinity for BMP 2,4) | Yes | Failure of neural tube closure, broad club-shaped limbs, loss of caudal vertebrae, shortened body axis and retention of small vestigial tail |
| <i>Chordin</i> (highest affinity for BMP2,4) | | Still born | Normal early development and Neural induction, defects in inner and outer ear development, pharyngeal and cardiovascular organization at later stages of embryogenesis | (Bachiller, Klingensmith et al. 2000) |
| <i>Follistatin</i> (highest affinity for BMP7) | | Postnatal lethal | Smaller than heterozygotes, less muscle, fail to breath after birth | (Matzuk, Lu et al. 1995) |
| <i>DAN</i> (highest affinity for BMP2) | | No | No defects in head, mesoderm, somites, facial structures and limbs, normal neural tube development, viable and fertile | (Dionne, Skarnes et al. 2001) |

All knockout mouse models described above are homozygous for gene of interest

1.4.3.2 Intracellular modulation

As mentioned above, inhibitory Smads or I-Smads (Smad 6 & 7) function within the cell to antagonize TGF- β /BMP signalling. These Smads have the ability to interact with type I receptors but are never released and thus prevent R-Smads from interacting with these same receptors¹⁹⁰. Smad7 has the ability to inhibit TGF- β and BMP signalling, whereas Smad6 has been shown to preferentially inhibit BMP signalling²⁰⁵. I-Smads have also been shown to have activity within the nucleus. Smad7, for example, is able to bind to Smad-responsive DNA elements and disrupt the formation of a functional Smad-DNA complex²⁰⁶. On the other hand, Smad6, functions by recruiting transcriptional corepressors, such as histone deacetylases and C-terminal binding proteins (CtBP)^{207,208}.

Another way that Smad activity is regulated is through ubiquitin-mediated degradation. Smad ubiquitin regulatory factors 1 & 2 (Smurfs 1 & 2) are E3 ubiquitin ligases that selectively target R-Smads as well as activated type I receptors for degradation^{209,210}. Smurf1 specifically interacts with Smads 1 and 5 to inhibit BMP signalling, whereas, Smurf2 acts more broadly to inhibit Smads 1 and 2 in order to repress both BMP and TGF- β signalling^{188,204}. Smurf1 is also able to enhance the interaction between I-Smads and type I receptors in order to inhibit BMP signalling²¹¹.

1.4.4 Smad-independent signalling

Smads are not only phosphorylated at the C-terminus by type I receptors in a ligand-dependent manner, but can also be phosphorylated within their linker region by kinases from other pathways (ie: MAPKs, ERKs, JNK, p38)²⁰⁴. The Smad linker region is easily accessed by a number of kinases since it is loosely organized and highly flexible. Specifically, epidermal growth factor (EGF) treatment, which activates Ras/MAPK signalling, results in phosphorylation of the Smad1 linker region. This phosphorylation blocks the nuclear translocation of Smad1, inhibiting BMP signalling²¹². Additionally, expression of a dominant negative mutant of Ras or treatment of intestinal epithelial cells with a MAP and ERK kinase (MEK) inhibitor decreased the ability of the BMP pathway to induce Smad1 phosphorylation²¹³. From this it was proposed that these two pathways converge on Smad1 by phosphorylation of the C-terminus (BMP pathway) and the linker

region (Ras/MAPK pathway). It is the balance of these two inputs that determines Smad1 activation and nuclear translocation²¹⁴. The crosstalk between BMP signalling and other signalling pathways could have important implications not only in development but also in cancer.

1.4.5 BMP signalling in cancer

The BMP signalling pathway can exhibit both tumour suppressive and oncogenic functions depending not only on the type of cancer but also the stage. In some cancers, BMP signaling is growth inhibitory and induces apoptosis^{153,215-220} via activation of downstream Smad-dependent pathways that promote apoptosis or inhibition of pathways that prevent apoptosis. Alternatively, the BMP signaling pathway can also increase metastatic potential^{221,222} and tumour angiogenesis²²³. In fact, it has been reported in different cancers that BMPs serve a dual role, acting as a tumour suppressor at early stages of carcinogenesis and as a promoter of tumour metastasis at later stages^{224,225}.

1.4.5.1 *Cancer promoting activities*

The BMP signalling pathway has been shown to increase metastatic potential^{221,222} and tumour angiogenesis²²³ in a number of different cancers. For example, BMP2 is expressed in non-small-cell lung carcinoma (NSCLC) and has the ability to enhance the growth of lung cancer cell lines *in vitro* and *in vivo*²²⁶. In addition to enhancing tumour growth, BMP2 has also been shown to play an important role in angiogenesis. Four days following injection of recombinant BMP2 a large increase in the size and number of blood vessels was observed in a NSCLC tumour xenograft model²²³. In addition to this, BMP7 has been shown to enhance vascular endothelial growth factor (VEGF) expression in metastatic prostate cancer cells²²⁷. The tumour-promoting properties of various components of the BMP signalling pathway have been illustrated in a number of other cancer sites including osteosarcoma, prostate, breast and colorectal²²⁸⁻²³¹.

1.4.5.2 *Anti-cancer activities*

The potential tumour suppressive function of the BMP signalling pathway was highlighted in the early 2000s with the discovery of germline mutations in the type I BMP receptor, BMPR1A (Alk3), and Smad4 in up to 40% of juvenile polyposis patients²³²⁻²³⁷. This is an autosomal dominant syndrome characterized by multiple hamartomatous polyps and predisposition for gastrointestinal cancers²³³. A role for the BMP signaling pathway in this inherited syndrome was further supported by a transgenic mouse model expressing the BMP inhibitor noggin. At two to three months of age, these mice displayed a phenotype similar to that observed in juvenile polyposis patients. At a later age (6 to 8 months), adenomatous polyps could be observed in these mice, resembling the syndrome in humans²³⁸. In addition to this, recent studies have suggested that the BMP signalling pathway may in fact be inactivated in a number of cases of sporadic colorectal cancer²³⁹.

1.4.6 BMP signalling in ovarian cancer

BMPs serve critical functions in the normal ovary, controlling processes such as steroidogenesis, follicle formation, and apoptosis²⁴⁰⁻²⁴⁴. In addition to this, double knockout mouse models for either Smad 1 & 5 or BMPRIA & BMPRIB develop granulosa cell tumours by three and eight months of age respectively^{245,246}. Given the importance of BMP signalling pathway in maintaining normal ovarian function, it is not surprising to that it may play a role in the development of ovarian cancer.

Human EOC cells have been reported to possess an autocrine BMP4 signalling loop²⁴⁷ and treatment of EOC cells with exogenous BMP4 or constitutively-active type I BMP receptor (Alk3^{QD}) resulted in an increase in cell adhesion and invasion, as well as a cell spreading response indicative of enhanced cell motility^{187,247}. Additionally, BMP2 expression has been shown to be elevated in malignant ascites cells and solid tumour samples with expression positively correlating with tumour grade¹⁸⁴. Perhaps some of the most convincing evidence for the cancer promoting functions of the BMP signalling pathway in ovarian cancer came from the Buckanovich lab in 2011. They demonstrated that activation of BMP signalling significantly increased the proportion of ovarian cancer

stem cells. Additionally, inhibiting BMP signalling *in vivo* resulted in a decreased proportion of ovarian cancer stem cells and decreased tumour growth²⁴⁸. Taken together these results indicate a cellular response which could contribute to EOC progression in response to BMP signalling, however, given the complexity of this pathway, it is likely that it serves different functions throughout ovarian cancer pathogenesis. The use of relevant models to dissect the role of this pathway during ovarian cancer metastasis could provide additional insight into the therapeutic potential for targeting this pathway for treatment of ovarian cancer.

1.5 LKB1/AMPK signalling

1.5.1 Overview

As mentioned previously, the objective of my research was to identify signalling pathways that potentially interact and have a pro-survival effect on spheroid cells in ovarian cancer. In this vein, recent work uncovered a unique connection between the TGF- β /BMP signalling pathway and a tumour suppressor protein that plays an important role in the metabolic reprogramming of cancer cells, liver kinase B1 (LKB1). In this study they found that LKB1 is able to phosphorylate Smad4 and prevent it from binding to DNA, thus inhibiting both TGF- β /BMP signalling pathways²⁴⁹.

Metabolic reprogramming of tumour cells is an important disease driver that allows cells to survive in unfavourable conditions where oxygen and nutrients are scarce²⁵⁰⁻²⁵³. This is especially relevant to the ovarian cancer environment where cancer cells are released into the ascites fluid an environment where oxygen and nutrient access is severely compromised which necessitates a unique metabolic response for survival. In this context, Adenosine monophosphate-activated protein kinase (AMPK) is important in that it functions as a sensor of cellular energy and allows cells to cope with various forms of metabolic stress, such as nutrient and energy deprivation²⁵⁴. AMPK is the only kinase that has the ability to respond to adenosine nucleotide levels within a cell and is thus one of the most important mediators of metabolic reprogramming. This section will discuss how the LKB1/AMPK signalling pathway is activated, how each of these kinases

contributes to oncogenesis, and the potential contribution of this pathway to ovarian cancer pathogenesis.

1.5.2 Pathway activation and attenuation

1.5.2.1 *AMPK structure and activity*

AMPK was originally discovered in 1987 as the protein kinase responsible for phosphorylating and inactivating acetyl-CoA carboxylase (ACC) and 3-hydroxy-3-methylglutaryl-CoA reductase (HMGR), enzymes crucial for fatty acid and sterol biosynthesis, respectively²⁵⁵. In response to cellular stress that results in ATP depletion either by inhibiting its production or accelerating its consumption, AMPK switches off ATP-consuming anabolic processes and turns on ATP-producing catabolic pathways in order to restore energy homeostasis²⁵⁶. This prevents cells from proliferating in situations where nutrients are scarce and allows them to survive periods of stress, an important attribute that many cancer cells have adapted especially ovarian cancer cells in ascites fluid.

AMPK is a highly conserved sensor of intracellular adenosine nucleotide levels that exists as a heterotrimeric complex consisting of catalytic α subunits and regulatory β and γ subunits²⁵⁷. In mammals, there are two isoforms of the α subunit ($\alpha 1$ and $\alpha 2$), two of the β ($\beta 1$ and $\beta 2$), and three of the γ subunit ($\gamma 1$, $\gamma 2$, and $\gamma 3$), each of which is encoded by a distinct gene²⁵⁸. The α subunits contain a serine/threonine kinase domain in the N-terminus and are activated by phosphorylation of Threonine (Thr) 172 within the activation loop of this domain^{259,260}. The γ subunits contain four tandem repeats known as CBS motifs. These repeats are arranged in a pseudo-symmetrical manner, yielding four potential adenosine nucleotide-binding clefts²⁵⁶. Site 4 binds only to AMP, site 2 appears to remain unoccupied while sites 1 and 3 competitively bind ADP, ATP or AMP^{261,262}. The β subunits link the C-terminus of the α subunit to the N-terminal domain of the γ subunit²⁶²⁻²⁶⁴. In a cell that is not stressed and ATP:ADP ratios are high, sites 1 and 3 of the γ subunit are occupied primarily by ATP. However, when cells are exposed to metabolic stress and levels of ADP and AMP increase, ATP is gradually replaced at these sites²⁵⁶. When AMP or ADP is bound to the γ subunit a conformational change occurs in

the complex that promotes phosphorylation of the α subunit, which is required for its activation²⁵⁷.

For many years the upstream kinase responsible for activating AMPK remained elusive. In 2003, after over 20 years of work and the combination of studies in yeast and mammals, three different groups published consecutive papers identifying liver kinase B1 (LKB1) as the primary kinase responsible for phosphorylating AMPK²⁶⁵⁻²⁶⁷. Since this time, calmodulin-dependent protein kinase β (CAMKK β) has also been shown to phosphorylate AMPK at Thr172 in response to calcium flux²⁶⁸⁻²⁷⁰ (Figure 1.3).

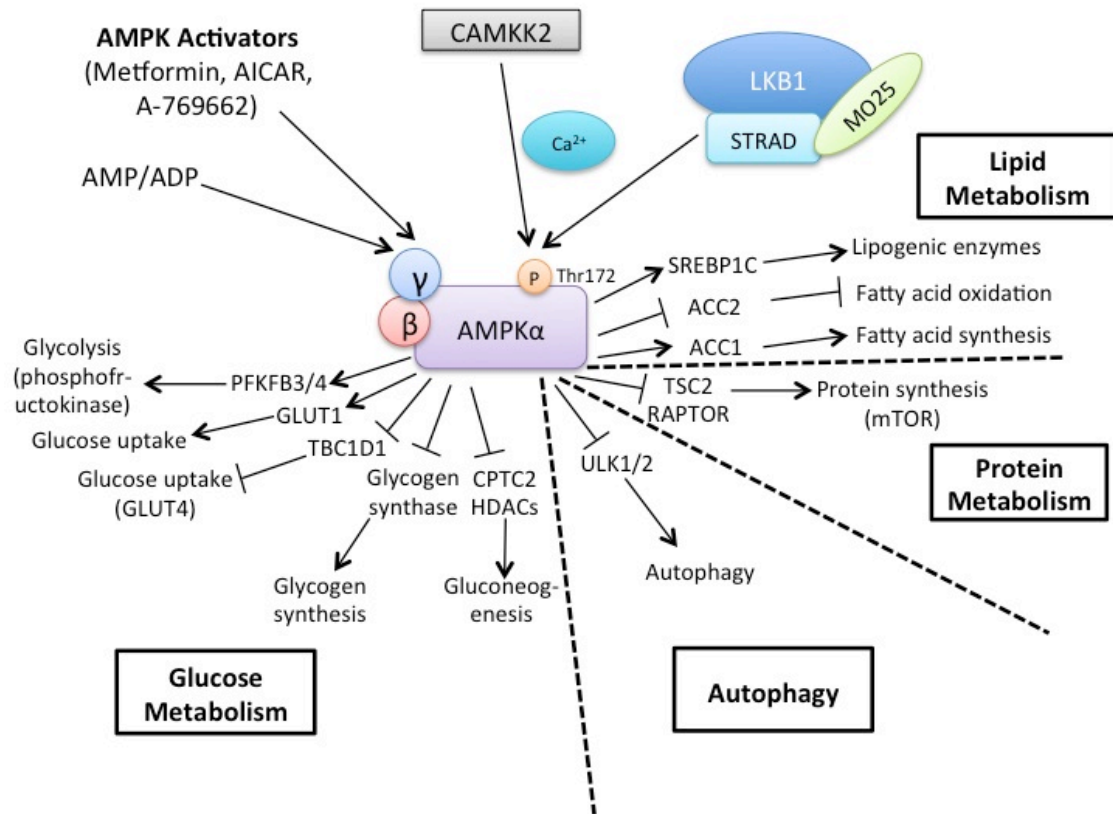


Figure 1.3: Activation of the LKB1/AMPK signalling cascade.

AMPK is activated when AMP or ADP levels increase due to a number of physiological stresses. It can also be activated pharmacologically (AICAR, A-769662). LKB1, in complex with STRAD and MO25, is the major upstream kinase that phosphorylates Thr172 on the α -subunit of AMPK in response to a rise in AMP or ADP. AMPK can also be phosphorylated by CAMKK2 in response to calcium flux. Activated AMPK directly phosphorylates a number of substrates to affect cellular metabolism and growth.

1.5.2.2 *LKB1 structure and activity*

The human LKB1 gene also referred to as serine threonine kinase 11 (*STK11*), spans 23kb with ten exons, nine of which are coding. LKB1 is phosphorylated on at least eight different residues, 4 of which are phosphorylated by upstream kinases (Ser31, Ser325, Thr366 and Ser428), while the other 4 are autophosphorylation sites (Thr185, Thr189, Thr336, and Ser 404)²⁷¹. Mutation of these sites to an alanine (Ala) or glutamic acid (Glu) does not appear to have any effect on the catalytic activity or subcellular localization of LKB1²⁷²⁻²⁷⁴. However, mutation of Ser428 rendered LKB1 unable to suppress cell growth *in vitro*, suggesting that phosphorylation of this residue may contribute to LKB1 tumour suppressor function²⁷⁴. This particular site can be phosphorylated by the p90 ribosomal S6 protein kinase (RSK) as well as Protein kinase A (PKA), suggesting that phosphorylation of LKB1 may be an avenue through which these kinases can regulate cell growth^{274,275}.

LKB1 exists in mammalian cells in a complex with STE20-related adaptor (STRAD) and mouse protein 25 (MO25)²⁷⁶⁻²⁷⁸. STRAD α and STRAD β are referred to as pseudokinases because although they exhibit high sequence homology to the STE20 family of protein kinases, they lack several key catalytic residues, rendering them inactive²⁷⁶. MO25 α and MO25 β are closely related to each other but don't appear to resemble any other protein. They were originally identified as genes expressed at the early cleavage stage during mouse embryogenesis²⁷⁹. STRAD and MO25 are required not only to enhance the activity of LKB1 but also to ensure proper localization within the cell.

LKB1 on its own is located predominantly in the nucleus, with only a small proportion in the cytoplasm^{280,281}. This nuclear retention is mediated by a nuclear localization signal (NLS) located within the N-terminal non-catalytic region of LKB1^{271,280,282-284}. When the NLS is mutated, LKB1 becomes distributed throughout the cell but retains its ability to suppress cell growth²⁸⁵. This suggests that the cytosolic pool of LKB1 may be the primary mediator of its tumour suppressive function²⁷¹. When STRAD and MO25 are present LKB1 is relocalized to the cytoplasm where the catalytic

activity towards its substrates is 10-fold higher. When a mutant of LKB1 that is unable to bind STRAD is introduced into the G361 melanoma cell line, it is unable to induce cell cycle arrest. Thus, MO25/STRAD/LKB1 complex is essential for the tumour suppressive function of LKB1^{272,276,282}.

1.5.2.3 *LKB1-mediated activation of AMPK*

LKB1 does not respond to changes in AMP concentration, rather, it is constitutively active, constantly phosphorylating the Thr172 residue within the activation loop of AMPK^{286,287}. When cells have an adequate supply of energy and nutrients, this site is immediately dephosphorylated, a process mediated by the conformational change induced in the γ subunit when adenosine nucleotides bind. This allows the phosphorylation state and activity of AMPK to change according to cellular energy status²⁸⁸. Specifically, in the presence of ADP or AMP, dephosphorylation of Thr172 by protein phosphatase 2C (PP2C) is inhibited^{289,290}, LKB1-mediated phosphorylation of Thr172 is promoted^{291,292}, and further activation is achieved by allosteric binding of AMP^{288,293}.

One of the initial papers identifying LKB1 as the upstream kinase for AMPK also highlighted the importance of this kinase in mediating AMPK stress responses. They showed that LKB1/*STK11*-null cells failed to activate AMPK in response to metabolic stress and that this response could be rescued by re-expression of LKB1²⁶⁵. This has more recently also been demonstrated *in vivo* where mice lacking LKB1 expression in skeletal muscle have significantly lower AMPK activity, fatty acid oxidation and glucose uptake in response to muscle contraction, a process which normally significantly enhances AMPK activation²⁹⁴. This was the first genetic evidence demonstrating the ability of the LKB1/AMPK pathway to regulate and maintain cellular energy levels.

1.5.2.4 *LKB1-mediated activation of AMPK-related kinases (ARKs)*

In the early 2000s, as we became more aware of various protein kinases and how they interact functionally as well as their sequence similarities, came the development of the human kinome dendrogram²⁹⁵. It is from this that a group of 12 protein kinases closely related to AMPK were discovered and are now referred to as AMPK-related kinases

(ARKs; BRSK1/SAD-A, BRSK2/SAD-B, NUA1/ARK5, NUA2/SNARK, SIK1, OIK/SIK2, SIK3, SNRK, MARK1, MARK2, MARK3 and MARK4)²⁷¹. LKB1 is the master kinase of this entire subfamily of protein kinases, phosphorylating and activating the residue equivalent to Thr172 within each AMPK-related kinase. Correspondingly, the activity of these kinases is decreased significantly in LKB1-deficient cells^{286,296}. The catalytic subunits of the ARK subfamily do not interact with the γ subunits that provide AMPK with its ability to respond to changes in AMP/ADP concentrations, therefore, these kinases do not appear to be regulated by energy stress^{256,297}. ARKs have been shown to play roles in cell polarity (MARK, BRSK/SAD)²⁹⁸⁻³⁰¹, cell proliferation (NUAKs)^{271,302} and CREB-regulated gene transcription (SIKs)^{303,304}, although their regulation and function is poorly understood in comparison to AMPK²⁵⁶. Further study of the ARKs is important in cancer because they may mediate some of the tumour suppressor effects previously ascribed to LKB1 (Figure 1.4).

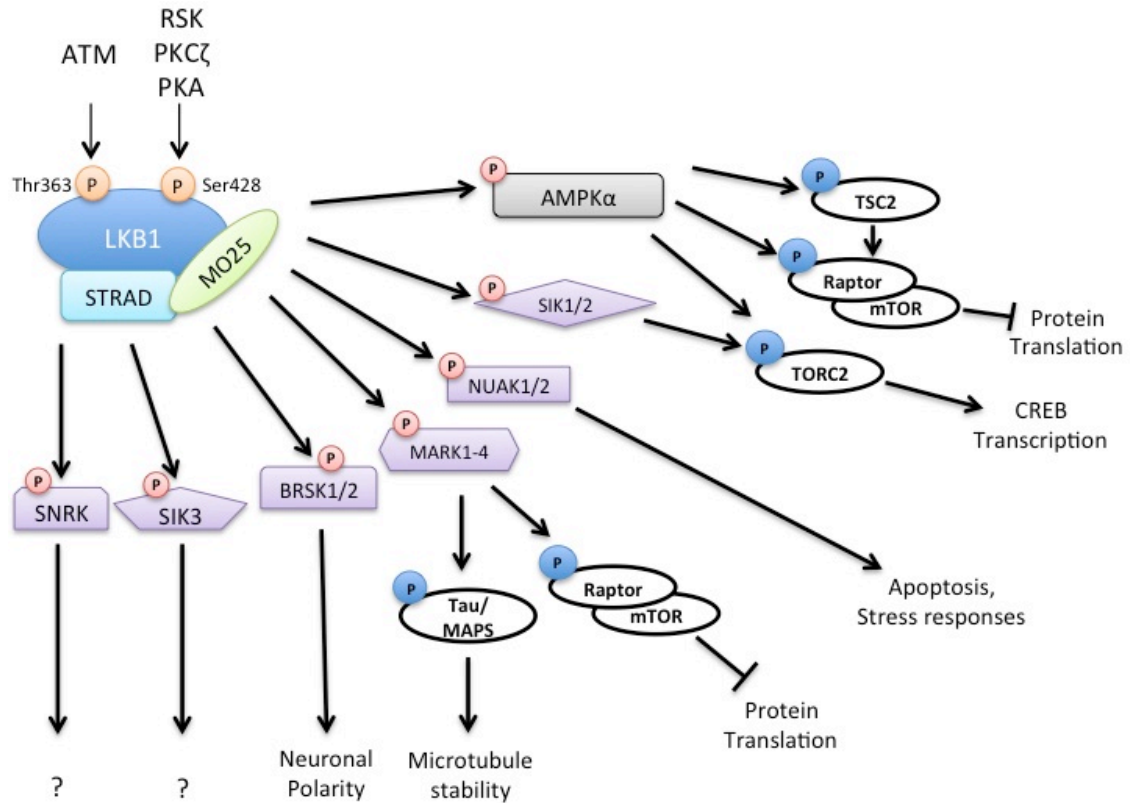


Figure 1.4: LKB1 is a master kinase, phosphorylating a number of AMPK-related kinases (ARKs).

LKB1, in a complex with STRAD and MO25, phosphorylates 12 AMPK-related kinases (ARKs) in addition to AMPK itself. These ARKs play roles in many important cellular processes, including microtubule stability, protein translation, CREB transcription and apoptosis. Upstream, LKB1 is phosphorylated by RSK, PKCζ or PKA at Ser428 and ATM at Thr 363.

1.5.3 LKB1/AMPK signalling in cancer

1.5.3.1 *Peutz-Jeghers syndrome and LKB1*

In 1922, Dr. Johannes Peutz was the first to describe Peutz-Jeghers Syndrome (PJS)³⁰⁵. This was followed by additional characterization provided by Dr. Harold Jeghers in the 1940s³⁰⁶. PJS is an autosomal dominant disorder characterized by development of benign hamartomatous polyps (benign tumour-like growths) within the gastrointestinal tract and marked cutaneous pigmentation (discolouration) of mucous membranes²⁷¹. PJS patients also have a significantly greater chance of developing malignant tumours in a number of different tissues, including the breast, ovary, and pancreas³⁰⁷⁻³⁰⁹. In fact, 93% of PJS patients develop cancer by the age of 43 with 8% of patients developing a gynaecological cancer^{310,311}.

In 1998, parallel studies from two laboratories identified a number of mutations in the LKB1/STK11 gene in PJS families, providing the first evidence for LKB1's function as a tumour suppressor^{312,313}. Since that time, 144 different mutations in the LKB1 gene have been identified in PJS families and a limited number of sporadic cancers. The majority of which result in significant truncation of the catalytic domain, impairing catalytic activity³¹⁴⁻³²⁶. These findings indicate that the tumour suppressive functions of LKB1 are mediated by its downstream targets (AMPK and ARKs).

1.5.3.2 *LKB1/AMPK function as tumour suppressors*

Given the tumour suppressive function LKB1 plays in PJS, its mutation status in a number of sporadic cancers has also been examined. Surprisingly, the occurrence of somatic LKB1/STK11 mutations in sporadic cancers is relatively rare, except in the case of NSCLC and cervical cancers where mutations in this gene have been identified in 30% and 20% of tumours, respectively³²⁷⁻³²⁹. Additional evidence to support the tumour suppressive function of LKB1 was provided by overexpression studies whereby wild-type LKB1 induced a G1 cell-cycle arrest in the HeLa cervical cancer and G361 melanoma cell lines³³⁰. Mice heterozygous for LKB1^{+/-} are viable with no overt phenotype until 45 weeks of age, at which point most animals develop polyps in the

gastrointestinal tract. Histology performed on these polyps revealed that they are remarkably similar to those found in PJS patients^{271,331,332}. When LKB1/STK11^{+/-} mice are aged beyond 50 weeks of age, the majority of animals will develop hepatocellular carcinomas. These tumours have no LKB1 mRNA or protein expression, indicating that complete loss of LKB1 may be required for carcinogenesis³³³.

Prior to the discovery that AMPK activation involves a tumour suppressor (LKB1), AMPK had solely been viewed as kinase with important roles in metabolism and was not on the radar of many cancer biologists. Although AMPK mediates some of the tumour suppressor functions of LKB1, some of these effects are also likely mediated by AMPK-related kinases²⁵⁶. A recent publication in which whole-animal knockout of AMPK α 1 accelerates the development of B cell lymphomas in mice overexpressing c-myc supports the idea that AMPK may function as a tumour suppressor³³⁴.

As part of its energy sensing capabilities, AMPK has a unique ability to control the cell-cycle under conditions of metabolic stress. This can occur through AMPK phosphorylation and stabilization of p53, which causes cells to arrest in the G1/S phase of the cell-cycle^{335,336}. This effect was mediated by upregulation of cyclin-dependent kinase inhibitors p21^{WAF1/CIP1}, which is a transcriptional target of p53, and p27^{KIP1}, which is phosphorylated by AMPK³³⁷.

Perhaps the best characterized mechanism through which AMPK controls cell growth is by suppressing the mechanistic Target of Rapamycin 1 (mTORC1) pathway. mTOR is a crucial hub through which a number of kinases signal, integrating signals from nutrient and energy sensors in order to ensure that growth and proliferation are only triggered when conditions are favourable³³⁸. AMPK is able to directly phosphorylate two crucial components of the mTORC1 signalling cascade, Tuberous sclerosis complex2 (TSC2/Tuberin)³³⁹ and regulatory-associated protein of mTOR (RAPTOR)³⁴⁰. AMPK phosphorylation of both TSC2 and RAPTOR results in inhibition of mTORC1 signalling, thereby decreasing protein translation and inducing prosurvival process such as autophagy.

1.5.3.3 *LKB1/AMPK pathway is tumour-promoting*

Although many of the functions of the LKB1/AMPK pathway discussed above seem to support the idea that these kinases function as tumour suppressors, it has also been suggested that this may be highly context-dependent, based not only on the type of cancer but also the stage of metastasis. In fact, LKB1/AMPK may act as conditional tumour suppressors or oncogenes, depending on the magnitude or duration of stress^{254,341}.

It has also been suggested that LKB1 and AMPK may not always act in concert. Interestingly, unlike LKB1, AMPK subunits are more frequently amplified than mutated in human cancer and there is no evidence of a germline cancer predisposition syndrome involving AMPK subunits²⁵⁴. In addition to this, high levels of AMPK activity are observed in NSCLCs, where loss of LKB1 is common³⁴². Given the lack of genetic evidence to support loss of AMPK function in cancer, AMPK may in fact be required for cancer cell survival in some instances²⁵⁴. In solid tumours, for example, AMPK is activated in areas of hypoxia allowing cells to tolerate nutrient starvation²⁵³. In this context, some of the aforementioned ‘tumour suppressive’ functions of AMPK can actually contribute to cell survival during periods of energetic stress. The prosurvival role of AMPK is likely mediated at least in part by its ability to inhibit mTORC1 signalling, thereby inducing proliferative quiescence and autophagy.

AMPK is able to induce autophagy, a highly conserved cellular process through which cellular content is degraded and recycled through lysosomal machinery. This process has been shown to be upregulated during periods of starvation in order to generate nutrients essential to maintain basic cellular function. mTORC1 activity suppresses autophagy by phosphorylating autophagy-related 13 (ATG 13) and Unc-51 like autophagy activating kinase 1 (ULK1) and preventing autophagosome initiation^{343,344}. AMPK has the ability to indirectly induce autophagy when nutrients are scarce through its inhibition of mTORC1 signalling. It has also been reported that AMPK has the ability to directly phosphorylate ULK1^{345,346}, another mechanism through which AMPK directly promotes autophagy. The protective nature of AMPK activation and autophagy induction was illustrated in a recent study by Avivar *et al.*. In this study autophagy-induction mediated by the LKB1/AMPK/mTORC1 signalling axis promoted

anoikis-resistance in mammary epithelial cells. This effect was also found to be mediated by suspension-induced PERK activation, a member of the unfolded protein response (UPR) pathway³⁴⁷.

1.5.3.4 Therapeutic manipulation of LKB1/AMPK signalling in cancer

Based on the proposed tumour suppressive function of the LKB1/AMPK pathway and its ability to suppress mTORC1 activity, it has been proposed that AMPK-activating drugs may be useful as cancer therapeutics³⁴⁸. One of the most commonly used AMPK agonists is the drug metformin, which is taken by approximately 120 million type 2 diabetics daily³⁴⁹. This activation, however, is not direct as metformin fails to activate AMPK in cell-free assays, rather it has been hypothesized to be through metformin's inhibition of the mitochondrial respiratory chain complex I³⁵⁰. Retrospective studies have demonstrated a strong correlation between metformin use and a reduction in cancer risk of up to 30%³⁵¹⁻³⁵³. The most significant risk-reduction was observed for pancreatic and hepatocellular carcinomas³⁵⁴. It has been suggested that these associations between cancer incidence and metformin use may be due to other effects that metformin has on the tumour cells themselves, rather than AMPK activation alone. This provoked studies in tumour-prone PTEN^{+/-} mice crossed to mice with decreased LKB1 expression (hypomorphic LKB1), in which development of lymphomas was delayed by administration of metformin or A-769662 (an allosteric AMPK agonist)³⁵⁵. Since metformin and A-769662 have completely different mechanisms through which they activate AMPK, it is unlikely that the effects of either of these compounds, is AMPK-independent³⁵⁶. Therefore, these data strongly suggest that metformin may be used as an AMPK-agonist in a therapeutic setting for cancer treatment.

As discussed above, the role of the LKB1/AMPK pathway largely depends on the stage of the tumour in question. In pre-neoplastic lesions, LKB1/AMPK may in fact function as a tumour suppressor through its ability to inhibit cell proliferation. Once a tumour is established, however, LKB1/AMPK may be needed to allow cells to survive periods of metabolic stress²⁵⁶. Before we use AMPK-activators as a cancer therapeutic, we need to better understand the unique metabolic requirements of cancer cells during

different stages of the carcinogenic process. In some cases, like when cells lose ECM-attachment or become hypoxic, specific inhibitors of LKB1 or AMPK may in fact be more appropriate.

1.5.4 LKB1/AMPK signalling in ovarian cancer

The observation that females with PJS have a significantly higher risk of developing gynecological cancers lead researchers to suspect that LKB1 may play an important role in the female reproductive tract³⁵⁷. In fact, 61% (176/288) of high-grade serous ovarian tumours analyzed within The Cancer Genome Atlas (TCGA) exhibit deletion of one or more of the alleles of the LKB1/STK11 gene. Correspondingly, immunofluorescence performed on 92 human high-grade serous ovarian carcinomas revealed complete loss of protein expression in 54% of samples and partial/scattered or no loss in the remaining specimens³⁵⁸. The consequences of LKB1 loss in high-grade serous ovarian cancer was examined using a conditional knockout mouse model in which LKB1 is lost in the OSE and stromal cells of the ovary using the *Amhr2*-cre driver mouse strain. Although adult LKB1^{cko} mice exhibit a high degree of surface papillary hyperplasia of the ovary, tumour formation was not observed. Perhaps this was due to the fact that it is now well-recognized that the cell of origin of high grade serous cancer is the secretory cell of the fimbria in the fallopian tube. When LKB1^{cko} mice are crossed to conditional knockout *PTEN* mice under control of the same promotor, however, adnexal (adnexa of uterus; i.e. fallopian tubes or ovaries) tumours were observed with 100% penetrance. When these tumours are examined histologically and compared to human ovarian cancer specimens, they strongly resemble that of high-grade serous ovarian carcinomas³⁵⁸. These studies provided the first evidence that LKB1 loss and its synergy with other tumour suppressors may be important for the initiation of high-grade serous ovarian cancer.

Contrary to LKB1, when tumour specimens from ovarian cancer patients were examined for expression of the various AMPK subunits, higher levels were observed in ovarian carcinomas compared to normal ovarian controls³⁵⁹. Additional studies have demonstrated that activation of AMPK by metformin or AMP mimetic, 5-Aminoimidazole-4-carboxamide ribonucleotide (AICAR) inhibits cell growth and

induces apoptosis^{360,361}. The functional consequences of AMPK subunit overexpression in ovarian carcinoma specimens have yet to be determined with targeted knockdown experiments.

1.5.5 Summary

The LKB1/AMPK signalling pathway is unique in that it allows cells to respond to various forms of metabolic stress, such as nutrient deprivation, hypoxia, and energy depletion. The importance of metabolic reprogramming in allowing cancer cells to survive adverse microenvironments has become apparent over the last few years. It is clear that LKB1/AMPK may in fact play many context-specific roles throughout tumorigenesis and may not simply be classified as oncogenes or tumour suppressors. For example, loss of LKB1/AMPK signalling may be necessary during the initial stages of tumour development where there is need for rapid proliferation to support tumour growth. Subsequent to this, when this growth has stripped many of the available nutrient supplies, reactivation of LKB1/AMPK signalling may allow cells to survive until nutrients are replenished. Given the studies that have begun to implicate this pathway in ovarian carcinogenesis, there is a critical need for a more thorough molecular analysis and functional studies to determine the role of the LKB1/AMPK signalling pathway in ovarian cancer pathogenesis. This is particularly important given the unique way that ovarian cancer metastasizes and the crucial role that LKB1/AMPK signalling plays in mediating anoikis-resistance^{347,362}.

1.6 Scope of Thesis

Mechanisms of anoikis-resistance and spheroid formation are of particular importance when studying ovarian cancer given the way this disease metastasizes. Cells shed into the peritoneal cavity from the primary tumour must survive under non-adherent conditions until they reach the serosal surface of various abdominal organs at which point they are able to reattach and form secondary metastatic lesions. We developed an *in vitro* system with which to model suspension-induced spheroid formation and re-implantation to an adherent substratum. This allowed us to examine two signalling pathways we

hypothesized to play important, although not necessarily overlapping roles, in the process of ovarian cancer spheroid formation and re-implantation.

Our investigations began with the BMP signalling pathway, which we demonstrated is autonomously down-regulated during spheroid formation (Chapter 2). Correspondingly, over-activation of this pathway has a detrimental effect on the ability of cells to aggregate in suspension, resulting in much smaller spheroids. Further to this, we also demonstrate that when cells are reattached to an adherent substratum, BMP signalling is activated and enhances cell dispersion. Global gene expression analyses revealed a number of molecular aberrations associated with activated BMP signalling in ovarian cancer cells under both adherent and suspension conditions. Of these, Akt, which is also autonomously down-regulated when cells are in suspension, was shown to be enhanced in spheroids with activated BMP signalling. We also demonstrate that the BMP and Akt signalling pathways have the ability to act in concert to mediate suspension-induced cell aggregation and subsequent reattachment to an adherent surface. This study highlights the context-dependent role for the BMP signalling pathway throughout the various stages of ovarian cancer metastasis and provides a crucial link between this pathway and the PI3K/AKT signalling cascade. Given the important role that AKT plays in mediating the phenotypic alterations associated with activated BMP signalling in spheroids and other studies in our laboratory demonstrating that AKT signalling is a crucial mediator of reversible spheroid formation-induced dormancy, we became interested in other pathways that may cooperate with the PI3K/AKT pathway in our system.

AMPK is an important sensor of cellular energy status that converges with the PI3K/AKT signalling cascade on mTOR. These kinases have opposing regulatory effects on mTOR and therefore, may act in concert to allow ovarian cancer cells to survive in suspension. Indeed, in contrast to AKT, the activity of AMPK and its upstream kinase, LKB1, are enhanced in ovarian cancer spheroids (Chapter 3). Further pharmacological activation of the AMPK pathway is detrimental to adherent cells but much less so when cells are in suspension. Interestingly, targeted knockdown experiments demonstrated that LKB1 is crucial for suspension-induced spheroid formation and survival and that this

effect is AMPK-independent. These studies have begun to uncover the diverse range of signalling aberrations that occur when cells form multicellular spheroids and how these pathways interact to promote aggregation and survival in suspension.

1.7 References

1. Erickson, B.K., Conner, M.G. & Landen, C.N., Jr. The role of the fallopian tube in the origin of ovarian cancer. *Am J Obstet Gynecol* (2013).
2. Auersperg, N., Wong, A.S., Choi, K.C., Kang, S.K. & Leung, P.C. Ovarian surface epithelium: biology, endocrinology, and pathology. *Endocr Rev* **22**, 255-288 (2001).
3. Landen, C.N., Jr., Birrer, M.J. & Sood, A.K. Early events in the pathogenesis of epithelial ovarian cancer. *Journal of clinical oncology : official journal of the American Society of Clinical Oncology* **26**, 995-1005 (2008).
4. Lengyel, E., *et al.* Epithelial ovarian cancer experimental models. *Oncogene* (2013).
5. Karst, A.M. & Drapkin, R. Ovarian cancer pathogenesis: a model in evolution. *J Oncol* **2010**, 932371 (2010).
6. Paclitaxel plus carboplatin versus standard chemotherapy with either single-agent carboplatin or cyclophosphamide, doxorubicin, and cisplatin in women with ovarian cancer: the ICON3 randomised trial. *Lancet* **360**, 505-515 (2002).
7. du Bois, A., *et al.* A randomized clinical trial of cisplatin/paclitaxel versus carboplatin/paclitaxel as first-line treatment of ovarian cancer. *J Natl Cancer Inst* **95**, 1320-1329 (2003).
8. Gilks, C.B. Molecular abnormalities in ovarian cancer subtypes other than high-grade serous carcinoma. *J Oncol* **2010**, 740968 (2010).
9. Gilks, C.B. & Prat, J. Ovarian carcinoma pathology and genetics: recent advances. *Human pathology* **40**, 1213-1223 (2009).
10. Galic, V., Coleman, R.L. & Herzog, T.J. Unmet needs in ovarian cancer: dividing histologic subtypes to exploit novel targets and pathways. *Curr Cancer Drug Targets* **13**, 698-707 (2013).
11. Winter, W.E., 3rd, *et al.* Prognostic factors for stage III epithelial ovarian cancer: a Gynecologic Oncology Group Study. *Journal of clinical oncology : official journal of the American Society of Clinical Oncology* **25**, 3621-3627 (2007).
12. Shih Ie, M. & Kurman, R.J. Ovarian tumorigenesis: a proposed model based on morphological and molecular genetic analysis. *Am J Pathol* **164**, 1511-1518 (2004).
13. Nik, N.N., Vang, R., Shih, I.M. & Kurman, R.J. Origin and Pathogenesis of Pelvic (Ovarian, Tubal, and Primary Peritoneal) Serous Carcinoma. *Annu Rev Pathol* (2013).
14. Wiegand, K.C., *et al.* ARID1A mutations in endometriosis-associated ovarian carcinomas. *N Engl J Med* **363**, 1532-1543 (2010).
15. Kurman, R.J. & Shih Ie, M. Molecular pathogenesis and extraovarian origin of epithelial ovarian cancer--shifting the paradigm. *Human pathology* **42**, 918-931 (2011).

16. Chan, W.Y., *et al.* Bcl-2 and p53 protein expression, apoptosis, and p53 mutation in human epithelial ovarian cancers. *Am J Pathol* **156**, 409-417 (2000).
17. Kohler, M.F., *et al.* Mutation and overexpression of p53 in early-stage epithelial ovarian cancer. *Obstet Gynecol* **81**, 643-650 (1993).
18. Kupryjanczyk, J., *et al.* p53 gene mutations and protein accumulation in human ovarian cancer. *Proceedings of the National Academy of Sciences of the United States of America* **90**, 4961-4965 (1993).
19. Wen, W.H., *et al.* p53 mutations and expression in ovarian cancers: correlation with overall survival. *Int J Gynecol Pathol* **18**, 29-41 (1999).
20. Singer, G., Shih Ie, M., Truskinovsky, A., Umudum, H. & Kurman, R.J. Mutational analysis of K-ras segregates ovarian serous carcinomas into two types: invasive MPSC (low-grade tumor) and conventional serous carcinoma (high-grade tumor). *Int J Gynecol Pathol* **22**, 37-41 (2003).
21. Singer, G., *et al.* Patterns of p53 mutations separate ovarian serous borderline tumors and low- and high-grade carcinomas and provide support for a new model of ovarian carcinogenesis: a mutational analysis with immunohistochemical correlation. *Am J Surg Pathol* **29**, 218-224 (2005).
22. Permuth-Wey, J. & Sellers, T.A. Epidemiology of ovarian cancer. *Methods Mol Biol* **472**, 413-437 (2009).
23. Erzen, M. & Kovacic, J. Relationship between endometriosis and ovarian cancer. *Eur J Gynaecol Oncol* **19**, 553-555 (1998).
24. Goumenou, A., Matalliotakis, I., Mahutte, N. & Koumantakis, E. Endometriosis mimicking advanced ovarian cancer. *Fertil Steril* **86**, 219 e223-215 (2006).
25. Iwanari, O., *et al.* Differential diagnosis of ovarian cancer, benign ovarian tumor and endometriosis by a combination assay of serum sialyl SSEA-1 antigen and CA125 levels. *Gynecol Obstet Invest* **29**, 71-74 (1990).
26. Mandai, M., Yamaguchi, K., Matsumura, N., Baba, T. & Konishi, I. Ovarian cancer in endometriosis: molecular biology, pathology, and clinical management. *Int J Clin Oncol* **14**, 383-391 (2009).
27. Steed, H., Chapman, W. & Laframboise, S. Endometriosis-associated ovarian cancer: a clinicopathologic review. *J Obstet Gynaecol Can* **26**, 709-715 (2004).
28. Vercellini, P., *et al.* Endometriosis and ovarian cancer. *Am J Obstet Gynecol* **169**, 181-182 (1993).
29. Vlahos, N.F., Kalampokas, T. & Fotiou, S. Endometriosis and ovarian cancer: a review. *Gynecol Endocrinol* **26**, 213-219 (2010).
30. Yoshikawa, H., *et al.* Prevalence of endometriosis in ovarian cancer. *Gynecol Obstet Invest* **50 Suppl 1**, 11-17 (2000).
31. Callahan, M.J., *et al.* Primary fallopian tube malignancies in BRCA-positive women undergoing surgery for ovarian cancer risk reduction. *Journal of clinical oncology : official journal of the American Society of Clinical Oncology* **25**, 3985-3990 (2007).
32. Crum, C.P., *et al.* Lessons from BRCA: the tubal fimbria emerges as an origin for pelvic serous cancer. *Clin Med Res* **5**, 35-44 (2007).
33. Crum, C.P., *et al.* The distal fallopian tube: a new model for pelvic serous carcinogenesis. *Curr Opin Obstet Gynecol* **19**, 3-9 (2007).

34. Gross, A.L., Kurman, R.J., Vang, R., Shih Ie, M. & Visvanathan, K. Precursor lesions of high-grade serous ovarian carcinoma: morphological and molecular characteristics. *J Oncol* **2010**, 126295 (2010).
35. Piek, J.M., *et al.* Dysplastic changes in prophylactically removed Fallopian tubes of women predisposed to developing ovarian cancer. *J Pathol* **195**, 451-456 (2001).
36. Saleemuddin, A., *et al.* Risk factors for a serous cancer precursor ("p53 signature") in women with inherited BRCA mutations. *Gynecologic oncology* **111**, 226-232 (2008).
37. Piek, J.M., *et al.* BRCA1/2-related ovarian cancers are of tubal origin: a hypothesis. *Gynecologic oncology* **90**, 491 (2003).
38. Erickson, B.K., Conner, M.G. & Landen, C.N., Jr. The role of the fallopian tube in the origin of ovarian cancer. *Am J Obstet Gynecol* **209**, 409-414 (2013).
39. Kessler, M., Fotopoulou, C. & Meyer, T. The molecular fingerprint of high grade serous ovarian cancer reflects its fallopian tube origin. *Int J Mol Sci* **14**, 6571-6596 (2013).
40. O'Shannessy, D.J., *et al.* Gene expression analyses support fallopian tube epithelium as the cell of origin of epithelial ovarian cancer. *Int J Mol Sci* **14**, 13687-13703 (2013).
41. Kindelberger, D.W., *et al.* Intraepithelial carcinoma of the fimbria and pelvic serous carcinoma: Evidence for a causal relationship. *Am J Surg Pathol* **31**, 161-169 (2007).
42. Perets, R., *et al.* Transformation of the fallopian tube secretory epithelium leads to high-grade serous ovarian cancer in *brca*; *tp53*; *pten* models. *Cancer cell* **24**, 751-765 (2013).
43. Statistics, C.C.S.s.A.C.o.C. Canadian Cancer Statistics 2013. *Canadian Cancer Society* (2013).
44. Bast, R.C., Jr., Hennessy, B. & Mills, G.B. The biology of ovarian cancer: new opportunities for translation. *Nature reviews. Cancer* **9**, 415-428 (2009).
45. Herzog, T.J. & Pothuri, B. Ovarian cancer: a focus on management of recurrent disease. *Nat Clin Pract Oncol* **3**, 604-611 (2006).
46. Jemal, A., *et al.* Cancer statistics, 2008. *CA Cancer J Clin* **58**, 71-96 (2008).
47. Burleson, K.M., *et al.* Ovarian carcinoma ascites spheroids adhere to extracellular matrix components and mesothelial cell monolayers. *Gynecol Oncol* **93**, 170-181 (2004).
48. Burleson, K.M., Hansen, L.K. & Skubitz, A.P. Ovarian carcinoma spheroids disaggregate on type I collagen and invade live human mesothelial cell monolayers. *Clinical & experimental metastasis* **21**, 685-697 (2004).
49. Kenny, H.A., Nieman, K.M., Mitra, A.K. & Lengyel, E. The first line of intra-abdominal metastatic attack: breaching the mesothelial cell layer. *Cancer Discov* **1**, 100-102 (2011).
50. Milliken, D., Scotton, C., Raju, S., Balkwill, F. & Wilson, J. Analysis of chemokines and chemokine receptor expression in ovarian cancer ascites. *Clinical cancer research : an official journal of the American Association for Cancer Research* **8**, 1108-1114 (2002).

51. Kipps, E., Tan, D.S. & Kaye, S.B. Meeting the challenge of ascites in ovarian cancer: new avenues for therapy and research. *Nature reviews. Cancer* **13**, 273-282 (2013).
52. Holtfreter, J. A study of the mechanics of gastrulation. *J Exp Zool* **95**, 171-212 (1944).
53. Holtfreter, J. Neural induction in explants which have passed through sublethal cytolysis. *J Exp Zool* **106**, 197-222 (1947).
54. Moscana, A. Cell suspension from organ rudiments of chick embryos. *Exp Cell Res* **3**, 535-539 (1952).
55. Moscana, A. The development in vitro of chimeric aggregates of dissociated embryonic chick and mouse cells. *Proceedings of the National Academy of Sciences of the United States of America* **43**, 184-194 (1957).
56. Sutherland, R.M., Inch, W.R., McCredie, J.A. & Kruuv, J. A multi-component radiation survival curve using an in vitro tumour model. *Int J Radiat Biol Relat Stud Phys Chem Med* **18**, 491-495 (1970).
57. Sutherland, R.M., MacDonald, H.R. & Howell, R.L. Multicellular spheroids: a new model target for in vitro studies of immunity to solid tumor allografts. *J Natl Cancer Inst* **58**, 1849-1853 (1977).
58. Sutherland, R.M., McCredie, J.A. & Inch, W.R. Growth of multicell spheroids in tissue culture as a model of nodular carcinomas. *J Natl Cancer Inst* **46**, 113-120 (1971).
59. Ahammer, H., DeVaney, T.T. & Tritthart, H.A. Fractal dimension of K1735 mouse melanoma clones and spheroid invasion in vitro. *Eur Biophys J* **30**, 494-499 (2001).
60. Burleson, K.M., Boente, M.P., Pambuccian, S.E. & Skubitz, A.P. Disaggregation and invasion of ovarian carcinoma ascites spheroids. *Journal of translational medicine* **4**, 6 (2006).
61. Carey, S.P., Starchenko, A., McGregor, A.L. & Reinhart-King, C.A. Leading malignant cells initiate collective epithelial cell invasion in a three-dimensional heterotypic tumor spheroid model. *Clinical & experimental metastasis* **30**, 615-630 (2013).
62. de Ridder, L., Cornelissen, M. & de Ridder, D. Autologous spheroid culture: a screening tool for human brain tumour invasion. *Crit Rev Oncol Hematol* **36**, 107-122 (2000).
63. De Wever, O., *et al.* Single cell and spheroid collagen type I invasion assay. *Methods Mol Biol* **1070**, 13-35 (2014).
64. Del Duca, D., Werbowetski, T. & Del Maestro, R.F. Spheroid preparation from hanging drops: characterization of a model of brain tumor invasion. *J Neurooncol* **67**, 295-303 (2004).
65. Naber, H.P., Wiercinska, E., Ten Dijke, P. & van Laar, T. Spheroid assay to measure TGF-beta-induced invasion. *J Vis Exp* (2011).
66. Sutherland, R.M. Cell and environment interactions in tumor microregions: the multicell spheroid model. *Science* **240**, 177-184 (1988).
67. Mueller-Klieser, W. Multicellular spheroids. A review on cellular aggregates in cancer research. *Journal of cancer research and clinical oncology* **113**, 101-122 (1987).

68. Santini, M.T., Rainaldi, G. & Indovina, P.L. Apoptosis, cell adhesion and the extracellular matrix in the three-dimensional growth of multicellular tumor spheroids. *Crit Rev Oncol Hematol* **36**, 75-87 (2000).
69. Aoshiba, K., Rennard, S.I. & Spurzem, J.R. Cell-matrix and cell-cell interactions modulate apoptosis of bronchial epithelial cells. *Am J Physiol* **272**, L28-37 (1997).
70. Fukai, F., *et al.* Modulation of apoptotic cell death by extracellular matrix proteins and a fibronectin-derived antiadhesive peptide. *Experimental cell research* **242**, 92-99 (1998).
71. Rozzo, C., Chiesa, V., Caridi, G., Pagnan, G. & Ponzoni, M. Induction of apoptosis in human neuroblastoma cells by abrogation of integrin-mediated cell adhesion. *International journal of cancer. Journal international du cancer* **70**, 688-698 (1997).
72. Scott, G., Cassidy, L. & Busacco, A. Fibronectin suppresses apoptosis in normal human melanocytes through an integrin-dependent mechanism. *J Invest Dermatol* **108**, 147-153 (1997).
73. Frisch, S.M. & Francis, H. Disruption of epithelial cell-matrix interactions induces apoptosis. *The Journal of cell biology* **124**, 619-626 (1994).
74. Chiarugi, P. & Giannoni, E. Anoikis: a necessary death program for anchorage-dependent cells. *Biochemical pharmacology* **76**, 1352-1364 (2008).
75. Bissell, M.J. & Radisky, D. Putting tumours in context. *Nature reviews. Cancer* **1**, 46-54 (2001).
76. Eble, J.A. & Haier, J. Integrins in cancer treatment. *Curr Cancer Drug Targets* **6**, 89-105 (2006).
77. Reddig, P.J. & Juliano, R.L. Clinging to life: cell to matrix adhesion and cell survival. *Cancer Metastasis Rev* **24**, 425-439 (2005).
78. Valentijn, A.J., Zouq, N. & Gilmore, A.P. Anoikis. *Biochemical Society transactions* **32**, 421-425 (2004).
79. Frisch, S.M. & Ruoslahti, E. Integrins and anoikis. *Current opinion in cell biology* **9**, 701-706 (1997).
80. Ruoslahti, E. & Reed, J.C. Anchorage dependence, integrins, and apoptosis. *Cell* **77**, 477-478 (1994).
81. Giancotti, F.G. Complexity and specificity of integrin signalling. *Nat Cell Biol* **2**, E13-14 (2000).
82. Chiarugi, P. From anchorage dependent proliferation to survival: lessons from redox signalling. *IUBMB Life* **60**, 301-307 (2008).
83. Liotta, L.A. & Kohn, E. Anoikis: cancer and the homeless cell. *Nature* **430**, 973-974 (2004).
84. Wang, L.H. Molecular signaling regulating anchorage-independent growth of cancer cells. *Mt Sinai J Med* **71**, 361-367 (2004).
85. Day, M.L., *et al.* E-cadherin mediates aggregation-dependent survival of prostate and mammary epithelial cells through the retinoblastoma cell cycle control pathway. *J Biol Chem* **274**, 9656-9664 (1999).
86. Kantak, S.S. & Kramer, R.H. E-cadherin regulates anchorage-independent growth and survival in oral squamous cell carcinoma cells. *J Biol Chem* **273**, 16953-16961 (1998).

87. St Croix, B., *et al.* E-Cadherin-dependent growth suppression is mediated by the cyclin-dependent kinase inhibitor p27(KIP1). *The Journal of cell biology* **142**, 557-571 (1998).
88. Davies, C.D., Muller, H., Hagen, I., Garseth, M. & Hjelstuen, M.H. Comparison of extracellular matrix in human osteosarcomas and melanomas growing as xenografts, multicellular spheroids, and monolayer cultures. *Anticancer research* **17**, 4317-4326 (1997).
89. Nederman, T., Norling, B., Glimelius, B., Carlsson, J. & Brunk, U. Demonstration of an extracellular matrix in multicellular tumor spheroids. *Cancer Res* **44**, 3090-3097 (1984).
90. Paulus, W., Huettner, C. & Tonn, J.C. Collagens, integrins and the mesenchymal drift in glioblastomas: a comparison of biopsy specimens, spheroid and early monolayer cultures. *International journal of cancer. Journal international du cancer* **58**, 841-846 (1994).
91. Hauptmann, S., *et al.* Integrin expression on colorectal tumor cells growing as monolayers, as multicellular tumor spheroids, or in nude mice. *International journal of cancer. Journal international du cancer* **61**, 819-825 (1995).
92. Waleh, N.S., *et al.* Selective down-regulation of integrin receptors in spheroids of squamous cell carcinoma. *Cancer Res* **54**, 838-843 (1994).
93. Boyd, M., *et al.* Transfectant mosaic spheroids: a new model for evaluation of tumour cell killing in targeted radiotherapy and experimental gene therapy. *J Gene Med* **4**, 567-576 (2002).
94. Christensen, T., Moan, J., Sandquist, T. & Smedshammer, L. Multicellular spheroids as an in vitro model system for photoradiation therapy in the presence of HpD. *Prog Clin Biol Res* **170**, 381-390 (1984).
95. Dubessy, C., Merlin, J.M., Marchal, C. & Guillemin, F. Spheroids in radiobiology and photodynamic therapy. *Crit Rev Oncol Hematol* **36**, 179-192 (2000).
96. Durand, R.E. & Olive, P.L. Resistance of tumor cells to chemo- and radiotherapy modulated by the three-dimensional architecture of solid tumors and spheroids. *Methods Cell Biol* **64**, 211-233 (2001).
97. Griffon, G., *et al.* Radiosensitivity of multicellular tumour spheroids obtained from human ovarian cancers. *Eur J Cancer* **31A**, 85-91 (1995).
98. Guirado, D., *et al.* Low-dose radiation hyper-radiosensitivity in multicellular tumour spheroids. *Br J Radiol* **85**, 1398-1406 (2012).
99. Ho, J.T., *et al.* Effects of fractionated radiation therapy on human brain tumor multicellular spheroids. *Int J Radiat Oncol Biol Phys* **25**, 251-258 (1993).
100. Kelly, C.J., Hussien, K. & Muschel, R.J. 3D tumour spheroids as a model to assess the suitability of [18F]FDG-PET as an early indicator of response to PI3K inhibition. *Nucl Med Biol* **39**, 986-992 (2012).
101. Kim, T.H., Mount, C.W., Gombotz, W.R. & Pun, S.H. The delivery of doxorubicin to 3-D multicellular spheroids and tumors in a murine xenograft model using tumor-penetrating triblock polymeric micelles. *Biomaterials* **31**, 7386-7397.
102. Langmuir, V.K., Mendonca, H.L. & Woo, D.V. Comparisons between two monoclonal antibodies that bind to the same antigen but have differing affinities:

- uptake kinetics and ¹²⁵I-antibody therapy efficacy in multicell spheroids. *Cancer Res* **52**, 4728-4734 (1992).
103. Mandujano-Tinoco, E.A., Gallardo-Perez, J.C., Marin-Hernandez, A., Moreno-Sanchez, R. & Rodriguez-Enriquez, S. Anti-mitochondrial therapy in human breast cancer multi-cellular spheroids. *Biochimica et biophysica acta* **1833**, 541-551 (2013).
 104. Mehta, G., Hsiao, A.Y., Ingram, M., Luker, G.D. & Takayama, S. Opportunities and challenges for use of tumor spheroids as models to test drug delivery and efficacy. *J Control Release* **164**, 192-204 (2012).
 105. Nederman, T. & Twentyman, P. Spheroids for studies of drug effects. *Recent Results Cancer Res* **95**, 84-102 (1984).
 106. Nichols, M.G. & Foster, T.H. Oxygen diffusion and reaction kinetics in the photodynamic therapy of multicell tumour spheroids. *Phys Med Biol* **39**, 2161-2181 (1994).
 107. Perche, F. & Torchilin, V.P. Cancer cell spheroids as a model to evaluate chemotherapy protocols. *Cancer Biol Ther* **13**, 1205-1213 (2012).
 108. Sutherland, R.M., Eddy, H.A., Bareham, B., Reich, K. & Vanantwerp, D. Resistance to adriamycin in multicellular spheroids. *Int J Radiat Oncol Biol Phys* **5**, 1225-1230 (1979).
 109. Durand, R.E. & Sutherland, R.M. Effects of intercellular contact on repair of r radiation damage. *Experimental cell research* **71**, 75-80 (1972).
 110. Durand, R.E. & Sutherland, R.M. Dependence of the radiation response of an in vitro tumor model on cell cycle effects. *Cancer Res* **33**, 213-219 (1973).
 111. Sutherland, R.M. & Durand, R.E. Cell contact as a possible contribution to radiation resistance of some tumours. *Br J Radiol* **45**, 788-789 (1972).
 112. Hirschhaeuser, F., *et al.* Multicellular tumor spheroids: an underestimated tool is catching up again. *Journal of biotechnology* **148**, 3-15.
 113. Brammer, I., Zywiets, F. & Jung, H. Changes of histological and proliferative indices in the Walker carcinoma with tumour size and distance from blood vessel. *European journal of cancer* **15**, 1329-1336 (1979).
 114. Burns, F.J. & Tannock, I.F. On the existence of a G 0 -phase in the cell cycle. *Cell Tissue Kinet* **3**, 321-334 (1970).
 115. Denekamp, J. & Kallman, R.F. In vitro and in vivo labelling of animal tumours with tritiated thymidine. *Cell Tissue Kinet* **6**, 217-227 (1973).
 116. Tannock, I.F. The relation between cell proliferation and the vascular system in a transplanted mouse mammary tumour. *British journal of cancer* **22**, 258-273 (1968).
 117. Dethlefsen, L.A., Bauer, K.D. & Riley, R.M. Analytical cytometric approaches to heterogeneous cell populations in solid tumors: a review. *Cytometry* **1**, 89-108 (1980).
 118. Hlatky, L. & Alpen, E.L. Two-dimensional diffusion limited system for cell growth. *Cell Tissue Kinet* **18**, 597-611 (1985).
 119. Bauer, K.D., Keng, P., Sutherland, R.M. Isolation of quiescent cells from multicellular tumour spheroids using centrifugal elutriation. *Cancer Res* **42**, 72-78 (1982).

120. Inch, W.R., McCredie, J.A. & Sutherland, R.M. Growth of nodular carcinomas in rodents compared with multi-cell spheroids in tissue culture. *Growth* **34**, 271-282 (1970).
121. Hudson, L.G., Zeineldin, R. & Stack, M.S. Phenotypic plasticity of neoplastic ovarian epithelium: unique cadherin profiles in tumor progression. *Clinical & experimental metastasis* **25**, 643-655 (2008).
122. Sawada, K., *et al.* Loss of E-cadherin promotes ovarian cancer metastasis via alpha 5-integrin, which is a therapeutic target. *Cancer Res* **68**, 2329-2339 (2008).
123. Symowicz, J., *et al.* Engagement of collagen-binding integrins promotes matrix metalloproteinase-9-dependent E-cadherin ectodomain shedding in ovarian carcinoma cells. *Cancer Res* **67**, 2030-2039 (2007).
124. Shield, K., Ackland, M.L., Ahmed, N. & Rice, G.E. Multicellular spheroids in ovarian cancer metastases: Biology and pathology. *Gynecol Oncol* **113**, 143-148 (2009).
125. Valcarcel, M., *et al.* Three-dimensional growth as multicellular spheroid activates the proangiogenic phenotype of colorectal carcinoma cells via LFA-1-dependent VEGF: implications on hepatic micrometastasis. *Journal of translational medicine* **6**, 57 (2008).
126. Patel, I.S., Madan, P., Getsios, S., Bertrand, M.A. & MacCalman, C.D. Cadherin switching in ovarian cancer progression. *International journal of cancer. Journal international du cancer* **106**, 172-177 (2003).
127. Imai, T., *et al.* Hypoxia attenuates the expression of E-cadherin via up-regulation of SNAIL in ovarian carcinoma cells. *Am J Pathol* **163**, 1437-1447 (2003).
128. Casey, R.C., *et al.* Beta 1-integrins regulate the formation and adhesion of ovarian carcinoma multicellular spheroids. *Am J Pathol* **159**, 2071-2080 (2001).
129. Iwanicki, M.P., *et al.* Ovarian cancer spheroids use myosin-generated force to clear the mesothelium. *Cancer Discov* **1**, 144-157 (2011).
130. Sato, K. & Urist, M.R. Induced regeneration of calvaria by bone morphogenetic protein (BMP) in dogs. *Clin Orthop Relat Res*, 301-311 (1985).
131. Takahashi, S. & Urist, M.R. Differentiation of cartilage on three substrata under the influence of an aggregate of morphogenetic protein and other bone tissue noncollagenous proteins (BMP/iNCP). *Clin Orthop Relat Res*, 227-238 (1986).
132. Urist, M.R., *et al.* Bone regeneration under the influence of a bone morphogenetic protein (BMP) beta tricalcium phosphate (TCP) composite in skull trephine defects in dogs. *Clin Orthop Relat Res*, 295-304 (1987).
133. Bin, S., *et al.* BMP-7 attenuates TGF-beta1-induced fibroblast-like differentiation of rat dermal papilla cells. *Wound Repair Regen* **21**, 275-281 (2013).
134. Cai, J., *et al.* BMP and TGF-beta pathway mediators are critical upstream regulators of Wnt signaling during midbrain dopamine differentiation in human pluripotent stem cells. *Dev Biol* **376**, 62-73 (2013).
135. Ghosh-Choudhury, N., *et al.* Requirement of BMP-2-induced phosphatidylinositol 3-kinase and Akt serine/threonine kinase in osteoblast differentiation and Smad-dependent BMP-2 gene transcription. *J Biol Chem* **277**, 33361-33368 (2002).

136. Liu, D.D., Zhang, J.C., Zhang, Q., Wang, S.X. & Yang, M.S. TGF-beta/BMP signaling pathway is involved in cerium-promoted osteogenic differentiation of mesenchymal stem cells. *Journal of cellular biochemistry* **114**, 1105-1114 (2013).
137. Lorda-Diez, C.I., Montero, J.A., Choe, S., Garcia-Porrero, J.A. & Hurler, J.M. Ligand- and stage-dependent divergent functions of BMP signaling in the differentiation of embryonic skeletogenic progenitors in vitro. *J Bone Miner Res* (2013).
138. Matsumoto, T., *et al.* BMP-2 Induced Expression of Alx3 That Is a Positive Regulator of Osteoblast Differentiation. *PLoS One* **8**, e68774 (2013).
139. Onishi, M., Fujita, Y., Yoshikawa, H. & Yamashita, T. Inhibition of Rac1 promotes BMP-2-induced osteoblastic differentiation. *Cell death & disease* **4**, e698 (2013).
140. Schneider, H., Sedaghati, B., Naumann, A., Hacker, M.C. & Schulz-Siegmund, M. Gene Silencing of Chordin Improves BMP-2 Effects on Osteogenic Differentiation of Human Adipose Tissue-Derived Stromal Cells. *Tissue Eng Part A* (2013).
141. Sharff, K.A., *et al.* Hey1 basic helix-loop-helix protein plays an important role in mediating BMP9-induced osteogenic differentiation of mesenchymal progenitor cells. *J Biol Chem* **284**, 649-659 (2009).
142. Sui, L., Geens, M., Sermon, K., Bouwens, L. & Mfopou, J.K. Role of BMP signaling in pancreatic progenitor differentiation from human embryonic stem cells. *Stem Cell Rev* **9**, 569-577 (2013).
143. Vinals, F., Lopez-Rovira, T., Rosa, J.L. & Ventura, F. Inhibition of PI3K/p70 S6K and p38 MAPK cascades increases osteoblastic differentiation induced by BMP-2. *FEBS Lett* **510**, 99-104 (2002).
144. Wei, X., *et al.* Effects of bone morphogenetic protein-4 (BMP-4) on adipocyte differentiation from mouse adipose-derived stem cells. *Cell Prolif* **46**, 416-424 (2013).
145. Yang, Z., *et al.* Cessation of Epithelial Bmp Signaling Switches the Differentiation of Crown Epithelia to the Root Lineage in a beta-Catenin-Dependent Manner. *Mol Cell Biol* **33**, 4732-4744 (2013).
146. Zhang, J., *et al.* BMP induces cochlin expression to facilitate self-renewal and suppress neural differentiation of mouse embryonic stem cells. *J Biol Chem* **288**, 8053-8060 (2013).
147. Guha, U., Gomes, W.A., Kobayashi, T., Pestell, R.G. & Kessler, J.A. In vivo evidence that BMP signaling is necessary for apoptosis in the mouse limb. *Dev Biol* **249**, 108-120 (2002).
148. Jernvall, J., Aberg, T., Kettunen, P., Keranen, S. & Thesleff, I. The life history of an embryonic signaling center: BMP-4 induces p21 and is associated with apoptosis in the mouse tooth enamel knot. *Development* **125**, 161-169 (1998).
149. Kawamura, C., Kizaki, M. & Ikeda, Y. Bone morphogenetic protein (BMP)-2 induces apoptosis in human myeloma cells. *Leuk Lymphoma* **43**, 635-639 (2002).
150. Pi, W., Guo, X., Su, L. & Xu, W. BMP-2 up-regulates PTEN expression and induces apoptosis of pulmonary artery smooth muscle cells under hypoxia. *PLoS One* **7**, e35283 (2012).

151. Shimizu, T., Kayamori, T., Murayama, C. & Miyamoto, A. Bone morphogenetic protein (BMP)-4 and BMP-7 suppress granulosa cell apoptosis via different pathways: BMP-4 via PI3K/PDK-1/Akt and BMP-7 via PI3K/PDK-1/PKC. *Biochemical and biophysical research communications* **417**, 869-873 (2012).
152. Smith, A. & Graham, A. Restricting Bmp-4 mediated apoptosis in hindbrain neural crest. *Dev Dyn* **220**, 276-283 (2001).
153. Wach, S., Schirmacher, P., Protschka, M. & Blessing, M. Overexpression of bone morphogenetic protein-6 (BMP-6) in murine epidermis suppresses skin tumor formation by induction of apoptosis and downregulation of fos/jun family members. *Oncogene* **20**, 7761-7769 (2001).
154. Wang, Z. & Guo, J. Mechanical Induction of BMP-7 in Osteocyte Blocks Glucocorticoid-Induced Apoptosis Through PI3K/AKT/GSK3beta Pathway. *Cell Biochem Biophys* **67**, 567-574 (2013).
155. Zhang, Y., *et al.* Binding of carbon nanotube to BMP receptor 2 enhances cell differentiation and inhibits apoptosis via regulating bHLH transcription factors. *Cell death & disease* **3**, e308 (2012).
156. Zou, H. & Niswander, L. Requirement for BMP signaling in interdigital apoptosis and scale formation. *Science* **272**, 738-741 (1996).
157. Alarmo, E.L., *et al.* BMP7 influences proliferation, migration, and invasion of breast cancer cells. *Cancer Lett* **275**, 35-43 (2009).
158. Busch, C., Drews, U., Garbe, C., Eisele, S.R. & Oppitz, M. Neural crest cell migration of mouse B16-F1 melanoma cells transplanted into the chick embryo is inhibited by the BMP-antagonist noggin. *International journal of oncology* **31**, 1367-1378 (2007).
159. Christiaen, L., Stolfi, A. & Levine, M. BMP signaling coordinates gene expression and cell migration during precardiac mesoderm development. *Dev Biol* **340**, 179-187 (2010).
160. Coles, E., Christiansen, J., Economou, A., Bronner-Fraser, M. & Wilkinson, D.G. A vertebrate crossveinless 2 homologue modulates BMP activity and neural crest cell migration. *Development* **131**, 5309-5317 (2004).
161. Crouzier, T., Fourel, L., Boudou, T., Albiges-Rizo, C. & Picart, C. Presentation of BMP-2 from a soft biopolymeric film unveils its activity on cell adhesion and migration. *Adv Mater* **23**, H111-118 (2011).
162. Fong, Y.C., *et al.* BMP-2 increases migration of human chondrosarcoma cells via PI3K/Akt pathway. *J Cell Physiol* **217**, 846-855 (2008).
163. Fong, Y.C., *et al.* BMP-2 increases migration of human chondrosarcoma cells via PI3K/Akt pathway. *J Cell Physiol* **217**, 846-855 (2008).
164. Fu, M., Vohra, B.P., Wind, D. & Heuckeroth, R.O. BMP signaling regulates murine enteric nervous system precursor migration, neurite fasciculation, and patterning via altered Ncam1 polysialic acid addition. *Dev Biol* **299**, 137-150 (2006).
165. Fu, M., Vohra, B.P., Wind, D. & Heuckeroth, R.O. BMP signaling regulates murine enteric nervous system precursor migration, neurite fasciculation, and patterning via altered Ncam1 polysialic acid addition. *Dev Biol* **299**, 137-150 (2006).

166. Gamell, C., *et al.* BMP2 induction of actin cytoskeleton reorganization and cell migration requires PI3-kinase and Cdc42 activity. *J Cell Sci* **121**, 3960-3970 (2008).
167. Gamell, C., Susperregui, A.G., Bernard, O., Rosa, J.L. & Ventura, F. The p38/MK2/Hsp25 pathway is required for BMP-2-induced cell migration. *PLoS One* **6**, e16477 (2011).
168. Goldstein, A.M., Brewer, K.C., Doyle, A.M., Nagy, N. & Roberts, D.J. BMP signaling is necessary for neural crest cell migration and ganglion formation in the enteric nervous system. *Mech Dev* **122**, 821-833 (2005).
169. Ichikawa, T., Suenaga, Y., Koda, T., Ozaki, T. & Nakagawara, A. DeltaNp63/BMP-7-dependent expression of matrilin-2 is involved in keratinocyte migration in response to wounding. *Biochemical and biophysical research communications* **369**, 994-1000 (2008).
170. Inai, K., Burnside, J.L., Hoffman, S., Toole, B.P. & Sugi, Y. BMP-2 Induces Versican and Hyaluronan That Contribute to Post-EMT AV Cushion Cell Migration. *PLoS One* **8**, e77593 (2013).
171. Inai, K., Norris, R.A., Hoffman, S., Markwald, R.R. & Sugi, Y. BMP-2 induces cell migration and periostin expression during atrioventricular valvulogenesis. *Dev Biol* **315**, 383-396 (2008).
172. Inai, K., Norris, R.A., Hoffman, S., Markwald, R.R. & Sugi, Y. BMP-2 induces cell migration and periostin expression during atrioventricular valvulogenesis. *Dev Biol* **315**, 383-396 (2008).
173. Kim, M., *et al.* Gremlin-1 induces BMP-independent tumor cell proliferation, migration, and invasion. *PLoS One* **7**, e35100 (2012).
174. Lenhart, K.F., Holtzman, N.G., Williams, J.R. & Burdine, R.D. Integration of nodal and BMP signals in the heart requires FoxH1 to create left-right differences in cell migration rates that direct cardiac asymmetry. *PLoS Genet* **9**, e1003109 (2013).
175. Li, B., *et al.* Adenovirus-mediated overexpression of BMP-9 inhibits human osteosarcoma cell growth and migration through downregulation of the PI3K/AKT pathway. *International journal of oncology* **41**, 1809-1819 (2012).
176. Maegdefrau, U. & Bosserhoff, A.K. BMP activated Smad signaling strongly promotes migration and invasion of hepatocellular carcinoma cells. *Exp Mol Pathol* **92**, 74-81 (2012).
177. Park, J.E., *et al.* BMP-9 induced endothelial cell tubule formation and inhibition of migration involves Smad1 driven endothelin-1 production. *PLoS One* **7**, e30075 (2012).
178. Pi, X., *et al.* Sequential roles for myosin-X in BMP6-dependent filopodial extension, migration, and activation of BMP receptors. *The Journal of cell biology* **179**, 1569-1582 (2007).
179. Wang, X.Y., *et al.* Construction of a eukaryotic expression vector pEGFP-C1-BMP-2 and its effect on cell migration. *J Zhejiang Univ Sci B* **13**, 356-363 (2012).
180. Wu, J.B., Fu, H.Q., Huang, L.Z., Liu, A.W. & Zhang, J.X. Effects of siRNA-targeting BMP-2 on the abilities of migration and invasion of human liver cancer SMMC7721 cells and its mechanism. *Cancer Gene Ther* **18**, 20-25 (2011).

181. Buijs, J.T., *et al.* BMP7, a putative regulator of epithelial homeostasis in the human prostate, is a potent inhibitor of prostate cancer bone metastasis in vivo. *Am J Pathol* **171**, 1047-1057 (2007).
182. Darby, S., Cross, S.S., Brown, N.J., Hamdy, F.C. & Robson, C.N. BMP-6 over-expression in prostate cancer is associated with increased Id-1 protein and a more invasive phenotype. *J Pathol* **214**, 394-404 (2008).
183. Kang, M.H., Kim, J.S., Seo, J.E., Oh, S.C. & Yoo, Y.A. BMP2 accelerates the motility and invasiveness of gastric cancer cells via activation of the phosphatidylinositol 3-kinase (PI3K)/Akt pathway. *Exp Cell Res* **316**, 24-37.
184. Le Page, C., *et al.* BMP-2 signaling in ovarian cancer and its association with poor prognosis. *J Ovarian Res* **2**, 4 (2009).
185. Peart, T.M., Correa, R.J., Valdes, Y.R., Dimattia, G.E. & Shepherd, T.G. BMP signalling controls the malignant potential of ascites-derived human epithelial ovarian cancer spheroids via AKT kinase activation. *Clinical & experimental metastasis* **29**, 293-313 (2012).
186. Shepherd, T.G., Theriault, B.L. & Nachtigal, M.W. Autocrine BMP4 signalling regulates ID3 proto-oncogene expression in human ovarian cancer cells. *Gene* **414**, 95-105 (2008).
187. Theriault, B.L., Shepherd, T.G., Mujoomdar, M.L. & Nachtigal, M.W. BMP4 induces EMT and Rho GTPase activation in human ovarian cancer cells. *Carcinogenesis* **28**, 1153-1162 (2007).
188. Derynck, R. & Zhang, Y.E. Smad-dependent and Smad-independent pathways in TGF-beta family signalling. *Nature* **425**, 577-584 (2003).
189. Heldin, C.H., Miyazono, K. & ten Dijke, P. TGF-beta signalling from cell membrane to nucleus through SMAD proteins. *Nature* **390**, 465-471 (1997).
190. Miyazono, K., Kamiya, Y. & Morikawa, M. Bone morphogenetic protein receptors and signal transduction. *J Biochem* **147**, 35-51 (2010).
191. Balemans, W. & Van Hul, W. Extracellular regulation of BMP signaling in vertebrates: a cocktail of modulators. *Dev Biol* **250**, 231-250 (2002).
192. Derynck, R. SMAD proteins and mammalian anatomy. *Nature* **393**, 737-739 (1998).
193. Kawabata, M. & Miyazono, K. Signal transduction of the TGF-beta superfamily by Smad proteins. *J Biochem* **125**, 9-16 (1999).
194. Raftery, L.A. & Sutherland, D.J. TGF-beta family signal transduction in Drosophila development: from Mad to Smads. *Dev Biol* **210**, 251-268 (1999).
195. Macias-Silva, M., *et al.* MADR2 is a substrate of the TGFbeta receptor and its phosphorylation is required for nuclear accumulation and signaling. *Cell* **87**, 1215-1224 (1996).
196. Zhang, Y., Feng, X., We, R. & Derynck, R. Receptor-associated Mad homologues synergize as effectors of the TGF-beta response. *Nature* **383**, 168-172 (1996).
197. Hoodless, P.A., *et al.* MADR1, a MAD-related protein that functions in BMP2 signaling pathways. *Cell* **85**, 489-500 (1996).
198. Kawai, S., *et al.* Mouse smad8 phosphorylation downstream of BMP receptors ALK-2, ALK-3, and ALK-6 induces its association with Smad4 and transcriptional activity. *Biochemical and biophysical research communications* **271**, 682-687 (2000).

199. Nishimura, R., *et al.* Smad5 and DPC4 are key molecules in mediating BMP-2-induced osteoblastic differentiation of the pluripotent mesenchymal precursor cell line C2C12. *J Biol Chem* **273**, 1872-1879 (1998).
200. Massague, J., Seoane, J. & Wotton, D. Smad transcription factors. *Genes & development* **19**, 2783-2810 (2005).
201. Casellas, R. & Brivanlou, A.H. Xenopus Smad7 inhibits both the activin and BMP pathways and acts as a neural inducer. *Dev Biol* **198**, 1-12 (1998).
202. Imamura, T., *et al.* Smad6 inhibits signalling by the TGF-beta superfamily. *Nature* **389**, 622-626 (1997).
203. Yu, P.B., Beppu, H., Kawai, N., Li, E. & Bloch, K.D. Bone morphogenetic protein (BMP) type II receptor deletion reveals BMP ligand-specific gain of signaling in pulmonary artery smooth muscle cells. *J Biol Chem* **280**, 24443-24450 (2005).
204. Blanco Calvo, M., *et al.* Biology of BMP signalling and cancer. *Clin Transl Oncol* **11**, 126-137 (2009).
205. Goto, K., Kamiya, Y., Imamura, T., Miyazono, K. & Miyazawa, K. Selective inhibitory effects of Smad6 on bone morphogenetic protein type I receptors. *J Biol Chem* **282**, 20603-20611 (2007).
206. Zhang, S., *et al.* Smad7 antagonizes transforming growth factor beta signaling in the nucleus by interfering with functional Smad-DNA complex formation. *Mol Cell Biol* **27**, 4488-4499 (2007).
207. Bai, S., Shi, X., Yang, X. & Cao, X. Smad6 as a transcriptional corepressor. *J Biol Chem* **275**, 8267-8270 (2000).
208. Lin, X., *et al.* Smad6 recruits transcription corepressor CtBP to repress bone morphogenetic protein-induced transcription. *Mol Cell Biol* **23**, 9081-9093 (2003).
209. Ebisawa, T., *et al.* Smurf1 interacts with transforming growth factor-beta type I receptor through Smad7 and induces receptor degradation. *J Biol Chem* **276**, 12477-12480 (2001).
210. Kavsak, P., *et al.* Smad7 binds to Smurf2 to form an E3 ubiquitin ligase that targets the TGF beta receptor for degradation. *Mol Cell* **6**, 1365-1375 (2000).
211. Gazzerro, E. & Canalis, E. Bone morphogenetic proteins and their antagonists. *Rev Endocr Metab Disord* **7**, 51-65 (2006).
212. Kretschmar, M., Doody, J. & Massague, J. Opposing BMP and EGF signalling pathways converge on the TGF-beta family mediator Smad1. *Nature* **389**, 618-622 (1997).
213. Yue, J., Frey, R.S. & Mulder, K.M. Cross-talk between the Smad1 and Ras/MEK signaling pathways for TGFbeta. *Oncogene* **18**, 2033-2037 (1999).
214. Massague, J. Integration of Smad and MAPK pathways: a link and a linker revisited. *Genes & development* **17**, 2993-2997 (2003).
215. Buckley, S., *et al.* BMP4 signaling induces senescence and modulates the oncogenic phenotype of A549 lung adenocarcinoma cells. *Am J Physiol Lung Cell Mol Physiol* **286**, L81-86 (2004).
216. Hjertner, O., *et al.* Bone morphogenetic protein-4 inhibits proliferation and induces apoptosis of multiple myeloma cells. *Blood* **97**, 516-522 (2001).

217. Kawamura, C., *et al.* Bone morphogenetic protein-2 induces apoptosis in human myeloma cells with modulation of STAT3. *Blood* **96**, 2005-2011 (2000).
218. Yamada, N., *et al.* Bone morphogenetic protein type IB receptor is progressively expressed in malignant glioma tumours. *British journal of cancer* **73**, 624-629 (1996).
219. Ide, H., *et al.* Growth regulation of human prostate cancer cells by bone morphogenetic protein-2. *Cancer Res* **57**, 5022-5027 (1997).
220. Ro, T.B., *et al.* Bone morphogenetic protein-5, -6 and -7 inhibit growth and induce apoptosis in human myeloma cells. *Oncogene* **23**, 3024-3032 (2004).
221. Autzen, P., *et al.* Bone morphogenetic protein 6 in skeletal metastases from prostate cancer and other common human malignancies. *British journal of cancer* **78**, 1219-1223 (1998).
222. Kim, I.Y., *et al.* Expression of bone morphogenetic protein receptors type-IA, -IB and -II correlates with tumor grade in human prostate cancer tissues. *Cancer Res* **60**, 2840-2844 (2000).
223. Langenfeld, E.M. & Langenfeld, J. Bone morphogenetic protein-2 stimulates angiogenesis in developing tumors. *Mol Cancer Res* **2**, 141-149 (2004).
224. Buijs, J.T., *et al.* TGF-beta and BMP7 interactions in tumour progression and bone metastasis. *Clinical & experimental metastasis* **24**, 609-617 (2007).
225. Kodach, L.L., *et al.* The bone morphogenetic protein pathway is active in human colon adenomas and inactivated in colorectal cancer. *Cancer* **112**, 300-306 (2008).
226. Langenfeld, E.M., *et al.* The mature bone morphogenetic protein-2 is aberrantly expressed in non-small cell lung carcinomas and stimulates tumor growth of A549 cells. *Carcinogenesis* **24**, 1445-1454 (2003).
227. Dai, J., *et al.* Vascular endothelial growth factor contributes to the prostate cancer-induced osteoblast differentiation mediated by bone morphogenetic protein. *Cancer Res* **64**, 994-999 (2004).
228. Guo, W., *et al.* Expression of bone morphogenetic proteins and receptors in sarcomas. *Clin Orthop Relat Res*, 175-183 (1999).
229. Deng, H., *et al.* Bone morphogenetic protein-4 is overexpressed in colonic adenocarcinomas and promotes migration and invasion of HCT116 cells. *Experimental cell research* **313**, 1033-1044 (2007).
230. Clement, J.H., *et al.* Bone morphogenetic protein 2 (BMP-2) induces in vitro invasion and in vivo hormone independent growth of breast carcinoma cells. *International journal of oncology* **27**, 401-407 (2005).
231. Hamdy, F.C., *et al.* Immunolocalization and messenger RNA expression of bone morphogenetic protein-6 in human benign and malignant prostatic tissue. *Cancer Res* **57**, 4427-4431 (1997).
232. Friedl, W., *et al.* Juvenile polyposis: massive gastric polyposis is more common in MADH4 mutation carriers than in BMPR1A mutation carriers. *Hum Genet* **111**, 108-111 (2002).
233. Howe, J.R., *et al.* Germline mutations of the gene encoding bone morphogenetic protein receptor 1A in juvenile polyposis. *Nat Genet* **28**, 184-187 (2001).

234. Howe, J.R., *et al.* The prevalence of MADH4 and BMPR1A mutations in juvenile polyposis and absence of BMPR2, BMPR1B, and ACVR1 mutations. *J Med Genet* **41**, 484-491 (2004).
235. Sayed, M.G., *et al.* Germline SMAD4 or BMPR1A mutations and phenotype of juvenile polyposis. *Ann Surg Oncol* **9**, 901-906 (2002).
236. Zhou, X.P., *et al.* Germline mutations in BMPR1A/ALK3 cause a subset of cases of juvenile polyposis syndrome and of Cowden and Bannayan-Riley-Ruvalcaba syndromes. *Am J Hum Genet* **69**, 704-711 (2001).
237. Rahimi, R.A. & Leof, E.B. TGF-beta signaling: a tale of two responses. *Journal of cellular biochemistry* **102**, 593-608 (2007).
238. Haramis, A.P., *et al.* De novo crypt formation and juvenile polyposis on BMP inhibition in mouse intestine. *Science* **303**, 1684-1686 (2004).
239. Kodach, L.L., *et al.* The bone morphogenetic protein pathway is inactivated in the majority of sporadic colorectal cancers. *Gastroenterology* **134**, 1332-1341 (2008).
240. Otsuka, F., Moore, R.K. & Shimasaki, S. Biological function and cellular mechanism of bone morphogenetic protein-6 in the ovary. *J Biol Chem* **276**, 32889-32895 (2001).
241. Shimasaki, S., *et al.* A functional bone morphogenetic protein system in the ovary. *Proceedings of the National Academy of Sciences of the United States of America* **96**, 7282-7287 (1999).
242. Shimizu, T., *et al.* Involvement of the bone morphogenetic protein/receptor system during follicle development in the bovine ovary: Hormonal regulation of the expression of bone morphogenetic protein 7 (BMP-7) and its receptors (ActRII and ALK-2). *Mol Cell Endocrinol* **249**, 78-83 (2006).
243. Lee, W.S., *et al.* Effects of bone morphogenetic protein-7 (BMP-7) on primordial follicular growth in the mouse ovary. *Mol Reprod Dev* **69**, 159-163 (2004).
244. Sun, R.Z., *et al.* Expression of GDF-9, BMP-15 and their receptors in mammalian ovary follicles. *J Mol Histol* **41**, 325-332 (2010).
245. Edson, M.A., *et al.* Granulosa cell-expressed BMPR1A and BMPR1B have unique functions in regulating fertility but act redundantly to suppress ovarian tumor development. *Mol Endocrinol* **24**, 1251-1266 (2010).
246. Pangas, S.A., *et al.* Conditional deletion of Smad1 and Smad5 in somatic cells of male and female gonads leads to metastatic tumor development in mice. *Mol Cell Biol* **28**, 248-257 (2008).
247. Shepherd, T.G. & Nachtigal, M.W. Identification of a putative autocrine bone morphogenetic protein-signaling pathway in human ovarian surface epithelium and ovarian cancer cells. *Endocrinology* **144**, 3306-3314 (2003).
248. McLean, K., *et al.* Human ovarian carcinoma-associated mesenchymal stem cells regulate cancer stem cells and tumorigenesis via altered BMP production. *The Journal of clinical investigation* **121**, 3206-3219 (2011).
249. Moren, A., Raja, E., Heldin, C.H. & Moustakas, A. Negative regulation of TGFbeta signaling by the kinase LKB1 and the scaffolding protein LIP1. *J Biol Chem* **286**, 341-353 (2011).
250. Caino, M.C., *et al.* Metabolic stress regulates cytoskeletal dynamics and metastasis of cancer cells. *The Journal of clinical investigation* **123**, 2907-2920 (2013).

251. Buchakjian, M.R. & Kornbluth, S. The engine driving the ship: metabolic steering of cell proliferation and death. *Nature reviews. Molecular cell biology* **11**, 715-727 (2010).
252. Kroemer, G. & Pouyssegur, J. Tumor cell metabolism: cancer's Achilles' heel. *Cancer cell* **13**, 472-482 (2008).
253. Laderoute, K.R., *et al.* 5'-AMP-activated protein kinase (AMPK) is induced by low-oxygen and glucose deprivation conditions found in solid-tumor microenvironments. *Mol Cell Biol* **26**, 5336-5347 (2006).
254. Liang, J. & Mills, G.B. AMPK: a contextual oncogene or tumor suppressor? *Cancer Res* **73**, 2929-2935 (2013).
255. Carling, D., Zammit, V.A. & Hardie, D.G. A common bicyclic protein kinase cascade inactivates the regulatory enzymes of fatty acid and cholesterol biosynthesis. *FEBS Lett* **223**, 217-222 (1987).
256. Hardie, D.G. & Alessi, D.R. LKB1 and AMPK and the cancer-metabolism link - ten years after. *BMC Biol* **11**, 36 (2013).
257. Mihaylova, M.M. & Shaw, R.J. The AMPK signalling pathway coordinates cell growth, autophagy and metabolism. *Nat Cell Biol* **13**, 1016-1023 (2011).
258. Hardie, D.G. AMP-activated protein kinase: an energy sensor that regulates all aspects of cell function. *Genes & development* **25**, 1895-1908 (2011).
259. Hawley, S.A., *et al.* Characterization of the AMP-activated protein kinase kinase from rat liver and identification of threonine 172 as the major site at which it phosphorylates AMP-activated protein kinase. *J Biol Chem* **271**, 27879-27887 (1996).
260. Stein, S.C., Woods, A., Jones, N.A., Davison, M.D. & Carling, D. The regulation of AMP-activated protein kinase by phosphorylation. *The Biochemical journal* **345 Pt 3**, 437-443 (2000).
261. Scott, J.W., *et al.* CBS domains form energy-sensing modules whose binding of adenosine ligands is disrupted by disease mutations. *The Journal of clinical investigation* **113**, 274-284 (2004).
262. Xiao, B., *et al.* Structural basis for AMP binding to mammalian AMP-activated protein kinase. *Nature* **449**, 496-500 (2007).
263. Amodeo, G.A., Rudolph, M.J. & Tong, L. Crystal structure of the heterotrimer core of *Saccharomyces cerevisiae* AMPK homologue SNF1. *Nature* **449**, 492-495 (2007).
264. Townley, R. & Shapiro, L. Crystal structures of the adenylate sensor from fission yeast AMP-activated protein kinase. *Science* **315**, 1726-1729 (2007).
265. Hawley, S.A., *et al.* Complexes between the LKB1 tumor suppressor, STRAD alpha/beta and MO25 alpha/beta are upstream kinases in the AMP-activated protein kinase cascade. *J Biol* **2**, 28 (2003).
266. Shaw, R.J., *et al.* The tumor suppressor LKB1 kinase directly activates AMP-activated kinase and regulates apoptosis in response to energy stress. *Proceedings of the National Academy of Sciences of the United States of America* **101**, 3329-3335 (2004).
267. Woods, A., *et al.* LKB1 is the upstream kinase in the AMP-activated protein kinase cascade. *Current biology : CB* **13**, 2004-2008 (2003).

268. Hawley, S.A., *et al.* Calmodulin-dependent protein kinase kinase-beta is an alternative upstream kinase for AMP-activated protein kinase. *Cell Metab* **2**, 9-19 (2005).
269. Hurley, R.L., *et al.* The Ca²⁺/calmodulin-dependent protein kinase kinases are AMP-activated protein kinase kinases. *J Biol Chem* **280**, 29060-29066 (2005).
270. Woods, A., *et al.* Ca²⁺/calmodulin-dependent protein kinase kinase-beta acts upstream of AMP-activated protein kinase in mammalian cells. *Cell Metab* **2**, 21-33 (2005).
271. Alessi, D.R., Sakamoto, K. & Bayascas, J.R. LKB1-dependent signaling pathways. *Annu Rev Biochem* **75**, 137-163 (2006).
272. Boudeau, J., *et al.* Functional analysis of LKB1/STK11 mutants and two aberrant isoforms found in Peutz-Jeghers Syndrome patients. *Hum Mutat* **21**, 172 (2003).
273. Sapkota, G.P., *et al.* Identification and characterization of four novel phosphorylation sites (Ser31, Ser325, Thr336 and Thr366) on LKB1/STK11, the protein kinase mutated in Peutz-Jeghers cancer syndrome. *The Biochemical journal* **362**, 481-490 (2002).
274. Sapkota, G.P., *et al.* Phosphorylation of the protein kinase mutated in Peutz-Jeghers cancer syndrome, LKB1/STK11, at Ser431 by p90(RSK) and cAMP-dependent protein kinase, but not its farnesylation at Cys(433), is essential for LKB1 to suppress cell growth. *J Biol Chem* **276**, 19469-19482 (2001).
275. Collins, S.P., Reoma, J.L., Gamm, D.M. & Uhler, M.D. LKB1, a novel serine/threonine protein kinase and potential tumour suppressor, is phosphorylated by cAMP-dependent protein kinase (PKA) and prenylated in vivo. *The Biochemical journal* **345 Pt 3**, 673-680 (2000).
276. Baas, A.F., *et al.* Activation of the tumour suppressor kinase LKB1 by the STE20-like pseudokinase STRAD. *The EMBO journal* **22**, 3062-3072 (2003).
277. Boudeau, J., *et al.* MO25alpha/beta interact with STRADalpha/beta enhancing their ability to bind, activate and localize LKB1 in the cytoplasm. *The EMBO journal* **22**, 5102-5114 (2003).
278. Brajenovic, M., Joberty, G., Kuster, B., Bouwmeester, T. & Drewes, G. Comprehensive proteomic analysis of human Par protein complexes reveals an interconnected protein network. *J Biol Chem* **279**, 12804-12811 (2004).
279. Miyamoto, H., Matsushiro, A. & Nozaki, M. Molecular cloning of a novel mRNA sequence expressed in cleavage stage mouse embryos. *Mol Reprod Dev* **34**, 1-7 (1993).
280. Nezu, J., Oku, A. & Shimane, M. Loss of cytoplasmic retention ability of mutant LKB1 found in Peutz-Jeghers syndrome patients. *Biochemical and biophysical research communications* **261**, 750-755 (1999).
281. Smith, D.P., Spicer, J., Smith, A., Swift, S. & Ashworth, A. The mouse Peutz-Jeghers syndrome gene *Lkb1* encodes a nuclear protein kinase. *Human molecular genetics* **8**, 1479-1485 (1999).
282. Boudeau, J., *et al.* Analysis of the LKB1-STRAD-MO25 complex. *J Cell Sci* **117**, 6365-6375 (2004).
283. Karos, M. & Fischer, R. Molecular characterization of HymA, an evolutionarily highly conserved and highly expressed protein of *Aspergillus nidulans*. *Mol Gen Genet* **260**, 510-521 (1999).

284. Nozaki, M., Onishi, Y., Togashi, S. & Miyamoto, H. Molecular characterization of the Drosophila Mo25 gene, which is conserved among Drosophila, mouse, and yeast. *DNA Cell Biol* **15**, 505-509 (1996).
285. Tiainen, M., Vaahtomeri, K., Ylikorkala, A. & Makela, T.P. Growth arrest by the LKB1 tumor suppressor: induction of p21(WAF1/CIP1). *Human molecular genetics* **11**, 1497-1504 (2002).
286. Lizcano, J.M., *et al.* LKB1 is a master kinase that activates 13 kinases of the AMPK subfamily, including MARK/PAR-1. *The EMBO journal* **23**, 833-843 (2004).
287. Sakamoto, K., Goransson, O., Hardie, D.G. & Alessi, D.R. Activity of LKB1 and AMPK-related kinases in skeletal muscle: effects of contraction, phenformin, and AICAR. *Am J Physiol Endocrinol Metab* **287**, E310-317 (2004).
288. Gowans, G.J., Hawley, S.A., Ross, F.A. & Hardie, D.G. AMP is a true physiological regulator of AMP-activated protein kinase by both allosteric activation and enhancing net phosphorylation. *Cell Metab* **18**, 556-566 (2013).
289. Davies, S.P., Helps, N.R., Cohen, P.T. & Hardie, D.G. 5'-AMP inhibits dephosphorylation, as well as promoting phosphorylation, of the AMP-activated protein kinase. Studies using bacterially expressed human protein phosphatase-2C alpha and native bovine protein phosphatase-2AC. *FEBS Lett* **377**, 421-425 (1995).
290. Park, S., Scheffler, T.L., Rossie, S.S. & Gerrard, D.E. AMPK activity is regulated by calcium-mediated protein phosphatase 2A activity. *Cell Calcium* **53**, 217-223 (2013).
291. Hawley, S.A., *et al.* 5'-AMP activates the AMP-activated protein kinase cascade, and Ca²⁺/calmodulin activates the calmodulin-dependent protein kinase I cascade, via three independent mechanisms. *J Biol Chem* **270**, 27186-27191 (1995).
292. Oakhill, J.S., *et al.* beta-Subunit myristoylation is the gatekeeper for initiating metabolic stress sensing by AMP-activated protein kinase (AMPK). *Proceedings of the National Academy of Sciences of the United States of America* **107**, 19237-19241 (2010).
293. Corton, J.M., Gillespie, J.G., Hawley, S.A. & Hardie, D.G. 5-aminoimidazole-4-carboxamide ribonucleoside. A specific method for activating AMP-activated protein kinase in intact cells? *Eur J Biochem* **229**, 558-565 (1995).
294. Sakamoto, K., *et al.* Deficiency of LKB1 in skeletal muscle prevents AMPK activation and glucose uptake during contraction. *The EMBO journal* **24**, 1810-1820 (2005).
295. Manning, G., Whyte, D.B., Martinez, R., Hunter, T. & Sudarsanam, S. The protein kinase complement of the human genome. *Science* **298**, 1912-1934 (2002).
296. Jaleel, M., *et al.* Identification of the sucrose non-fermenting related kinase SNRK, as a novel LKB1 substrate. *FEBS Lett* **579**, 1417-1423 (2005).
297. Al-Hakim, A.K., *et al.* 14-3-3 cooperates with LKB1 to regulate the activity and localization of QSK and SIK. *J Cell Sci* **118**, 5661-5673 (2005).
298. Martin, S.G. & St Johnston, D. A role for Drosophila LKB1 in anterior-posterior axis formation and epithelial polarity. *Nature* **421**, 379-384 (2003).

299. Munro, E.M. PAR proteins and the cytoskeleton: a marriage of equals. *Current opinion in cell biology* **18**, 86-94 (2006).
300. Nance, J. PAR proteins and the establishment of cell polarity during *C. elegans* development. *Bioessays* **27**, 126-135 (2005).
301. Kishi, M., Pan, Y.A., Crump, J.G. & Sanes, J.R. Mammalian SAD kinases are required for neuronal polarization. *Science* **307**, 929-932 (2005).
302. Sun, X., Rikkerink, E.H., Jones, W.T. & Uversky, V.N. Multifarious Roles of Intrinsic Disorder in Proteins Illustrate Its Broad Impact on Plant Biology. *Plant Cell* (2013).
303. Katoh, Y., *et al.* Salt-inducible kinase-1 represses cAMP response element-binding protein activity both in the nucleus and in the cytoplasm. *Eur J Biochem* **271**, 4307-4319 (2004).
304. Screaton, R.A., *et al.* The CREB coactivator TORC2 functions as a calcium- and cAMP-sensitive coincidence detector. *Cell* **119**, 61-74 (2004).
305. Peutz, J.L.A. Over een zeer merkwaardige, gecombineerde familiale polyposis van de slijmvliezen van den tractus intestinalis met die van de neuskeelholte en gepaard met eigenaardige pigmentaties van huiden slijmvliezen. *Ned Maandschr v Geneesk* **10**, 134-146 (1921).
306. Jeghers, H., Mc, K.V. & Katz, K.H. Generalized intestinal polyposis and melanin spots of the oral mucosa, lips and digits; a syndrome of diagnostic significance. *N Engl J Med* **241**, 993, illust; passim (1949).
307. Hemminki, A. The molecular basis and clinical aspects of Peutz-Jeghers syndrome. *Cellular and molecular life sciences : CMLS* **55**, 735-750 (1999).
308. Tomlinson, I.P. & Houlston, R.S. Peutz-Jeghers syndrome. *J Med Genet* **34**, 1007-1011 (1997).
309. Westerman, A.M., *et al.* Peutz-Jeghers syndrome: 78-year follow-up of the original family. *Lancet* **353**, 1211-1215 (1999).
310. Giardiello, F.M., *et al.* Very high risk of cancer in familial Peutz-Jeghers syndrome. *Gastroenterology* **119**, 1447-1453 (2000).
311. Giardiello, F.M., *et al.* Increased risk of cancer in the Peutz-Jeghers syndrome. *N Engl J Med* **316**, 1511-1514 (1987).
312. Hemminki, A., *et al.* A serine/threonine kinase gene defective in Peutz-Jeghers syndrome. *Nature* **391**, 184-187 (1998).
313. Jenne, D.E., *et al.* Peutz-Jeghers syndrome is caused by mutations in a novel serine threonine kinase. *Nat Genet* **18**, 38-43 (1998).
314. Abed, A.A., Gunther, K., Kraus, C., Hohenberger, W. & Ballhausen, W.G. Mutation screening at the RNA level of the STK11/LKB1 gene in Peutz-Jeghers syndrome reveals complex splicing abnormalities and a novel mRNA isoform (STK11 c.597(insertion mark)598insIVS4). *Hum Mutat* **18**, 397-410 (2001).
315. Alhopuro, P., *et al.* Mutation analysis of three genes encoding novel LKB1-interacting proteins, BRG1, STRADalpha, and MO25alpha, in Peutz-Jeghers syndrome. *British journal of cancer* **92**, 1126-1129 (2005).
316. Chen, C., *et al.* One novel deletion and one splicing mutation of the LKB1 gene in two Chinese patients with Peutz-Jeghers syndrome. *DNA Cell Biol* **31**, 1535-1540 (2012).

317. Guldberg, P., *et al.* Somatic mutation of the Peutz-Jeghers syndrome gene, LKB1/STK11, in malignant melanoma. *Oncogene* **18**, 1777-1780 (1999).
318. Hastings, M.L., *et al.* An LKB1 AT-AC intron mutation causes Peutz-Jeghers syndrome via splicing at noncanonical cryptic splice sites. *Nat Struct Mol Biol* **12**, 54-59 (2005).
319. Hernan, I., *et al.* De novo germline mutation in the serine-threonine kinase STK11/LKB1 gene associated with Peutz-Jeghers syndrome. *Clin Genet* **66**, 58-62 (2004).
320. Liu, L., Du, X. & Nie, J. A novel de novo mutation in LKB1 gene in a Chinese Peutz Jeghers syndrome patient significantly diminished p53 activity. *Clin Res Hepatol Gastroenterol* **35**, 221-226 (2011).
321. Qiu, W., Schonleben, F., Thaker, H.M., Goggins, M. & Su, G.H. A novel mutation of STK11/LKB1 gene leads to the loss of cell growth inhibition in head and neck squamous cell carcinoma. *Oncogene* **25**, 2937-2942 (2006).
322. Scott, R.J., *et al.* Mutation analysis of the STK11/LKB1 gene and clinical characteristics of an Australian series of Peutz-Jeghers syndrome patients. *Clin Genet* **62**, 282-287 (2002).
323. Su, G.H., *et al.* Germline and somatic mutations of the STK11/LKB1 Peutz-Jeghers gene in pancreatic and biliary cancers. *Am J Pathol* **154**, 1835-1840 (1999).
324. Takahashi, M., *et al.* A novel germline mutation of the LKB1 gene in a patient with Peutz-Jeghers syndrome with early-onset gastric cancer. *J Gastroenterol* **39**, 1210-1214 (2004).
325. Tate, G., Suzuki, T. & Mitsuya, T. A new mutation of LKB1 gene in a Japanese patient with Peutz-Jeghers syndrome. *Acta Med Okayama* **57**, 305-308 (2003).
326. Zhong, D., *et al.* LKB1 mutation in large cell carcinoma of the lung. *Lung Cancer* **53**, 285-294 (2006).
327. Ding, L., *et al.* Somatic mutations affect key pathways in lung adenocarcinoma. *Nature* **455**, 1069-1075 (2008).
328. Sanchez-Cespedes, M., *et al.* Inactivation of LKB1/STK11 is a common event in adenocarcinomas of the lung. *Cancer Res* **62**, 3659-3662 (2002).
329. Wingo, S.N., *et al.* Somatic LKB1 mutations promote cervical cancer progression. *PLoS One* **4**, e5137 (2009).
330. Tiainen, M., Ylikorkala, A. & Makela, T.P. Growth suppression by Lkb1 is mediated by a G(1) cell cycle arrest. *Proceedings of the National Academy of Sciences of the United States of America* **96**, 9248-9251 (1999).
331. Jishage, K., *et al.* Role of Lkb1, the causative gene of Peutz-Jegher's syndrome, in embryogenesis and polyposis. *Proceedings of the National Academy of Sciences of the United States of America* **99**, 8903-8908 (2002).
332. Miyoshi, H., *et al.* Gastrointestinal hamartomatous polyposis in Lkb1 heterozygous knockout mice. *Cancer Res* **62**, 2261-2266 (2002).
333. Nakau, M., *et al.* Hepatocellular carcinoma caused by loss of heterozygosity in Lkb1 gene knockout mice. *Cancer Res* **62**, 4549-4553 (2002).
334. Faubert, B., *et al.* AMPK is a negative regulator of the Warburg effect and suppresses tumor growth in vivo. *Cell Metab* **17**, 113-124 (2013).

335. Imamura, K., Ogura, T., Kishimoto, A., Kaminishi, M. & Esumi, H. Cell cycle regulation via p53 phosphorylation by a 5'-AMP activated protein kinase activator, 5-aminoimidazole- 4-carboxamide-1-beta-D-ribofuranoside, in a human hepatocellular carcinoma cell line. *Biochemical and biophysical research communications* **287**, 562-567 (2001).
336. Jones, K.R., *et al.* p53-Dependent accelerated senescence induced by ionizing radiation in breast tumour cells. *Int J Radiat Biol* **81**, 445-458 (2005).
337. Liang, J., *et al.* The energy sensing LKB1-AMPK pathway regulates p27(kip1) phosphorylation mediating the decision to enter autophagy or apoptosis. *Nat Cell Biol* **9**, 218-224 (2007).
338. Efeyan, A. & Sabatini, D.M. mTOR and cancer: many loops in one pathway. *Current opinion in cell biology* **22**, 169-176.
339. Inoki, K., *et al.* TSC2 integrates Wnt and energy signals via a coordinated phosphorylation by AMPK and GSK3 to regulate cell growth. *Cell* **126**, 955-968 (2006).
340. Pacholec, M., *et al.* SRT1720, SRT2183, SRT1460, and resveratrol are not direct activators of SIRT1. *J Biol Chem* **285**, 8340-8351 (2010).
341. Herrmann, J.L., Byekova, Y., Elmets, C.A. & Athar, M. Liver kinase B1 (LKB1) in the pathogenesis of epithelial cancers. *Cancer Lett* **306**, 1-9 (2011).
342. William, W.N., *et al.* The impact of phosphorylated AMP-activated protein kinase expression on lung cancer survival. *Annals of oncology : official journal of the European Society for Medical Oncology / ESMO* **23**, 78-85 (2012).
343. Chan, E.Y. mTORC1 phosphorylates the ULK1-mAtg13-FIP200 autophagy regulatory complex. *Science signaling* **2**, pe51 (2009).
344. Hosokawa, N., *et al.* Nutrient-dependent mTORC1 association with the ULK1-Atg13-FIP200 complex required for autophagy. *Mol Biol Cell* **20**, 1981-1991 (2009).
345. Kim, J., Kundu, M., Viollet, B. & Guan, K.L. AMPK and mTOR regulate autophagy through direct phosphorylation of Ulk1. *Nat Cell Biol* **13**, 132-141 (2011).
346. Egan, D.F., *et al.* Phosphorylation of ULK1 (hATG1) by AMP-activated protein kinase connects energy sensing to mitophagy. *Science* **331**, 456-461 (2011).
347. Avivar-Valderas, A., *et al.* Regulation of autophagy during ECM detachment is linked to a selective inhibition of mTORC1 by PERK. *Oncogene* **32**, 4932-4940 (2013).
348. Hardie, D.G. AMP-activated protein kinase as a drug target. *Annu Rev Pharmacol Toxicol* **47**, 185-210 (2007).
349. Shackelford, D.B. Unravelling the connection between metabolism and tumorigenesis through studies of the liver kinase B1 tumour suppressor. *J Carcinog* **12**, 16 (2013).
350. Hardie, D.G. Neither LKB1 nor AMPK are the direct targets of metformin. *Gastroenterology* **131**, 973; author reply 974-975 (2006).
351. Bowker, S.L., Majumdar, S.R., Veugelers, P. & Johnson, J.A. Increased cancer-related mortality for patients with type 2 diabetes who use sulfonylureas or insulin. *Diabetes Care* **29**, 254-258 (2006).

352. Evans, J.M., Donnelly, L.A., Emslie-Smith, A.M., Alessi, D.R. & Morris, A.D. Metformin and reduced risk of cancer in diabetic patients. *Bmj* **330**, 1304-1305 (2005).
353. Pollak, M. Metformin and other biguanides in oncology: advancing the research agenda. *Cancer Prev Res (Phila)* **3**, 1060-1065 (2010).
354. Decensi, A., *et al.* Metformin and cancer risk in diabetic patients: a systematic review and meta-analysis. *Cancer Prev Res (Phila)* **3**, 1451-1461 (2010).
355. Huang, X., *et al.* Important role of the LKB1-AMPK pathway in suppressing tumorigenesis in PTEN-deficient mice. *The Biochemical journal* **412**, 211-221 (2008).
356. Hawley, S.A., *et al.* Use of cells expressing gamma subunit variants to identify diverse mechanisms of AMPK activation. *Cell Metab* **11**, 554-565 (2010).
357. Sanchez-Cespedes, M. A role for LKB1 gene in human cancer beyond the Peutz-Jeghers syndrome. *Oncogene* **26**, 7825-7832 (2007).
358. Tanwar, P.S., *et al.* Loss of LKB1 and PTEN tumor suppressor genes in the ovarian surface epithelium induces papillary serous ovarian cancer. *Carcinogenesis* (2013).
359. Li, C., Liu, V.W., Chiu, P.M., Chan, D.W. & Ngan, H.Y. Over-expressions of AMPK subunits in ovarian carcinomas with significant clinical implications. *BMC cancer* **12**, 357 (2012).
360. Gotlieb, W.H., *et al.* In vitro metformin anti-neoplastic activity in epithelial ovarian cancer. *Gynecologic oncology* **110**, 246-250 (2008).
361. Yasmeen, A., *et al.* Induction of apoptosis by metformin in epithelial ovarian cancer: involvement of the Bcl-2 family proteins. *Gynecologic oncology* **121**, 492-498 (2011).
362. Ng, T.L., *et al.* The AMPK stress response pathway mediates anoikis resistance through inhibition of mTOR and suppression of protein synthesis. *Cell Death Differ* **19**, 501-510 (2012).

Chapter 2

2 BMP signalling controls the malignant potential of ascites-derived human epithelial ovarian cancer spheroids via AKT kinase activation

2.1 Introduction

Metastasis of epithelial ovarian cancer (EOC) is unique among most carcinomas in that spread occurs by direct dissemination of malignant cells from the primary tumour into the peritoneal cavity. EOC cells exist in suspension as single cells or aggregates called spheroids, until they adhere to the serosal surfaces of abdominal organs to establish and grow as secondary tumours^{1,2}. It is becoming increasingly evident that EOC spheroids harbour unique characteristics that render them more resistant to chemotherapeutics, and perhaps more aggressive in establishing metastatic implants³. From an experimental perspective, we know that the gene expression patterns of cancer cells within multicellular spheroids more closely resemble that of the tumour, when compared with adherent monolayer cell cultures^{4,5}. Therefore, cell culture systems that better mimic this metastatic program of EOC are favoured because they will more accurately reflect the pathophysiology of native EOC spheroids and provide relevant data regarding the signalling pathways important for spheroid formation and survival.

The transforming growth factor beta (TGF- β)/bone morphogenetic protein (BMP) signalling superfamily has been implicated in numerous aspects of the pathogenesis of many different cancers including EOC^{4,5}. Both normal human ovarian surface epithelial (OSE) cells and EOC cells possess the signalling components necessary for activation of this pathway in response to ligands of this superfamily, including TGF- β , BMPs, activin and Mullerian inhibiting substance (MIS)⁶⁻¹³. For example, EOC cells respond to exogenous TGF- β by inducing growth arrest due to upregulation of p15 expression¹⁴. MIS treatment targets EOC-initiating cells of both cell lines and patient ascites cells by reducing their stem-like characteristics and thereby blocking their tumour-forming ability when injected in mice¹⁵. BMP signalling through BMP4 increases the adhesion, motility and invasiveness of ascites-derived primary human EOC cells and induces epithelial-

mesenchymal transition (EMT); treatment with the BMP2/4 antagonist Noggin blocks these activities as well as autocrine BMP4 signalling¹³. In addition, BMP2 expression in EOC cells from ascites fluid is elevated compared to matched solid tumour samples⁷. Regulated expression of a constitutively-active BMP2/4 receptor in the human OVCA429 ovarian cancer cell line recapitulates many of the changes modulated by BMP ligands, however, the ability of these cells to form ascites and secondary tumours in immunocompromised mice is dramatically reduced¹¹. Thus, we propose that BMP signalling has different effects at specific stages of EOC progression including dissemination from the primary tumour, spread through the ascites as spheroids, and reattachment to form secondary tumours. Determining the molecular changes controlled by activated BMP signalling in an *in vitro* cell culture system that closely mimics EOC pathogenesis would provide additional mechanistic insight into the functional implications of this pathway during the disease process in patients.

Herein, we describe the characterization of activated BMP signalling using a three-dimensional cell culture system whereby ascites-derived primary human EOC cells are grown in suspension where they naturally and rapidly form viable multicellular aggregates that closely resemble those observed directly in the malignant ascites collected from patients. Endogenous BMP signalling is decreased during EOC spheroid formation yet re-established during the process of spheroid reattachment. Ectopic expression of the constitutively-active BMP type I receptor ALK3^{QD}, however, reduces the formation of large multicellular spheroids, yet enhances the immediate reattachment of EOC spheroids via increased cell motility. In addition, we provide evidence that activated BMP signalling in EOC cells and spheroids induces AKT phosphorylation, which is a necessary intracellular mediator of activated BMP signalling regulating the malignant features of metastatic disease.

2.2 Materials and Methods

2.2.1 Cell culture

Ascitic fluid collected from chemotherapy-naive patients at time of paracentesis or debulking surgery was used to generate primary ascites cell cultures from patients with

stage III or IV ovarian cancer as described previously¹⁶. Briefly, ascitic fluid containing cells was mixed 1:1 with growth medium [MCDB105 (Sigma, St. Louis, MO)/M199 (Invitrogen, Carlsbad, CA) supplemented with 10% fetal bovine serum (FBS) (Wisent, St. Bruno, Quebec, Canada) and 50 µg/ml penicillin-streptomycin]. Cells were grown in a 37°C humidified atmosphere of 95% air and 5% CO₂. All experiments with primary EOC cells were performed between passages 3 and 5.

Adherent cells were maintained on tissue culture-treated polystyrene (Sarstedt, Newton, NC). Non-adherent cells were maintained on Ultra Low-Attachment (ULA[®]) cultureware (Corning, Corning, NY) which is coated with a hydrophilic, neutrally charged hydrogel to prevent cell attachment. Single-cell suspensions of 5 x 10⁴ cells/mL were seeded to ULA plates to form spheroids over time.

2.2.2 Adenovirus vectors and cell transduction

The virus Ad-ALK3^{QD}, which encodes constitutively-active BMP type IA receptor was previously constructed using the AdEasy Vector System (Qbiogene, Irvine, CA, USA)¹¹. Adenovirus expressing green fluorescent protein (Ad-GFP) was a kind gift from Dr. B. C. Vanderhyden (Ottawa Health Research Institute). Primary ovarian cancer cells were transduced at 80% confluence with a multiplicity of infection of 25 with either Ad-ALK3^{QD} or Ad-GFP in a minimal volume of medium containing 10% FBS for 2 hours with occasional agitation. Following transduction, complete growth medium was replenished. ALK3^{QD} is tagged with a hemagglutinin (HA) epitope at the carboxyl-terminus, therefore expression was detected by western analysis using anti-HA. All experiments were performed or initiated 24 hours following transduction.

2.2.3 RNA expression analysis

Total RNA was isolated from cells grown either as a monolayer on tissue-culture-treated polystyrene or as spheroids on ULA[®] cultureware using Qiagen RNeasy Mini Kit (Qiagen, Valencia, CA). Quantity and quality of purified RNA was determined using an ND-1000 spectrophotometer (NanoDrop Technologies, Wilmington, DE) and Agilent 2100 bioanalyzer (Agilent Technologies, Santa Clara, CA). Monolayer and spheroid

RNA samples from five different primary EOC patient samples that were transduced with either Ad-GFP (control) or Ad-ALK3^{QD} (activated BMP signalling) were hybridized to Affymetrix® Human Genome U133A GeneChips (Affymetrix, Santa Clara, CA) at Precision Biomarker Resources Inc. (Evanston, IL).

2.2.4 Real-time quantitative RT-PCR

Reverse transcription was performed using total RNA isolated from five independent patient samples (adherent & spheroid, Ad-GFP & Ad-ALK3^{QD}-transduced) and Superscript II reverse transcriptase (Invitrogen) as per manufacturer's instructions. PCR reactions were carried out using Brilliant® SYBR® Green QPCR Master Mix (Agilent Technologies/Stratagene) and a Stratagene Mx3000P machine with data exported to Microsoft® Excel for data analysis. Human-specific primers sequences and annealing temperatures used for *CDH1*, *SNAI1*, *SNAI2*, *TWIST1*, *TWIST2*, *ZEB2*, *SMAD6*, *NOG*, *MSX2*, *TBX3*, *HEY1* and *DLX2* are available upon request. *GAPDH* served as an internal control for RNA input using previously published primer sequences¹¹.

2.2.5 Cell number a viability assays

Primary EOC cells were transduced in complete growth medium with either Ad-GFP or Ad-ALK3^{QD}. Twenty-four hours following transduction, cells were seeded to either tissue-culture treated or ULA cultureware. Adherent cells were exposed to 0.25% trypsin-EDTA for 3 minutes and, following detachment, trypsin was inactivated using complete growth medium. Spheroids were exposed to 0.25% trypsin-EDTA for 10 minutes with vortexing and trituration to disaggregate spheroids. Trypsin was then inactivated using a small volume of FBS. To evaluate total cell number, single-cell suspensions were counted in a hemacytometer. To assess cell viability, single-cell suspensions were first diluted 1:1 in Trypan Blue reagent (Invitrogen, Carlsbad, CA) and all dye-excluding, viable cells counted in a hemacytometer. All treatments were performed in triplicate and two hemacytometer counts were performed per replicate.

2.2.6 Spheroid formation and reattachment assays

Primary EOC cells were transduced at 80% confluence with either Ad-GFP or Ad-ALK3^{QD}. Twenty four hours later, spheroids were formed on ULA cultureware for three days at which point phase contrast images were captured of each well containing spheroids using an Olympus IX70 inverted microscope and ImagePro image capture software. The size of each of the spheroids was quantified for each image using the area measurement tool in the *ImageJ* image processing program (NIH, Bethesda, MD). In some cases, instead of transduction with virus, cells were incubated in media with minimal serum (0.5%-1%) for 24 hours prior to seeding to ULA culture ware, at which point, cells were treated with either Fc-Noggin or LDN-193189.

Spheroids were collected and re-plated to: (i) 18 mm diameter round glass coverslips placed in 22 mm diameter culture dishes for subsequent BrdU immunocytochemical analysis (see below), or (ii) directly to tissue-culture-treated 24-well polystyrene plates to quantify spheroid reattachment and dispersion. Phase contrast images were captured using an Olympus IX70 inverted microscope and ImagePro software of individual reattaching spheroids at initial point of attachment prior to dispersion (3 hours) and 24 hours following re-attachment. At this point, the experiment was terminated and re-attached spheroids were fixed and stained with using Hema-3 Stain kit (Fisher, Kalamazoo, MI). Spheroid dispersion was quantified using the area measurement tool in *ImageJ* (NIH, Bethesda, MD). Dispersion area at 24 hours was calculated as a percentage of the original spheroid size at 3 hours of attachment.

2.2.7 Spheroid disaggregation assay

Primary EOC cells were transduced as described above with either virus (Ad-GFP or Ad-ALK3^{QD}) and 24 hours later plated to ULA cultureware to form spheroids. Spheroids that had formed for 3 days were then exposed to 0.25% trypsin-EDTA for specified periods of time (*i.e.*, 2-30mins) at which point the trypsin was inactivated with a small volume of FBS and single cells were counted in a hemacytometer. All treatments were performed in triplicate and two hemacytometer counts were performed per replicate.

2.2.8 Flow cytometry

Primary EOC cells were transduced with Ad-GFP or Ad-ALK3^{QD} and 24 hours later plated to ULA culture ware to form spheroids or to standard tissue culture plastic for adherent culture. After three days in culture, adherent cells and spheroids were detached and disaggregated, respectively, using 0.25% trypsin-EDTA. Cells were rinsed with PBS and fixed for 5 minutes using 10% neutral-buffered formalin. Cells were then rinsed with PBS/1% BSA and incubated with primary anti-E-cadherin antibody (#3195; Cell Signalling) for 1 hour, rinsed in PBS/1% BSA, and incubated with AlexaFluor 488-conjugated anti-rabbit secondary antibody (#4412; Cell Signalling). The proportion of E-cadherin-positive cells was determined using a Beckman Coulter Epics XL-MCL flow cytometer with at least 10,000 events counted per test. Four independent patient samples were tested in triplicate and included cells-only and secondary antibody-only controls for each.

2.2.9 BrdU cytochemistry

Spheroids formed over a 3 day period were allowed to re-attach and disperse on glass coverslips for 24 hours at which point they were pulse labelled overnight with 10 μ M bromodeoxyuridine (BrdU; GE Healthcare, Buckinghamshire, UK). Spheroids on coverslips were then fixed in a buffered 10% formalin solution, washed with PBS, and permeabilized with 0.1% TritonX-100 in PBS. This was followed by sequential washes and incubations in 2N HCl/0.5% TritonX-100 for DNA denaturation, 0.1M NaB₄O₄ pH 8.5 for neutralization, mouse anti-BrdU primary antibody (1:100; Becton Dickinson), anti-Mouse FITC-conjugated secondary antibody (1:100; Vector Laboratories), and 4',6-diamidino-2-phenylindole (DAPI; 1:5000; Sigma). Stained coverslips were washed in PBS, inverted and mounted on glass slides with VectaShield mounting medium (Vector Laboratories). Fluorescence images were captured using an Olympus AX70 upright microscope and ImagePro image capture software.

2.2.10 Western blotting

Total cellular protein was isolated from adherent and non-adherent EOC cells. Cells were washed once briefly in ice-cold PBS, dissolved in lysis buffer [50 mM HEPES

pH7.4, 150 mM NaCl, 10% glycerol, 1.5 mM MgCl₂, 1 mM EGTA, 1 mM sodium orthovanadate, 10 mM sodium pyrophosphate, 10 mM NaF, 1% Triton X-100, 1% sodium deoxycholate, 0.1% SDS, 1 mM PMSF, 1X protease inhibitor cocktail (Roche, Laval, Quebec, Canada)], clarified by centrifugation (20 min at 15,000 x g), and quantified by Bradford analysis (Bio-Rad Laboratories, Mississauga, Ontario, Canada). Thirty to fifty micrograms of protein extract per lane were separated by SDS-PAGE in the presence of 1% β-mercaptoethanol using 8% or 12% gels. Proteins were then transferred to a polyvinylidene difluoride membrane (PVDF; Roche, Laval, Quebec, Canada), blocked with 5% skim milk in Tris-buffered saline with Tween-20 [TBST; 10 mM Tris.HCl, pH 8.0, 150 mM NaCl, 0.1% Tween-20]. Membranes were washed in TBST and incubated (overnight, 4°C) with appropriate antibodies (1:1000 in 5% skim milk/TBST or 5% BSA/TBST). Immunoreactive bands were visualized by incubating (1h, room temperature) with a peroxidase-conjugated anti-rabbit (1:10,000 in 1% skim milk/TBST; GE Healthcare) followed by exposure to enhanced chemiluminescence reagent (ECL Plus; GE Healthcare).

2.2.11 Antibodies and other reagents

Antibodies against phospho-Smad1/5/8 (#9511), phospho-Smad2 (#3108), phospho-Smad3 (#9520), total Smad1 (#9743), total Smad2 (#3122), total Smad3 (#9528), Smurf1 (#2174), and E-cadherin (#3195) were purchased from Cell Signaling Technologies (Danvers, MA). HA-probe (Y-11; sc-805) and Smad4 (H-552; sc-7154) antibodies were purchased from Santa Cruz Biotechnology (Santa Cruz, CA). The antibody against ID1 was purchased from Biocheck (Foster City, CA). Antibody to detect phosphorylated AKT (Ser473) was purchased from Cell Signaling Technology (#9271; Danvers, MA), and for total AKT1/2/3 from Santa Cruz Biotechnology (H-136 sc-8312; Santa Cruz, CA). Anti-actin antibody (A 2066) was purchased from Sigma (Mississauga, ON).

Recombinant human Noggin (Fc-NG; 6057-NG) was purchased from R&D systems (Minneapolis, MN) and used at 50 or 100 ng/mL, as indicated. The BMP type I receptor inhibitor LDN-193189 was purchased from Stemgent (San Diego, CA) and prepared in DMSO: chloroform (3:1) according to manufacturer's instructions, and used at a concentration of 10 or 100 nM, as indicated. Akt inhibitor VIII (Akti-1/2) was purchased

from EMD/Calbiochem (Merck, Darmstadt, Germany), prepared in DMSO according to manufacturer's instructions, and used at a concentration of 5 mM. The PI3K inhibitor LY294002 was purchased from (Cell Signaling) and used at a concentration of 50 mM. Mammalian target of rapamycin inhibitors were used at a concentration of 20 nM for rapamycin (Sigma) and 500 nM for temsirolimus (Torisel[®]; Pfizer).

2.2.12 Statistical analysis

Statistical analysis was performed using GraphPad Prism[®] software. Data were expressed as mean \pm SEM. Statistical analysis was performed using two-tailed Student's *t*-tests or one-way ANOVA and Tukey's *post-hoc* test with significances set at * $p < 0.05$, ** $p < 0.01$ and *** $p < 0.001$ as indicated.

2.3 Results

2.3.1 Reduced BMP signalling activity in primary human EOC spheroids

We have previously reported that primary human EOC cells possess an intact BMP signalling pathway^{11,12,17}. To determine whether the critical BMP signalling components are present in EOC spheroids we prepared protein extracts from several independent primary human EOC cells that were grown as suspension cultures for three days. We have selected this time point because primary EOC cells will autonomously form multicellular aggregates or spheroids with morphological characteristics mimicking those observed directly in patient ascites within this time frame. Western blotting using protein lysates isolated from EOC spheroids and matched adherent cultures demonstrated expression of phosphorylated Smad1/5/8 levels. Interestingly, total Smad1/5 protein was significantly increased in all primary EOC spheroids as compared with their adherent cell counterparts (Figure 2.1A). Thus, when BMP-activated R-Smad levels are normalized to total Smad1/5 protein, endogenous BMP signalling activity is in effect decreased by >50% upon spheroid formation.

To follow this observation, we performed quantitative RT-PCR on RNA isolated from primary EOC adherent cells and spheroids and directly measured the expression of

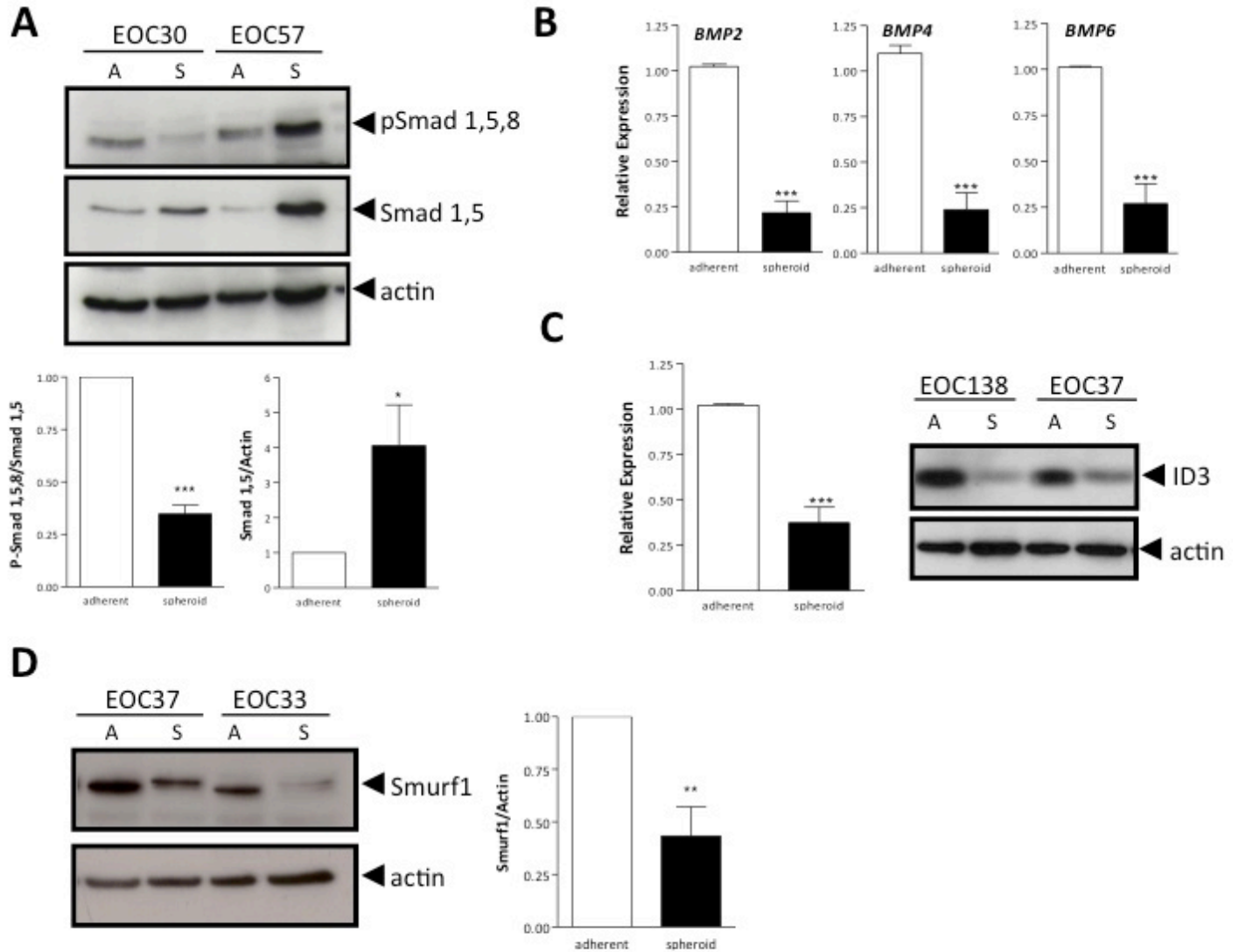


Figure 2.1: BMP signalling is decreased during EOC spheroid formation.

(A) Western blot analysis of phosphorylated and total Smad1/5/8 in adherent [A] and spheroid [S] samples in two independent EOC patient samples. Densitometric quantification of phosphorylated and total Smad1/5/8 (n=8) levels from Western blots. (B) Quantitative RT-PCR analysis of *BMP2*, *BMP4*, *BMP6* and *ID3* mRNA in adherent and spheroid samples in four independent EOC patient samples. (C, D) Western blot and densitometric quantification of *ID3* and *SMURF1* levels respectively in spheroids compared to adherent EOC cells (n=6). * $p < 0.05$; ** $p < 0.01$; *** $p < 0.001$ as determined by Student's *t*-test.

ligands BMP 2, 4 and 6, known to be present in EOC cells ^{7,9,17}. The mRNA levels of all three of these BMP ligands were significantly reduced in EOC spheroids compared with matched adherent cells (Figure 2.1B). Quantitative RT-PCR analysis of BMP7, however, did not yield a consistently detectable product in all samples analyzed (data not shown). In addition, the expression of the BMP signalling target gene *ID3* ^{12,17} was significantly reduced in EOC spheroids (Figure 2.1C). To address the potential mechanism by which EOC spheroids exhibit increased Smad1/5 protein, we assessed the expression level of the E3 ubiquitin-protein ligase SMURF1. SMURF1 is a Smad1/5-specific ubiquitin ligase and functions to target the degradation of R-Smad1/5/8 as a form of negative feedback regulation ^{18,19}. Indeed, SMURF1 protein levels were significantly decreased in EOC spheroids as compared to adherent cells from multiple patient samples (Figure 2.1D), which could account for the observed increase in total Smad1/5 in EOC spheroids.

To determine whether this phenomenon of downregulated signalling could be applied broadly to the TGF β superfamily, we also assessed the levels of the related R-Smad2/3. Phosphorylated Smad2 and Smad3 were detectable in both adherent EOC cells and spheroids, but there was no statistically significant difference in expression between culture conditions (Figure 2.2). Additionally, levels of the common-mediator Smad4 were not significantly altered in EOC spheroids (data not shown). Thus, it appears that differential R-Smad expression and activity in three-dimensional EOC spheroids is specific to the BMP pathway, with the net result being a downregulation of its endogenous signalling capacity in EOC spheroids.

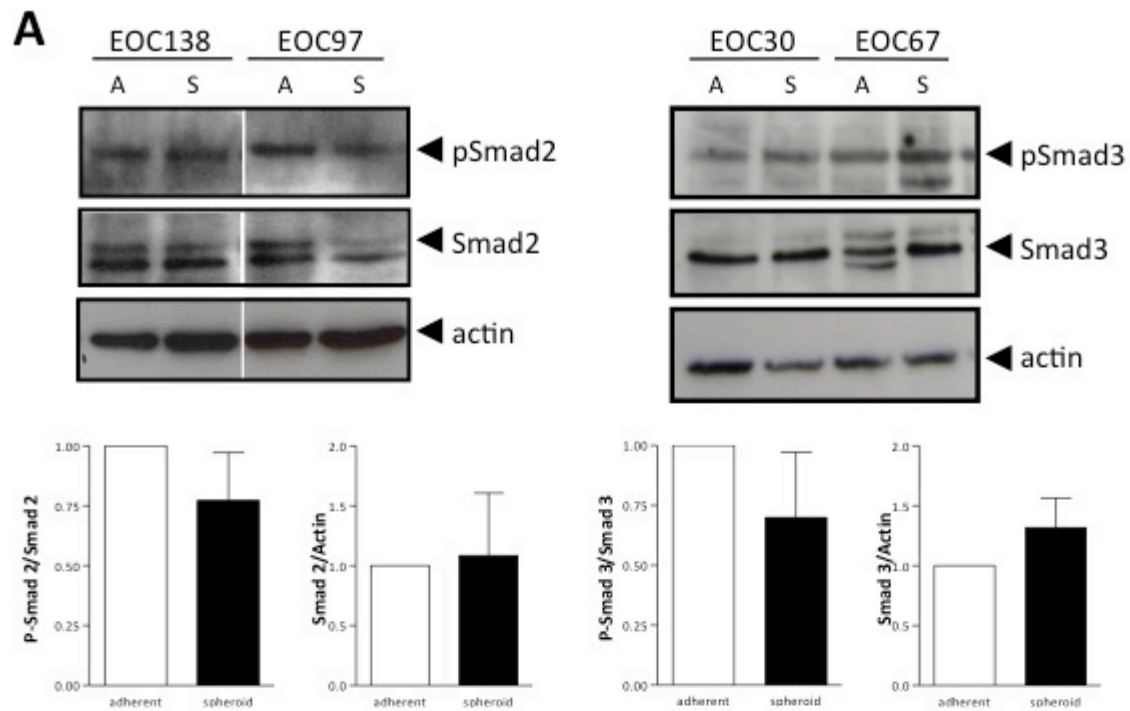


Figure 2.2: TGF- β signalling is not altered during EOC spheroid formation.

(A) Western blot and densitometric analysis of Smad2 and Smad3 levels in adherent [A] and spheroid [S] EOC cells (n=4).

2.3.2 Forced BMP activity in EOC spheroids alters cell adhesion

Given that endogenous BMP signalling activity was decreased in EOC spheroids, we postulated that this change was important for the optimal formation of spheroids. To examine this further, we tested the effect of ectopic re-activation of BMP signalling within these structures. To accomplish this, we transduced primary human EOC cells grown as adherent monolayer with adenovirus constructs expressing an HA-tagged constitutively-active mutant of the BMP type I receptor ALK3 (Ad-ALK3^{QD}), or control virus expressing green fluorescent protein (Ad-GFP). We chose this method to sustain BMP signalling during spheroid formation and reattachment experiments to ensure cell autonomous BMP signalling without the limitation of BMP ligand access to all cells within the three-dimensional multicellular aggregate during the time course of the experiment. Transducing cells as adherent cultures ensured homogeneous and efficient transduction and resultant expression of ALK3^{QD} (Figure 2.3A); direct transduction of established spheroids yielded uptake of virus into surface cells only, as visualized by Ad-GFP (data not shown). To confirm that ALK3^{QD} expression resulted in activation of BMP signalling in transduced EOC cells, western immunoblotting was performed to detect downstream targets of the pathway. As predicted, forced ALK3^{QD} expression resulted in increased phosphorylated Smad1/5/8 and ID1 protein levels as compared with EOC cells transduced with Ad-GFP (Figure 2.3B).

Since endogenous BMP signalling is naturally reduced in EOC spheroids, we hypothesized that sustained BMP signalling activity via ALK3^{QD} would abrogate their formation and resultant morphological phenotype. Indeed, primary human EOC cells expressing ALK3^{QD} generates EOC spheroids that are much smaller in size as compared with Ad-GFP transduced control spheroids (Figure 2.3C&D). This result is consistent with previous results using OVCA429 cells expressing ALK3^{QD}¹¹.

In addition, we noted that ALK3^{QD}-expressing spheroids consist of cells that are much more loosely-aggregated than the compact spheroids observed from control cells (Figure 2.3C). To verify that this phenotype is not just due to decreased cell viability from overexpression of ALK3^{QD}, we performed viable cell counting of Trypan blue-excluding cells over 72 hours of spheroid formation. ALK3^{QD} signalling had no effect on

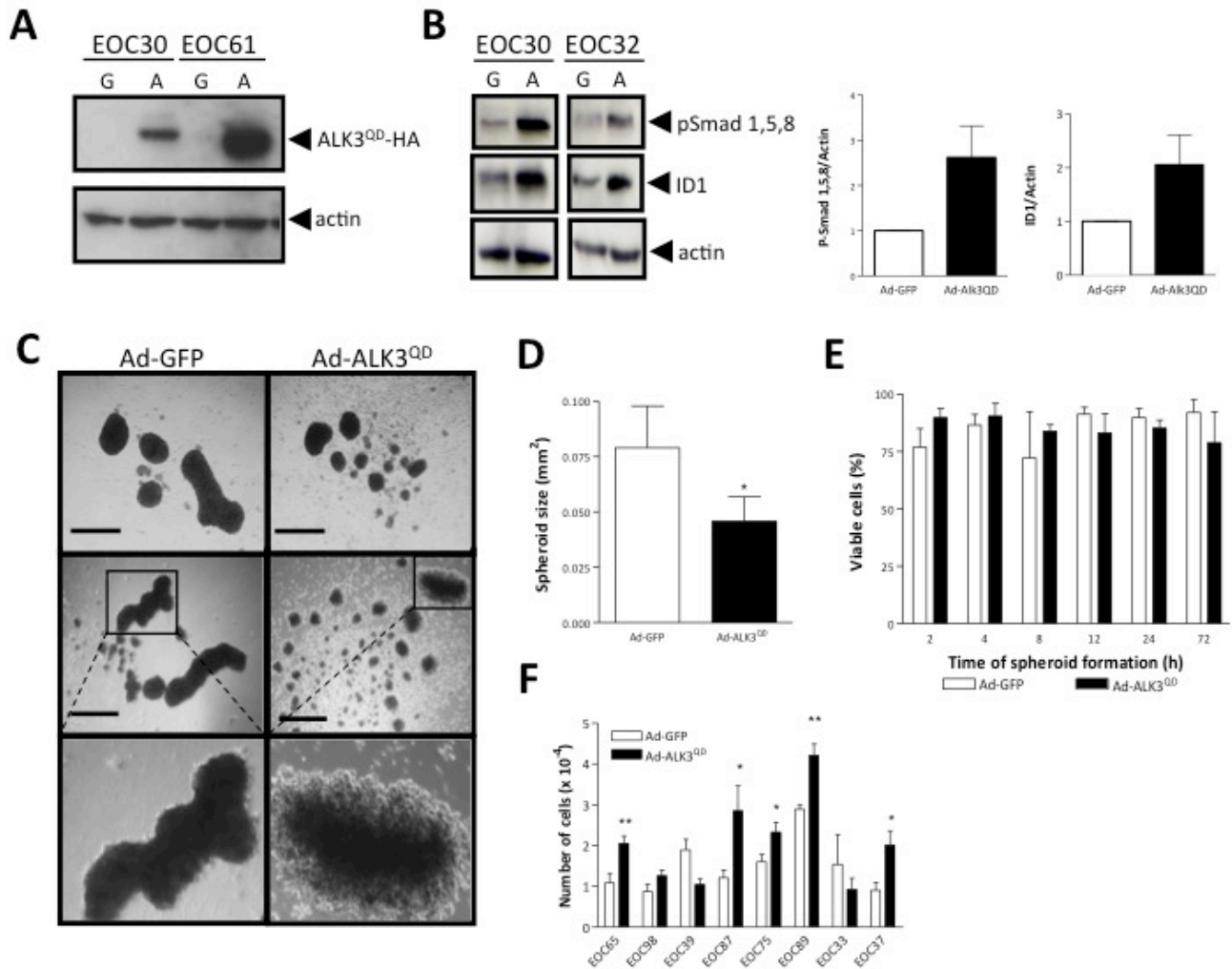


Figure 2.3: Activated BMP signalling results in smaller EOC spheroids that are more loosely aggregated.

(A) ALK3^{QD} expression was achieved by adenoviral transduction of primary EOC cells using Ad-ALK3^{QD} [A] and compared to Ad-GFP [G] control vector. (B) ALK3^{QD} expression results in activation of BMP signalling pathway as confirmed by increased phosphorylated Smad1/5/8 and ID1 protein levels 24 hours following transduction. (C) ALK3^{QD} dramatically reduces the ability of primary EOC cells to form large multicellular spheroids as compared with Ad-GFP transduced controls. Scale bar = 200 μ m. (D) ALK3^{QD} reduces the size of EOC spheroids as quantified using *ImageJ* software and averaged among seven experiments using independent patient samples. (E) ALK3^{QD} expression in EOC cells has no effect on cell viability within the first 72 hours of seeding to non-adherent culture as determined by Trypan blue exclusion. (F) ALK3^{QD}-expressing primary EOC spheroids (5 out of 8 individual patient samples) are more readily disaggregated compared to Ad-GFP controls, as determined by single-cell counting after a 2-minute trypsinization. * $p < 0.05$; ** $p < 0.01$ as determined by Student's *t*-test.

EOC cell viability in suspension culture, indicating that enhanced anoikis is not triggered by elevated BMP signalling during spheroid formation (Figure 2.2E). To assay cell cohesion directly, spheroid disaggregation experiments were performed on several patient samples (n=8) expressing ALK3^{QD}, or Ad-GFP controls. Timed exposure to trypsin followed by quantification of single cells demonstrated that activated BMP signalling caused decreased cell cohesion of spheroids in 5 of 8 independent primary EOC samples (Figure 2.3F).

Activated BMP signalling in adherent EOC cells induces epithelial-mesenchymal transition (EMT), a hallmark of which is the downregulation of E-cadherin^{11,13}. Since E-cadherin may be involved in mediating cell-cell interactions in 3D spheroids^{2,20}, we sought to determine if ALK3^{QD} was downregulating E-cadherin expression via inducing EMT in EOC spheroids, thereby resulting in decreased cell cohesion. Using real-time quantitative RT-PCR analysis of several EMT markers, we observed that EOC cells naturally undergo an EMT response during spheroid formation with an upregulation of Snail, Slug, ZEB2, Twist1 and Twist2 transcriptional repressors and concomitant downregulation of E-cadherin (*CDH1*) expression (Figure 2.4A). In contrast, we observed that spheroid cells expressing ALK3^{QD} possess increased E-cadherin mRNA expression compared with control cells, and this correlated with an increase in the proportion of cells that were E-cadherin positive as determined by flow cytometry (Figure 2.4B). Therefore, constitutively active BMP signalling appeared to counteract the natural dynamics of transitions between epithelial and mesenchymal cell phenotypes in EOC spheroids.

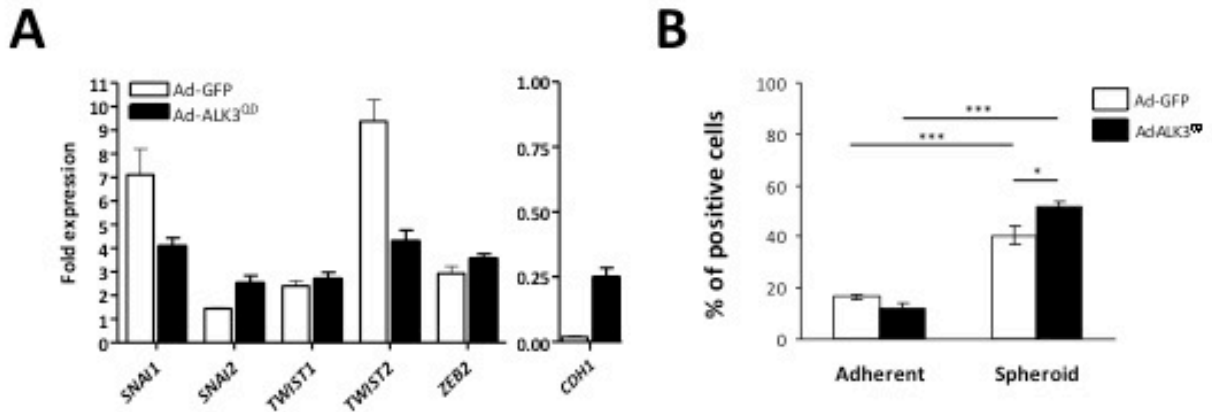


Figure 2.4: EMT is induced during EOC spheroid formation.

(A) EMT is induced in EOC spheroids, both in the absence or presence of activated ALK3^{OD} signalling, as determined by real-time quantitative RT-PCR of E-cadherin (*CDH1*), Snail (*SNAI1*), Slug (*SNAI2*), *TWIST1*, *TWIST2* and *ZEB2*. Fold expression was quantified against adherent cultures (set to 1) using pooled data from 5 independent patient samples performed in duplicate; *GAPDH* served as an internal control. (B) Flow cytometry for E-cadherin protein expression across 5 independent patient samples in the presence or absence of Alk3^{OD} signalling. * $p < 0.05$; *** $p < 0.001$ as determined by Student's *t*-test.

The capacity of EOC spheroids for reattachment, growth and motility defines their ability to form secondary metastases². Since activated BMP signalling consistently reduces cell-cell cohesion within EOC spheroids, we next sought to determine whether activated BMP signalling affects the ability of EOC spheroid cells to reattach and migrate. ALK3^{QD}-expressing EOC spheroids and GFP controls were plated for reattachment using standard tissue culture-treated plastic by directly transferring spheroids into new dishes with fresh growth medium. We observed an increased cell dispersion area and number of motile cells emanating from ALK3^{QD}-expressing EOC spheroids within the first 24 hours of replating, as compared with controls (Figure 2.5A&B). This was not due to cell proliferation since there was no significant difference in BrdU-incorporated cytochemistry in dispersing cells of ALK3^{QD}-expressing spheroids compared to GFP controls (data not shown). This observed effect on EOC cell motility upon spheroid reattachment was consistent with our previous results of increased motility in adherent primary human EOC cells using recombinant human BMP4 and ALK3^{QD} expression in conventional scratch wound assays^{11,13}.

2.3.3 Inhibition of endogenous BMP signalling affects EOC spheroid adhesion

Given the enhanced effect of activated BMP signalling during EOC spheroid reattachment, we wanted to determine if the reduction in endogenous BMP signalling, which was observed during EOC spheroid formation, would be restored during reattachment. Indeed, there is a significant increase in the levels of phosphorylated Smad1/5/8 when normalized to total protein levels in a number of different EOC patient samples (Figure 2.5C). These results indicate that the activity of the BMP signalling pathway is restored during EOC spheroid reattachment.

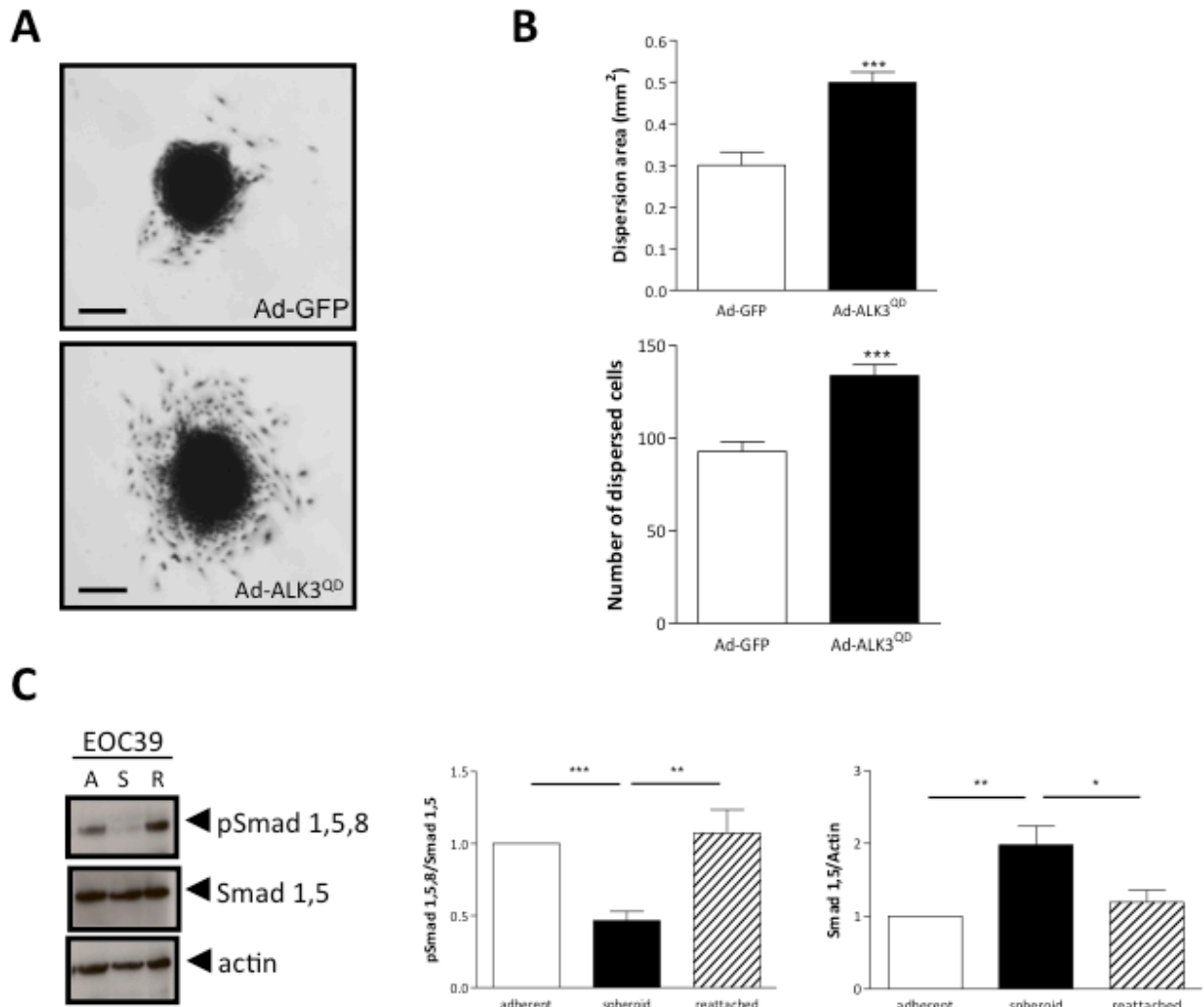


Figure 2.5: Alk3^{QD} expression enhances the movement of EOC cells from spheroids after reattachment.

(A) ALK3^{QD} enhances the ability of EOC spheroids to migrate from the spheroid. (B) ALK3^{QD} increases the dispersion area generated by reattached EOC spheroids as quantified using *ImageJ* software and averaged among six experiments using independent patient samples. Dispersion area was calculated 24 hours after spheroids have been replated to standard tissue culture plastic and normalized to the size of original spheroid. ALK3^{QD} increases the number of dispersed cells 24 hours following spheroid reattachment as determined by counting DAPI-stained nuclei. (C) Western blot and densitometric analysis of phosphorylated and total Smad1/5/8 in adherent, spheroid and reattached EOC spheroid cells (n=7). (* $p < 0.05$; ** $p < 0.001$; *** $p < 0.001$ as determined by Student's *t*-test). Scale Bar: 200 μ m.

Given our results in EOC spheroids thus far, we postulated that blocking endogenous BMP activity may further facilitate spheroid formation yet decrease subsequent reattachment and dispersion. Primary human EOC cells express several BMP ligands, chiefly BMP2, BMP4 and BMP6 (Figure 2.1B) and their ability to promote signalling in EOC cells can be efficiently blocked using natural antagonists such as Noggin (NG) and Chordin^{9,13}. Additionally, LDN-193189 is a small molecule that selectively inhibits BMP type I receptors and can be used to block this pathway^{21,22}. Treatment of EOC cells with a single bolus of 50 ng/mL Fc-NG or with a range of concentrations of LDN-193189 resulted in a rapid and sustained reduction in phosphorylated BMP R-Smad1/5/8 over 72 hours (Figure 2.6A). Primary EOC cells were seeded to Ultra-Low Attachment dishes and treatment with Fc-NG (50 ng/mL) or LDN-193189 (10 nM and 100 nM) was initiated immediately. From this, we observed a statistically significant increase in the average size of EOC spheroids as compared with control cultures (Figure 2.6B&C). In addition to this, when EOC spheroids were treated with either Fc-NG or LDN-193189 upon reattachment, dispersion areas were significantly reduced. A reduction in the number of dispersing cells was observed at 100 nM of LDN-193189, but no difference in the number of cells arising from the attached spheroids by treatment with Fc-NG. Taken together, these results suggest a functional requirement for differential regulation of EOC spheroid formation and subsequent motility of EOC cells upon spheroid reattachment by BMP signalling.

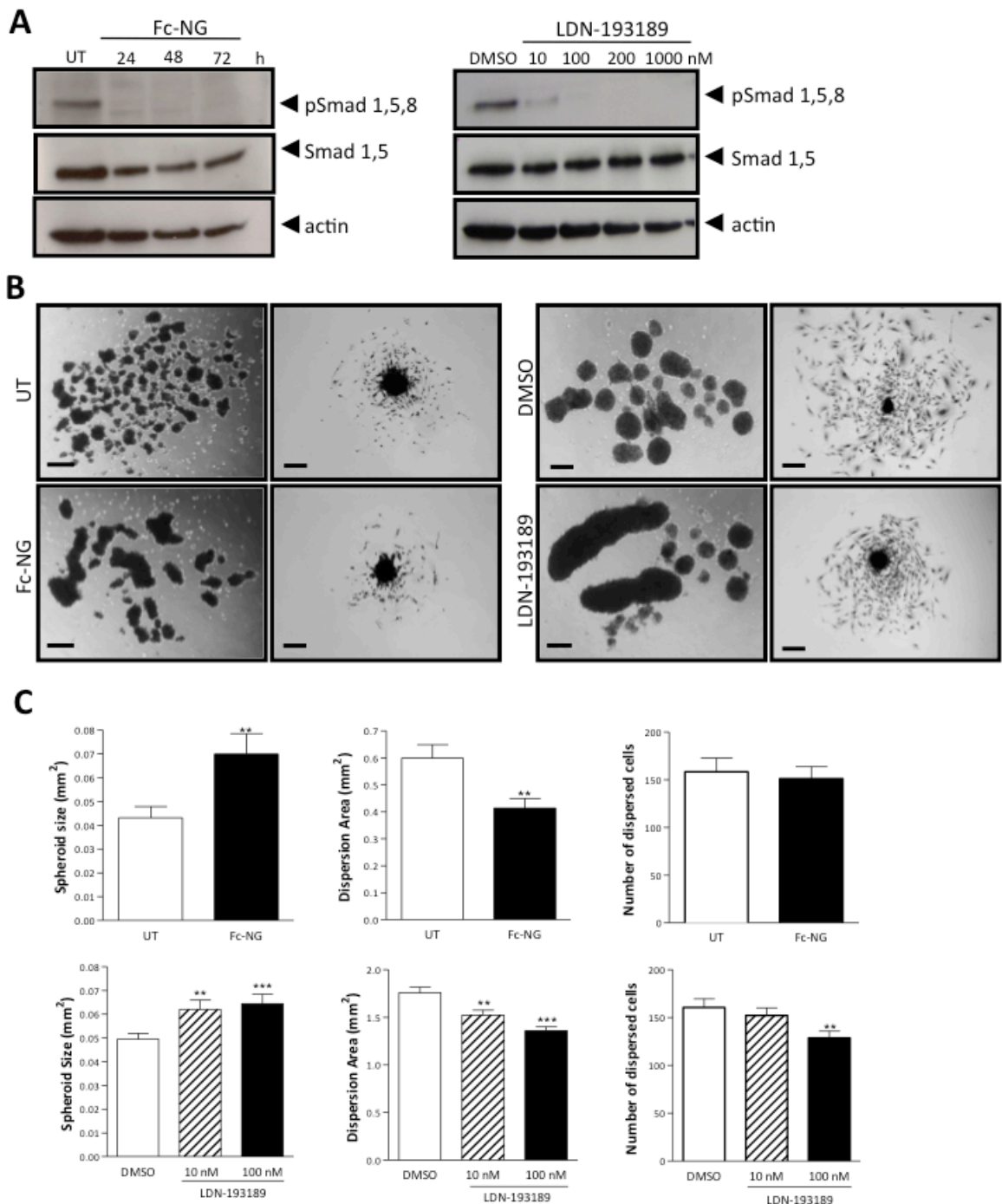


Figure 2.6: Inhibition of BMP signalling enhances EOC spheroid formation and decreases reattachment.

(A) Treatment of primary EOC cells with extracellular antagonist of BMP signalling Fc-Noggin (Fc-NG, 50 ng/mL) and small molecule inhibitor LDN-193189 results in potent inhibition of BMP signalling as visualized by Western blot analysis of pSmad1/5/8. (B) Treatment with Fc-NG (50 ng/mL) or LDN-193189 (100 nM) increases the ability of EOC cells to form large multicellular spheroids and a subsequent decreased ability to disperse on tissue culture plastic. Scale bar=50 μ m. (C) Quantification of spheroid size and dispersion area following treatment with Fc-NG or LDN-193189 using *ImageJ* software (n=3; n=7 respectively). (** $p < 0.01$; *** $p < 0.001$ using Student's *t*-test).

2.3.4 BMP signalling activates the AKT pathway in EOC cells & spheroids

The phenotypic changes in EOC spheroid adhesion and motility due to ALK3^{QD} signalling likely result from a combination of both direct and indirect alterations in expression of many genes and their products. Activation of BMP signalling leads to the regulation of target gene expression primarily via Smad-dependent mechanisms. Several genes are direct targets of BMP signalling in EOC cells, including genes encoding the inhibitory Smad6/7 and the helix-loop-helix negative regulatory transcription factors ID1 and ID3^{12,17}. Thus, to uncover many potential targets on a genome-wide scale, we performed an expression microarray using Ad-ALK3^{QD}- and Ad-GFP-transduced cells of five independent EOC patient samples, and compared mRNA expression between adherent and spheroid cultures as well. We selected primary human EOC cells from patients with high-grade serous adenocarcinoma since they represent the most common histologic subtype of EOC and also to minimize potential experimental variability among patient samples. Using Affymetrix® Human U133A 2.0 plus arrays, we uncovered a plethora of altered gene expression characteristics which were consistent among all five patient samples ($p < 0.05$): 444 annotated genes were elevated in expression due to ALK3^{QD} in EOC spheroids compared to GFP controls, and 314 annotated genes were reduced (Table S2.1). The subset of genes that were commonly-regulated by ALK3^{QD} in both adherent EOC cells and spheroids, comprising 96 up-regulated and 45 down-regulated genes (Tables 2.1 & 2.2 and Figure 2.7A) were used to focus our analysis. Some known BMP target genes were identified in this subset, namely the transcription factors *SMAD6* and *SMAD7*, *MSX2*, *DLX2*, and *JUND*. In addition, the BMP signalling antagonists *NOG* (Noggin) and *GREM2* (Gremlin 2) were also increased due to ALK3^{QD} signalling in both adherent cells and spheroids. We have since validated the expression of several of these genes, with *SMAD6*, *NOG*, *MSX2*, *HEY1* and *TBX3* demonstrating reproducible upregulation by ALK3^{QD} signalling as determined by qRT-PCR (Figure S2.1).

Table 2.1: Up-regulated genes in response to Alk3QD expression and common between adherent and spheroid EOC cells.

| Gene Name | Gene Description | Probe Set | Adherent Fold Change | Spheroid Fold Change |
|---|--|--------------|----------------------|----------------------|
| <i>BMP signalling & target genes</i> | | | | |
| <i>DLX2*</i> | distal-less homeobox 2 | 207147_at | 8.543 | 20.206 |
| <i>SMAD6*</i> | SMAD family member 6 | 207069_s_at | 5.782 | 10.538 |
| <i>SMAD7</i> | SMAD family member 7 | 204790_at | 2.078 | 2.813 |
| <i>GREM2</i> | gremlin 2 | 235504_at | 5.071 | 2.982 |
| | | 240509_s_at | 4.665 | 2.535 |
| <i>NOG*</i> | noggin | 231798_at | 3.683 | 10.343 |
| <i>MSX2*</i> | msh homeobox 2 | 210319_x_at | 2.581 | 4.527 |
| | | 205555_s_at | 2.118 | 4.689 |
| <i>JUND</i> | jun D proto-oncogene | 203751_x_at | 2.146 | 2.291 |
| <i>ECM & cell adhesion</i> | | | | |
| <i>GJD3</i> | gap junction protein, delta 3, 31.9kDa | 230025_at | 7.533 | 10.917 |
| <i>HAS2</i> | hyaluronan synthase 2 | 206432_at | 4.122 | 2.696 |
| <i>CD24</i> | CD24 molecule | 209772_s_at | 4.078 | 39.195 |
| | | 208650_s_at | 3.376 | 24.444 |
| | | 266_s_at | 2.927 | 37.327 |
| | | 208651_x_at | 2.861 | 21.376 |
| <i>LRRC4</i> | leucine rich repeat containing 4 | 223552_at | 4.043 | 6.963 |
| <i>PCDH10</i> | protocadherin 10 | 1552925_at | 3.641 | 2.624 |
| <i>CD300LG</i> | CD300 molecule-like family member g | 1552509_a_at | 3.316 | 6.675 |
| <i>SSX2IP</i> | synovial sarcoma, X breakpoint 2 interacting protein | 203018_s_at | 2.858 | 3.122 |
| | | 210871_x_at | 2.788 | 3.153 |
| | | 203016_s_at | 2.759 | 3.056 |
| | | 203015_s_at | 2.675 | 3.625 |
| | | 203019_x_at | 2.655 | 3.195 |
| | | 203017_s_at | 2.19 | 2.175 |
| <i>FBLN2</i> | fibulin 2 | 203886_s_at | 2.542 | 2.905 |
| <i>CDH24</i> | cadherin-like 24 | 1553166_at | 2.321 | 2.181 |
| <i>CNTNAP2</i> | contactin associated protein-like 2 | 219301_s_at | 2.309 | 25.559 |
| <i>Ligands</i> | | | | |
| <i>TNFSF9</i> | tumor necrosis factor, member 9 | 206907_at | 4.802 | 8.53 |
| <i>CCL26</i> | chemokine (C-C motif) ligand 26 | 223710_at | 4.725 | 11.408 |
| <i>CCK</i> | cholecystokinin | 205827_at | 7.97 | 3.831 |
| <i>JAG1</i> | jagged 1 | 231183_s_at | 3.146 | 2.306 |
| | | 209098_s_at | 2.639 | 2.546 |
| <i>PGF</i> | placental growth factor | 209652_s_at | 2.84 | 3.963 |
| <i>INSL3</i> | insulin-like 3 | 1553594_a_at | 2.472 | 2.875 |
| <i>Receptors & membrane proteins</i> | | | | |
| <i>FOLR3</i> | folate receptor 3 | 206371_at | 6.787 | 12.253 |
| <i>SYT15</i> | synaptotagmin XV | 1560879_a_at | 6.497 | 6.516 |
| | | 1560878_at | 3.835 | 2.825 |
| <i>FIBCD1</i> | fibrinogen C domain containing 1 | 240042_at | 4.27 | 4.389 |

Table 2.1 cont'd

| | | | | |
|--|--|--------------|--------|--------|
| <i>SEMA7A</i> | semaphorin 7A | 230345_at | 4.226 | 2.382 |
| <i>TMEM132E</i> | transmembrane protein 132E | 243708_at | 4.196 | 3.56 |
| <i>MALL</i> | mal, T-cell differentiation protein-like | 209373_at | 3.705 | 4.481 |
| <i>SLC25A15</i> | solute carrier family 25, member 15 | 222705_s_at | 3.524 | 2.879 |
| <i>KCNQ5</i> | potassium voltage-gated channel, member 5 | 244623_at | 3.489 | 6.034 |
| <i>STRA6</i> | stimulated by retinoic acid gene 6 | 221701_s_at | 3.465 | 3.08 |
| <i>PLXNA2</i> | plexin A2 | 213030_s_at | 2.758 | 4.575 |
| | | 227032_at | 2.413 | 2.938 |
| <i>PAQR9</i> | progesterone and adiponectin receptor family member IX | 1558322_a_at | 2.7 | 2.681 |
| <i>LIN7B</i> | lin-7 homolog B | 241957_x_at | 2.583 | 4.773 |
| <i>FZD8</i> | frizzled homolog 8 | 227405_s_at | 2.513 | 3.713 |
| <i>PITPNM2</i> | phosphatidylinositol transfer protein, membrane-associated 2 | 1552924_a_at | 2.476 | 2.579 |
| <i>TRPC3</i> | transient receptor potential cation channel, subfamily C, member 3 | 210814_at | 2.223 | 4.341 |
| <i>TRPV2</i> | transient receptor potential cation channel, subfamily V, member 2 | 219282_s_at | 2.1 | 2.149 |
| <i>FGFR3</i> | fibroblast growth factor receptor 3 | 204379_s_at | 2.184 | 2.227 |
| Intracellular signalling proteins | | | | |
| <i>DUSP5P</i> | dual specificity phosphatase 5 | 1553299_at | 2.305 | 3.296 |
| <i>DUSP26</i> | dual specificity phosphatase 26 | 219144_at | 4.234 | 2.56 |
| <i>SPRY2</i> | sprouty homolog 2 | 204011_at | 2.598 | 2.061 |
| <i>SOCS2</i> | suppressor of cytokine signaling 2 | 203372_s_at | 2.473 | 6.416 |
| | | 203373_at | 2.065 | 4.938 |
| <i>SHC4</i> | SHC family, member 4 | 230538_at | 2.132 | 2.765 |
| <i>NCLN</i> | nicalin | 222206_s_at | 2.007 | 2.055 |
| Structural proteins | | | | |
| <i>LOR</i> | loricrin | 207720_at | 63.124 | 49.49 |
| <i>IVL</i> | involucrin | 214599_at | 4.612 | 14.951 |
| <i>KRTAP2-4</i> | keratin associated protein 2-4 | 1555673_at | 4.146 | 3.112 |
| <i>KIF7</i> | kinesin family member 7 | 229405_at | 4.102 | 2.224 |
| <i>EML1</i> | echinoderm microtubule associated protein like 1 | 204797_s_at | 3.853 | 2.712 |
| <i>ACTC1</i> | actin, alpha, cardiac muscle 1 | 205132_at | 3.766 | 40.174 |
| <i>DCDC5</i> | doublecortin domain containing 5 | 232603_at | 3.346 | 4.783 |
| <i>TUBB2A ///</i> | tubulin, beta 2A /// tubulin, beta 2B | 209372_x_at | 2.684 | 2.546 |
| <i>TUBB2B</i> | | | | |
| <i>TPM1</i> | tropomyosin 1 | 206117_at | 2.454 | 3.223 |
| <i>SPTBN1</i> | spectrin, beta, non-erythrocytic 1 | 226342_at | 2.437 | 2.422 |
| <i>TLN2</i> | talin 2 | 212701_at | 2.239 | 3.438 |
| <i>MAP1B</i> | microtubule-associated protein 1B | 212233_at | 2.193 | 3.056 |
| Transcription factors | | | | |
| <i>FEZF2</i> | FEZ family zinc finger 2 | 233972_s_at | 5.611 | 16.35 |
| <i>MYB</i> | v-myb myeloblastosis viral oncogene | 204798_at | 3.721 | 3.094 |
| <i>ATOX1</i> | atonal homolog 8 | 1558706_a_at | 3.716 | 4.353 |
| | | 228890_at | 2.873 | 4.266 |
| <i>KLF4</i> | Kruppel-like factor 4 | 220266_s_at | 3.638 | 3.033 |
| | | 221841_s_at | 2.701 | 2.962 |
| <i>LMO2</i> | LIM domain only 2 | 204249_s_at | 3.592 | 4.971 |
| <i>AFF2</i> | AF4/FMR2 family, member 2 | 206105_at | 3.356 | 3.267 |

Table 2.1 cont'd

| | | | | |
|-------------------|---|--------------|-------|-------|
| <i>TBX3*</i> | T-box 3 | 225544_at | 2.737 | 2.183 |
| | | 229576_s_at | 2.707 | 2.416 |
| <i>GATA2</i> | GATA binding protein 2 | 209710_at | 2.422 | 2.501 |
| <i>GATA3</i> | GATA binding protein 3 | 209604_s_at | 2.123 | 2.301 |
| <i>HEY1*</i> | hairy/enhancer-of-split related with YRPW motif 1 | 44783_s_at | 2.053 | 3.736 |
| | | 218839_at | 2.047 | 3.216 |
| <i>PRRX2</i> | paired related homeobox 2 | 219729_at | 2.037 | 4.659 |
| Other | | | | |
| <i>AKR1C1</i> | aldo-keto reductase family 1, member C1 | 204151_x_at | 4.2 | 4.254 |
| | | 216594_x_at | 3.321 | 3.725 |
| <i>AKR1C2</i> | aldo-keto reductase family 1, member C2 | 211653_x_at | 5.339 | 4.759 |
| | | 209699_x_at | 3.62 | 3.771 |
| <i>CCDC68</i> | coiled-coil domain containing 68 | 220180_at | 2.022 | 2.067 |
| <i>CCDC85A</i> | coiled-coil domain containing 85A | 235228_at | 3.596 | 5.131 |
| <i>TRNP1</i> | TMF1-regulated nuclear protein 1 | 227862_at | 3.268 | 4.095 |
| <i>CRYAB</i> | crystallin, alpha B | 209283_at | 3.058 | 4.708 |
| <i>GPX3</i> | glutathione peroxidase 3 | 214091_s_at | 3.03 | 4.534 |
| <i>THAP2</i> | THAP domain containing, apoptosis associated protein 2 | 230380_at | 2.893 | 4.04 |
| <i>DNAJA4</i> | DnaJ homolog, subfamily A, member 4 | 1554334_a_at | 2.89 | 3.921 |
| <i>PEG10</i> | paternally expressed 10 | 212092_at | 2.875 | 2.108 |
| <i>RPA4</i> | replication protein A4 | 221143_at | 2.733 | 4.239 |
| <i>KANK4</i> | KN motif and ankyrin repeat domains 4 | 229125_at | 2.522 | 2.414 |
| <i>DCBLD2</i> | discoidin, CUB and LCCL domain containing 2 | 213873_at | 2.497 | 3.841 |
| | | 213865_at | 2.323 | 2.769 |
| <i>NHEDC2</i> | Na ⁺ /H ⁺ exchanger domain containing 2 | 1564746_at | 2.438 | 3.347 |
| | | 229491_at | 2.358 | 4.648 |
| <i>ALAS2</i> | aminolevulinate synthase 2 | 244205_at | 2.355 | 2.621 |
| <i>HSPD1 ///</i> | heat shock 60kDa protein 1 /// | 243372_at | 2.34 | 2.642 |
| <i>HSPDIP4</i> | pseudogene 4 | | | |
| <i>HSPA1A ///</i> | heat shock 70kDa protein 1A /// | 200800_s_at | 2.145 | 7.074 |
| <i>HSPA1B</i> | | | | |
| <i>MEX3C</i> | mex-3 homolog C | 1556874_a_at | 2.326 | 2.37 |
| <i>CASQ1</i> | calsequestrin 1 | 219645_at | 2.285 | 3.64 |
| <i>PSG6</i> | pregnancy specific beta-1-glycoprotein 6 | 208106_x_at | 2.195 | 2.017 |
| <i>YWHAH</i> | tyrosine 3-monooxygenase/tryptophan 5-monooxygenase activation protein, eta polypeptide | 201020_at | 2.188 | 2.704 |
| <i>ME2</i> | malic enzyme 2 | 210154_at | 2.068 | 2.187 |
| <i>HECW2</i> | HECT, C2 and WW domain containing | 232080_at | 2.04 | 3.641 |
| <i>ATP13A3</i> | ATPase type 13A3 | 219558_at | 2.018 | 3.262 |

*- Expression was validated by real-time quantitative RT-PCR as described in Materials & Methods.

Table 2.2: Down-regulated genes in response to Alk3QD expression common between adherent and spheroid EOC cells.

| Gene Name | Gene Description | Probe Sets | Adherent Fold Change | Spheroid Fold Change |
|---|---|--------------|----------------------|----------------------|
| <i>ECM & cell adhesion</i> | | | | |
| <i>CHI3L1</i> | chitinase 3-like 1 | 209396_s_at | 23.81 | 4.35 |
| | | 209395_at | 14.08 | 3.25 |
| <i>VCAM1</i> | vascular cell adhesion molecule 1 | 203868_s_at | 3.82 | 3.38 |
| <i>CCDC80</i> | coiled-coil domain containing 80 | 225241_at | 3 | 3.27 |
| | | 225242_s_at | 2.38 | 2.72 |
| <i>Ligands</i> | | | | |
| <i>PDGFD</i> | platelet derived growth factor D | 219304_s_at | 4.55 | 3.3 |
| <i>CXCL16</i> | chemokine (C-X-C motif) ligand 16 | 223454_at | 3.57 | 2.85 |
| <i>Receptors & membrane proteins</i> | | | | |
| <i>PDPN</i> | podoplanin | 221898_at | 5.88 | 3.64 |
| | | 204879_at | 3.46 | 2.72 |
| <i>KCNH2</i> | potassium voltage-gated channel, subfamily H, member 2 | 210036_s_at | 4.37 | 3.21 |
| <i>KCNJ12</i> | potassium inwardly-rectifying channel, subfamily J, member 12 | 232289_at | 2.51 | 2 |
| | | 207110_at | 2.5 | 2.01 |
| <i>VNN1</i> | vanin 1 | 205844_at | 3.48 | 3.72 |
| <i>PLSCR4</i> | phospholipid scramblase 4 | 218901_at | 3.17 | 2.43 |
| <i>EPHB3</i> | EPH receptor B3 | 204600_at | 2.91 | 5.95 |
| <i>PLSCR1</i> | phospholipid scramblase 1 | 202430_s_at | 2.81 | 2.1 |
| <i>PTGFRN</i> | prostaglandin F2 receptor negative regulator | 224937_at | 2.66 | 2.43 |
| <i>TNFRSF21</i> | tumor necrosis factor receptor superfamily, | 218856_at | 2.39 | 2.72 |
| <i>ITGB8</i> | integrin, beta 8 | 226189_at | 2.21 | 2.41 |
| <i>SORT1</i> | sortilin 1 | 224818_at | 2.17 | 2.57 |
| <i>PGRMC2</i> | progesterone receptor membrane component 2 | 213227_at | 2.04 | 2.32 |
| <i>Intracellular signalling proteins</i> | | | | |
| <i>RAP1A</i> | RAP1A, member of RAS oncogene family | 1555340_x_at | 1000 | 333.33 |
| | | 1555339_at | 333.33 | 333.33 |
| <i>PKIB</i> | protein kinase inhibitor beta | 231120_x_at | 18.18 | 3.23 |
| <i>REPS2</i> | RALBP1 associated Eps domain containing 2 | 227425_at | 6.21 | 5.08 |
| | | 205645_at | 4.61 | 3.19 |
| <i>CASP10</i> | caspase 10 | 205467_at | 2.43 | 2.28 |
| <i>ELMO1</i> | engulfment and cell motility 1 | 204513_s_at | 2.22 | 2.15 |
| <i>ARHGEF3</i> | Rho guanine nucleotide exchange factor 3 | 218501_at | 2.19 | 2.01 |
| <i>Structural proteins</i> | | | | |
| <i>PPL</i> | periplakin | 203407_at | 15.15 | 4.42 |
| <i>MYO5B</i> | myosin VB | 225299_at | 3.04 | 3.1 |
| | | 225301_s_at | 3.04 | 3.7 |
| <i>MBP</i> | myelin basic protein | 210136_at | 2.97 | 2.51 |

Table 2.2 cont'd.

| | | | | |
|------------------------------|---|---------------------------|-------------|--------------|
| <i>MAP7</i> | microtubule-associated protein 7 | 1554544_a_at 202890_at | 2.56 2.5 | 3.15 2.39 |
| Transcription factors | | | | |
| <i>NFE2L3</i> | nuclear factor (erythroid-derived 2)-like 3 | 204702_s_at | 3.06 | 2.19 |
| <i>KAT2B</i> | lysine acetyltransferase 2B | 203845_at | 2.39 | 2.75 |
| <i>BNC1</i> | basonuclin 1 | 1552487_a_at | 2.1 | 2.2 |
| Other | | | | |
| <i>LRIG3</i> | leucine-rich repeats and immunoglobulin-like domains 3 | 226908_at | 4.31 | 3.65 |
| <i>SLC46A3</i> | solute carrier family 46, member 3 | 214719_at | 3.77 | 2.22 |
| <i>ALDH6A1</i> | aldehyde dehydrogenase 6 family, member A1 | 221589_s_at | 3.68 | 2.86 |
| <i>ALDH6A1</i> | | 221588_x_at | 2.84 | 2.39 |
| <i>ALDH6A1</i> | | 204290_s_at | 2.51 | 2.31 |
| <i>CYP7B1</i> | cytochrome P450, family 7, subfamily B, polypeptide 1 | 207386_at | 3.64 | 2.67 |
| <i>CYP39A1</i> | cytochrome P450, family 39, subfamily A, polypeptide 1 | 1553977_a_at | 2.73 | 2.12 |
| <i>IFIT1</i> | interferon-induced protein with tetratricopeptide repeats 1 | 203153_at | 3.19 | 2.7 |
| <i>ERO1LB</i> | ERO1-like beta | 231944_at | 2.69 | 2.06 |
| <i>FTH1</i> | ferritin, heavy polypeptide 1 | 214211_at | 2.59 | 2.16 |
| <i>FTH1</i> | | | | |
| <i>FTH1</i> | | | | |
| <i>CMBL</i> | carboxymethylenebutenolidase | 227522_at | 2.46 | 2.74 |
| <i>AOXI</i> | aldehyde oxidase 1 | 205083_at | 2.28 | 6.25 |
| <i>SLC27A1</i> | solute carrier family 27, member 1 | 226728_at | 2.2 | 2.15 |
| <i>ZFYVE16</i> | zinc finger, FYVE domain containing 16 | 1555982_at | 2.14 | 2.14 |
| <i>B3GNT1</i> | beta-1,3-N-acetylglucosaminyl-transferase 1 | 203188_at | 2.07 | 2.92 |
| <i>PSITP4</i> | HBV preS1-transactivated protein 4 | 226381_at | 2.06 | 2.04 |
| <i>FUCA1</i> | fucosidase, alpha-L-1, tissue | 202838_at | 2.02 | 2.06 |

Uncovering potential novel mechanisms of disease hidden within a gene expression signature is more readily attainable when compared to the large number of published datasets available. One such useful resource is Connectivity Map (CMAP) that was established and made available by the Broad Institute and MIT (<http://www.broadinstitute.org/cmap>)²³⁻²⁵. CMAP facilitates the discovery of connections among human diseases, chiefly cancer, with gene expression changes and drug action. By uploading the up-regulated and down-regulated probe set lists (*i.e.* 96 up- and 45 down-regulated genes) from our microarray study to CMAP (Figure 2.7A), we identified that three of the top ten drugs are inhibitors targeting the phosphatidylinositol 3-kinase (PI3K)-mammalian target of rapamycin (mTOR) pathway (Figure 2.7B). The PI3K inhibitors LY294002 and wortmannin were ranked first and seventh respectively, and the mTOR inhibitor sirolimus, also known as rapamycin, was ranked second. Interestingly, the compiled data of these three drugs from CMAP had a strong negative correlation with our ALK3^{QD} gene expression signature. Given that the ALK3^{QD} gene expression dataset was negatively-correlated with those from all three of the PI3K-mTOR pathway inhibitors, we reasoned that activated BMP signalling induces the PI3K-mTOR pathway in primary EOC cells. To determine if this was the case, we performed western blotting to detect phosphorylated AKT levels as a direct readout of PI3K-mTOR pathway activity in EOC cells and spheroids expressing the constitutively-active BMP receptor. Indeed, ALK3^{QD} expression significantly increased phospho-AKT in EOC cells (Figure 2.8C).

We and others have demonstrated that active PI3K-mTOR signalling is vital to promoting the metastatic potential of EOC cells and spheroids²⁶⁻²⁹. Indeed, treatment of reattaching primary EOC spheroids with any of three different inhibitors of the PI3K-mTOR pathway, LY294002, rapamycin and temsirolimus (Torisel[®]), resulted in a significant reduction in cell dispersion (Figure S2.2). To address whether this pathway is required for the phenotypic changes imparted by active BMP signalling, we targeted its central mediator AKT directly and specifically using the AKT inhibitor, Akti-1/2. Reattaching EOC spheroids transduced with either Ad-ALK3^{QD} or Ad-GFP were treated with 5 μ M AKTi-1/2, or DMSO as a vehicle control. As early as 24 hours after treatment with Akti-1/2, the dispersion area of ALK3^{QD} spheroids was reduced, although not

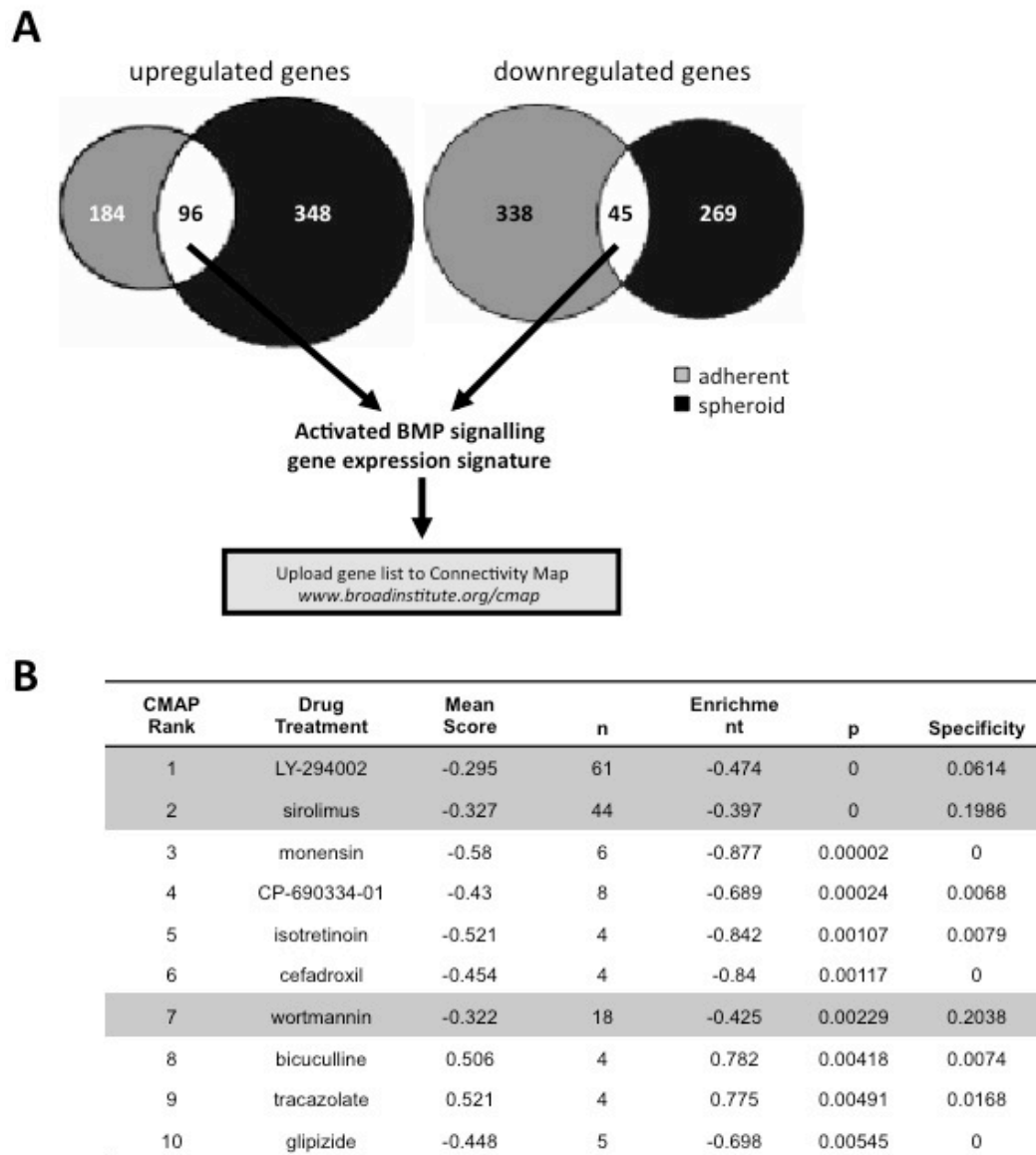


Figure 2.7: The PI3K-AKT-mTOR pathway is activated by BMP signalling in EOC cells and spheroids.

(A) Venn diagrams (based on Genespring analysis of microarray data using Affymetrix Human U133 plus 2.0 arrays) representing a total of 96 genes which are increased and 45 genes which are decreased in expression in response to ALK3QD in both EOC cells and spheroids. The up-regulated and down-regulated probe set lists from the microarray study were uploaded to Connectivity Map (CMAP) which was established and made available by the Broad Institute and MIT (<http://www.broadinstitute.org/cmap>). (B) The top ten drugs with gene expression signatures correlating with the ALK3QD gene expression signatures. Inhibitors targeting the PI3K-AKT-mTOR pathway, specifically LY294002, sirolimus, and wortmannin, result in gene expression patterns exhibiting a negative correlation with the ALK3QD gene expression signature.

completely down to levels observed in Ad-GFP control spheroids (Figure 2.8D). This suggests that enhanced AKT activity is required, at least in part, for the enhanced reattachment and dispersion of EOC cells observed as a result of active BMP signalling.

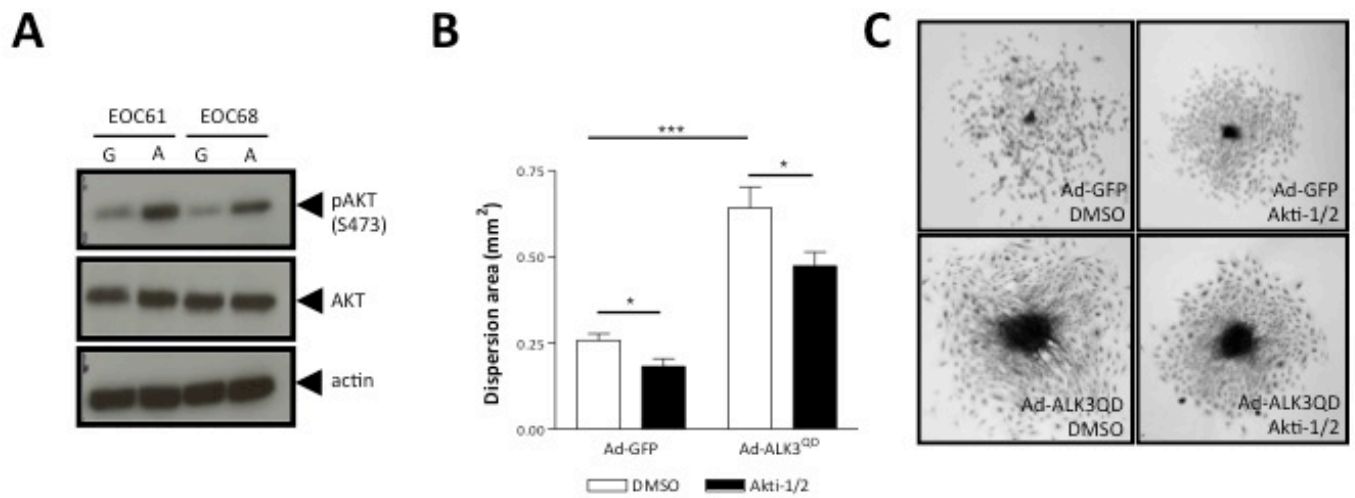


Figure 2.8: BMP-enhanced spheroid reattachment is partially mediated by AKT signalling.

(A) ALK3QD results in increased levels of phosphorylated AKT (at residue Ser473) in EOC cells. (B, C) Enhanced EOC spheroid dispersion due to ALK3QD is decreased by treatment with the AKT inhibitor, Akti-1/2 (5 mM).

2.4 Discussion

The multicellular spheroids found in EOC malignant ascites possess distinct biological properties due to their 3D architecture and downstream signalling afforded by the tumour sphere structure^{2,30}. For example, the formation of EOC multi-cellular clusters provides protection against anoikis allowing these cancer cells to survive in ascites and seed metastatic tumours³¹. Therefore, identifying signalling pathways that contribute to the formation or disruption of EOC spheroids will provide new potential therapeutic targets that may also facilitate killing of solid tumour cells given their common 3D structure. We have shown previously that EOC cells express an intact and functional BMP signalling pathway, which directly impacts several key characteristics of a transformed cell phenotype^{12,13}. Here we have exploited the *in vitro* EOC spheroid model system, to uncover novel actions of the BMP signalling pathway in EOC pathobiology (Figure 2.9). Interestingly, we have found that endogenous BMP signalling in EOC cells is down-regulated during spheroid formation. To determine whether this reduction in BMP signalling has functional implications for the formation of EOC spheroids we generated cells with constitutive activation of the pathway. Indeed, expression of the constitutively-active BMP type I receptor ALK3QD caused a decrease in EOC cell cohesion during spheroid formation. Additionally, enhanced BMP signalling activity subsequently resulted in increased motility of EOC cells dispersing from spheroids that attached to the culture dish. At the protein level we determined that activated BMP signalling resulted in activation of the AKT signalling pathway in human EOC cells. Therefore, the phenotypic changes induced by BMP signalling in EOC spheroids may, in part, be mediated by its effects on AKT signalling.

The process of forming multi-cellular aggregates in suspension, akin to what occurs in malignant ascites, results in the down-regulation of endogenous BMP signalling. The genes encoding several BMP ligands showed significantly reduced expression during spheroid formation when compared to proliferating adherent monolayer cells, which was directly correlated with reduced levels of phosphorylated BMP R-Smad protein, thus implying that autocrine activation of the pathway is reduced in spheroid EOC cells. The downregulation of BMP signalling in EOC spheroid cells could occur through several

mechanisms. Several extracellular antagonists exist for BMP signalling, including Noggin, Chordin and Gremlin and other related proteins³². Moreover, BMP signalling induces the transcriptional activation of target genes encoding inhibitory Smad proteins, Smad6 and Smad7. Smad6/7 function at several points in the pathway, namely to inhibit R-Smad phosphorylation, and Smad complex formation and its transcriptional activity³³⁻³⁵. This mechanism is likely not operational in EOC spheroid cells because Smad6/7 mRNA expression does not change in EOC spheroids, and Smad6 protein levels are not consistent among EOC cells and spheroids generated from patient samples (data not shown). We also demonstrate that increased turnover of R-Smads by SMURF1-mediated ubiquitinylation is not a likely mechanism, since SMURF1 levels are in fact decreased in expression in EOC spheroids. This indicates that turnover of Smads is reduced in spheroids leading to the subsequent accumulation of Smad1/5 as we observed. This increase in BMP R-Smad protein levels may represent a compensatory response to the decrease in endogenous BMP signalling during EOC cell spheroid formation. Consequently, the reduction in expression of the major BMP ligands expressed in EOC cells, *i.e.* BMP4, BMP2, and BMP6, likely represents the mechanism for downregulated BMP signalling in EOC spheroids. This is the first time that decreased endogenous BMP signalling has been observed during spheroid formation. This is in contrast to the data demonstrating that BMP signalling is elevated in primary EOC cells and in solid tumour samples compared to normal ovarian surface epithelial cells^{7,12,17}. Thus, our results provide new insight about the dynamics of BMP signalling within EOC spheroids, which represent a unique transitional step for malignant cells between the primary tumour and secondary metastases².

The process of multicellular spheroid formation is complex and involves the coordinated action of different cell adhesion molecules. During the initial stages of spheroid formation, cell-cell adhesion is primarily mediated by the actions of integrins and cadherins^{20,36,37}. By analysing several markers for EMT, we observed that EOC cells induce an EMT phenotype during spheroid formation, defined by a substantial decrease in the gene expression of the cell-cell adhesion molecule E-cadherin. This implies that EOC spheroid compaction likely depends on additional molecules or processes, such as fibronectin, vimentin or actomyosin-mediated contractility as seen in other spheroid

systems^{2,37-39}. Since endogenous BMP signalling is reduced during spheroid formation, we propose that induction of the EMT phenotype in EOC spheroid cells does not require activation of BMP signalling. We noted, however, that the general induction of EMT in EOC spheroids is sustained in the presence of ectopic activated BMP signalling, a result which is supported by previous studies showing that BMP stimulation can induce EMT^{11,13,40}. We also observed an unexpected slight but significantly greater increase in the induction of E-cadherin expression in ALK3^{QD} expressing patient derived EOC spheroid cells relative to GFP transduced cells. This up regulation may be related to the unique microenvironment of the spheroid counteracting the EMT inducing properties of activated BMP signalling to maintain cell-cell contacts. The decreased spheroid integrity that occurs as a result of activated BMP signalling may be due to the lack of typical late-step spheroid compaction. In fact, the reduction in EOC spheroid compaction in the presence of activated BMP signalling may provide cells with an increased propensity to attach and disperse during secondary metastasis formation (as modeled by spheroid reattachment and dispersion *in vitro*).

Reattachment of EOC spheroids to a hospitable substratum and the subsequent dispersion of cells and expansion via cell proliferation and motility are necessary to achieve secondary metastasis^{2,41,42}. In response to activated BMP signalling, EOC spheroids have a significantly increased ability to reattach and disperse due to increased cell adhesion and motility and not cell proliferation. This result conforms to previous data indicating that BMP signalling has no effect on EOC cell proliferation, but induces a cell spreading phenotype, enhances motility and adhesion to several ECM components^{13,17}.

The phenotypic response of altered cell motility due to BMP signalling usually occurs in a Smad-independent manner utilizing other converging intracellular signalling pathways^{43,44}. In this report, we determined that levels of phosphorylated AKT were significantly elevated in EOC cells and spheroids in response to activated BMP signalling, thus providing a further mechanism for BMP-mediated changes in cell adhesion and motility. There has been growing evidence for crosstalk between the BMP and PI3K-AKT-mTOR signalling pathways. For example, AKT kinase is activated by BMP2 stimulation of mouse myoblast C2C12 cells, an effect that is inhibited by the BMP

type I receptor specific inhibitor LDN-193189²¹. Stimulation of vascular smooth muscle cells with BMP2 induces cell motility in a phospho-AKT dependent manner via the action of Rac1 and RhoA GTPases⁴⁵. In addition, activated BMP signalling enhances cell motility, invasion and EMT via the PI3K-AKT pathway in other cancer cell types⁴⁶⁻⁵⁰. Thus, it will be important to identify whether BMP activation of AKT employs common or different mechanisms in EOC cells and spheroids, as well as the functional implications of this signalling on the malignant characteristics of EOC.

Our laboratory has independent evidence that the PI3K-AKT pathway is down-regulated endogenously during EOC spheroid formation, yet its activation is required again during spheroid reattachment and cell dispersion. Taken together, AKT and BMP signalling are co-ordinately down-regulated during EOC spheroid formation. Perhaps sustained AKT activity due to enforced BMP signalling leads to less-cohesive spheroid formation yet enhances cell dispersion after re-attachment (Figure 2.9). This idea is supported by our studies in which treatment of ALK3^{QD}-expressing spheroids with an Akt1/2 inhibitor results in a partial restoration of spheroid dispersion area to that of controls. Thus, we believe that activation of the AKT pathway is functionally required and plays an important role in BMP-induced changes in spheroid behaviour and ultimately EOC metastasis. As mentioned previously, the presence of BMP signalling in EOC is correlated with significantly shorter survival periods for patients with advanced stage disease⁷. One mechanism for the deleterious effects of active BMP signalling in EOC may be downstream activation of the AKT pathway, another established marker for poor patient prognosis^{51,52}. Thus, further exploration of the interaction between these two pathways is currently underway and may determine the therapeutic potential of targeting BMP signalling or AKT activity during EOC metastasis.

Our previous and current studies implicate disparate roles for BMP signalling during different steps of the metastatic cascade in EOC pathogenesis. Overall, the data supports the notion that BMP signalling has bi-phasic influences: reduced activity may be required for EOC spheroid formation during dissemination of cells from the primary tumour, yet reactivation is required for more efficient establishment of secondary metastases (Figure 2.9). As such, the conflicting roles for BMP signalling during EOC progression are

similar to the multifaceted effects of the related TGF β pathway at early and late stages of multiple human cancers⁵³. Collectively our data indicates the critical necessity to assess the effects of signalling systems at each step of the EOC metastatic process to assess the overall therapeutic potential of targeting a particular pathway.

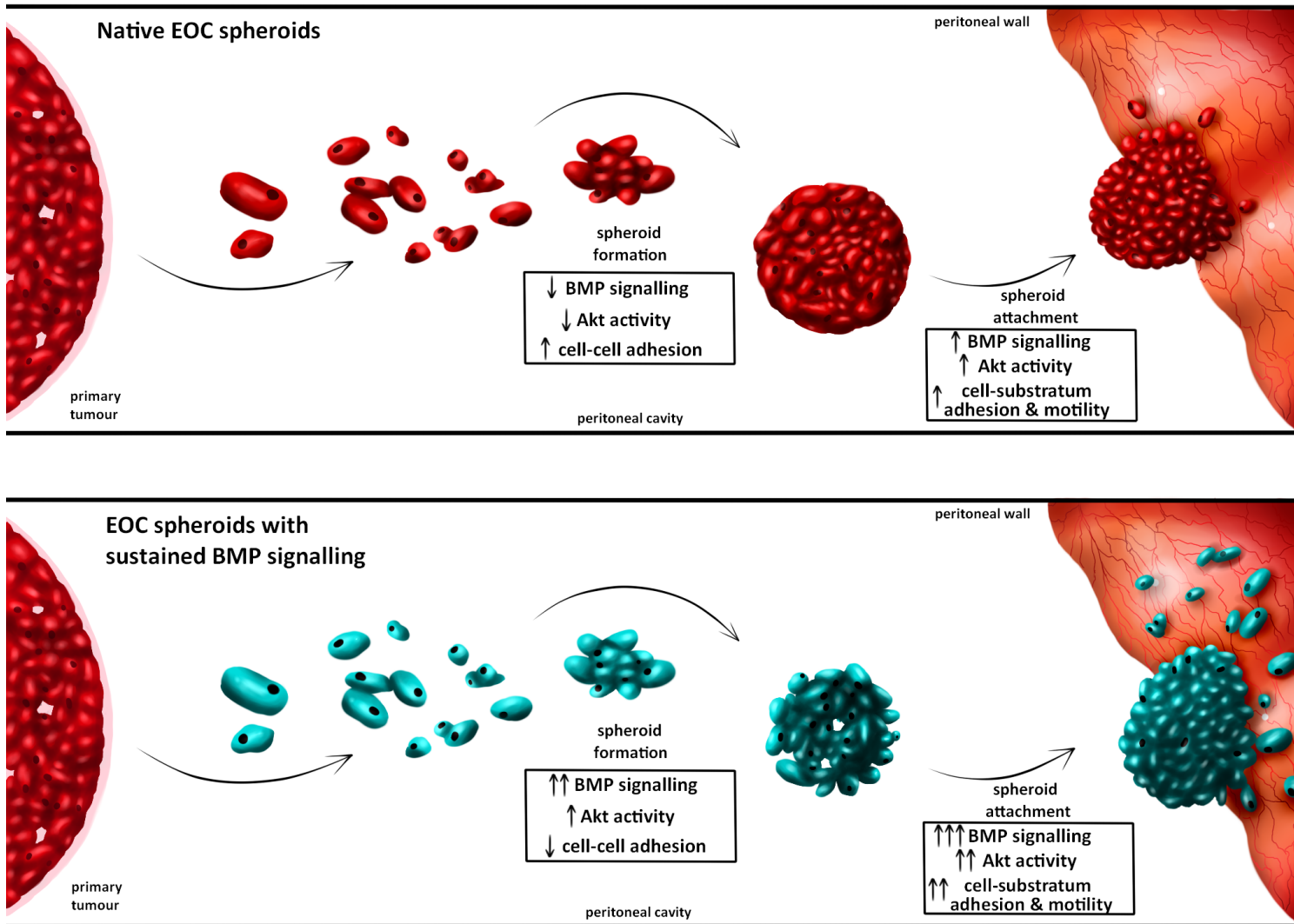


Figure 2.9: Proposed model of BMP signalling in EOC metastasis.

Metastatic EOC cells disseminating from the primary tumour naturally aggregate to form multicellular spheroids while in suspension in ascites in the peritoneal cavity. EOC spheroids endogenously down-regulate both BMP and AKT signalling, which may be required for tight cell-cell cohesion. Upon reattachment of EOC spheroids, however, cells reactivate the BMP and AKT pathways for efficient adhesion and dispersion to establish secondary metastases (*e.g.* on peritoneal wall). Ectopic activation of BMP signalling using $ALK3^{QD}$, with the concomitant increase in AKT activity, alters this dynamic process by rendering EOC spheroids more loosely-aggregated while in suspension, which ultimately enhances their ability to disperse upon reattachment.

2.5 References

1. Lengyel, E. Ovarian cancer development and metastasis. *American Journal of Pathology* **177**, 1053-1064 (2010).
2. Shield, K., Ackland, M.L., Ahmed, N. & Rice, G.E. Multicellular spheroids in ovarian cancer metastases: Biology and pathology. *Gynecol Oncol* **113**, 143-148 (2009).
3. Kim, T.H., Mount, C.W., Gombotz, W.R. & Pun, S.H. The delivery of doxorubicin to 3-D multicellular spheroids and tumors in a murine xenograft model using tumor-penetrating triblock polymeric micelles. *Biomaterials* **31**, 7386-7397 (2010).
4. Grun, B., *et al.* Three-dimensional in vitro cell biology models of ovarian and endometrial cancer. *Cell Prolif* **42**, 219-228 (2009).
5. Kim, J.B. Three-dimensional tissue culture models in cancer biology. *Seminars in cancer biology* **15**, 365-377 (2005).
6. Herrera, B., van Dinther, M., Ten Dijke, P. & Inman, G.J. Autocrine bone morphogenetic protein-9 signals through activin receptor-like kinase-2/Smad1/Smad4 to promote ovarian cancer cell proliferation. *Cancer Res* **69**, 9254-9262 (2009).
7. Le Page, C., *et al.* BMP-2 signaling in ovarian cancer and its association with poor prognosis. *Journal of ovarian research* **2**, 4 (2009).
8. Ma, Y., Ma, L., Guo, Q. & Zhang, S. Expression of bone morphogenetic protein-2 and its receptors in epithelial ovarian cancer and their influence on the prognosis of ovarian cancer patients. *J Exp Clin Cancer Res* **29**, 85.
9. Moll, F., *et al.* Chordin is underexpressed in ovarian tumors and reduces tumor cell motility. *Faseb J* **20**, 240-250 (2006).
10. Pils, D., *et al.* BAMBI is overexpressed in ovarian cancer and co-translocates with Smads into the nucleus upon TGF-beta treatment. *Gynecol Oncol* **117**, 189-197.
11. Shepherd, T.G., Mujoomdar, M.L. & Nachtigal, M.W. Constitutive activation of BMP signalling abrogates experimental metastasis of OVCA429 cells via reduced cell adhesion. *Journal of ovarian research* **3**, 5 (2010).
12. Shepherd, T.G., Theriault, B.L. & Nachtigal, M.W. Autocrine BMP4 signalling regulates ID3 proto-oncogene expression in human ovarian cancer cells. *Gene* **414**, 95-105 (2008).
13. Theriault, B.L., Shepherd, T.G., Mujoomdar, M.L. & Nachtigal, M.W. BMP4 induces EMT and Rho GTPase activation in human ovarian cancer cells. *Carcinogenesis* **28**, 1153-1162 (2007).
14. Dunfield, L.D., Dwyer, E.J. & Nachtigal, M.W. TGF beta-induced Smad signaling remains intact in primary human ovarian cancer cells. *Endocrinology* **143**, 1174-1181 (2002).
15. Wei, X., *et al.* Mullerian inhibiting substance preferentially inhibits stem/progenitors in human ovarian cancer cell lines compared with chemotherapeutics. *Proceedings of the National Academy of Sciences of the United States of America* **107**, 18874-18879 (2010).

16. Shepherd, T.G., Theriault, B.L., Campbell, E.J. & Nachtigal, M.W. Primary culture of ovarian surface epithelial cells and ascites-derived ovarian cancer cells from patients. *Nature protocols* **1**, 2643-2649 (2006).
17. Shepherd, T.G. & Nachtigal, M.W. Identification of a putative autocrine bone morphogenetic protein-signaling pathway in human ovarian surface epithelium and ovarian cancer cells. *Endocrinology* **144**, 3306-3314 (2003).
18. Murakami, G., Watabe, T., Takaoka, K., Miyazono, K. & Imamura, T. Cooperative inhibition of bone morphogenetic protein signaling by Smurf1 and inhibitory Smads. *Mol Biol Cell* **14**, 2809-2817 (2003).
19. Zhu, H., Kavsak, P., Abdollah, S., Wrana, J.L. & Thomsen, G.H. A SMAD ubiquitin ligase targets the BMP pathway and affects embryonic pattern formation. *Nature* **400**, 687-693 (1999).
20. Ivascu, A. & Kubbies, M. Diversity of cell-mediated adhesions in breast cancer spheroids. *International journal of oncology* **31**, 1403-1413 (2007).
21. Boergemann, J.H., Kopf, J., Yu, P.B. & Knaus, P. Dorsomorphin and LDN-193189 inhibit BMP-mediated Smad, p38 and Akt signalling in C2C12 cells. *International Journal of Biochemistry and Cell Biology* **42**, 1802-1807 (2010).
22. Cuny, G.D., *et al.* Structure-activity relationship study of bone morphogenetic protein (BMP) signaling inhibitors. *Bioorg Med Chem Lett* **18**, 4388-4392 (2008).
23. Lamb, J. The Connectivity Map: a new tool for biomedical research. *Nature reviews* **7**, 54-60 (2007).
24. Lamb, J., *et al.* The Connectivity Map: using gene-expression signatures to connect small molecules, genes, and disease. *Science* **313**, 1929-1935 (2006).
25. Zhang, S.D. & Gant, T.W. A simple and robust method for connecting small-molecule drugs using gene-expression signatures. *BMC bioinformatics* **9**, 258 (2008).
26. Bast, R.C., Jr., Hennessy, B. & Mills, G.B. The biology of ovarian cancer: new opportunities for translation. *Nature reviews* **9**, 415-428 (2009).
27. Correa, R.J., Peart, T., Valdes, Y.R., Dimattia, G.E. & Shepherd, T.G. Modulation of AKT activity is associated with reversible dormancy in ascites-derived epithelial ovarian cancer spheroids. *Carcinogenesis* **33**, 49-58 (2012).
28. Arboleda, M.J., *et al.* Overexpression of AKT2/protein kinase Bbeta leads to up-regulation of beta1 integrins, increased invasion, and metastasis of human breast and ovarian cancer cells. *Cancer Res* **63**, 196-206 (2003).
29. Meng, Q., Xia, C., Fang, J., Rojanasakul, Y. & Jiang, B.H. Role of PI3K and AKT specific isoforms in ovarian cancer cell migration, invasion and proliferation through the p70S6K1 pathway. *Cell Signal* **18**, 2262-2271 (2006).
30. Ahmed, N., Thompson, E.W. & Quinn, M.A. Epithelial-mesenchymal interconversions in normal ovarian surface epithelium and ovarian carcinomas: an exception to the norm. *J Cell Physiol* **213**, 581-588 (2007).
31. Tang, M.K., Zhou, H.Y., Yam, J.W. & Wong, A.S. c-Met overexpression contributes to the acquired apoptotic resistance of nonadherent ovarian cancer cells through a cross talk mediated by phosphatidylinositol 3-kinase and extracellular signal-regulated kinase 1/2. *Neoplasia* **12**, 128-138 (2010).
32. Balemans, W. & Van Hul, W. Extracellular regulation of BMP signaling in vertebrates: a cocktail of modulators. *Dev Biol* **250**, 231-250 (2002).

33. Goto, K., Kamiya, Y., Imamura, T., Miyazono, K. & Miyazawa, K. Selective inhibitory effects of Smad6 on bone morphogenetic protein type I receptors. *J Biol Chem* **282**, 20603-20611 (2007).
34. Itoh, F., *et al.* Promoting bone morphogenetic protein signaling through negative regulation of inhibitory Smads. *Embo J* **20**, 4132-4142 (2001).
35. Kamiya, Y., Miyazono, K. & Miyazawa, K. Smad7 inhibits transforming growth factor-beta family type I receptors through two distinct modes of interaction. *Journal of Biological Chemistry* **285**, 30804-30813 (2010).
36. Casey, R.C., *et al.* Beta 1-integrins regulate the formation and adhesion of ovarian carcinoma multicellular spheroids. *Am J Pathol* **159**, 2071-2080 (2001).
37. Kim, Y.J., *et al.* Modulating the strength of cadherin adhesion: evidence for a novel adhesion complex. *J Cell Sci* **118**, 3883-3894 (2005).
38. Napolitano, A.P., Chai, P., Dean, D.M. & Morgan, J.R. Dynamics of the self-assembly of complex cellular aggregates on micromolded nonadhesive hydrogels. *Tissue Eng* **13**, 2087-2094 (2007).
39. Tzanakakis, E.S., Hansen, L.K. & Hu, W.S. The role of actin filaments and microtubules in hepatocyte spheroid self-assembly. *Cell Motil Cytoskeleton* **48**, 175-189 (2001).
40. Gamell, C., *et al.* BMP2 induction of actin cytoskeleton reorganization and cell migration requires PI3-kinase and Cdc42 activity. *J Cell Sci* **121**, 3960-3970 (2008).
41. Burleson, K.M., Boente, M.P., Pambuccian, S.E. & Skubitz, A.P. Disaggregation and invasion of ovarian carcinoma ascites spheroids. *Journal of translational medicine* **4**, 6 (2006).
42. Iwanicki, M., *et al.* Ovarian cancer spheroids use myosin-generated force to clear the mesothelium. *Cancer Discov* (2011).
43. Derynck, R. & Zhang, Y.E. Smad-dependent and Smad-independent pathways in TGF-beta family signalling. *Nature* **425**, 577-584 (2003).
44. Guo, X. & Wang, X.F. Signaling cross-talk between TGF-beta/BMP and other pathways. *Cell Res* **19**, 71-88 (2009).
45. Perez, V.A., *et al.* BMP promotes motility and represses growth of smooth muscle cells by activation of tandem Wnt pathways. *Journal of Cell Biology* **192**, 171-188 (2011).
46. Chen, X., Liao, J., Lu, Y., Duan, X. & Sun, W. Activation of the PI3K/Akt Pathway Mediates Bone Morphogenetic Protein 2-Induced Invasion of Pancreatic Cancer Cells Panc-1. *Pathology Oncology Research* (2011).
47. Graham, T.R., *et al.* PI3K/Akt-dependent transcriptional regulation and activation of BMP-2-Smad signaling by NF-kappaB in metastatic prostate cancer cells. *Prostate* **69**, 168-180 (2009).
48. Kang, M.H., *et al.* Inhibition of PI3 kinase/Akt pathway is required for BMP2-induced EMT and invasion. *Oncol Rep* **22**, 525-534 (2009).
49. Kang, M.H., Kim, J.S., Seo, J.E., Oh, S.C. & Yoo, Y.A. BMP2 accelerates the motility and invasiveness of gastric cancer cells via activation of the phosphatidylinositol 3-kinase (PI3K)/Akt pathway. *Experimental cell research* **316**, 24-37 (2010).

50. Langenfeld, E.M., Kong, Y. & Langenfeld, J. Bone morphogenetic protein-2-induced transformation involves the activation of mammalian target of rapamycin. *Mol Cancer Res* **3**, 679-684 (2005).
51. Davidson, B., *et al.* Proteomic analysis of malignant ovarian cancer effusions as a tool for biologic and prognostic profiling. *Clinical Cancer Research* **12**, 791-799 (2006).
52. Schilder, R.J., *et al.* Phase II evaluation of imatinib mesylate in the treatment of recurrent or persistent epithelial ovarian or primary peritoneal carcinoma: a Gynecologic Oncology Group Study. *Journal of Clinical Oncology* **26**, 3418-3425 (2008).
53. Massague, J. TGFbeta in Cancer. *Cell* **134**, 215-230 (2008).

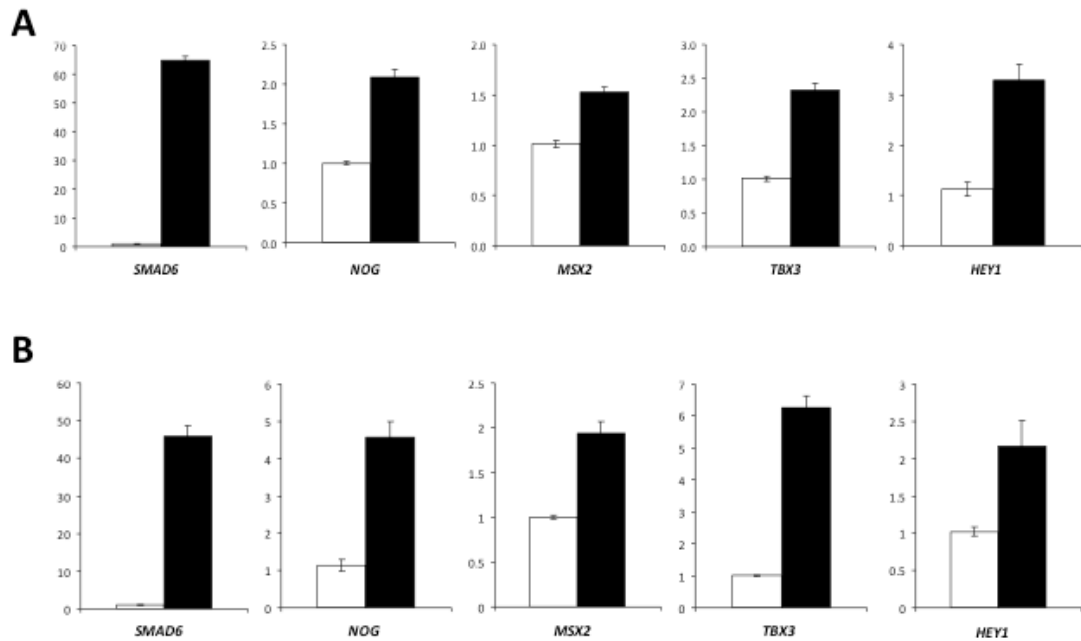


Figure S2.1: Validation of microarray results by quantitative RT-PCR analysis of specific up-regulated genes.

SMAD6, *NOG*, *MSX2*, *TBX3*, and *HEY1* mRNA expression was detected using human-specific primers for each and cDNA samples generated from adherent primary human EOC cells (A) and spheroids (B) transduced with either Ad-ALK3^{QD} or Ad-GFP control virus. Relative expression was normalized to Ad-GFP transduced cells (set to 1) and *GAPDH* mRNA served as an internal control.

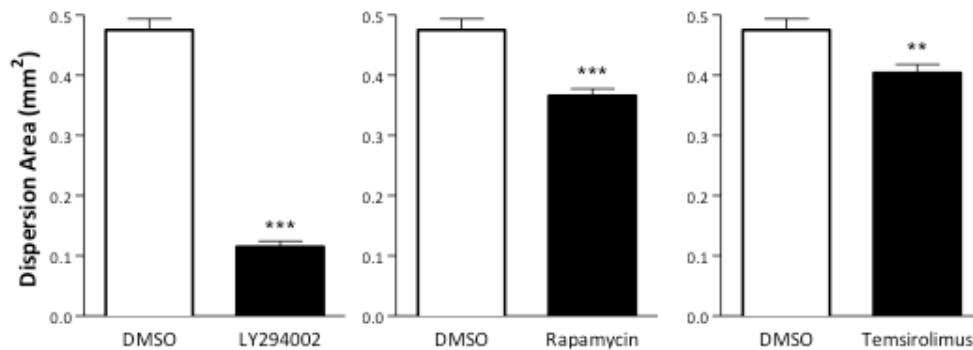


Figure S2.2: Inhibition of PI3K-mTOR signalling reduces EOC cell dispersion upon spheroid reattachment.

EOC cells from patient ascites samples (EOC30 and EOC67) were seeded to ULA cluster plates to generate spheroids over three days. EOC spheroids were individually seeded to standard tissue culture plastic and treated with LY294002, rapamycin, or temsirolimus (Torisel[®]) or DMSO vehicle control. Images of spheroids were captured (>40 per treatment group) at 24 h post-reattachment and dispersion area was quantified using *ImageJ* software. (** $p < 0.01$; *** $p < 0.001$ using Student's *t*-test).

Table S2.1: Genes with increased expression due to Alk3QD in adherent EOC cells.

| Gene Title | Gene Symbol | Probe Set ID | Fold Change |
|--|--------------|--------------|-------------|
| loricrin | LOR | 207720_at | 63.124 |
| calcitonin-related polypeptide beta | CALCB | 214636_at | 17.708 |
| S100 calcium binding protein P | S100P | 204351_at | 14.716 |
| heat shock 70kDa protein 6 (HSP70B) | HSPA6 | 213418_at | 9.249 |
| distal-less homeobox 2 | DLX2 | 207147_at | 8.543 |
| cholecystokinin | CCK | 205827_at | 7.97 |
| pregnancy specific beta-1-glycoprotein 5 | PSG5 | 204830_x_at | 7.951 |
| FLJ35409 protein | FLJ35409 | 1559506_x_at | 7.665 |
| gap junction protein, delta 3, 31.9kDa | GJD3 | 230025_at | 7.533 |
| acetoacetyl-CoA synthetase-like | AACSL | 1570020_at | 6.901 |
| pregnancy specific beta-1-glycoprotein 3 | PSG3 | 211741_x_at | 6.892 |
| folate receptor 3 (gamma) | FOLR3 | 206371_at | 6.787 |
| synaptotagmin XV | SYT15 | 1560879_a_at | 6.497 |
| similar to hCG2038656 | LOC100129058 | 1564300_at | 6.285 |
| KIT ligand | KITLG | 211124_s_at | 6.282 |
| dual specificity phosphatase 2 | DUSP2 | 204794_at | 6.138 |
| podocalyxin-like | PODXL | 201578_at | 6.085 |
| claudin 4 | CLDN4 | 201428_at | 6.019 |
| SMAD family member 6 | SMAD6 | 207069_s_at | 5.782 |
| FEZ family zinc finger 2 | FEZF2 | 233972_s_at | 5.611 |
| keratin associated protein 4-12 | KRTAP4-12 | 224269_at | 5.553 |
| chloride intracellular channel 2 | CLIC2 | 213415_at | 5.416 |
| aldo-keto reductase family 1, member C2 (dihydrodiol dehydrogenase 2; bile acid binding protein; 3- α - | AKR1C2 | 211653_x_at | 5.339 |
| glutamate receptor, ionotropic, AMPA 2 | GRIA2 | 241172_at | 5.324 |
| solute carrier family 16, member 14 (monocarboxylic acid transporter 14) | SLC16A14 | 238029_s_at | 5.109 |
| interleukin 9 | IL9 | 208193_at | 5.086 |
| gremlin 2, cysteine knot superfamily, homolog (Xenopus laevis) | GREM2 | 235504_at | 5.071 |
| tumor necrosis factor (ligand) superfamily, member 9 | TNFSF9 | 206907_at | 4.802 |
| chemokine (C-C motif) ligand 26 | CCL26 | 223710_at | 4.725 |
| gremlin 2, cysteine knot superfamily, homolog (Xenopus laevis) | GREM2 | 240509_s_at | 4.665 |
| involucrin | IVL | 214599_at | 4.612 |
| hypothetical protein MGC16121 | MGC16121 | 228235_at | 4.348 |
| XK, Kell blood group complex subunit-related family, member 6 | XKR6 | 1557436_at | 4.344 |
| hemicentin 2 | HMCN2 | 241650_x_at | 4.341 |
| ameloblastin (enamel matrix protein) | AMBN | 221114_at | 4.3 |
| fibrinogen C domain containing 1 | FIBCD1 | 240042_at | 4.27 |
| dual specificity phosphatase 26 (putative) | DUSP26 | 219144_at | 4.234 |
| semaphorin 7A, GPI membrane anchor (John Milton Hagen blood group) | SEMA7A | 230345_at | 4.226 |
| aldo-keto reductase family 1, member C1 (dihydrodiol dehydrogenase 1; 20- α (3- α)-hydroxyster | AKR1C1 | 204151_x_at | 4.2 |
| transmembrane protein 132E | TMEM132E | 243708_at | 4.196 |
| keratin associated protein 2-4 | KRTAP2-4 | 1555673_at | 4.146 |
| hypothetical LOC441052 | LOC441052 | 232443_at | 4.131 |
| hyaluronan synthase 2 | HAS2 | 206432_at | 4.122 |
| kinesin family member 7 | KIF7 | 229405_at | 4.102 |
| keratin associated protein 4-1 | KRTAP4-1 | 234635_at | 4.082 |
| CD24 molecule | CD24 | 209772_s_at | 4.078 |
| leucine rich repeat containing 4 | LRRC4 | 223552_at | 4.043 |
| polymerase (RNA) II (DNA directed) polypeptide A, 220kDa | POLR2A | 217415_at | 4.005 |
| G protein-coupled receptor 56 | GPR56 | 212070_at | 3.941 |
| gremlin 2, cysteine knot superfamily, homolog (Xenopus laevis) | GREM2 | 220794_at | 3.908 |
| folate receptor 2 (fetal) | FOLR2 | 204829_s_at | 3.882 |
| hypothetical protein LOC284542 | LOC284542 | 230920_at | 3.88 |
| zinc finger protein 114 | ZNF114 | 1552946_at | 3.878 |
| echinoderm microtubule associated protein like 1 | EML1 | 204797_s_at | 3.853 |
| neuregulin 1 | NRG1 | 206343_s_at | 3.837 |
| synaptotagmin XV | SYT15 | 1560878_at | 3.835 |
| hypothetical protein MGC16121 | MGC16121 | 227488_at | 3.823 |
| neuronal cell adhesion molecule | NRCAM | 204105_s_at | 3.777 |
| actin, alpha, cardiac muscle 1 | ACTC1 | 205132_at | 3.766 |
| zinc finger protein 831 | ZNF831 | 1558826_at | 3.752 |
| extra spindle pole bodies homolog 1 (S. cerevisiae) | ESPL1 | 204817_at | 3.747 |
| v-myb myeloblastosis viral oncogene homolog (avian) | MYB | 204798_at | 3.721 |
| Atonal homolog 8 (Drosophila) | ATOH8 | 1558706_a_at | 3.716 |
| pregnancy specific beta-1-glycoprotein 9 | PSG9 | 209594_x_at | 3.712 |
| mal, T-cell differentiation protein-like | MALL | 209373_at | 3.705 |
| synaptopodin | SYNPO | 235914_at | 3.697 |
| noggin | NOG | 231798_at | 3.683 |
| synapsin I | SYN1 | 221914_at | 3.657 |

Table S2.1 cont'd.

| | | | |
|--|--------------|--------------|-------|
| protocadherin 10 | PCDH10 | 1552925_at | 3.641 |
| Kruppel-like factor 4 (gut) | KLF4 | 220266_s_at | 3.638 |
| clusterin | CLU | 222043_at | 3.632 |
| aldo-keto reductase family 1, member C2 (dihydrodiol dehydrogenase 2; bile acid binding protein; 3- α - | AKR1C2 | 209699_x_at | 3.62 |
| GIPC PDZ domain containing family, member 3 | GIPC3 | 236730_at | 3.617 |
| glutathione peroxidase 3 (plasma) | GPX3 | 201348_at | 3.601 |
| coiled-coil domain containing 85A | CCDC85A | 235228_at | 3.596 |
| LIM domain only 2 (rhombotin-like 1) | LMO2 | 204249_s_at | 3.592 |
| vasoactive intestinal peptide | VIP | 206577_at | 3.532 |
| solute carrier family 25 (mitochondrial carrier; ornithine transporter) member 15 | SLC25A15 | 222705_s_at | 3.524 |
| DIRAS family, GTP-binding RAS-like 3 | DIRAS3 | 215506_s_at | 3.49 |
| potassium voltage-gated channel, KQT-like subfamily, member 5 | KCNQ5 | 244623_at | 3.489 |
| trafficking protein particle complex 2 | TRAPPC2 | 1562349_at | 3.483 |
| WD repeat domain 33 | WDR33 | 243832_at | 3.466 |
| stimulated by retinoic acid gene 6 homolog (mouse) | STRA6 | 221701_s_at | 3.465 |
| acidic (leucine-rich) nuclear phosphoprotein 32 family, member C | ANP32C | 208538_at | 3.454 |
| pappalysin 2 | PAPPA2 | 228237_at | 3.404 |
| CD24 molecule | CD24 | 208650_s_at | 3.376 |
| hypothetical gene supported by AK026773 | LOC440863 | 234478_at | 3.368 |
| myosin binding protein H | MYBPH | 206304_at | 3.363 |
| RASD family, member 2 | RASD2 | 223634_at | 3.36 |
| AF4/FMR2 family, member 2 | AFF2 | 206105_at | 3.356 |
| doublecortin domain containing 5 | DCDC5 | 232603_at | 3.346 |
| aldo-keto reductase family 1, member C1 (dihydrodiol dehydrogenase 1; 20- α (3- α)-hydroxyster | AKR1C1 | 216594_x_at | 3.321 |
| CD300 molecule-like family member g | CD300LG | 1552509_a_at | 3.316 |
| pleckstrin homology domain containing, family A member 7 | PLEKHA7 | 228450_at | 3.276 |
| TMF1-regulated nuclear protein 1 | TRNP1 | 227862_at | 3.268 |
| myosin, heavy chain 13, skeletal muscle | MYH13 | 208208_at | 3.243 |
| hypothetical LOC100126784 | LOC100126784 | 240407_at | 3.228 |
| hypothetical protein LOC254057 | LOC254057 | 232370_at | 3.226 |
| RAB39B, member RAS oncogene family | RAB39B | 230075_at | 3.204 |
| UPF0632 protein A | LOC388630 | 244472_at | 3.199 |
| ankyrin repeat domain 20 family, member A pseudogene | LOC375010 | 1566147_a_at | 3.182 |
| small nucleolar RNA host gene 4 (non-protein coding) | SNHG4 | 1565325_at | 3.172 |
| TIMP metalloproteinase inhibitor 4 | TIMP4 | 206243_at | 3.169 |
| similar to Primase, DNA, polypeptide 2 (58kDa) /// primase, DNA, polypeptide 2 (58kDa) | LOC100134355 | 215709_at | 3.162 |
| family with sequence similarity 83, member G | FAM83G | 228587_at | 3.158 |
| Jagged 1 (Alagille syndrome) | JAG1 | 231183_s_at | 3.146 |
| neuronal cell adhesion molecule 1 | NCAM1 | 212843_at | 3.145 |
| solute carrier family 6 (neutral amino acid transporter), member 15 | SLC6A15 | 232263_at | 3.138 |
| X-ray repair complementing defective repair in Chinese hamster cells 4 | XRCC4 | 210812_at | 3.109 |
| breast cancer 1, early onset | BRCA1 | 211851_x_at | 3.096 |
| similar to TLK2 protein /// similar to TLK2 protein /// similar to Serine/threonine-protein kinase tousled-lik | LOC100128729 | 232585_at | 3.088 |
| echinoderm microtubule associated protein like 1 | EML1 | 204796_at | 3.062 |
| crystallin, alpha B | CRYAB | 209283_at | 3.058 |
| exoribonuclease 2 | ERI2 | 240604_at | 3.048 |
| retinoic acid induced 2 | RAI2 | 219440_at | 3.039 |
| glutathione peroxidase 3 (plasma) | GPX3 | 214091_s_at | 3.03 |
| IGF-like family member 2 | IGFL2 | 231148_at | 3.027 |
| retinitis pigmentosa 1 (autosomal dominant) | RP1 | 224021_at | 3.013 |
| chromosome 14 open reading frame 145 | C14orf145 | 244033_at | 3.01 |
| Hypothetical LOC150538 | FLJ32063 | 235147_at | 3.005 |
| ELMO/CED-12 domain containing 1 | ELMOD1 | 231930_at | 2.984 |
| jagged 1 (Alagille syndrome) | JAG1 | 216268_s_at | 2.974 |
| glycerol-3-phosphate dehydrogenase 2 (mitochondrial) | GPD2 | 211613_s_at | 2.971 |
| extra spindle pole bodies homolog 1 (S. cerevisiae) | ESPL1 | 38158_at | 2.953 |
| chromosome 14 open reading frame 145 | C14orf145 | 1557755_at | 2.936 |
| CD24 molecule | CD24 | 266_s_at | 2.927 |
| aurora kinase B | AURKB | 209464_at | 2.912 |
| dynein, axonemal, heavy chain 12 | DNAH12 | 1563097_at | 2.91 |
| hypothetical protein LOC283278 | LOC283278 | 242417_at | 2.907 |
| fatty acid binding protein 5 (psoriasis-associated) | FABP5 | 202345_s_at | 2.898 |
| THAP domain containing, apoptosis associated protein 2 | THAP2 | 230380_at | 2.893 |
| DnaJ (Hsp40) homolog, subfamily A, member 4 | DNAJA4 | 1554334_a_at | 2.89 |
| formin 2 | FMN2 | 1555471_a_at | 2.877 |
| paternally expressed 10 | PEG10 | 212092_at | 2.875 |
| atonal homolog 8 (Drosophila) | ATOH8 | 228890_at | 2.873 |
| T-box 3 | TBX3 | 219682_s_at | 2.871 |
| X-ray repair complementing defective repair in Chinese hamster cells 4 | XRCC4 | 210813_s_at | 2.866 |
| CD24 molecule | CD24 | 208651_x_at | 2.861 |

Table S2.1 cont'd.

| | | | |
|---|-------------------|--------------|-------|
| synovial sarcoma, X breakpoint 2 interacting protein | SSX2IP | 203018_s_at | 2.858 |
| RGD motif, leucine rich repeats, tropomodulin domain and proline-rich containing | RLTPR | 227216_at | 2.854 |
| placental growth factor | PGF | 209652_s_at | 2.84 |
| transketolase | TKT | 228205_at | 2.83 |
| formin 2 | FMN2 | 223618_at | 2.826 |
| cancer susceptibility candidate 4 | CASC4 | 1559635_at | 2.798 |
| t-complex 11 homolog (mouse) | TCP11 | 220378_at | 2.798 |
| synovial sarcoma, X breakpoint 2 interacting protein | SSX2IP | 210871_x_at | 2.788 |
| cholecystokinin A receptor | CKKAR | 211174_s_at | 2.772 |
| Na ⁺ /K ⁺ transporting ATPase interacting 2 | NKAIN2 | 242002_at | 2.762 |
| matrix metalloproteinase 3 (stromelysin 1, progelatinase) | MMP3 | 205828_at | 2.762 |
| synovial sarcoma, X breakpoint 2 interacting protein | SSX2IP | 203016_s_at | 2.759 |
| plexin A2 | PLXNA2 | 213030_s_at | 2.758 |
| ATP-binding cassette, sub-family C (CFTR/MRP), member 9 | ABCC9 | 208561_at | 2.758 |
| hypothetical protein LOC144481 | LOC144481 | 1559315_s_at | 2.755 |
| T-box 3 | TBX3 | 225544_at | 2.737 |
| replication protein A4, 34kDa | RPA4 | 221143_at | 2.733 |
| WD repeat domain 4 | WDR4 | 241937_s_at | 2.725 |
| X-ray repair complementing defective repair in Chinese hamster cells 4 | XRCC4 | 205071_x_at | 2.713 |
| T-box 3 | TBX3 | 229576_s_at | 2.707 |
| transient receptor potential cation channel, subfamily C, member 4 | TRPC4 | 224219_s_at | 2.703 |
| pyrophosphatase (inorganic) 2 | PPA2 | 1554499_s_at | 2.701 |
| Kruppel-like factor 4 (gut) | KLF4 | 221841_s_at | 2.701 |
| progesterin and adipoQ receptor family member IX | PAQR9 | 1558322_a_at | 2.7 |
| v-maf musculoaponeurotic fibrosarcoma oncogene homolog B (avian) | MAFB | 218559_s_at | 2.691 |
| tubulin, beta 2A /// tubulin, beta 2B | TUBB2A /// TUBB2B | 209372_x_at | 2.684 |
| cysteine-rich protein 2 | CRIP2 | 208978_at | 2.682 |
| pregnancy specific beta-1-glycoprotein 9 | PSG9 | 207733_x_at | 2.681 |
| actinin, alpha 2 | ACTN2 | 203861_s_at | 2.678 |
| synovial sarcoma, X breakpoint 2 interacting protein | SSX2IP | 203015_s_at | 2.675 |
| RNA binding motif protein, Y-linked, family 3, member A pseudogene | RBM3AP | 1565320_at | 2.669 |
| synovial sarcoma, X breakpoint 2 interacting protein | SSX2IP | 203019_x_at | 2.655 |
| serine/threonine/tyrosine kinase 1 | STYK1 | 220030_at | 2.649 |
| transforming growth factor, alpha | TGFA | 211258_s_at | 2.642 |
| jagged 1 (Alagille syndrome) | JAG1 | 209098_s_at | 2.639 |
| sperm specific antigen 2 | SSFA2 | 236207_at | 2.639 |
| v-maf musculoaponeurotic fibrosarcoma oncogene homolog B (avian) | MAFB | 222670_s_at | 2.619 |
| zinc finger and BTB domain containing 45 | ZBTB45 | 240551_at | 2.602 |
| regulator of G-protein signaling 4 | RGS4 | 204339_s_at | 2.602 |
| sprouty homolog 2 (Drosophila) | SPRY2 | 204011_at | 2.598 |
| X-ray repair complementing defective repair in Chinese hamster cells 4 | XRCC4 | 205072_s_at | 2.593 |
| E2F transcription factor 7 | E2F7 | 228033_at | 2.586 |
| lin-7 homolog B (C. elegans) | LIN7B | 241957_x_at | 2.583 |
| msh homeobox 2 | MSX2 | 210319_x_at | 2.581 |
| MAP/microtubule affinity-regulating kinase 2 | MARK2 | 211082_x_at | 2.581 |
| cystic fibrosis transmembrane conductance regulator (ATP-binding cassette sub-family C, member 7) | CFTR | 234706_x_at | 2.581 |
| solute carrier family 4, sodium bicarbonate cotransporter, member 4 | SLC4A4 | 210738_s_at | 2.565 |
| regulator of G-protein signaling 4 | RGS4 | 204338_s_at | 2.563 |
| synaptotagmin-like 3 | SYTL3 | 238423_at | 2.558 |
| fibulin 2 | FBLN2 | 203886_s_at | 2.542 |
| Hypothetical protein LOC100132244 | LOC100132244 | 229438_at | 2.538 |
| ELOVL family member 6, elongation of long chain fatty acids (FEN1/Elo2, SUR4/Elo3-like, yeast) | ELOVL6 | 204256_at | 2.531 |
| Fc receptor-like A | FCRLA | 235401_s_at | 2.527 |
| KN motif and ankyrin repeat domains 4 | KANK4 | 229125_at | 2.522 |
| jagged 1 (Alagille syndrome) | JAG1 | 209099_x_at | 2.519 |
| Sperm specific antigen 2 | SSFA2 | 229744_at | 2.516 |
| chromosome 10 open reading frame 116 | C10orf116 | 203571_s_at | 2.516 |
| frizzled homolog 8 (Drosophila) | FZD8 | 227405_s_at | 2.513 |
| cerebellin 2 precursor | CBLN2 | 242301_at | 2.508 |
| potassium voltage-gated channel, subfamily G, member 1 | KCNG1 | 214595_at | 2.507 |
| diacylglycerol kinase, gamma 90kDa | DGKG | 206395_at | 2.504 |
| olfactory receptor, family 2, subfamily J, member 2 | OR2J2 | 208508_s_at | 2.502 |
| microtubule-associated protein 1A | MAP1A | 203151_at | 2.502 |
| discoidin, CUB and LCCL domain containing 2 | DCBLD2 | 213873_at | 2.497 |
| ELOVL family member 6, elongation of long chain fatty acids (FEN1/Elo2, SUR4/Elo3-like, yeast) | ELOVL6 | 210868_s_at | 2.493 |
| solute carrier family 29 (nucleoside transporters), member 2 | SLC29A2 | 1560149_at | 2.484 |
| ubiquitin-like with PHD and ring finger domains 1 | UHRF1 | 225655_at | 2.484 |
| angiotensin II receptor, type 2 | AGTR2 | 222321_at | 2.481 |
| phosphatidylinositol transfer protein, membrane-associated 2 | PITPNM2 | 1552924_a_at | 2.476 |
| suppressor of cytokine signaling 2 | SOCS2 | 203372_s_at | 2.473 |

Table S2.1 cont'd.

| | | | |
|--|----------------|--------------|-------|
| insulin-like 3 (Leydig cell) | INSL3 | 1553594_a_at | 2.472 |
| peroxisome proliferator-activated receptor gamma | PPARG | 208510_s_at | 2.47 |
| non-protein coding RNA 161 | NCRNA00161 | 1554405_a_at | 2.467 |
| phosphatidylinositol-5-phosphate 4-kinase, type II, beta | PIP4K2B | 1553047_at | 2.464 |
| integrin, alpha 2 (CD49B, alpha 2 subunit of VLA-2 receptor) | ITGA2 | 205032_at | 2.456 |
| tropomyosin 1 (alpha) | TPM1 | 206117_at | 2.454 |
| TOX high mobility group box family member 2 | TOX2 | 228737_at | 2.446 |
| kelch-like 17 (Drosophila) | KLHL17 | 229792_at | 2.44 |
| Na ⁺ /H ⁺ exchanger domain containing 2 | NHEDC2 | 1564746_at | 2.438 |
| spectrin, beta, non-erythrocytic 1 | SPTBN1 | 226342_at | 2.437 |
| TruB pseudouridine (psi) synthase homolog 1 (E. coli) | TRUB1 | 236020_s_at | 2.432 |
| p21 protein (Cdc42/Rac)-activated kinase 7 | PAK7 | 213990_s_at | 2.428 |
| GATA binding protein 2 | GATA2 | 209710_at | 2.422 |
| similar to hCG2042915 | LOC100129673 | 236611_at | 2.419 |
| plexin A2 | PLXNA2 | 227032_at | 2.413 |
| testis specific, 14 | TSGA14 | 215637_at | 2.403 |
| acyl-CoA thioesterase 7 | ACOT7 | 215728_s_at | 2.399 |
| Spectrin repeat containing, nuclear envelope 1 | SYNE1 | 232027_at | 2.391 |
| hypothetical locus MGC42157 | MGC42157 | 1552987_a_at | 2.376 |
| transcription factor 19 | TCF19 | 223274_at | 2.369 |
| Na ⁺ /H ⁺ exchanger domain containing 2 | NHEDC2 | 229491_at | 2.358 |
| aminolevulinate, delta-, synthase 2 | ALAS2 | 244205_at | 2.355 |
| claudin domain containing 2 | CLDN2 | 231162_at | 2.343 |
| heat shock 60kDa protein 1 (chaperonin) /// heat shock 60kDa protein 1 (chaperonin) pseudogene 4 | HSPD1 /// HSPD | 243372_at | 2.34 |
| purinergic receptor P2Y, G-protein coupled, 8 | P2RY8 | 229686_at | 2.336 |
| GINS complex subunit 4 (Sid5 homolog) | GINS4 | 211767_at | 2.332 |
| ADAMTS-like 1 | ADAMTSL1 | 229585_at | 2.33 |
| mex-3 homolog C (C. elegans) | MEX3C | 1556874_a_at | 2.326 |
| discoidin, CUB and LCCL domain containing 2 | DCBLD2 | 213865_at | 2.323 |
| cadherin-like 24 | CDH24 | 1553166_at | 2.321 |
| homeobox A4 | HOXA4 | 206289_at | 2.321 |
| erythrocyte membrane protein band 4.2 | EPB42 | 210746_s_at | 2.315 |
| contactin associated protein-like 2 | CNTNAP2 | 219301_s_at | 2.309 |
| dual specificity phosphatase 5 pseudogene | DUSP5P | 1553299_at | 2.305 |
| choroideremia (Rab escort protein 1) | CHM | 1569183_a_at | 2.303 |
| interleukin 21 receptor | IL21R | 221658_s_at | 2.301 |
| FERM domain containing 8 | FRMD8 | 227964_at | 2.293 |
| nuclear factor of kappa light polypeptide gene enhancer in B-cells inhibitor-like 2 | NFKBIL2 | 1558329_at | 2.286 |
| calsequestrin 1 (fast-twitch, skeletal muscle) | CASQ1 | 219645_at | 2.285 |
| OTU domain, ubiquitin aldehyde binding 2 | OTUB2 | 222878_s_at | 2.281 |
| sterile alpha motif domain containing 11 | SAMD11 | 1560477_a_at | 2.28 |
| leucine-rich repeats and WD repeat domain containing 1 | LRWD1 | 225680_at | 2.28 |
| aquaporin 5 | AQP5 | 213611_at | 2.268 |
| high mobility group AT-hook 2 | HMGA2 | 1567224_at | 2.267 |
| acyl-Coenzyme A dehydrogenase, long chain | ACADL | 206068_s_at | 2.265 |
| A kinase (PRKA) anchor protein 6 | AKAP6 | 205359_at | 2.262 |
| tetraspanin 13 | TSPAN13 | 217979_at | 2.262 |
| minichromosome maintenance complex component 5 | MCM5 | 201755_at | 2.257 |
| calcium activated nucleotidase 1 | CANT1 | 1554327_a_at | 2.252 |
| plexin A2 | PLXNA2 | 207290_at | 2.239 |
| taln 2 | TLN2 | 212701_at | 2.239 |
| pregnancy specific beta-1-glycoprotein 3 | PSG3 | 203399_x_at | 2.233 |
| carbohydrate (chondroitin 6) sulfotransferase 3 | CHST3 | 32094_at | 2.228 |
| Janus kinase 2 | JAK2 | 205842_s_at | 2.224 |
| pre-B-cell leukemia homeobox 4 | PBX4 | 230536_at | 2.223 |
| transient receptor potential cation channel, subfamily C, member 3 | TRPC3 | 210814_at | 2.223 |
| poliovirus receptor | PVR | 214443_at | 2.221 |
| retinoic acid receptor, gamma | RARG | 204188_s_at | 2.217 |
| clusterin | CLU | 208791_at | 2.211 |
| ADAM metallopeptidase domain 11 | ADAM11 | 207880_at | 2.204 |
| FERM domain containing 8 | FRMD8 | 1554903_at | 2.196 |
| pregnancy specific beta-1-glycoprotein 6 | PSG6 | 208106_x_at | 2.195 |
| microtubule-associated protein 1B | MAP1B | 212233_at | 2.193 |
| synovial sarcoma, X breakpoint 2 interacting protein | SSX2IP | 203017_s_at | 2.19 |
| prolactin | PRL | 205445_at | 2.19 |
| connector enhancer of kinase suppressor of Ras 2 | CNKSR2 | 1554607_at | 2.189 |
| tyrosine 3-monooxygenase/tryptophan 5-monooxygenase activation protein, eta polypeptide | YWHAH | 201020_at | 2.188 |
| MyoD family inhibitor domain containing | MDFIC | 1559942_at | 2.186 |
| fibroblast growth factor receptor 3 | FGFR3 | 204379_s_at | 2.184 |
| cadherin 6, type 2, K-cadherin (fetal kidney) | CDH6 | 205532_s_at | 2.183 |

Table S2.1 cont'd.

| | | | |
|--|----------------|--------------|-------|
| annexin A10 | ANXA10 | 210143_at | 2.183 |
| intermediate filament family orphan 2 | IFFO2 | 225615_at | 2.179 |
| coiled-coil-helix-coiled-coil-helix domain containing 10 | CHCHD10 | 224932_at | 2.176 |
| monoglyceride lipase | MGLL | 211026_s_at | 2.175 |
| oxysterol binding protein-like 6 | OSBPL6 | 223805_at | 2.169 |
| glycerol-3-phosphate acyltransferase, mitochondrial | GPAM | 225420_at | 2.162 |
| collagen, type XIII, alpha 1 | COL13A1 | 211343_s_at | 2.157 |
| SHC (Src homology 2 domain containing) family, member 4 | SHC4 | 235238_at | 2.156 |
| FERM domain containing 3 | FRMD3 | 230645_at | 2.153 |
| carbonic anhydrase I | CA1 | 205949_at | 2.148 |
| small VCP/p97-interacting protein | SVIP | 230005_at | 2.148 |
| jun D proto-oncogene | JUND | 203751_x_at | 2.146 |
| heat shock 70kDa protein 1A /// heat shock 70kDa protein 1B | HSPA1A /// HSP | 200800_s_at | 2.145 |
| Ankyrin-repeat and fibronectin type III domain containing 1 | ANKFN1 | 1559640_at | 2.139 |
| arylsulfatase B | ARSB | 1554032_at | 2.139 |
| nucleolar and coiled-body phosphoprotein 1 | NOLC1 | 205895_s_at | 2.133 |
| SHC (Src homology 2 domain containing) family, member 4 | SHC4 | 230538_at | 2.132 |
| TRM1 tRNA methyltransferase 1 homolog (S. cerevisiae) | TRMT1 | 203701_s_at | 2.127 |
| GATA binding protein 3 | GATA3 | 209604_s_at | 2.123 |
| heme oxygenase (decycling) 1 | HMOX1 | 203665_at | 2.123 |
| chromosome 14 open reading frame 34 | C14orf34 | 1555786_s_at | 2.123 |
| similar to HSPC047 protein | LOC100134722 | 220692_at | 2.122 |
| ATP-binding cassette, sub-family C (CFTR/MRP), member 4 | ABCC4 | 203196_at | 2.121 |
| msh homeobox 2 | MSX2 | 205555_s_at | 2.118 |
| Insulin receptor substrate 1 | IRS1 | 235392_at | 2.112 |
| chondroitin sulfate synthase 3 | CHSY3 | 242100_at | 2.106 |
| transient receptor potential cation channel, subfamily V, member 2 | TRPV2 | 219282_s_at | 2.1 |
| RGM domain family, member B | RGMB | 227339_at | 2.099 |
| TRM1 tRNA methyltransferase 1 homolog (S. cerevisiae) | TRMT1 | 210463_x_at | 2.099 |
| BTB (POZ) domain containing 11 | BTBD11 | 238692_at | 2.097 |
| ATPase family, AAA domain containing 3A /// ATPase family, AAA domain containing 3B /// similar to A/ATAD3A /// ATAI | ATAD3A | 1552641_s_at | 2.092 |
| notchless homolog 1 (Drosophila) | NLE1 | 203867_s_at | 2.086 |
| FERM domain containing 3 | FRMD3 | 229893_at | 2.079 |
| SMAD family member 7 | SMAD7 | 204790_at | 2.078 |
| Sp8 transcription factor | SP8 | 239743_at | 2.072 |
| clusterin | CLU | 208792_s_at | 2.071 |
| ATP-binding cassette, sub-family C (CFTR/MRP), member 4 | ABCC4 | 1554918_a_at | 2.069 |
| malic enzyme 2, NAD(+)-dependent, mitochondrial | ME2 | 210154_at | 2.068 |
| thromboxane A2 receptor | TBXA2R | 336_at | 2.068 |
| KIAA1609 | KIAA1609 | 221843_s_at | 2.067 |
| suppressor of cytokine signaling 2 | SOCS2 | 203373_at | 2.065 |
| myosin VA (heavy chain 12, myosin) | MYO5A | 204527_at | 2.06 |
| hairy/enhancer-of-split related with YRPW motif 1 | HEY1 | 44783_s_at | 2.053 |
| solute carrier family 4, sodium bicarbonate cotransporter, member 4 | SLC4A4 | 1554027_a_at | 2.051 |
| YOD1 OTU deubiquinating enzyme 1 homolog (S. cerevisiae) | YOD1 | 215150_at | 2.049 |
| hairy/enhancer-of-split related with YRPW motif 1 | HEY1 | 218839_at | 2.047 |
| glutamate receptor, ionotropic, kainate 2 | GRIK2 | 1560265_at | 2.046 |
| smoothelin | SMTN | 207390_s_at | 2.046 |
| BTB (POZ) domain containing 11 | BTBD11 | 228570_at | 2.044 |
| protein phosphatase 3 (formerly 2B), catalytic subunit, beta isoform | PPP3CB | 209817_at | 2.043 |
| septin 13 | 13-Sep | 230355_at | 2.042 |
| potassium inwardly-rectifying channel, subfamily J, member 8 | KCNJ8 | 205304_s_at | 2.042 |
| HECT, C2 and WW domain containing E3 ubiquitin protein ligase 2 | HECW2 | 232080_at | 2.04 |
| Kruppel-like factor 2 (lung) | KLF2 | 226646_at | 2.037 |
| paired related homeobox 2 | PRRX2 | 219729_at | 2.037 |
| gamma-aminobutyric acid (GABA) A receptor, gamma 1 | GABRG1 | 241805_at | 2.032 |
| acyl-CoA thioesterase 7 | ACOT7 | 208002_s_at | 2.026 |
| coiled-coil domain containing 68 | CCDC68 | 220180_at | 2.022 |
| SET domain and mariner transposase fusion gene | SETMAR | 1554060_s_at | 2.021 |
| ATPase type 13A3 | ATP13A3 | 219558_at | 2.018 |
| glycerol-3-phosphate acyltransferase, mitochondrial | GPAM | 225424_at | 2.018 |
| KIAA1609 | KIAA1609 | 65438_at | 2.013 |
| zinc finger protein 175 | ZNF175 | 205497_at | 2.01 |
| prominin 2 | PROM2 | 1552797_s_at | 2.009 |
| nicalin homolog (zebrafish) | NCLN | 222206_s_at | 2.007 |
| BAI1-associated protein 2 | BAIAP2 | 205293_x_at | 2.005 |
| P antigen family, member 1 (prostate associated) | PAGE1 | 206897_at | 2.004 |
| monoglyceride lipase | MGLL | 225102_at | 2 |
| collagen, type IV, alpha 6 | COL4A6 | 210945_at | 2 |

Table S2.2: Genes with increased expression due to Alk3QD in EOC spheroids.

| Gene Title | Gene Symbol | Probe Set ID | Fold Change |
|--|----------------|--------------|-------------|
| lipopolysaccharide binding protein | LBP | 214461_at | 72.27 |
| loricrin | LOR | 207720_at | 49.49 |
| hairy/enhancer-of-split related with YRPW motif 2 | HEY2 | 222921_s_at | 48.379 |
| actin, alpha, cardiac muscle 1 | ACTC1 | 205132_at | 40.174 |
| CD24 molecule | CD24 | 209772_s_at | 39.195 |
| CD24 molecule | CD24 | 266_s_at | 37.327 |
| CD24 molecule | CD24 | 209771_x_at | 34.274 |
| CD24 molecule | CD24 | 216379_x_at | 30.311 |
| contactin associated protein-like 2 | CNTNAP2 | 219301_s_at | 25.559 |
| CD24 molecule | CD24 | 208650_s_at | 24.444 |
| cut-like homeobox 2 | CUX2 | 213920_at | 24.245 |
| CD24 molecule | CD24 | 208651_x_at | 21.376 |
| distal-less homeobox 2 | DLX2 | 207147_at | 20.206 |
| FEZ family zinc finger 2 | FEZF2 | 233972_s_at | 16.35 |
| involutrin | IVL | 214599_at | 14.951 |
| dickkopf homolog 1 (Xenopus laevis) | DKK1 | 204602_at | 13.536 |
| cannabinoid receptor 1 (brain) | CNR1 | 213436_at | 13.412 |
| gamma-aminobutyric acid (GABA) B receptor, 2 | GABBR2 | 209990_s_at | 12.811 |
| folate receptor 3 (gamma) | FOLR3 | 206371_at | 12.253 |
| chromosome 5 open reading frame 23 | C5orf23 | 219054_at | 11.902 |
| chemokine (C-C motif) ligand 26 | CCL26 | 223710_at | 11.408 |
| gap junction protein, delta 3, 31.9kDa | GJD3 | 230025_at | 10.917 |
| SMAD family member 9 | SMAD9 | 206320_s_at | 10.709 |
| SMAD family member 6 | SMAD6 | 207069_s_at | 10.538 |
| noggin | NOG | 231798_at | 10.343 |
| chromosome 2 open reading frame 88 | C2orf88 | 223754_at | 10.294 |
| guanine nucleotide binding protein (G protein), gamma transducing activity polypeptide 1 | GNGT1 | 207166_at | 9.878 |
| lipopolysaccharide binding protein | LBP | 211652_s_at | 9.867 |
| keratin 81 | KRT81 | 213711_at | 9.186 |
| Interleukin 1 receptor-like 1 | IL1RL1 | 234066_at | 9.109 |
| distal-less homeobox 1 | DLX1 | 242138_at | 8.579 |
| tumor necrosis factor (ligand) superfamily, member 9 | TNFSF9 | 206907_at | 8.53 |
| chemokine (C-C motif) ligand 2 | CCL2 | 216598_s_at | 8.503 |
| solute carrier family 25 (mitochondrial carrier; ornithine transporter) member 2 | SLC25A2 | 224166_at | 8.37 |
| hypothetical protein LOC90246 | LOC90246 | 233835_at | 7.669 |
| neural cell adhesion molecule 1 | NCAM1 | 227394_at | 7.19 |
| Inhibitor of growth family, member 2 | ING2 | 213544_at | 7.105 |
| heat shock 70kDa protein 1A /// heat shock 70kDa protein 1B | HSPA1A /// HSP | 200800_s_at | 7.074 |
| hypothetical gene supported by BC011527; BC021928; BC011527; BC021928 | LOC284260 | 1570208_at | 7.018 |
| leucine rich repeat containing 4 | LRRC4 | 223552_at | 6.963 |
| protocadherin 9 | PCDH9 | 219738_s_at | 6.945 |
| neutrophil cytosolic factor 2 | NCF2 | 209949_at | 6.843 |
| tubulin, beta 2B | TUBB2B | 214023_x_at | 6.831 |
| hypothetical LOC100127940 | LOC100127940 | 1564299_at | 6.828 |
| calcitonin-related polypeptide alpha | CALCA | 217561_at | 6.805 |
| CD300 molecule-like family member g | CD300LG | 1552509_a_at | 6.675 |
| FEZ family zinc finger 2 | FEZF2 | 221086_s_at | 6.65 |
| chromosome 2 open reading frame 88 | C2orf88 | 228195_at | 6.64 |
| Tropomyosin 4 | TPM4 | 1559989_at | 6.591 |
| neurofilament, medium polypeptide | NEFM | 205113_at | 6.543 |
| synaptotagmin XV | SYT15 | 1560879_a_at | 6.516 |
| heparan sulfate 6-O-sulfotransferase 3 | HS6ST3 | 232275_s_at | 6.499 |
| myozenin 2 | MYO22 | 207148_x_at | 6.44 |
| suppressor of cytokine signaling 2 | SOCS2 | 203372_s_at | 6.416 |
| UPF0632 protein A | LOC388630 | 244472_at | 6.388 |
| hypothetical protein LOC254057 | LOC254057 | 232370_at | 6.369 |
| hypothetical protein LOC284542 | LOC284542 | 230920_at | 6.349 |
| collagen, type XXIII, alpha 1 | COL23A1 | 229168_at | 6.304 |
| hypothetical LOC84983 | MGC14436 | 1553811_at | 6.267 |
| contactin associated protein-like 2 | CNTNAP2 | 219302_s_at | 6.263 |
| sterile alpha motif domain containing 4A | SAMD4A | 215120_s_at | 6.246 |
| A kinase (PRKA) anchor protein 5 | AKAP5 | 230846_at | 6.169 |
| myozenin 2 | MYO22 | 213782_s_at | 6.144 |
| potassium voltage-gated channel, KQT-like subfamily, member 5 | KCNQ5 | 244623_at | 6.034 |
| solute carrier family 37 (glycerol-3-phosphate transporter), member 1 | SLC37A1 | 218928_s_at | 6.029 |
| pyruvate dehydrogenase kinase, isozyme 4 | PKD4 | 225207_at | 5.985 |
| matrix metalloproteinase 24 (membrane-inserted) | MMP24 | 213171_s_at | 5.825 |
| NEL-like 1 (chicken) | NELL1 | 206089_at | 5.742 |
| cartilage oligomeric matrix protein | COMP | 205713_s_at | 5.662 |
| hedgehog interacting protein | HHIP | 1556037_s_at | 5.573 |
| cyclic AMP-regulated phosphoprotein, 21 kD /// hypothetical protein LOC100130503 | ARPP-21 /// LO | 1556599_s_at | 5.243 |
| KIAA1128 | KIAA1128 | 1554131_at | 5.23 |
| ribonuclease, RNase A family, 1 (pancreatic) | RNASE1 | 201785_at | 5.165 |

Table S2.2 cont'd.

| | | | |
|--|----------------|--------------|-------|
| SV2 related protein homolog (rat) | SVOP | 229818_at | 5.14 |
| coiled-coil domain containing 85A | CCDC85A | 235228_at | 5.131 |
| heat shock 70kDa protein 1A /// heat shock 70kDa protein 1B | HSPA1A /// HSI | 202581_at | 5.082 |
| chromosome 14 open reading frame 81 | C14orf81 | 1564499_at | 5.047 |
| LIM domain only 2 (rhombotin-like 1) | LMO2 | 204249_s_at | 4.971 |
| keratin associated protein 19-3 | KRTAP19-3 | 240967_at | 4.965 |
| retinol binding protein 2, cellular | RBP2 | 231734_at | 4.96 |
| suppressor of cytokine signaling 2 | SOCS2 | 203373_at | 4.938 |
| chromosome 1 open reading frame 14 | C1orf14 | 220996_s_at | 4.936 |
| neuron navigator 2 | NAV2 | 218330_s_at | 4.868 |
| Syntrophin, gamma 1 | SNTG1 | 1562287_at | 4.854 |
| G protein-coupled receptor 83 | GPR83 | 222953_at | 4.849 |
| doublecortin domain containing 5 | DCDC5 | 232603_at | 4.783 |
| lin-7 homolog B (C. elegans) | LIN7B | 241957_x_at | 4.773 |
| acyl-CoA thioesterase 11 | ACOT11 | 214763_at | 4.76 |
| aldo-keto reductase family 1, member C2 (dihydrodiol dehydrogenase 2; bile acid binding protein; 3-alpha | AKR1C2 | 211653_x_at | 4.759 |
| UDP-Gal:betaGlcNAc beta 1,3-galactosyltransferase, polypeptide 5 | B3GALT5 | 206947_at | 4.757 |
| crystallin, alpha B | CRYAB | 209283_at | 4.708 |
| tachykinin, precursor 1 | TAC1 | 206552_s_at | 4.698 |
| msh homeobox 2 | MSX2 | 205555_s_at | 4.689 |
| epiplakin 1 | EPPK1 | 232165_at | 4.664 |
| paired related homeobox 2 | PRRX2 | 219729_at | 4.659 |
| chromosome 10 open reading frame 126 | C10orf126 | 1553915_at | 4.65 |
| Na ⁺ /H ⁺ exchanger domain containing 2 | NHEDC2 | 229491_at | 4.648 |
| complement component (3b/4b) receptor 1-like | CR1L | 239206_at | 4.631 |
| chromosome 12 open reading frame 59 | C12orf59 | 236646_at | 4.616 |
| chromosome 12 open reading frame 47 | C12orf47 | 212868_x_at | 4.586 |
| plexin A2 | PLXNA2 | 213030_s_at | 4.575 |
| heparan sulfate 6-O-sulfotransferase 3 | HS6ST3 | 232276_at | 4.547 |
| glutathione peroxidase 3 (plasma) | GPX3 | 214091_s_at | 4.534 |
| neural cell adhesion molecule 1 | NCAM1 | 209968_s_at | 4.53 |
| msh homeobox 2 | MSX2 | 210319_x_at | 4.527 |
| pyruvate dehydrogenase kinase, isozyme 4 | PKD4 | 1562321_at | 4.525 |
| G protein-coupled receptor 137C | GPR137C | 242592_at | 4.515 |
| mal, T-cell differentiation protein-like | MALL | 209373_at | 4.481 |
| phospholipase C, eta 1 | PLCH1 | 216634_at | 4.47 |
| G protein-coupled receptor 158 | GPR158 | 232195_at | 4.448 |
| kynurenine 3-monooxygenase (kynurenine 3-hydroxylase) | KMO | 205306_x_at | 4.438 |
| fibrinogen C domain containing 1 | FIBCD1 | 240042_at | 4.389 |
| uronyl-2-sulfotransferase | UST | 205138_s_at | 4.359 |
| Atonal homolog 8 (Drosophila) | ATOH8 | 1558706_a_at | 4.353 |
| chromosome 13 open reading frame 38 | C13orf38 | 234085_at | 4.351 |
| hypothetical protein LOC641364 | LOC641364 | 1562253_at | 4.35 |
| transient receptor potential cation channel, subfamily C, member 3 | TRPC3 | 210814_at | 4.341 |
| neurofilament, light polypeptide | NEFL | 221801_x_at | 4.293 |
| placenta-specific 1 | PLAC1 | 219702_at | 4.286 |
| maestro | MRO | 224324_at | 4.283 |
| atonal homolog 8 (Drosophila) | ATOH8 | 228890_at | 4.266 |
| aldo-keto reductase family 1, member C1 (dihydrodiol dehydrogenase 1; 20-alpha (3-alpha)-hydroxysteroid | AKR1C1 | 204151_x_at | 4.254 |
| replication protein A4, 34kDa | RPA4 | 221143_at | 4.239 |
| hypothetical protein LOC652821 /// variable charge, Y-linked /// variable charge, Y-linked 1B | LOC652821 /// | 206922_at | 4.209 |
| serpin peptidase inhibitor, clade B (ovalbumin), member 5 | SERPINB5 | 155551_at | 4.159 |
| hypothetical protein MGC16121 | MGC16121 | 228235_at | 4.159 |
| par-3 partitioning defective 3 homolog B (C. elegans) | PARD3B | 1555113_at | 4.144 |
| slit homolog 3 (Drosophila) | SLIT3 | 216216_at | 4.107 |
| caspase 12 (gene/pseudogene) | CASP12 | 1564736_a_at | 4.104 |
| DnaJ (Hsp40) homolog, subfamily A, member 4 | DNAJA4 | 225061_at | 4.102 |
| A kinase (PRKA) anchor protein 5 | AKAP5 | 207800_at | 4.1 |
| activating transcription factor 3 | ATF3 | 202672_s_at | 4.099 |
| TMF1-regulated nuclear protein 1 | TRNP1 | 227862_at | 4.095 |
| arginine-glutamic acid dipeptide (RE) repeats | RERE | 200939_s_at | 4.089 |
| solute carrier family 23 (nucleobase transporters), member 3 | SLC23A3 | 1553265_at | 4.076 |
| Cell division cycle 20 homolog B (S. cerevisiae) | CDC20B | 240161_s_at | 4.069 |
| coiled-coil domain containing 3 | CCDC3 | 223316_at | 4.062 |
| THAP domain containing, apoptosis associated protein 2 | THAP2 | 230380_at | 4.04 |
| calponin 1, basic, smooth muscle | CNN1 | 203951_at | 4.023 |
| natriuretic peptide receptor A/guanylate cyclase A (atrionatriuretic peptide receptor A) | NPR1 | 204648_at | 4.018 |
| glycoprotein V (platelet) | GP5 | 211525_s_at | 3.984 |
| interleukin 8 | IL8 | 211506_s_at | 3.977 |
| hypothetical LOC100268168 | LOC100268168 | 233491_at | 3.975 |
| placental growth factor | PGF | 209652_s_at | 3.963 |
| bone morphogenetic protein receptor, type IB | BMPRI1B | 210523_at | 3.961 |
| immunoglobulin-like and fibronectin type III domain containing 1 | IGFN1 | 229275_at | 3.928 |
| DnaJ (Hsp40) homolog, subfamily A, member 4 | DNAJA4 | 1554334_a_at | 3.921 |
| parathyroid hormone-like hormone | PTH1LH | 211756_at | 3.915 |

Table S2.2 cont'd.

| | | | |
|--|--------------|--------------|-------|
| transducin-like enhancer of split 6 (E(sp1) homolog, Drosophila) | TLE6 | 1553813_s_at | 3.895 |
| aggregran | ACAN | 207692_s_at | 3.883 |
| protein phosphatase 1, regulatory (inhibitor) subunit 14C | PPP1R14C | 226907_at | 3.88 |
| similar to hCG41624 | LOC100128071 | 1556560_a_at | 3.865 |
| isopentenyl-diphosphate delta isomerase 2 | IDI2 | 1552491_at | 3.86 |
| Triple functional domain (PTPRF interacting) | TRIO | 216700_at | 3.845 |
| discoidin, CUB and LCCL domain containing 2 | DCBLD2 | 213873_at | 3.841 |
| cholecystokinin | CCK | 205827_at | 3.831 |
| T-box, brain, 1 | TBR1 | 220025_at | 3.801 |
| Phospholamban | PLN | 228202_at | 3.777 |
| aldo-keto reductase family 1, member C2 (dihydrodiol dehydrogenase 2; bile acid binding protein; 3-alpha | AKR1C2 | 209699_x_at | 3.771 |
| nescent helix loop helix 2 | NHLH2 | 215228_at | 3.765 |
| AT rich interactive domain 1A (SWI-like) | ARID1A | 207591_s_at | 3.739 |
| hairy/enhancer-of-split related with YRPW motif 1 | HEY1 | 44783_s_at | 3.736 |
| dynein, axonemal, heavy chain 1 | DNAH1 | 239059_at | 3.729 |
| aldo-keto reductase family 1, member C1 (dihydrodiol dehydrogenase 1; 20-alpha (3-alpha)-hydroxysteroid | AKR1C1 | 216594_x_at | 3.725 |
| DiGeorge syndrome critical region gene 12 | DGCR12 | 1566235_at | 3.722 |
| frizzled homolog 8 (Drosophila) | FZD8 | 227405_s_at | 3.713 |
| acid phosphatase 5, tartrate resistant | ACP5 | 204638_at | 3.709 |
| frizzled homolog 8 (Drosophila) | FZD8 | 224325_at | 3.698 |
| distal-less homeobox 3 | DLX3 | 231778_at | 3.698 |
| cAMP responsive element binding protein 5 | CREB5 | 229228_at | 3.695 |
| similar to hCG1815045 | LOC100131781 | 240320_at | 3.694 |
| epiplakin 1 | EPPK1 | 208156_x_at | 3.684 |
| chromodomain helicase DNA binding protein 5 | CHD5 | 213965_s_at | 3.683 |
| KH domain containing, RNA binding, signal transduction associated 2 | KHDRBS2 | 215527_at | 3.679 |
| peptidase domain containing associated with muscle regeneration 1 | PAMR1 | 213661_at | 3.667 |
| WNK lysine deficient protein kinase 2 | WNK2 | 1557536_at | 3.665 |
| catenin (cadherin-associated protein), delta 2 (neural plakophilin-related arm-repeat protein) | CTNND2 | 209617_s_at | 3.665 |
| HECT, C2 and WW domain containing E3 ubiquitin protein ligase 2 | HECW2 | 232080_at | 3.641 |
| parathyroid hormone-like hormone | PTH1H | 206300_s_at | 3.641 |
| casepuestrin 1 (fast-twitch, skeletal muscle) | CASQ1 | 219645_at | 3.64 |
| synovial sarcoma, X breakpoint 2 interacting protein | SSX2IP | 203015_s_at | 3.625 |
| heat shock 70kDa protein 1A | HSPA1A | 200799_at | 3.62 |
| Hypothetical LOC150538 | FLJ32063 | 235147_at | 3.618 |
| gap junction protein, gamma 1, 45kDa | GJC1 | 228563_at | 3.617 |
| transmembrane protein 132E | TMEM132E | 243708_at | 3.56 |
| gamma-aminobutyric acid (GABA) B receptor, 2 | GABBR2 | 217077_s_at | 3.544 |
| microtubule-associated protein 1B | MAP1B | 226084_at | 3.528 |
| chromosome 1 open reading frame 129 | C1orf129 | 221182_at | 3.525 |
| signal transducer and activator of transcription 3 (acute-phase response factor) | STAT3 | 243213_at | 3.509 |
| insulin-like growth factor binding protein 5 | IGFBP5 | 1555997_s_at | 3.487 |
| calmodulin binding transcription activator 1 | CAMTA1 | 213268_at | 3.465 |
| chymotrypsin-like elastase family, member 3A | CELA3A | 210080_x_at | 3.457 |
| homeobox C13 | HOXC13 | 219832_s_at | 3.44 |
| talin 2 | TLN2 | 212701_at | 3.438 |
| chondroitin sulfate proteoglycan 4 | CSPG4 | 214297_at | 3.436 |
| atlastin GTPase 2 | ATL2 | 237968_at | 3.429 |
| elastin microfibril interfacer 2 | EMILIN2 | 224374_s_at | 3.429 |
| ArfGAP with dual PH domains 1 | ADAP1 | 219150_s_at | 3.411 |
| Neural cell adhesion molecule 1 | NCAM1 | 231532_at | 3.405 |
| Kruppel-like factor 6 | KLF6 | 208960_s_at | 3.401 |
| growth arrest and DNA-damage-inducible, beta | GADD45B | 209304_x_at | 3.387 |
| hypothetical protein LOC144481 | LOC144481 | 1559315_s_at | 3.383 |
| UL16 binding protein 2 | ULBP2 | 238542_at | 3.378 |
| oxytocin, prepropeptide | OXT | 207576_x_at | 3.368 |
| met proto-oncogene (hepatocyte growth factor receptor) | MET | 203510_at | 3.364 |
| copine IV | CPNE4 | 231336_at | 3.362 |
| Na ⁺ /H ⁺ exchanger domain containing 2 | NHEDC2 | 1564746_at | 3.347 |
| makorin ring finger protein 2 | MKRN2 | 216995_x_at | 3.338 |
| potassium voltage-gated channel, Shaw-related subfamily, member 4 | KCNK4 | 208251_at | 3.335 |
| neuron navigator 2 | NAV2 | 222598_s_at | 3.326 |
| hypothetical LOC100126784 | LOC100126784 | 240407_at | 3.326 |
| Fc receptor-like A | FCRLA | 235400_at | 3.312 |
| eukaryotic translation initiation factor 4A, isoform 2 | EIF4A2 | 1556350_a_at | 3.305 |
| melanoma cell adhesion molecule | MCAM | 209087_x_at | 3.3 |
| dual specificity phosphatase 5 pseudogene | DUSP5P | 1553299_at | 3.296 |
| glycoprotein, alpha-galactosyltransferase 1 | GGTA1 | 228376_at | 3.291 |
| Hypothetical protein LOC203274 | LOC203274 | 232034_at | 3.29 |
| kazrin | RP1-21018.1 | 229144_at | 3.286 |
| brain-derived neurotrophic factor | BDNF | 206382_s_at | 3.278 |
| AF4/FMR2 family, member 2 | AFF2 | 206105_at | 3.267 |
| ATPase type 13A3 | ATP13A3 | 219558_at | 3.262 |
| GPRIN family member 3 | GPRIN3 | 1556697_at | 3.253 |
| Atonal homolog 8 (Drosophila) | ATOH8 | 1558705_at | 3.247 |

Table S2.2 cont'd.

| | | | |
|--|----------------|--------------|-------|
| keratin 73 | KRT73 | 1553537_at | 3.238 |
| adrenergic, beta-1-, receptor | ADRB1 | 229309_at | 3.225 |
| tropomyosin 1 (alpha) | TPM1 | 206117_at | 3.223 |
| kazrin | RP1-21O18.1 | 213478_at | 3.222 |
| muscle RAS oncogene homolog | MRAS | 225185_at | 3.218 |
| hairy/enhancer-of-split related with YRPW motif 1 | HEY1 | 218839_at | 3.216 |
| mitogen-activated protein kinase kinase kinase kinase 1 | MAP4K1 | 214339_s_at | 3.207 |
| echinoderm microtubule associated protein like 2 | EML2 | 204399_s_at | 3.204 |
| hyaluronoglucosaminidase 1 | HYAL1 | 210619_s_at | 3.197 |
| synovial sarcoma, X breakpoint 2 interacting protein | SSX2IP | 203019_x_at | 3.195 |
| stimulated by retinoic acid gene 6 homolog (mouse) | STRA6 | 1569334_at | 3.185 |
| Kruppel-like factor 6 | KLF6 | 208961_s_at | 3.185 |
| tripartite motif-containing 14 | TRIM14 | 211044_at | 3.184 |
| SERTA domain containing 4 | SERTAD4 | 229674_at | 3.181 |
| cAMP responsive element binding protein 5 | CREB5 | 205931_s_at | 3.167 |
| histone cluster 1, H3g | HIST1H3G | 208496_x_at | 3.156 |
| cysteinyl-tRNA synthetase | CARS | 240982_at | 3.155 |
| synovial sarcoma, X breakpoint 2 interacting protein | SSX2IP | 210871_x_at | 3.153 |
| hypothetical protein LOC149086 | LOC149086 | 1566647_s_at | 3.152 |
| hypothetical protein LOC731477 | LOC731477 | 237312_at | 3.146 |
| Glycoprotein, synaptic 2 | GPSN2 | 231556_at | 3.146 |
| growth arrest and DNA-damage-inducible, beta | GADD45B | 209305_s_at | 3.14 |
| cartilage acidic protein 1 | CRTAC1 | 221204_s_at | 3.131 |
| synovial sarcoma, X breakpoint 2 interacting protein | SSX2IP | 203018_s_at | 3.122 |
| msh homeobox 1 | MSX1 | 205932_s_at | 3.121 |
| Hypothetical protein DKFZp686O24166 | DKFZp686O24 | 229715_at | 3.115 |
| SLAM family member 9 | SLAMF9 | 1553770_a_at | 3.113 |
| keratin associated protein 2-4 | KRTAP2-4 | 1555673_at | 3.112 |
| family with sequence similarity 83, member G | FAM83G | 228587_at | 3.108 |
| SMAD family member 9 | SMAD9 | 227719_at | 3.101 |
| interleukin 1 family, member 5 (delta) | IL1F5 | 222223_s_at | 3.098 |
| v-myb myeloblastosis viral oncogene homolog (avian) | MYB | 204798_at | 3.094 |
| natriuretic peptide receptor A/guanylate cyclase A (atrionatriuretic peptide receptor A) | NPR1 | 32625_at | 3.083 |
| heat shock protein 90kDa alpha (cytosolic), class A member 1 | HSP90AA1 | 211968_s_at | 3.081 |
| stimulated by retinoic acid gene 6 homolog (mouse) | STRA6 | 221701_s_at | 3.08 |
| hypothetical protein MGC16121 | MGC16121 | 227488_at | 3.072 |
| peptidylprolyl isomerase A (cyclophilin A)-like 4A /// peptidylprolyl isomerase A (cyclophilin A)-like 4B /// pe | PPIAL4A /// PP | 217136_at | 3.066 |
| HHIP-like 2 | HHIPL2 | 220283_at | 3.056 |
| synovial sarcoma, X breakpoint 2 interacting protein | SSX2IP | 203016_s_at | 3.056 |
| microtubule-associated protein 1B | MAP1B | 212233_at | 3.056 |
| hypothetical protein LOC100132388 | LOC100132388 | 224241_s_at | 3.045 |
| phospholipase C, epsilon 1 | PLCE1 | 205111_s_at | 3.04 |
| tousled-like kinase 2 | TLK2 | 233349_at | 3.038 |
| leucine zipper protein 2 | LUZP2 | 215323_at | 3.034 |
| GATA binding protein 3 | GATA3 | 209602_s_at | 3.034 |
| Kruppel-like factor 4 (gut) | KLF4 | 220266_s_at | 3.033 |
| solute carrier family 4, sodium bicarbonate cotransporter, member 7 | SLC4A7 | 207604_s_at | 3.033 |
| kinesin family member 23 | KIF23 | 204709_s_at | 3.031 |
| hypothetical gene supported by AK098783 | FLJ25917 | 1564295_at | 3.03 |
| nuclear receptor interacting protein 3 | NRIP3 | 222900_at | 3.023 |
| methylenetetrahydrofolate dehydrogenase (NADP+ dependent) 1, methylenetetrahydrofolate cyclohydrolas | MTHFD1 | 202309_at | 3.005 |
| dual specificity phosphatase 1 | DUSP1 | 201044_x_at | 2.985 |
| gremlin 2, cysteine knot superfamily, homolog (Xenopus laevis) | GREM2 | 235504_at | 2.982 |
| UDP-N-acetyl-alpha-D-galactosamine:polypeptide N-acetylgalactosaminyltransferase 9 (GalNAc-T9) /// sii | GALNT9 /// LO | 229451_at | 2.974 |
| matrix metalloproteinase 25 | MMP25 | 207890_s_at | 2.973 |
| growth arrest and DNA-damage-inducible, beta | GADD45B | 207574_s_at | 2.973 |
| ovo-like 1(Drosophila) | OVOL1 | 229396_at | 2.969 |
| progesterone receptor | PGR | 228554_at | 2.967 |
| Kruppel-like factor 2 (lung) | KLF2 | 219371_s_at | 2.967 |
| 3-hydroxy-3-methylglutaryl-Coenzyme A synthase 1 (soluble) | HMGCS1 | 205822_s_at | 2.964 |
| Kruppel-like factor 4 (gut) | KLF4 | 221841_s_at | 2.962 |
| heat shock 27kDa protein 1 | HSPB1 | 201841_s_at | 2.961 |
| interleukin 8 | IL8 | 202859_x_at | 2.956 |
| glycerol kinase | GK | 215977_x_at | 2.955 |
| Kruppel-like factor 6 | KLF6 | 1555832_s_at | 2.953 |
| secretogranin II (chromogranin C) | SCG2 | 204035_at | 2.94 |
| plexin A2 | PLXNA2 | 227032_at | 2.938 |
| pleckstrin homology-like domain, family A, member 1 | PHLDA1 | 218000_s_at | 2.933 |
| somatostatin receptor 1 | SSTR1 | 235591_at | 2.932 |
| chromosome 18 open reading frame 1 | C18orf1 | 207996_s_at | 2.927 |
| brain-derived neurotrophic factor | BDNF | 239367_at | 2.919 |
| fibulin 2 | FBLN2 | 203886_s_at | 2.905 |
| parathyroid hormone-like hormone | PTH LH | 210355_at | 2.896 |
| hairy and enhancer of split 6 (Drosophila) | HES6 | 226446_at | 2.89 |
| ArfGAP with dual PH domains 1 | ADAP1 | 90265_at | 2.888 |

Table S2.2 cont'd.

| | | | |
|---|----------------|--------------|-------|
| poliovirus receptor | PVR | 212662_at | 2.888 |
| solute carrier family 25 (mitochondrial carrier; ornithine transporter) member 15 | SLC25A15 | 222705_s_at | 2.879 |
| insulin-like 3 (Leydig cell) | INSL3 | 1553594_a_at | 2.875 |
| similar to hCG2042915 | LOC100129673 | 236611_at | 2.871 |
| Collagen, type XXVII, alpha 1 | COL27A1 | 1564008_at | 2.87 |
| adaptor-related protein complex 1, sigma 3 subunit | AP1S3 | 1555731_a_at | 2.866 |
| prolactin receptor | PRLR | 216638_s_at | 2.865 |
| tubulin tyrosine ligase-like family, member 5 | TTL5 | 1566102_at | 2.851 |
| Threonyl-tRNA synthetase | TARS | 240206_at | 2.847 |
| glycine-N-acyltransferase-like 1 | GLYATL1 | 227794_at | 2.843 |
| one cut homeobox 2 | ONECUT2 | 233441_at | 2.842 |
| transient receptor potential cation channel, subfamily C, member 3 | TRPC3 | 206425_s_at | 2.834 |
| F-box protein 27 | FBXO27 | 235169_at | 2.825 |
| synaptotagmin XV | SYT15 | 1560878_at | 2.825 |
| chromosome 17 open reading frame 53 | C17orf53 | 219879_s_at | 2.823 |
| mucin 12, cell surface associated | MUC12 | 226654_at | 2.816 |
| SMAD family member 7 | SMAD7 | 204790_at | 2.813 |
| cysteine-rich, angiogenic inducer, 61 | CYR61 | 210764_s_at | 2.813 |
| DnaJ (Hsp40) homolog, subfamily C, member 6 | DNAJC6 | 204720_s_at | 2.807 |
| Kruppel-like factor 6 | KLF6 | 224606_at | 2.798 |
| carbonic anhydrase II | CA2 | 209301_at | 2.796 |
| TIMP metalloproteinase inhibitor 3 | TIMP3 | 201150_s_at | 2.787 |
| scavenger receptor class A, member 5 (putative) | SCARA5 | 235849_at | 2.778 |
| chimerin (chimaerin) 2 | CHN2 | 213385_at | 2.776 |
| chromosome 1 open reading frame 114 | C1orf114 | 1555112_a_at | 2.774 |
| discoidin, CUB and LCCL domain containing 2 | DCBLD2 | 213865_at | 2.769 |
| SHC (Src homology 2 domain containing) family, member 4 | SHC4 | 230538_at | 2.765 |
| aldehyde dehydrogenase 3 family, member B2 | ALDH3B2 | 204941_s_at | 2.76 |
| PDZ and LIM domain 3 | PDLIM3 | 238592_at | 2.758 |
| prostaglandin E synthase | PTGES | 207388_s_at | 2.757 |
| ubiquitin-like modifier activating enzyme 6 | UBA6 | 1555441_at | 2.756 |
| sema domain, seven thrombospondin repeats (type 1 and type 1-like), transmembrane domain (TM) and | SEMA5B | 223610_at | 2.752 |
| KIAA1826 | KIAA1826 | 223799_at | 2.752 |
| serine/threonine kinase 35 | STK35 | 1553673_at | 2.741 |
| hairy and enhancer of split 4 (Drosophila) | HES4 | 227347_x_at | 2.737 |
| fatty acid binding protein 3, muscle and heart (mammary-derived growth inhibitor) | FABP3 | 214285_at | 2.727 |
| phosphatidylinositol transfer protein, cytoplasmic 1 | PITPNC1 | 229414_at | 2.725 |
| brix domain containing 5 | BXDC5 | 234243_at | 2.718 |
| echinoderm microtubule associated protein like 1 | EML1 | 204797_s_at | 2.712 |
| tyrosine 3-monooxygenase/tryptophan 5-monooxygenase activation protein, eta polypeptide | YWHAH | 201020_at | 2.704 |
| KIT ligand | KITLG | 226534_at | 2.702 |
| protein phosphatase 4, regulatory subunit 1-like | PPP4R1L | 223733_s_at | 2.7 |
| hyaluronan synthase 2 | HAS2 | 206432_at | 2.696 |
| Similar to programmed cell death 6 interacting protein | LOC731884 | 217520_x_at | 2.689 |
| mucin 17, cell surface associated | MUC17 | 232321_at | 2.688 |
| chromosome 20 open reading frame 195 | C20orf195 | 220426_at | 2.685 |
| tubulin, beta 2A | TUBB2A | 204141_at | 2.682 |
| poly(A) binding protein, cytoplasmic 1-like | PABPC1L | 233104_at | 2.682 |
| progesterone and adipoQ receptor family member IX | PAQR9 | 1558322_a_at | 2.681 |
| neuron navigator 2 | NAV2 | 222599_s_at | 2.678 |
| interleukin 1 receptor accessory protein-like 1 | IL1RAPL1 | 222963_s_at | 2.666 |
| heat shock 60kDa protein 1 (chaperonin) /// heat shock 60kDa protein 1 (chaperonin) pseudogene 4 | HSPD1 /// HSP | 243372_at | 2.642 |
| gamma-aminobutyric acid (GABA) B receptor, 2 | GABBR2 | 211679_x_at | 2.641 |
| actinin, alpha 2 | ACTN2 | 203863_at | 2.635 |
| annexin A1 | ANXA1 | 201012_at | 2.631 |
| NPC1 (Niemann-Pick disease, type C1, gene)-like 1 | NPC1L1 | 220106_at | 2.631 |
| protocadherin 10 | PCDH10 | 1552925_at | 2.624 |
| lin-7 homolog B (C. elegans) | LIN7B | 219760_at | 2.621 |
| aminolevulinic acid, delta-, synthase 2 | ALAS2 | 244205_at | 2.621 |
| hypothetical protein LOC100132356 | hCG_2039148 | 1558310_s_at | 2.611 |
| v-src-1 Yamaguchi sarcoma viral related oncogene homolog | LYN | 202626_s_at | 2.609 |
| family with sequence similarity 84, member B | FAM84B | 225864_at | 2.594 |
| calpain 5 | CAPN5 | 205166_at | 2.584 |
| glycerol kinase | GK | 207387_s_at | 2.583 |
| phosphatidylinositol transfer protein, membrane-associated 2 | PITPNM2 | 1552924_a_at | 2.579 |
| leucine-rich repeat LGI family, member 2 | LGI2 | 219699_at | 2.579 |
| oxidative stress induced growth inhibitor 1 | OSGIN1 | 219475_at | 2.578 |
| serine incorporator 2 | SERINC2 | 224762_at | 2.578 |
| KIAA2018 | KIAA2018 | 242508_at | 2.571 |
| oxysterol binding protein-like 6 | OSBPL6 | 238575_at | 2.563 |
| dual specificity phosphatase 26 (putative) | DUSP26 | 219144_at | 2.56 |
| Kruppel-like factor 13 | KLF13 | 219878_s_at | 2.551 |
| KIAA1310 | KIAA1310 | 1558652_at | 2.548 |
| jagged 1 (Alagille syndrome) | JAG1 | 209098_s_at | 2.546 |
| tubulin, beta 2A /// tubulin, beta 2B | TUBB2A /// TUB | 209372_x_at | 2.546 |

Table S2.2 cont'd.

| | | | |
|---|--------------|--------------|-------|
| deleted in liver cancer 1 | DLC1 | 224822_at | 2.543 |
| UL16 binding protein 2 | ULBP2 | 221291_at | 2.537 |
| cysteine and glycine-rich protein 2 | CSRP2 | 207030_s_at | 2.537 |
| gremlin 2, cysteine knot superfamily, homolog (<i>Xenopus laevis</i>) | GREM2 | 240509_s_at | 2.535 |
| hypothetical LOC401317 | LOC401317 | 242329_at | 2.533 |
| protocadherin 9 | PCDH9 | 219737_s_at | 2.533 |
| cysteine and glycine-rich protein 2 | CSRP2 | 211126_s_at | 2.532 |
| lipopolysaccharide-induced TNF factor | LITAF | 200706_s_at | 2.532 |
| ADAM metalloproteinase domain 28 | ADAM28 | 208269_s_at | 2.531 |
| vaccinia related kinase 3 | VRK3 | 239190_at | 2.523 |
| zinc finger and BTB domain containing 1 | ZBTB1 | 213376_at | 2.516 |
| Anthrax toxin receptor 1 | ANTXR1 | 234832_at | 2.512 |
| armadillo repeat gene deletes in velocardiofacial syndrome | ARVCF | 217516_x_at | 2.508 |
| C-type lectin domain family 4, member E | CLEC4E | 222934_s_at | 2.507 |
| GATA binding protein 2 | GATA2 | 209710_at | 2.501 |
| nuclear receptor interacting protein 3 | NRIP3 | 219557_s_at | 2.495 |
| GINS complex subunit 3 (Psf3 homolog) | GINS3 | 218719_s_at | 2.481 |
| family with sequence similarity 62 (C2 domain containing), member C | FAM62C | 239770_at | 2.457 |
| carbohydrate (N-acetylgalactosamine 4-0) sulfotransferase 8 | CHST8 | 221065_s_at | 2.451 |
| gamma-aminobutyric acid (GABA) A receptor, beta 1 | GABRB1 | 207010_at | 2.448 |
| stanniocalcin 2 | STC2 | 203439_s_at | 2.441 |
| calmodulin binding transcription activator 1 | CAMTA1 | 1555370_a_at | 2.439 |
| T cell receptor beta variable 27 | TRBV27 | 241133_at | 2.439 |
| D-aspartate oxidase | DDO | 207418_s_at | 2.435 |
| Transforming, acidic coiled-coil containing protein 1 | TACC1 | 1557305_at | 2.433 |
| GATA binding protein 5 | GATA5 | 238095_at | 2.432 |
| insulin-like growth factor binding protein 5 | IGFBP5 | 203424_s_at | 2.423 |
| spectrin, beta, non-erythrocytic 1 | SPTBN1 | 226342_at | 2.422 |
| cancer susceptibility candidate 5 | CASC5 | 1552680_a_at | 2.42 |
| phospholipase inhibitor | LOC646627 | 238143_at | 2.417 |
| T-box 3 | TBX3 | 229576_s_at | 2.416 |
| KN motif and ankyrin repeat domains 4 | KANK4 | 229125_at | 2.414 |
| Norrie disease (pseudoglioma) | NDP | 206022_at | 2.408 |
| solute carrier family 7 (cationic amino acid transporter, y+ system), member 1 | SLC7A1 | 212290_at | 2.408 |
| solute carrier family 25 (mitochondrial carrier; ornithine transporter) member 15 | SLC25A15 | 218653_at | 2.4 |
| MHC class I polypeptide-related sequence A | MICA | 205904_at | 2.396 |
| aquaporin 1 (Colton blood group) | AQP1 | 209047_at | 2.395 |
| angiotensinogen (serpin peptidase inhibitor, clade A, member 8) | AGT | 202834_at | 2.393 |
| MAP/microtubule affinity-regulating kinase 1 | MARK1 | 226653_at | 2.386 |
| schlafen family member 5 | SLFN5 | 243999_at | 2.384 |
| semaphorin 7A, GPI membrane anchor (John Milton Hagen blood group) | SEMA7A | 230345_at | 2.382 |
| deleted in liver cancer 1 | DLC1 | 220511_s_at | 2.379 |
| PDZ and LIM domain 3 | PDLIM3 | 210170_at | 2.378 |
| mal, T-cell differentiation protein | MAL | 204777_s_at | 2.376 |
| zinc finger, MYM-type 2 | ZMYM2 | 210281_s_at | 2.375 |
| ATPase, class V, type 10A | ATP10A | 214255_at | 2.375 |
| bone morphogenetic protein 7 | BMP7 | 211259_s_at | 2.374 |
| glycine amidinotransferase (L-arginine:glycine amidinotransferase) | GATM | 216733_s_at | 2.371 |
| heat shock 70kD protein 12B | HSPA12B | 234610_at | 2.371 |
| mex-3 homolog C (<i>C. elegans</i>) | MEX3C | 1556874_a_at | 2.37 |
| tetraspanin 12 | TSPAN12 | 219274_at | 2.368 |
| matrix metalloproteinase 7 (matrilysin, uterine) | MMP7 | 204259_at | 2.368 |
| tetraspanin 10 | TSPAN10 | 223795_at | 2.366 |
| insulin-like growth factor binding protein 5 | IGFBP5 | 203426_s_at | 2.363 |
| cyclic nucleotide gated channel beta 1 | CNGB1 | 207342_at | 2.359 |
| ChaC, cation transport regulator homolog 1 (<i>E. coli</i>) | CHAC1 | 219270_at | 2.358 |
| RAB27B, member RAS oncogene family | RAB27B | 207017_at | 2.357 |
| spire homolog 2 (<i>Drosophila</i>) | SPIRE2 | 227706_at | 2.353 |
| small VCP/p97-interacting protein | SVIP | 230285_at | 2.353 |
| phosphatidylinositol transfer protein, cytoplasmic 1 | PITPNC1 | 238649_at | 2.351 |
| pyruvate dehydrogenase (lipoamide) alpha 2 | PDHA2 | 214518_at | 2.348 |
| rhodopsin | RHO | 206454_s_at | 2.344 |
| glycerol kinase | GK | 217167_x_at | 2.343 |
| small glutamine-rich tetratricopeptide repeat (TPR)-containing, beta | SGTB | 228745_at | 2.342 |
| N-acetylglucosamine-1-phosphate transferase, alpha and beta subunits | GNPTAB | 220398_at | 2.342 |
| tubulin tyrosine ligase-like family, member 7 | TTL7 | 219882_at | 2.339 |
| PH domain and leucine rich repeat protein phosphatase-like | PHLPPL | 213407_at | 2.337 |
| v-yes-1 Yamaguchi sarcoma viral related oncogene homolog | LYN | 210754_s_at | 2.337 |
| chloride intracellular channel 3 | CLIC3 | 219529_at | 2.336 |
| plasticity-related gene 2 | PRG2 | 220798_x_at | 2.336 |
| microRNA host gene 1 (non-protein coding) | MIRHG1 | 232291_at | 2.334 |
| Janus kinase 2 | JAK2 | 205841_at | 2.333 |
| serine/threonine protein kinase MST4 | RP6-213H19.1 | 224407_s_at | 2.332 |
| RAB27B, member RAS oncogene family | RAB27B | 207018_s_at | 2.331 |
| solute carrier family 14 (urea transporter), member 2 | SLC14A2 | 208409_at | 2.331 |

Table S2.2 cont'd.

| | | | |
|---|-------------------|--------------|-------|
| phosphatidylinositol transfer protein, cytoplasmic 1 | PITPNC1 | 219155_at | 2.312 |
| Tropomyosin 1 (alpha) | TPM1 | 238688_at | 2.312 |
| methyl-CpG binding domain protein 2 | MBD2 | 214397_at | 2.31 |
| T-box 2 | TBX2 | 213417_at | 2.309 |
| Jagged 1 (Alagille syndrome) | JAG1 | 231183_s_at | 2.306 |
| GATA binding protein 3 | GATA3 | 209604_s_at | 2.301 |
| tensin 4 | TNS4 | 230398_at | 2.297 |
| v-yes-1 Yamaguchi sarcoma viral related oncogene homolog | LYN | 202625_at | 2.295 |
| jumonji domain containing 4 | JMJD4 | 230810_at | 2.295 |
| small VCP/p97-interacting protein | SVIP | 226278_at | 2.293 |
| chromosome 20 open reading frame 57 | C20orf57 | 234829_at | 2.293 |
| contactin 3 (plasmacytoma associated) | CNTN3 | 229831_at | 2.292 |
| jun D proto-oncogene | JUND | 203751_x_at | 2.291 |
| nuclear receptor subfamily 1, group D, member 1 /// thyroid hormone receptor, alpha (erythroblastic leukemia) | NR1D1 /// THR | 204760_s_at | 2.291 |
| chondroitin sulfate proteoglycan 4 | CSPG4 | 204736_s_at | 2.282 |
| heparin-binding EGF-like growth factor | HBEGF | 38037_at | 2.28 |
| MHC class I polypeptide-related sequence A /// MHC class I polypeptide-related sequence B | MICA /// MICB | 205905_s_at | 2.277 |
| dishevelled associated activator of morphogenesis 1 | DAAM1 | 244062_at | 2.276 |
| natural cytotoxicity triggering receptor 2 | NCR2 | 217493_x_at | 2.269 |
| inhibitor of DNA binding 3, dominant negative helix-loop-helix protein | ID3 | 207826_s_at | 2.269 |
| acylphosphatase 1, erythrocyte (common) type | ACYP1 | 205260_s_at | 2.268 |
| pleckstrin homology-like domain, family A, member 1 | PHLDA1 | 217997_at | 2.268 |
| UDP glucuronosyltransferase 1 family, polypeptide A1 /// UDP glucuronosyltransferase 1 family, polypeptide A2 | UGT1A1 /// UGT1A2 | 208596_s_at | 2.265 |
| choroideremia-like (Rab escort protein 2) | CHML | 226350_at | 2.262 |
| echinoderm microtubule associated protein like 6 | EML6 | 229656_s_at | 2.261 |
| prostaglandin I2 (prostacyclin) synthase | PTGIS | 211892_s_at | 2.26 |
| karyopherin alpha 4 (importin alpha 3) | KPNA4 | 209653_at | 2.259 |
| ubiquitin specific peptidase 53 | USP53 | 231817_at | 2.258 |
| blood vessel epicardial substance | BVES | 223853_at | 2.256 |
| tetratricopeptide repeat domain 32 | TTC32 | 226838_at | 2.25 |
| glutamate receptor, ionotropic, kainate 2 | GRIK2 | 1563754_at | 2.25 |
| v-ets erythroblastosis virus E26 oncogene homolog 1 (avian) | ETS1 | 1553355_a_at | 2.249 |
| Hyaluronan synthase 2 | HAS2 | 230372_at | 2.244 |
| syndecan 1 | SDC1 | 201287_s_at | 2.244 |
| pleckstrin 2 | PLEK2 | 218644_at | 2.24 |
| T-box 18 | TBX18 | 1559840_s_at | 2.238 |
| fibroblast growth factor receptor 3 | FGFR3 | 204379_s_at | 2.227 |
| myosin X | MYO10 | 201976_s_at | 2.225 |
| kinesin family member 7 | KIF7 | 229405_at | 2.224 |
| GNAS complex locus | GNAS | 217673_x_at | 2.223 |
| non imprinted in Prader-Willi/Angelman syndrome 1 | NIPA1 | 225752_at | 2.223 |
| glycogen synthase kinase 3 alpha | GSK3A | 202210_x_at | 2.22 |
| radical S-adenosyl methionine domain containing 2 | RSAD2 | 213797_at | 2.22 |
| peptidoglycan recognition protein 4 | PGLYRP4 | 220944_at | 2.218 |
| WD repeat domain 69 | WDR69 | 242162_at | 2.215 |
| ADP-ribosylarginine hydrolase | ADPRH | 228042_at | 2.214 |
| tight junction protein 2 (zona occludens 2) | TJP2 | 202085_at | 2.213 |
| KIAA0182 | KIAA0182 | 212056_at | 2.209 |
| tubulin, beta 3 | TUBB3 | 202154_x_at | 2.204 |
| keratin 24 | KRT24 | 220267_at | 2.191 |
| malic enzyme 2, NAD(+)-dependent, mitochondrial | ME2 | 210154_at | 2.187 |
| abhydrolase domain containing 5 | ABHD5 | 218739_at | 2.185 |
| T-box 3 | TBX3 | 225544_at | 2.183 |
| cadherin-like 24 | CDH24 | 1553166_at | 2.181 |
| cadherin 4, type 1, R-cadherin (retinal) | CDH4 | 1563587_at | 2.177 |
| synovial sarcoma, X breakpoint 2 interacting protein | SSX2IP | 203017_s_at | 2.175 |
| blood vessel epicardial substance | BVES | 228783_at | 2.173 |
| similar to MCT /// solute carrier family 16, member 5 (monocarboxylic acid transporter 6) | LOC100133772 | 206600_s_at | 2.166 |
| transmembrane protein 70 | TMEM70 | 219449_s_at | 2.162 |
| inhibitor of DNA binding 4, dominant negative helix-loop-helix protein | ID4 | 209291_at | 2.158 |
| protein phosphatase 1, regulatory (inhibitor) subunit 15A | PPP1R15A | 202014_at | 2.157 |
| integrin, alpha 6 | ITGA6 | 201656_at | 2.155 |
| synaptotagmin XI | SYT11 | 209198_s_at | 2.15 |
| kelch domain containing 10 | KLHDC10 | 209254_at | 2.15 |
| transient receptor potential cation channel, subfamily V, member 2 | TRPV2 | 219282_s_at | 2.149 |
| tropomyosin 1 (alpha) | TPM1 | 1558532_at | 2.145 |
| serine hydrolase-like 2 | SERHL2 | 217276_x_at | 2.144 |
| beta-1,4-N-acetyl-galactosaminyl transferase 1 | B4GALNT1 | 206435_at | 2.14 |
| dual specificity phosphatase 8 | DUSP8 | 206374_at | 2.133 |
| progesterone and adiponectin receptor family member V | PAQR5 | 220333_at | 2.132 |
| hypothetical protein LOC149684 | LOC149684 | 244231_at | 2.132 |
| stanniocalcin 2 | STC2 | 203438_at | 2.131 |
| glutamate receptor interacting protein 2 | GRIP2 | 216481_at | 2.131 |
| connective tissue growth factor | CTGF | 209101_at | 2.131 |
| glycophorin B (MNS blood group) | GYPB | 207459_x_at | 2.121 |

Table S2.2 cont'd.

| | | | |
|---|-----------------|--------------|-------|
| staufen, RNA binding protein, homolog 2 (Drosophila) | STAU2 | 227179_at | 2.119 |
| zinc finger protein 83 | ZNF83 | 236429_at | 2.118 |
| transmembrane protein 8 (five membrane-spanning domains) | TMEM8 | 221882_s_at | 2.118 |
| myeloid/lymphoid or mixed-lineage leukemia (trithorax homolog, Drosophila); translocated to, 11 | MLLT11 | 211071_s_at | 2.115 |
| Rho-guanine nucleotide exchange factor | RGNEF | 1560348_at | 2.112 |
| ubiquilin 1 | UBQLN1 | 222989_s_at | 2.112 |
| lipopolysaccharide-induced TNF factor | LITAF | 200704_at | 2.111 |
| zinc finger CCCH-type containing 12C | ZC3H12C | 231899_at | 2.108 |
| paternally expressed 10 | PEG10 | 212092_at | 2.108 |
| Fraser syndrome 1 | FRAS1 | 226145_s_at | 2.106 |
| WD repeat domain 64 | WDR64 | 1553373_at | 2.105 |
| general transcription factor IIA, 1, 19/37kDa | GTF2A1 | 206521_s_at | 2.104 |
| anoctamin 10 | ANO10 | 218910_at | 2.102 |
| metastasis associated lung adenocarcinoma transcript 1 (non-protein coding) | MALAT1 | 224558_s_at | 2.099 |
| keratin 9 | KRT9 | 208188_at | 2.096 |
| acyl-CoA thioesterase 9 | ACOT9 | 221641_s_at | 2.093 |
| GA binding protein transcription factor, alpha subunit 60kDa | GABPA | 210188_at | 2.091 |
| thioredoxin-related transmembrane protein 3 | TMX3 | 1552822_at | 2.09 |
| zinc finger and BTB domain containing 1 | ZBTB1 | 205092_x_at | 2.086 |
| tropomyosin 1 (alpha) | TPM1 | 206116_s_at | 2.071 |
| hypothetical LOC284837 | LOC284837 | 1563088_s_at | 2.069 |
| coiled-coil domain containing 68 | CCDC68 | 220180_at | 2.067 |
| olfactory receptor, family 51, subfamily J, member 1 (gene/pseudogene) | OR51J1 | 233736_at | 2.066 |
| non imprinted in Prader-Willi/Angelman syndrome 1 | NIPA1 | 1552696_at | 2.065 |
| hairy and enhancer of split 1, (Drosophila) | HES1 | 203394_s_at | 2.064 |
| sprouty homolog 2 (Drosophila) | SPRY2 | 204011_at | 2.061 |
| Strawberry notch homolog 1 (Drosophila) | SBNO1 | 216162_at | 2.056 |
| nicalin homolog (zebrafish) | NCLN | 222206_s_at | 2.055 |
| cell division cycle 42 (GTP binding protein, 25kDa) | CDC42 | 210232_at | 2.055 |
| wingless-type MMTV integration site family, member 4 | WNT4 | 208606_s_at | 2.054 |
| forkhead box D1 | FOXO1 | 206307_s_at | 2.052 |
| v-Ki-ras2 Kirsten rat sarcoma viral oncogene homolog | KRAS | 214352_s_at | 2.05 |
| erythrocyte membrane protein band 4.1 like 4B | EPB41L4B | 220161_s_at | 2.049 |
| chromosome 16 open reading frame 11 | C16orf11 | 1553826_a_at | 2.042 |
| progesterone and adiponectin receptor family member III | PAQR3 | 213372_at | 2.04 |
| prefoldin subunit 2 | PFDN2 | 218336_at | 2.038 |
| cerebellar degeneration-related protein 2-like | CDR2L | 213230_at | 2.036 |
| heat shock protein 90kDa alpha (cytosolic), class A member 1 | HSP90AA1 | 211969_at | 2.031 |
| Kruppel-like factor 7 (ubiquitous) | KLF7 | 204334_at | 2.031 |
| hypothetical protein KIAA1434 | RP5-1022P6.2 | 224826_at | 2.031 |
| glycerol kinase 3 pseudogene | GK3P | 215966_x_at | 2.025 |
| pyruvate dehydrogenase kinase, isozyme 4 | PK4 | 205960_at | 2.025 |
| heat shock 22kDa protein 8 | HSPB8 | 221667_s_at | 2.025 |
| zinc finger protein 606 | ZNF606 | 229707_at | 2.024 |
| hypothetical protein FLJ23519 /// ribonuclease/angiogenin inhibitor 1 | FLJ23519 /// R1 | 216798_at | 2.021 |
| myosin X | MYO10 | 244350_at | 2.02 |
| pregnancy specific beta-1-glycoprotein 6 | PSG6 | 208106_x_at | 2.017 |
| Fraser syndrome 1 | FRAS1 | 1560153_at | 2.016 |
| forkhead box F2 | FOXO2 | 206377_at | 2.013 |
| BMP and activin membrane-bound inhibitor homolog (Xenopus laevis) | BAMBI | 203304_at | 2.011 |
| ring finger protein 112 | RNF112 | 223603_at | 2.01 |
| synaptotagmin XI | SYT11 | 209197_at | 2.007 |
| similar to mCG134545 | LOC342918 | 230814_at | 2.006 |
| myotubularin related protein 9 | MTMR9 | 204837_at | 2.006 |
| KIAA0182 | KIAA0182 | 212057_at | 2.006 |
| thrombospondin, type I, domain containing 4 | THSD4 | 222835_at | 2.003 |
| Inhibitor of DNA binding 4, dominant negative helix-loop-helix protein | ID4 | 226933_s_at | 2.003 |
| aryl hydrocarbon receptor | AHR | 202820_at | 2.002 |
| splicing factor, arginine/serine-rich 15 | SFRS15 | 233753_at | 2.001 |
| forkhead box C1 | FOXC1 | 1553613_s_at | 2.001 |

Table S2.3: Genes with decreased expression due to Alk3QD in adherent EOC cells.

| Gene Title | Gene Symbol | Probe Set ID | Fold Change |
|---|---------------|--------------|-------------|
| RAP1A, member of RAS oncogene family | RAP1A | 1555340_x_at | 1000.000 |
| RAP1A, member of RAS oncogene family | RAP1A | 1555339_at | 333.333 |
| serum amyloid A1 /// serum amyloid A2 | SAA1 /// SAA2 | 214456_x_at | 25.000 |
| chitinase 3-like 1 (cartilage glycoprotein-39) | CHI3L1 | 209396_s_at | 23.810 |
| major histocompatibility complex, class II, DR alpha | HLA-DRA | 210982_s_at | 20.000 |
| dipeptidyl-peptidase 6 | DPP6 | 228546_at | 19.231 |
| protein kinase (cAMP-dependent, catalytic) inhibitor beta | PKIB | 231120_x_at | 18.182 |
| periplakin | PPL | 203407_at | 15.152 |
| chitinase 3-like 1 (cartilage glycoprotein-39) | CHI3L1 | 209395_at | 14.085 |
| chloride channel accessory 2 | CLCA2 | 206165_s_at | 13.699 |
| serum amyloid A1 /// serum amyloid A2 | SAA1 /// SAA2 | 208607_s_at | 13.699 |
| toll-like receptor 7 | TLR7 | 220146_at | 12.821 |
| selenoprotein P, plasma, 1 | SEPP1 | 201427_s_at | 9.615 |
| family with sequence similarity 5, member B | FAM5B | 214822_at | 9.009 |
| hydroxy-delta-5-steroid dehydrogenase, 3 beta- and steroid delta-isomerase 2 | HSD3B2 | 206294_at | 9.009 |
| chloride channel accessory 2 | CLCA2 | 217528_at | 8.475 |
| dipeptidyl-peptidase 6 | DPP6 | 207789_s_at | 8.333 |
| alpha-2-macroglobulin | A2M | 217757_at | 7.634 |
| haptoglobin /// haptoglobin-related protein | HP /// HPR | 208470_s_at | 7.463 |
| chromosome 13 open reading frame 36 | C13orf36 | 241672_at | 6.536 |
| complement component 8, alpha polypeptide | C8A | 206305_s_at | 6.410 |
| asp (abnormal spindle) homolog, microcephaly associated (Drosophila) | ASPM | 232238_at | 6.369 |
| RALBP1 associated Eps domain containing 2 | REPS2 | 227425_at | 6.211 |
| chromosome 9 open reading frame 38 | C9orf38 | 208077_at | 6.098 |
| calbindin 1, 28kDa | CALB1 | 205625_s_at | 6.024 |
| benzodiazepine receptor (peripheral) associated protein 1 | BZRAP1 | 205839_s_at | 5.988 |
| podoplanin | PDPN | 221898_at | 5.882 |
| cadherin 1, type 1, E-cadherin (epithelial) | CDH1 | 201131_s_at | 5.814 |
| immunoglobulin heavy constant delta | IGHD | 214973_x_at | 5.714 |
| serine PI Kazal type 5-like 3 | SPINK5L3 | 233340_at | 5.682 |
| pyruvate carboxylase | PC | 204476_s_at | 5.682 |
| asp (abnormal spindle) homolog, microcephaly associated (Drosophila) | ASPM | 219918_s_at | 5.435 |
| bone morphogenetic protein 7 | BMP7 | 211259_s_at | 5.376 |
| netrin 3 | NTN3 | 207640_x_at | 5.319 |
| insulin-like growth factor 1 receptor | IGF1R | 203628_at | 5.181 |
| piwi-like 1 (Drosophila) | PIWIL1 | 214868_at | 5.128 |
| testicular cell adhesion molecule 1 homolog (mouse) | TCAM1 | 233320_at | 5.000 |
| ATPase, class I, type 8B, member 4 | ATP8B4 | 220416_at | 4.902 |
| keratin 36 | KRT36 | 214576_at | 4.785 |
| calcium/calmodulin-dependent protein kinase II beta | CAMK2B | 210404_x_at | 4.762 |
| carboxylesterase 8 (putative) | CES8 | 228903_at | 4.739 |
| thioredoxin interacting protein | TXNIP | 201010_s_at | 4.739 |
| chromosome 19 open reading frame 59 | C19orf59 | 235568_at | 4.717 |
| keratin 20 | KRT20 | 213953_at | 4.695 |
| sema domain, immunoglobulin domain (Ig), transmembrane domain (TM) and short cytoplasmic domain | SEMA4D | 228891_at | 4.673 |
| solute carrier family 39 (zinc transporter), member 2 | SLC39A2 | 220413_at | 4.630 |
| transmembrane and tetratricopeptide repeat containing 4 | TMTC4 | 225666_at | 4.630 |
| RALBP1 associated Eps domain containing 2 | REPS2 | 205645_at | 4.608 |
| haptoglobin /// haptoglobin-related protein | HP /// HPR | 206697_s_at | 4.608 |
| zinc finger protein 29 pseudogene | ZNF29 | 1567856_x_at | 4.587 |
| WD repeat domain 41 | WDR41 | 240637_at | 4.545 |
| platelet derived growth factor D | PDGFD | 219304_s_at | 4.545 |
| protein disulfide isomerase-like, testis expressed | PDILT | 1554970_at | 4.505 |
| retinoschisin 1 | RS1 | 216937_s_at | 4.484 |
| aryl-hydrocarbon receptor nuclear translocator 2 | ARNT2 | 202986_at | 4.464 |
| Oligodendrocyte myelin glycoprotein | OMG | 238720_at | 4.444 |
| heterogeneous nuclear ribonucleoprotein C (C1/C2) | HNRNPC | 235500_at | 4.425 |
| Immunoglobulin heavy constant gamma 1 (G1m marker) | IGHG1 | 217320_at | 4.367 |
| potassium voltage-gated channel, subfamily H (eag-related), member 2 | KCNH2 | 210036_s_at | 4.367 |
| solute carrier family 47, member 1 | SLC47A1 | 219525_at | 4.348 |
| chromosome 2 open reading frame 58 | C2orf58 | 1553829_at | 4.348 |
| hemoglobin, epsilon 1 | HBE1 | 205919_at | 4.348 |
| insulin-like growth factor binding protein 2, 36kDa | IGFBP2 | 202718_at | 4.310 |
| leucine-rich repeats and immunoglobulin-like domains 3 | LRIG3 | 226908_at | 4.310 |
| brain peptide A1 | BPA-1 | 1555547_at | 4.292 |
| chloride channel accessory 2 | CLCA2 | 206166_s_at | 4.255 |
| interferon stimulated exonuclease gene 20kDa-like 2 | ISG20L2 | 216502_at | 4.167 |

Table S2.3 cont'd.

| | | | |
|--|----------------------|--------------|-------|
| interleukin 18 (interferon-gamma-inducing factor) | IL18 | 206295_at | 4.167 |
| chromosome 14 open reading frame 162 | C14orf162 | 220887_at | 4.149 |
| transforming growth factor, beta receptor III | TGFBR3 | 204731_at | 4.132 |
| solute carrier family 27 (fatty acid transporter), member 2 | SLC27A2 | 205768_s_at | 4.065 |
| chromosome 14 open reading frame 83 | C14orf83 | 227544_at | 4.065 |
| NEDD4 binding protein 2-like 1 | N4BP2L1 | 213375_s_at | 4.016 |
| superoxide dismutase 2, mitochondrial | SOD2 | 221477_s_at | 4.016 |
| Hypothetical protein LOC100130458 | LOC100130458 | 239214_at | 3.968 |
| family with sequence similarity 84, member A | FAM84A | 234331_s_at | 3.953 |
| solute carrier family 4, sodium bicarbonate cotransporter, member 5 | SLC4A5 | 221723_s_at | 3.937 |
| vascular cell adhesion molecule 1 | VCAM1 | 203868_s_at | 3.817 |
| lysyl oxidase-like 4 | LOXL4 | 227145_at | 3.774 |
| solute carrier family 46, member 3 | SLC46A3 | 214719_at | 3.774 |
| Tripartite motif-containing 8 | TRIM8 | 228015_s_at | 3.731 |
| discs, large (Drosophila) homolog-associated protein 1 | DLGAP1 | 206490_at | 3.690 |
| CD28 molecule | CD28 | 206545_at | 3.690 |
| aldehyde dehydrogenase 6 family, member A1 | ALDH6A1 | 221589_s_at | 3.676 |
| potassium voltage-gated channel, Shal-related subfamily, member 3 | KCND3 | 213832_at | 3.663 |
| collagen, type XIV, alpha 1 | COL14A1 | 216866_s_at | 3.663 |
| cytochrome P450, family 7, subfamily B, polypeptide 1 | CYP7B1 | 207386_at | 3.636 |
| growth arrest-specific 7 | GAS7 | 202191_s_at | 3.636 |
| angiopoietin-like 1 | ANGPTL1 | 239183_at | 3.636 |
| vacuolar protein sorting 36 homolog (S. cerevisiae) | VPS36 | 240086_at | 3.623 |
| complement component 1, s subcomponent | C1S | 1555229_a_at | 3.623 |
| potassium voltage-gated channel, Shal-related subfamily, member 3 | KCND3 | 215014_at | 3.623 |
| synovial sarcoma, X breakpoint 3 | SSX3 | 207666_x_at | 3.623 |
| hook homolog 1 (Drosophila) | HOOK1 | 219976_at | 3.597 |
| chemokine (C-X-C motif) ligand 16 | CXCL16 | 223454_at | 3.571 |
| family with sequence similarity 170, member B | FAM170B | 1559828_at | 3.546 |
| sema domain, immunoglobulin domain (Ig), transmembrane domain (TM) and short cytoplasmic domain | SEMA4D | 203528_at | 3.534 |
| chromosome 13 open reading frame 31 | C13orf31 | 1553142_at | 3.521 |
| vanin 1 | VNN1 | 205844_at | 3.484 |
| endothelin 2 | EDN2 | 206758_at | 3.484 |
| synaptopodin 2 | SYNPO2 | 227662_at | 3.472 |
| cytochrome b5 type A (microsomal) | CYB5A | 217021_at | 3.472 |
| podoplanin | PDPN | 204879_at | 3.460 |
| 3-hydroxymethyl-3-methylglutaryl-Coenzyme A lyase-like 1 | HMGCLL1 | 232305_at | 3.413 |
| major facilitator superfamily domain containing 4 | MFSD4 | 229254_at | 3.401 |
| cytidine monophosphate-N-acetylneuraminic acid hydroxylase (CMP-N-acetylneuraminic acid hydroxylase) | CMAH | 205518_s_at | 3.401 |
| G protein-coupled receptor 112 | GPR112 | 1553006_at | 3.356 |
| E74-like factor 3 (ets domain transcription factor, epithelial-specific) | ELF3 | 210827_s_at | 3.344 |
| cyclin-dependent kinase 2 | CDK2 | 211803_at | 3.322 |
| KIAA1324 | KIAA1324 | 226248_s_at | 3.322 |
| chromosome 5 open reading frame 4 | C5orf4 | 220751_s_at | 3.322 |
| caspase 12 (gene/pseudogene) | CASP12 | 1564736_a_at | 3.322 |
| complement factor H /// complement factor H-related 1 | CFH /// CFHR1 | 215388_s_at | 3.322 |
| immunoglobulin kappa constant | IGKC | 214836_x_at | 3.300 |
| WW and C2 domain containing 1 | WWC1 | 216074_x_at | 3.300 |
| CUG triplet repeat, RNA binding protein 2 | CUGBP2 | 242268_at | 3.289 |
| vanin 1 | VNN1 | 1558549_s_at | 3.257 |
| cytochrome b reductase 1 | CYBRD1 | 222453_at | 3.247 |
| STEAP family member 4 | STEAP4 | 220187_at | 3.226 |
| interferon-induced protein with tetratricopeptide repeats 1 | IFIT1 | 203153_at | 3.195 |
| phospholipid scramblase 4 | PLSCR4 | 218901_at | 3.175 |
| baculoviral IAP repeat-containing 3 | BIRC3 | 210538_s_at | 3.175 |
| hypothetical LOC728475 | LOC728475 | 242010_at | 3.165 |
| interleukin-1 receptor-associated kinase 3 | IRAK3 | 213817_at | 3.165 |
| discs, large (Drosophila) homolog-associated protein 1 /// hypothetical protein LOC284214 | DLGAP1 /// LOC284214 | 235527_at | 3.145 |
| chromosome X open reading frame 56 | CXorf56 | 239444_at | 3.145 |
| ring finger protein 125 | RNF125 | 235199_at | 3.135 |
| hypothetical LOC653602 | LOC653602 | 229546_at | 3.115 |
| B-cell CLL/lymphoma 8 | BCL8 | 1560683_at | 3.086 |
| nuclear factor (erythroid-derived 2)-like 3 | NFE2L3 | 204702_s_at | 3.058 |
| tescalcin | TESC | 218872_at | 3.040 |
| myosin VB | MYO5B | 225299_at | 3.040 |
| myosin VB | MYO5B | 225301_s_at | 3.040 |
| sprouty homolog 1, antagonist of FGF signaling (Drosophila) | SPRY1 | 212558_at | 3.021 |
| hypothetical LOC401312 | LOC401312 | 1560520_at | 3.012 |
| golgi phosphoprotein 3-like | GOLPH3L | 218361_at | 3.012 |

Table S2.3 cont'd.

| | | | |
|---|----------------|--------------|-------|
| SWI/SNF related, matrix associated, actin dependent regulator of chromatin, subfamily a, member 4 | SMARCA4 | 213719_s_at | 3.003 |
| coiled-coil domain containing 80 | CCDC80 | 225241_at | 3.003 |
| chromobox homolog 2 (Pc class homolog, Drosophila) | CBX2 | 224138_at | 2.994 |
| interferon, alpha-inducible protein 6 | IFI6 | 204415_at | 2.985 |
| BCL2-interacting killer (apoptosis-inducing) | BIK | 205780_at | 2.976 |
| myelin basic protein | MBP | 210136_at | 2.967 |
| solute carrier family 44, member 3 | SLC44A3 | 228221_at | 2.967 |
| hypothetical protein LOC100129827 | LOC100129827 | 231595_at | 2.950 |
| calcyphosine | CAPS | 226424_at | 2.941 |
| calbindin 2 | CALB2 | 205428_s_at | 2.941 |
| OTU domain containing 1 | OTUD1 | 226140_s_at | 2.924 |
| WW and C2 domain containing 1 | WWC1 | 229180_at | 2.924 |
| armadillo repeat containing, X-linked 4 | ARMCX4 | 1552327_at | 2.924 |
| chromosome 13 open reading frame 31 | C13orf31 | 228937_at | 2.915 |
| Fc fragment of IgA, receptor for | FCAR | 211816_x_at | 2.915 |
| sphingomyelin phosphodiesterase 3, neutral membrane (neutral sphingomyelinase II) | SMPD3 | 231732_at | 2.915 |
| superoxide dismutase 2, mitochondrial | SOD2 | 215223_s_at | 2.915 |
| EPH receptor B3 | EPHB3 | 204600_at | 2.907 |
| potassium voltage-gated channel, subfamily H (eag-related), member 6 | KCNH6 | 211045_s_at | 2.899 |
| tumor necrosis factor, alpha-induced protein 2 | TNFAIP2 | 202510_s_at | 2.890 |
| plasticity related gene 3 | RP11-35N6.1 | 1570250_at | 2.890 |
| chromosome 5 open reading frame 4 | C5orf4 | 48031_r_at | 2.890 |
| E74-like factor 3 (ets domain transcription factor, epithelial-specific) | ELF3 | 201510_at | 2.874 |
| olfactory receptor, family 7, subfamily E, member 47 pseudogene | OR7E47P | 222304_x_at | 2.874 |
| cytidine monophosphate-N-acetylneuraminic acid hydroxylase (CMP-N-acetylneuraminate monooxygenase) | CMAH | 210571_s_at | 2.874 |
| chromosome 13 open reading frame 31 | C13orf31 | 1553141_at | 2.865 |
| par-6 partitioning defective 6 homolog beta (C. elegans) | PAR6B | 235165_at | 2.857 |
| aldehyde dehydrogenase 6 family, member A1 | ALDH6A1 | 221588_x_at | 2.841 |
| sushi, von Willebrand factor type A, EGF and pentraxin domain containing 1 | SVEP1 | 219552_at | 2.817 |
| synaptotagmin III | SYT3 | 223901_at | 2.817 |
| phospholipid scramblase 1 | PLSCR1 | 202430_s_at | 2.809 |
| Hypothetical protein LOC100128484 | LOC100128484 | 239308_at | 2.809 |
| solute carrier family 22 (organic cation transporter), member 2 | SLC22A2 | 207429_at | 2.809 |
| interleukin 23 receptor | IL23R | 1561853_a_at | 2.801 |
| glutamate receptor, ionotropic, N-methyl D-aspartate 2A | GRIN2A | 206534_at | 2.793 |
| EF-hand domain (C-terminal) containing 2 | EFHC2 | 220591_s_at | 2.770 |
| par-3 partitioning defective 3 homolog B (C. elegans) | PAR3B | 1553188_s_at | 2.762 |
| Solute carrier family 25, member 29 | SLC25A29 | 232280_at | 2.762 |
| E74-like factor 3 (ets domain transcription factor, epithelial-specific) | ELF3 | 229842_at | 2.762 |
| furry homolog (Drosophila) | FRY | 204072_s_at | 2.755 |
| transmembrane protein 140 | TMEM140 | 218999_at | 2.755 |
| collectin sub-family member 12 | COLEC12 | 221019_s_at | 2.740 |
| cytochrome P450, family 39, subfamily A, polypeptide 1 | CYP39A1 | 1553977_a_at | 2.732 |
| transforming growth factor, beta 3 | TGFB3 | 209747_at | 2.732 |
| solute carrier family 22, member 23 | SLC22A23 | 223194_s_at | 2.717 |
| KIAA1462 | KIAA1462 | 213316_at | 2.717 |
| colony stimulating factor 2 receptor, alpha, low-affinity (granulocyte-macrophage) /// hypothetical protein | CSF2RA /// LOC | 210340_s_at | 2.710 |
| annexin A4 | ANXA4 | 201302_at | 2.703 |
| glutaminase | GLS | 203157_s_at | 2.688 |
| interferon-induced protein with tetratricopeptide repeats 2 | IFIT2 | 226757_at | 2.688 |
| chromosome 10 open reading frame 11 | C10orf11 | 223703_at | 2.688 |
| ERO1-like beta (S. cerevisiae) | ERO1LB | 231944_at | 2.688 |
| transmembrane protein 37 | TMEM37 | 227190_at | 2.681 |
| T-cell activation RhoGTPase activating protein | TAGAP | 1552541_at | 2.674 |
| vitronectin | VTN | 204534_at | 2.674 |
| obscurin, cytoskeletal calmodulin and titin-interacting RhoGEF | OBSCN | 229854_at | 2.674 |
| vav 3 guanine nucleotide exchange factor | VAV3 | 218807_at | 2.667 |
| islet cell autoantigen 1,69kDa-like | ICA1L | 223881_at | 2.660 |
| PTPRF interacting protein, binding protein 2 (liprin beta 2) | PPFIBP2 | 212841_s_at | 2.660 |
| histone cluster 1, H2bc | HIST1H2BC | 236193_at | 2.660 |
| prostaglandin F2 receptor negative regulator | PTGFRN | 224937_at | 2.660 |
| cytochrome P450, family 27, subfamily A, polypeptide 1 | CYP27A1 | 203979_at | 2.639 |
| spectrin, beta, non-erythrocytic 4 | SPTBN4 | 224297_s_at | 2.632 |
| mesoderm specific transcript homolog (mouse) | MEST | 202016_at | 2.604 |
| chromosome 9 open reading frame 125 | C9orf125 | 224458_at | 2.597 |
| ferritin, heavy polypeptide 1 | FTH1 | 214211_at | 2.591 |
| ATP-binding cassette, sub-family B (MDR/TAP), member 1 | ABCB1 | 209993_at | 2.584 |
| Mannosidase, alpha, class 1A, member 1 | MAN1A1 | 221760_at | 2.577 |
| family with sequence similarity 38, member B | FAM38B | 219602_s_at | 2.571 |

Table S2.3 cont'd.

| | | | |
|--|----------------|--------------|-------|
| MACRO domain containing 2 | MACROD2 | 235278_at | 2.564 |
| myelin basic protein | MBP | 1554544_a_at | 2.558 |
| cyclin-dependent kinase inhibitor 1C (p57, Kip2) | CDKN1C | 219534_x_at | 2.551 |
| RAB7B, member RAS oncogene family | RAB7B | 1553982_a_at | 2.551 |
| ubiquitin protein ligase E3 component n-recogin 4 | UBR4 | 231889_at | 2.551 |
| hypothetical LOC151658 | LOC151658 | 238283_at | 2.545 |
| tensin 3 | TNS3 | 217853_at | 2.545 |
| calcium/calmodulin-dependent protein kinase kinase 2, beta | CAMKK2 | 207359_at | 2.538 |
| dymeclin | DYM | 220774_at | 2.538 |
| unc-51-like kinase 2 (C. elegans) | ULK2 | 215154_at | 2.538 |
| ATP/GTP binding protein-like 2 | AGBL2 | 220390_at | 2.538 |
| discs, large (Drosophila) homolog-associated protein 1 | DLGAP1 | 206489_s_at | 2.538 |
| hypothetical LOC100129550 | LOC100129550 | 229699_at | 2.532 |
| low density lipoprotein-related protein 2 | LRP2 | 205710_at | 2.525 |
| TAP binding protein (tapasin) | TAPBP | 210294_at | 2.525 |
| transmembrane protein 163 | TMEM163 | 1552626_a_at | 2.519 |
| chromosome 11 open reading frame 35 | C11orf35 | 236050_at | 2.519 |
| tumor necrosis factor receptor superfamily, member 21 | TNFRSF21 | 214581_x_at | 2.519 |
| potassium inwardly-rectifying channel, subfamily J, member 12 | KCNJ12 | 232289_at | 2.513 |
| chromosome 17 open reading frame 103 | C17orf103 | 226657_at | 2.513 |
| cathepsin F | CTSF | 203657_s_at | 2.506 |
| aldehyde dehydrogenase 6 family, member A1 | ALDH6A1 | 204290_s_at | 2.506 |
| 4-hydroxyphenylpyruvate dioxygenase | HPD | 206024_at | 2.500 |
| Mov1011, Moloney leukemia virus 10-like 1, homolog (mouse) | MOV10L1 | 239257_at | 2.500 |
| potassium inwardly-rectifying channel, subfamily J, member 12 | KCNJ12 | 207110_at | 2.500 |
| LRRN4 C-terminal like | LRRN4CL | 1556427_s_at | 2.500 |
| microtubule-associated protein 7 | MAP7 | 202890_at | 2.500 |
| WW and C2 domain containing 1 | WWC1 | 213085_s_at | 2.494 |
| spermatid perinuclear RNA binding protein | STRBP | 223246_s_at | 2.494 |
| chromosome 8 open reading frame 83 | C8orf83 | 224158_s_at | 2.494 |
| growth arrest-specific 7 | GAS7 | 202192_s_at | 2.488 |
| paired box 8 | PAX8 | 221990_at | 2.488 |
| glutamate decarboxylase 1 (brain, 67kDa) | GAD1 | 205278_at | 2.481 |
| ATP-binding cassette, sub-family A (ABC1), member 9 | ABCA9 | 235335_at | 2.481 |
| hypothetical gene supported by AK026416 | FLJ22763 | 233604_at | 2.475 |
| complement component 1, s subcomponent | C1S | 208747_s_at | 2.475 |
| ets variant 4 | ETV4 | 1554576_a_at | 2.463 |
| collagen, type XVI, alpha 1 | COL16A1 | 204345_at | 2.457 |
| acyl-CoA thioesterase 4 | ACOT4 | 229534_at | 2.457 |
| Kallmann syndrome 1 sequence | KAL1 | 205206_at | 2.457 |
| carboxymethylglutaminase homolog (Pseudomonas) | CMBL | 227522_at | 2.457 |
| chromosome 5 open reading frame 13 | C5orf13 | 201310_s_at | 2.457 |
| phospholipase A2, group X | PLA2G10 | 207222_at | 2.451 |
| CD6 molecule | CD6 | 213958_at | 2.445 |
| proprotein convertase subtilisin/kexin type 6 | PCSK6 | 211262_at | 2.445 |
| GM2 ganglioside activator | GM2A | 209727_at | 2.439 |
| caspase 10, apoptosis-related cysteine peptidase | CASP10 | 205467_at | 2.433 |
| receptor tyrosine kinase-like orphan receptor 1 | ROR1 | 232060_at | 2.433 |
| hydroxy-delta-5-steroid dehydrogenase, 3 beta- and steroid delta-isomerase 1 /// hydroxy-delta-5-steroid | HSD3B1 /// HSC | 215665_at | 2.433 |
| ureidopropionase, beta | UPB1 | 220507_s_at | 2.433 |
| C-terminal binding protein 1 | CTBP1 | 1557714_at | 2.427 |
| glutaminase | GLS | 203159_at | 2.421 |
| chromosome 10 open reading frame 54 | C10orf54 | 225372_at | 2.415 |
| family with sequence similarity 38, member B | FAM38B | 222908_at | 2.410 |
| ring finger protein 144B | RNF144B | 228153_at | 2.398 |
| keratinocyte growth factor-like protein 2 | KGFLP2 | 231031_at | 2.398 |
| cell adhesion molecule 4 | CADM4 | 222293_at | 2.398 |
| K(lysine) acetyltransferase 2B | KAT2B | 203845_at | 2.392 |
| aldehyde oxidase 1 | AOX1 | 205082_s_at | 2.392 |
| ubiquitin specific peptidase 2 | USP2 | 229337_at | 2.392 |
| chromosome 6 open reading frame 123 | C6orf123 | 207698_at | 2.387 |
| tumor necrosis factor receptor superfamily, member 21 | TNFRSF21 | 218856_at | 2.387 |
| ADAM metalloproteinase domain 12 | ADAM12 | 215613_at | 2.387 |
| phosphoinositide-3-kinase, regulatory subunit 3 (gamma) | PIK3R3 | 202743_at | 2.381 |
| solute carrier family 39 (metal ion transporter), member 11 | SLC39A11 | 227046_at | 2.381 |
| myelin-associated oligodendrocyte basic protein | MOBP | 242765_at | 2.375 |
| chromosome 18 open reading frame 2 | C18orf2 | 224045_x_at | 2.375 |
| superoxide dismutase 2, mitochondrial | SOD2 | 216841_s_at | 2.375 |
| coiled-coil domain containing 80 | CCDC80 | 225242_s_at | 2.375 |

Table S2.3 cont'd.

| | | | |
|--|----------------|--------------|-------|
| programmed cell death 4 (neoplastic transformation inhibitor) | PDCD4 | 212594_at | 2.370 |
| dual adaptor of phosphotyrosine and 3-phosphoinositides | DAPP1 | 219290_x_at | 2.370 |
| synovial sarcoma, X breakpoint 4 /// synovial sarcoma, X breakpoint 4B | SSX4 /// SSX4B | 211425_x_at | 2.364 |
| syndecan 4 | SDC4 | 202071_at | 2.358 |
| signal-regulatory protein gamma | SIRPG | 220485_s_at | 2.358 |
| palmelphin | PALMD | 218736_s_at | 2.358 |
| par-3 partitioning defective 3 homolog B (C. elegans) | PARD3B | 228411_at | 2.353 |
| hyaluronan and proteoglycan link protein 1 | HAPLN1 | 230204_at | 2.353 |
| mannosidase, alpha, class 1A, member 1 | MAN1A1 | 208116_s_at | 2.342 |
| chromosome 12 open reading frame 35 | C12orf35 | 227152_at | 2.342 |
| family with sequence similarity 35, member A | FAM35A | 233048_at | 2.336 |
| endoplasmic reticulum metalloproteinase 1 | ERMP1 | 222603_at | 2.331 |
| ribosomal modification protein rimK-like family member A | RIMKLA | 241075_at | 2.331 |
| mitogen-activated protein kinase kinase kinase 7 interacting protein 3 | MAP3K7IP3 | 1558518_at | 2.326 |
| hypothetical LOC79150 | MGC4859 | 207775_at | 2.326 |
| chromosome 5 open reading frame 13 | C5orf13 | 201309_x_at | 2.320 |
| ADAM metalloproteinase domain 12 | ADAM12 | 213790_at | 2.315 |
| cyclin-dependent kinase-like 2 (CDC2-related kinase) | CDKL2 | 236331_at | 2.309 |
| dopachrome tautomerase (dopachrome delta-isomerase, tyrosine-related protein 2) | DCT | 205338_s_at | 2.304 |
| yippee-like 3 (Drosophila) | YPEL3 | 223179_at | 2.304 |
| phospholipid scramblase 1 | PLSCR1 | 202446_s_at | 2.299 |
| histone cluster 1, H2bc | HIST1H2BC | 214455_at | 2.294 |
| serpin peptidase inhibitor, clade B (ovalbumin), member 9 | SERPINF9 | 242814_at | 2.294 |
| FERM domain containing 4B | FRMD4B | 213056_at | 2.294 |
| protein-L-isoaspartate (D-aspartate) O-methyltransferase domain containing 1 | PCMTD1 | 232382_s_at | 2.288 |
| copine VIII | CPNE8 | 243727_at | 2.288 |
| KIAA0247 | KIAA0247 | 202181_at | 2.288 |
| glutaminase | GLS | 203158_s_at | 2.288 |
| ST3 beta-galactoside alpha-2,3-sialyltransferase 5 | ST3GAL5 | 203217_s_at | 2.283 |
| ectonucleotide pyrophosphatase/phosphodiesterase 3 | ENPP3 | 232737_s_at | 2.283 |
| phospholipase D1, phosphatidylcholine-specific | PLD1 | 226636_at | 2.278 |
| endoplasmic reticulum metalloproteinase 1 | ERMP1 | 218342_s_at | 2.278 |
| KIAA0895 | KIAA0895 | 213424_at | 2.278 |
| aldehyde oxidase 1 | AOX1 | 205083_at | 2.278 |
| unc-51-like kinase 2 (C. elegans) | ULK2 | 1554112_a_at | 2.268 |
| transmembrane protein 151A | TMEM151A | 235614_at | 2.268 |
| six transmembrane epithelial antigen of the prostate 2 | STEAP2 | 225871_at | 2.262 |
| solute carrier family 27 (fatty acid transporter), member 2 | SLC27A2 | 205769_at | 2.262 |
| growth arrest-specific 6 /// similar to growth arrest-specific 6 | GAS6 /// LOC10 | 1598_g_at | 2.262 |
| interleukin 1 receptor, type I | IL1R1 | 202948_at | 2.262 |
| Hypothetical protein LOC100130353 | LOC100130353 | 1564449_at | 2.262 |
| Family with sequence similarity 92, member A1 | FAM92A1 | 237910_x_at | 2.257 |
| MAX dimerization protein 4 | MXD4 | 210778_s_at | 2.257 |
| mal, T-cell differentiation protein 2 | MAL2 | 224650_at | 2.257 |
| poly (ADP-ribose) polymerase family, member 14 | PARP14 | 224701_at | 2.252 |
| zinc finger and BTB domain containing 44 | ZBTB44 | 225845_at | 2.252 |
| annexin A4 | ANXA4 | 201301_s_at | 2.252 |
| myelin basic protein | MBP | 225408_at | 2.247 |
| UDP-N-acetyl-alpha-D-galactosamine:polypeptide N-acetylgalactosaminyltransferase 1 (GalNAc-T1) | GALNT1 | 201724_s_at | 2.242 |
| ubiquitously transcribed tetratricopeptide repeat gene, Y-linked | UTY | 210322_x_at | 2.242 |
| G protein-coupled receptor 87 | GPR87 | 219936_s_at | 2.237 |
| Tissue factor pathway inhibitor (lipoprotein-associated coagulation inhibitor) | TFPI | 215447_at | 2.232 |
| macrophage stimulating 1 receptor (c-met-related tyrosine kinase) | MST1R | 205455_at | 2.232 |
| DEAD (Asp-Glu-Ala-Asp) box polypeptide 60 | DDX60 | 218986_s_at | 2.232 |
| cyclin-dependent kinase inhibitor 2B (p15, inhibits CDK4) | CDKN2B | 236313_at | 2.222 |
| post-GPI attachment to proteins 1 | PGAP1 | 220576_at | 2.217 |
| engulfment and cell motility 1 | ELMO1 | 204513_s_at | 2.217 |
| actin-like 8 | ACTL8 | 214957_at | 2.217 |
| TP53 target 1 (non-protein coding) | TP53TG1 | 210241_s_at | 2.212 |
| macrophage stimulating 1 (hepatocyte growth factor-like) | MST1 | 205614_x_at | 2.212 |
| secretory leukocyte peptidase inhibitor | SLPI | 203021_at | 2.212 |
| solute carrier family 15, member 3 | SLC15A3 | 219593_at | 2.212 |
| integrin, beta 8 | ITGB8 | 226189_at | 2.208 |
| hypothetical LOC541472 | LOC541472 | 243977_at | 2.208 |
| aquaporin 2 (collecting duct) | AQP2 | 206672_at | 2.203 |
| solute carrier family 27 (fatty acid transporter), member 1 | SLC27A1 | 226728_at | 2.203 |
| fibroblast growth factor 7 (keratinocyte growth factor) | FGF7 | 205782_at | 2.203 |
| neuroblastoma, suppression of tumorigenicity 1 | NBL1 | 201621_at | 2.203 |
| cyclin-dependent kinase inhibitor 1C (p57, Kip2) | CDKN1C | 216894_x_at | 2.203 |

Table S2.3 cont'd.

| | | | |
|--|--|--------------|-------|
| fibulin 1 | FBLN1 | 207835_at | 2.198 |
| peroxisome proliferator-activated receptor gamma, coactivator 1 beta | PPARGC1B | 1553639_a_at | 2.193 |
| Rho guanine nucleotide exchange factor (GEF) 3 | ARHGEF3 | 218501_at | 2.193 |
| ciliary neurotrophic factor receptor | CNTFR | 205723_at | 2.188 |
| SH3 domain binding glutamic acid-rich protein like 2 | SH3BGL2 | 225354_s_at | 2.188 |
| TNFSF12-TNFSF13 readthrough transcript /// tumor necrosis factor (ligand) superfamily, member 13 | TNFSF12-TNFSF13 | 209500_x_at | 2.188 |
| hexose-6-phosphate dehydrogenase (glucose 1-dehydrogenase) | H6PD | 221892_at | 2.188 |
| sema domain, immunoglobulin domain (Ig), short basic domain, secreted, (semaphorin) 3E | SEMA3E | 206941_x_at | 2.183 |
| guanine nucleotide binding protein (G protein), gamma 7 | GNG7 | 228831_s_at | 2.183 |
| endothelin receptor type A | EDNRA | 204464_s_at | 2.183 |
| CD40 molecule, TNF receptor superfamily member 5 | CD40 | 222292_at | 2.179 |
| chromosome 9 open reading frame 126 | C9orf126 | 228174_at | 2.174 |
| solute carrier family 25, member 27 | SLC25A27 | 1554161_at | 2.174 |
| collagen, type XXII, alpha 1 | COL22A1 | 228873_at | 2.169 |
| pre T-cell antigen receptor alpha | PTCRA | 211837_s_at | 2.169 |
| mannosidase, alpha, class 2A, member 2 | MAN2A2 | 219999_at | 2.169 |
| interferon regulatory factor 1 | IRF1 | 238725_at | 2.169 |
| interleukin 16 (lymphocyte chemoattractant factor) | IL16 | 1555016_at | 2.169 |
| sortilin 1 | SORT1 | 224818_at | 2.169 |
| pleckstrin homology domain containing, family G (with RhoGef domain) member 1 | PLEKHG1 | 226122_at | 2.155 |
| phosphoinositide-3-kinase interacting protein 1 | PIK3IP1 | 221757_at | 2.155 |
| hypothetical LOC729970 | LOC729970 | 230433_at | 2.155 |
| leucine rich repeat containing 1 | LRRC1 | 218816_at | 2.146 |
| 2-5-oligoadenylate synthetase 3, 100kDa | OAS3 | 218400_at | 2.146 |
| zinc finger and BTB domain containing 44 | ZBTB44 | 226148_at | 2.146 |
| furry homolog (Drosophila) | FRY | 214318_s_at | 2.141 |
| zinc finger, FYVE domain containing 16 | ZFYVE16 | 1555982_at | 2.141 |
| growth arrest-specific 6 /// similar to growth arrest-specific 6 | GAS6 /// LOC10202177 | 202177_at | 2.137 |
| chromosome 12 open reading frame 35 | C12orf35 | 218614_at | 2.132 |
| interleukin 20 | IL20 | 224071_at | 2.132 |
| Transcription factor Dp-2 (E2F dimerization partner 2) | TFDP2 | 226157_at | 2.132 |
| plexin B1 | PLXNB1 | 215807_s_at | 2.132 |
| phosphoinositide-3-kinase, catalytic, delta polypeptide | PIK3CD | 203879_at | 2.128 |
| thioredoxin-related transmembrane protein 4 | TMX4 | 201580_s_at | 2.123 |
| complement factor H | CFH | 213800_at | 2.119 |
| T-cell lymphoma invasion and metastasis 2 | TIAM2 | 222942_s_at | 2.114 |
| hypothetical LOC283070 | LOC283070 | 226382_at | 2.114 |
| ezrin | EZR | 208621_s_at | 2.114 |
| ribonuclease T2 | RNASET2 | 217984_at | 2.114 |
| islet cell autoantigen 1,69kDa-like | ICA1L | 230454_at | 2.105 |
| transmembrane phosphatase with tensin homology | TPTE | 220205_at | 2.105 |
| basonuclin 1 | BNC1 | 1552487_a_at | 2.101 |
| cordons-bleu homolog (mouse) | COBL | 213050_at | 2.101 |
| ATPase, Cu++ transporting, beta polypeptide | ATP7B | 204624_at | 2.101 |
| mannan-binding lectin serine peptidase 1 (C4/C2 activating component of Ra-reactive factor) | MASP1 | 210680_s_at | 2.096 |
| chromosome 6 open reading frame 170 | C6orf170 | 232038_at | 2.096 |
| regulator of calcineurin 1 | RCAN1 | 215253_s_at | 2.092 |
| chromosome 1 open reading frame 133 | C1orf133 | 230121_at | 2.092 |
| Spermatid perinuclear RNA binding protein | STRBP | 229513_at | 2.092 |
| hypothetical protein DKFZp586l1420 | DKFZP586l1420 | 213546_at | 2.092 |
| C-terminal binding protein 2 | CTBP2 | 215377_at | 2.079 |
| serpin peptidase inhibitor, clade B (ovalbumin), member 3 | SERPINB3 | 209719_x_at | 2.079 |
| KIAA1217 | KIAA1217 | 231807_at | 2.079 |
| tumor necrosis factor receptor superfamily, member 8 | TNFRSF8 | 206729_at | 2.079 |
| prostaglandin F2 receptor negative regulator | PTGFRN | 224950_at | 2.079 |
| WD repeat and SOCS box-containing 1 | WSB1 | 201295_s_at | 2.075 |
| hypothetical protein LOC283867 | LOC283867 | 231518_at | 2.075 |
| KIAA1324 | KIAA1324 | 221874_at | 2.075 |
| protocadherin alpha 1 /// protocadherin alpha 10 /// protocadherin alpha 11 /// protocadherin alpha 12 /// | PCDHA1 /// PCDHA10 /// PCDHA11 /// PCDHA12 | 224212_s_at | 2.075 |
| UDP-GlcNAc:betaGal beta-1,3-N-acetylglucosaminyltransferase 1 | B3GNT1 | 203188_at | 2.075 |
| hemoglobin, alpha 1 /// hemoglobin, alpha 2 | HBA1 /// HBA2 | 209458_x_at | 2.070 |
| Ral GEF with PH domain and SH3 binding motif 1 | RALGPS1 | 204199_at | 2.070 |
| gastrokine 1 | GKN1 | 220191_at | 2.066 |
| UDP-Gal:betaGlcNAc beta 1,4- galactosyltransferase, polypeptide 6 | B4GALT6 | 235333_at | 2.066 |
| pre-B-cell leukemia homeobox 1 | PBX1 | 212148_at | 2.066 |
| HBV preS1-transactivated protein 4 | PS1TP4 | 226381_at | 2.062 |
| thioredoxin-related transmembrane protein 4 | TMX4 | 201581_at | 2.058 |
| salt-inducible kinase 2 | SIK2 | 213221_s_at | 2.058 |
| StAR-related lipid transfer (START) domain containing 10 | STARD10 | 232322_x_at | 2.058 |

Table S2.3 cont'd.

| | | | |
|---|-----------|--------------|-------|
| protein-L-isoaspartate (D-aspartate) O-methyltransferase domain containing 1 | PCMTD1 | 226119_at | 2.053 |
| RUN domain containing 3B | RUNDC3B | 241703_at | 2.053 |
| major facilitator superfamily domain containing 6 | MFSD6 | 225325_at | 2.049 |
| phospholipase A2 receptor 1, 180kDa | PLA2R1 | 210194_at | 2.049 |
| SPARC related modular calcium binding 2 | SMOC2 | 243946_at | 2.049 |
| hypothetical protein LOC90246 | LOC90246 | 233830_at | 2.049 |
| transient receptor potential cation channel, subfamily M, member 3 | TRPM3 | 216452_at | 2.049 |
| caspase 1, apoptosis-related cysteine peptidase (interleukin 1, beta, convertase) | CASP1 | 206011_at | 2.045 |
| complement component 3 | C3 | 217767_at | 2.045 |
| family with sequence similarity 53, member A | FAM53A | 1569139_s_at | 2.041 |
| cyclin D2 | CCND2 | 200953_s_at | 2.041 |
| progesterone receptor membrane component 2 | PGRMC2 | 213227_at | 2.037 |
| chromosome 12 open reading frame 26 | C12orf26 | 229018_at | 2.037 |
| isochorismatase domain containing 1 | ISOC1 | 218170_at | 2.037 |
| programmed cell death 4 (neoplastic transformation inhibitor) | PDCD4 | 202731_at | 2.033 |
| MU-2/AP1M2 domain containing, death-inducing | MUDENG | 232156_at | 2.033 |
| CCAAT/enhancer binding protein (C/EBP), delta | CEBPD | 203973_s_at | 2.033 |
| fibroblast growth factor receptor substrate 2 | FRS2 | 226045_at | 2.033 |
| KIAA0146 | KIAA0146 | 228325_at | 2.028 |
| phospholipase C, delta 3 | PLCD3 | 234971_x_at | 2.028 |
| family with sequence similarity 111, member A | FAM111A | 218248_at | 2.024 |
| regulator of calcineurin 1 | RCAN1 | 215254_at | 2.024 |
| dishevelled associated activator of morphogenesis 1 | DAAM1 | 216060_s_at | 2.024 |
| chromosome 11 open reading frame 54 | C11orf54 | 223268_at | 2.020 |
| hyaluronan synthase 3 | HAS3 | 223541_at | 2.020 |
| chromosome 8 open reading frame 68 | C8orf68 | 1557679_at | 2.016 |
| Cyclin E1 | CCNE1 | 242105_at | 2.016 |
| fucosidase, alpha-L- 1, tissue | FUCA1 | 202838_at | 2.016 |
| LAG1 homolog, ceramide synthase 6 | LASS6 | 212446_s_at | 2.012 |
| zinc finger protein 720 | ZNF720 | 242091_at | 2.012 |
| interleukin 2 receptor, gamma (severe combined immunodeficiency) | IL2RG | 204116_at | 2.012 |
| chromosome 10 open reading frame 4 | C10orf4 | 238596_at | 2.012 |
| chromosome 9 open reading frame 125 | C9orf125 | 213386_at | 2.008 |
| hypothetical LOC651250 | LOC651250 | 1566987_s_at | 2.004 |
| MAX dimerization protein 4 | MXD4 | 212346_s_at | 2.004 |

Table S2.4: Genes with decreased expression due to Alk3QD in EOC spheroids.

| Gene Title | Gene Symbol | Probe Set ID | Fold Change |
|---|--------------|--------------|-------------|
| RAP1A, member of RAS oncogene family | RAP1A | 1555340_x_at | 333.333 |
| RAP1A, member of RAS oncogene family | RAP1A | 1555339_at | 333.333 |
| centromere protein 1 | CENPI | 1555046_at | 10.870 |
| glutamate receptor, metabotropic 1 | GRM1 | 207299_s_at | 9.709 |
| interferon stimulated exonuclease gene 20kDa | ISG20 | 204698_at | 9.346 |
| chromosome 4 open reading frame 37 | C4orf37 | 1555096_at | 8.547 |
| UDP-N-acetyl-alpha-D-galactosamine:polypeptide N-acetylgalactosaminyltransferase-like | GALNTL6 | 1555273_at | 8.065 |
| platelet-derived growth factor receptor-like | PDGFRL | 205226_at | 7.752 |
| hydroxysteroid (17-beta) dehydrogenase 6 homolog (mouse) | HSD17B6 | 205700_at | 7.576 |
| folate hydrolase (prostate-specific membrane antigen) 1 | FOLH1 | 215363_x_at | 7.407 |
| hydroxysteroid (17-beta) dehydrogenase 6 homolog (mouse) | HSD17B6 | 37512_at | 7.194 |
| tumor necrosis factor (ligand) superfamily, member 10 | TNFSF10 | 202687_s_at | 6.667 |
| tumor necrosis factor (ligand) superfamily, member 10 | TNFSF10 | 202688_at | 6.452 |
| folate hydrolase (prostate-specific membrane antigen) 1 | FOLH1 | 205860_x_at | 6.289 |
| aldehyde oxidase 1 | AOX1 | 205083_at | 6.250 |
| EPH receptor B3 | EPHB3 | 204600_at | 5.952 |
| ATP-binding cassette, sub-family A (ABC1), member 9 | ABCA9 | 242541_at | 5.882 |
| similar to hCG2041313 | LOC100128178 | 235891_at | 5.814 |
| tumor necrosis factor (ligand) superfamily, member 10 | TNFSF10 | 214329_x_at | 5.714 |
| SH3 domain containing ring finger 2 | SH3RF2 | 228892_at | 5.587 |
| butyrobetaine (gamma), 2-oxoglutarate dioxygenase (gamma-butyrobetaine hydroxylase) | BBOX1 | 205363_at | 5.435 |
| transmembrane protein 170B | TMEM170B | 235798_at | 5.376 |
| ankyrin 1, erythrocytic | ANK1 | 205390_s_at | 5.155 |
| chromosome 18 open reading frame 20 | C18orf20 | 1553934_at | 5.128 |
| RALBP1 associated Eps domain containing 2 | REPS2 | 227425_at | 5.076 |
| actin filament associated protein 1-like 2 | AFAP1L2 | 226829_at | 4.902 |
| transmembrane protein 176B | TMEM176B | 220532_s_at | 4.878 |
| PRP18 pre-mRNA processing factor 18 homolog (S. cerevisiae) | PRPF18 | 232473_at | 4.854 |
| pre-B-cell leukemia homeobox 1 | PBX1 | 205253_at | 4.831 |
| protein kinase (cAMP-dependent, catalytic) inhibitor beta | PKIB | 223551_at | 4.762 |
| Hypothetical protein LOC650392 | LOC650392 | 1558463_s_at | 4.762 |
| signal transducer and activator of transcription 5B | STAT5B | 1555088_x_at | 4.717 |
| sperm protein associated with the nucleus, X-linked, family member A1 /// SPANX family, | SPANXA1 | 224032_x_at | 4.673 |
| MAM domain containing glycosylphosphatidylinositol anchor 1 | MDGA1 | 238543_x_at | 4.608 |
| katanin p60 subunit A-like 2 | KATNAL2 | 1554234_at | 4.608 |
| transmembrane protein 176A | TMEM176A | 218345_at | 4.608 |
| interferon-induced protein 44-like | IFI44L | 204439_at | 4.587 |
| wingless-type MMTV integration site family, member 6 | WNT6 | 221608_at | 4.587 |
| Protein tyrosine phosphatase, non-receptor type 9 | PTPN9 | 230140_at | 4.545 |
| plasticity related gene 3 | RP11-35N6.1 | 219732_at | 4.525 |
| periplakin | PPL | 203407_at | 4.425 |
| G0/G1switch 2 | G0S2 | 213524_s_at | 4.386 |
| dedicator of cytokinesis 2 | DOCK2 | 213160_at | 4.348 |
| chitinase 3-like 1 (cartilage glycoprotein-39) | CHI3L1 | 209396_s_at | 4.348 |
| phosphatase and actin regulator 3 | PHACTR3 | 227949_at | 4.329 |
| family with sequence similarity 20, member A | FAM20A | 226804_at | 4.237 |
| immunoglobulin heavy locus /// immunoglobulin heavy constant gamma 1 (G1m marker) / | IGHG | 211430_s_at | 4.237 |
| hypothetical LOC154872 | LOC154872 | 237271_at | 4.237 |
| MYC induced nuclear antigen | MINA | 229675_at | 4.219 |
| Rho GTPase activating protein 25 | ARHGAP25 | 204882_at | 4.202 |
| phosphodiesterase 3B, cGMP-inhibited | PDE3B | 214582_at | 4.202 |
| hypothetical LOC79100 | MGC4473 | 224020_at | 4.098 |
| protein tyrosine phosphatase, receptor type, F | PTPRF | 215066_at | 4.082 |
| lipocalin-like 1 | LCNL1 | 1564431_a_at | 3.984 |
| ATP-binding cassette, sub-family B (MDR/TAP), member 6 | ABCB6 | 203191_at | 3.968 |
| neuropeptide Y receptor Y1 | NPY1R | 205440_s_at | 3.937 |
| protein tyrosine phosphatase, non-receptor type 22 (lymphoid) | PTPN22 | 206060_s_at | 3.906 |
| aquaporin 3 (Gill blood group) | AQP3 | 39248_at | 3.861 |
| calcitonin receptor-like | CALCRL | 206331_at | 3.846 |

Table S2.4 cont'd.

| | | | |
|---|---------------|--------------|-------|
| postmeiotic segregation increased 2-like 5-like /// PMS2 postmeiotic segregation increase | LOC100132832 | 216039_at | 3.831 |
| RIMS binding protein 2 | RIMBP2 | 214811_at | 3.817 |
| thyroid hormone receptor, beta (erythroblastic leukemia viral (v-erb-a) oncogene homolog | THRB | 207044_at | 3.817 |
| ATP-binding cassette, sub-family A (ABC1), member 6 | ABCA6 | 217504_at | 3.817 |
| prematurely terminated mRNA decay factor-like | LOC91431 | 1565935_at | 3.802 |
| DNA-damage-inducible transcript 4-like | DDIT4L | 228057_at | 3.802 |
| ring finger protein 8 | RNF8 | 203161_s_at | 3.774 |
| protogenin homolog (Gallus gallus) | PRTG | 229073_at | 3.759 |
| decorin | DCN | 209335_at | 3.745 |
| IKAROS family zinc finger 2 (Helios) | IKZF2 | 231929_at | 3.731 |
| vanin 1 | VNN1 | 205844_at | 3.717 |
| myosin VB | MYO5B | 225301_s_at | 3.704 |
| zinc finger protein 224 | ZNF224 | 216991_at | 3.690 |
| leucine-rich repeats and immunoglobulin-like domains 3 | LRIG3 | 226908_at | 3.650 |
| podoplanin | PDPN | 221898_at | 3.636 |
| prostaglandin F receptor (FP) | PTGFR | 207177_at | 3.571 |
| Mdm2, transformed 3T3 cell double minute 2, p53 binding protein (mouse) binding protein | MTBP | 233436_at | 3.559 |
| SH3 domain containing ring finger 2 | SH3RF2 | 243582_at | 3.472 |
| Hypothetical gene supported by BC008048 | LOC440934 | 244159_at | 3.460 |
| A kinase (PRKA) anchor protein 13 | AKAP13 | 232188_at | 3.436 |
| spastic paraplegia 11 (autosomal recessive) | SPG11 | 1559747_at | 3.436 |
| vascular cell adhesion molecule 1 | VCAM1 | 203868_s_at | 3.378 |
| dpy-19-like 2 (C. elegans) | DPY19L2 | 230158_at | 3.378 |
| odontogenic, ameloblast associated | ODAM | 220133_at | 3.378 |
| casein alpha s1 | CSN1S1 | 208350_at | 3.367 |
| proteasome (prosome, macropain) subunit, alpha type, 3 | PSMA3 | 232648_at | 3.356 |
| laminin, beta 4 | LAMB4 | 215516_at | 3.356 |
| prostaglandin D2 synthase 21kDa (brain) | PTGDS | 211663_x_at | 3.356 |
| cyclin-dependent kinase-like 2 (CDC2-related kinase) | CDKL2 | 207073_at | 3.344 |
| formin-like 1 | FMNL1 | 204789_at | 3.333 |
| potassium voltage-gated channel, KQT-like subfamily, member 4 | KCNQ4 | 243209_at | 3.322 |
| baculoviral IAP repeat-containing 5 | BIRC5 | 202095_s_at | 3.322 |
| v-maf musculoaponeurotic fibrosarcoma oncogene homolog (avian) | MAF | 209347_s_at | 3.311 |
| DENN/MADD domain containing 2A | DENND2A | 221886_at | 3.311 |
| platelet derived growth factor D | PDGFD | 219304_s_at | 3.300 |
| homeobox D1 | HOXD1 | 205974_at | 3.289 |
| coiled-coil domain containing 80 | CCDC80 | 225241_at | 3.268 |
| chitinase 3-like 1 (cartilage glycoprotein-39) | CHI3L1 | 209395_at | 3.247 |
| protein kinase (cAMP-dependent, catalytic) inhibitor beta | PKIB | 231120_x_at | 3.226 |
| extracellular matrix protein 2, female organ and adipocyte specific | ECM2 | 206101_at | 3.215 |
| KIAA0644 gene product | KIAA0644 | 205151_s_at | 3.205 |
| potassium voltage-gated channel, subfamily H (eag-related), member 2 | KCNH2 | 210036_s_at | 3.205 |
| RALBP1 associated Eps domain containing 2 | REPS2 | 205645_at | 3.195 |
| TBC1 domain family, member 8 (with GRAM domain) | TBC1D8 | 204526_s_at | 3.175 |
| lipoprotein lipase | LPL | 203549_s_at | 3.155 |
| myelin basic protein | MBP | 1554544_a_at | 3.155 |
| heparan sulfate 6-O-sulfotransferase 2 | HS6ST2 | 230030_at | 3.125 |
| GTPase, IMAP family member 2 | GIMAP2 | 232024_at | 3.106 |
| kelch repeat and BTB (POZ) domain containing 10 | KBTBD10 | 219106_s_at | 3.106 |
| synaptotagmin XVII | SYT17 | 205613_at | 3.096 |
| myosin VB | MYO5B | 225299_at | 3.096 |
| V-ets erythroblastosis virus E26 oncogene homolog 2 (avian) | ETS2 | 241193_at | 3.086 |
| decorin | DCN | 211896_s_at | 3.067 |
| phosphodiesterase 1A, calmodulin-dependent | PDE1A | 233547_x_at | 3.040 |
| myosin light chain kinase family, member 4 | MYLK4 | 1556136_at | 3.030 |
| T-box 1 | TBX1 | 236926_at | 3.021 |
| teratocarcinoma-derived growth factor 1 /// teratocarcinoma-derived growth factor 3, pseu | TDGF1 /// TDG | 206286_s_at | 3.021 |
| coxsackie virus and adenovirus receptor | CXADR | 203917_at | 3.012 |
| GABA(A) receptors associated protein like 3 (pseudogene) | GABARAPL3 | 211457_at | 3.012 |
| chromosome 9 open reading frame 100 | C9orf100 | 230521_at | 3.003 |
| phosphorylase kinase, alpha 1 (muscle) | PHKA1 | 229876_at | 3.003 |

Table S2.4 cont'd.

| | | | |
|--|--------------|--------------|-------|
| KIAA1409 | KIAA1409 | 229550_at | 2.985 |
| hypothetical LOC100192378 | LOC100192378 | 1559965_at | 2.976 |
| WD repeat domain 91 | WDR91 | 222799_at | 2.967 |
| protein tyrosine phosphatase, receptor type, N polypeptide 2 | PTPRN2 | 203029_s_at | 2.959 |
| carboxypeptidase A4 | CPA4 | 205832_at | 2.950 |
| chromosome 1 open reading frame 88 | C1orf88 | 228100_at | 2.950 |
| dpy-19-like 2 pseudogene 2 (C. elegans) | DPY19L2P2 | 215143_at | 2.941 |
| potassium channel tetramerisation domain containing 12 | KCTD12 | 212192_at | 2.933 |
| coiled-coil domain containing 102B | CCDC102B | 220301_at | 2.933 |
| complement component 5 | C5 | 205500_at | 2.924 |
| dipeptidyl-peptidase 4 | DPP4 | 203717_at | 2.915 |
| protein tyrosine phosphatase, non-receptor type 13 (APO-1/CD95 (Fas)-associated phosphatase) | PTPN13 | 204201_s_at | 2.915 |
| UDP-GlcNAc:betaGal beta-1,3-N-acetylglucosaminyltransferase 1 | B3GNT1 | 203188_at | 2.915 |
| ADAMTS-like 1 | ADAMTSL1 | 224371_at | 2.899 |
| hypothetical LOC285780 | RP3-398D13.1 | 1553428_at | 2.890 |
| regulator of G-protein signaling 2, 24kDa | RGS2 | 202388_at | 2.890 |
| hypothetical protein FLJ10489 | FLJ10489 | 1562433_at | 2.890 |
| phosphodiesterase 7A | PDE7A | 1552343_s_at | 2.882 |
| epoxide hydrolase 2, cytoplasmic | EPHX2 | 209368_at | 2.865 |
| aldehyde dehydrogenase 6 family, member A1 | ALDH6A1 | 221589_s_at | 2.857 |
| Carbohydrate (chondroitin 4) sulfotransferase 11 | CHST11 | 226372_at | 2.857 |
| chemokine (C-X-C motif) ligand 16 | CXCL16 | 223454_at | 2.849 |
| Collagen, type III, alpha 1 | COL3A1 | 232458_at | 2.833 |
| family with sequence similarity 111, member B | FAM111B | 1557129_a_at | 2.825 |
| retinoic acid receptor responder (tazarotene induced) 3 | RARRES3 | 204070_at | 2.817 |
| ATP-binding cassette, sub-family A (ABC1), member 8 | ABCA8 | 204719_at | 2.817 |
| complement component 2 /// complement factor B | C2 /// CFB | 202357_s_at | 2.801 |
| tudor domain containing 6 | TDRD6 | 232692_at | 2.801 |
| ATP/GTP binding protein-like 3 | AGBL3 | 220649_at | 2.801 |
| podoplanin | PDPN | 226658_at | 2.793 |
| matrix metalloproteinase 8 (neutrophil collagenase) | MMP8 | 207329_at | 2.793 |
| dehydrogenase/reductase (SDR family) member 2 | DHRS2 | 214079_at | 2.778 |
| CD36 molecule (thrombospondin receptor) | CD36 | 206488_s_at | 2.770 |
| inter-alpha (globulin) inhibitor H5 | ITIH5 | 219064_at | 2.755 |
| K(lysine) acetyltransferase 2B | KAT2B | 203845_at | 2.755 |
| dihydropyrimidine dehydrogenase | DPYD | 204646_at | 2.747 |
| CD9 molecule | CD9 | 233322_at | 2.747 |
| 1-acylglycerol-3-phosphate O-acyltransferase 3 | AGPAT3 | 224282_s_at | 2.747 |
| carboxymethylenebutenolidase homolog (Pseudomonas) | CMBL | 227522_at | 2.740 |
| podocan-like 1 | PODNL1 | 220411_x_at | 2.740 |
| thyroglobulin | TG | 203673_at | 2.732 |
| sperm adhesion molecule 1 (PH-20 hyaluronidase, zona pellucida binding) | SPAM1 | 216989_at | 2.725 |
| RAB26, member RAS oncogene family | RAB26 | 50965_at | 2.725 |
| tumor necrosis factor receptor superfamily, member 21 | TNFRSF21 | 218856_at | 2.717 |
| podoplanin | PDPN | 204879_at | 2.717 |
| coiled-coil domain containing 80 | CCDC80 | 225242_s_at | 2.717 |
| collagen-like tail subunit (single strand of homotrimer) of asymmetric acetylcholinesterase | COLQ | 206073_at | 2.717 |
| fin bud initiation factor homolog (zebrafish) | FIBIN | 226769_at | 2.710 |
| coiled-coil domain-containing-like | hCG_29977 | 227043_at | 2.703 |
| interferon-induced protein with tetratricopeptide repeats 1 | IFIT1 | 203153_at | 2.703 |
| G protein-coupled receptor 115 | GPR115 | 237690_at | 2.695 |
| phospholipase C, beta 4 | PLCB4 | 203896_s_at | 2.688 |
| chromosome 14 open reading frame 143 | C14orf143 | 210525_x_at | 2.688 |
| neural precursor cell expressed, developmentally down-regulated 4-like | NEDD4L | 241396_at | 2.681 |
| BTG family, member 3 | BTG3 | 215425_at | 2.681 |
| similar to hCG2041586 | LOC730124 | 231337_at | 2.674 |
| mucin 12, cell surface associated | MUC12 | 1557906_at | 2.674 |
| DEAD (Asp-Glu-Ala-Asp) box polypeptide 50 | DDX50 | 1568814_at | 2.667 |
| formin-like 1 | FMNL1 | 1569257_at | 2.667 |
| paired immunoglobulin-like type 2 receptor alpha | PILRA | 219788_at | 2.667 |
| cytochrome P450, family 7, subfamily B, polypeptide 1 | CYP7B1 | 207386_at | 2.667 |

Table S2.4 cont'd.

| | | | |
|--|---------------|--------------|-------|
| zinc finger protein 3 | ZNF3 | 232497_at | 2.667 |
| heat shock 70kDa protein 12A | HSPA12A | 214434_at | 2.660 |
| protocadherin 18 | PCDH18 | 225975_at | 2.660 |
| Phospholipase C, beta 4 | PLCB4 | 240728_at | 2.646 |
| myosin light chain kinase | MYLK | 202555_s_at | 2.639 |
| myosin light chain kinase | MYLK | 224823_at | 2.632 |
| obscurin-like 1 | OBSL1 | 227573_s_at | 2.625 |
| cytochrome P450, family 39, subfamily A, polypeptide 1 | CYP39A1 | 220432_s_at | 2.618 |
| collagen, type 1, alpha 2 | COL1A2 | 229218_at | 2.611 |
| platelet-derived growth factor beta polypeptide (simian sarcoma viral (v-sis) oncogene hom | PDGFB | 216055_at | 2.611 |
| zinc finger, matrin type 1 | ZMAT1 | 226344_at | 2.611 |
| chromosome 3 open reading frame 65 | C3orf65 | 1563207_at | 2.591 |
| ribonucleotide reductase M2 polypeptide | RRM2 | 209773_s_at | 2.591 |
| sortilin 1 | SORT1 | 224818_at | 2.571 |
| CAP, adenylate cyclase-associated protein, 2 (yeast) | CAP2 | 212554_at | 2.571 |
| JMJD7-PLA2G4B readthrough transcript /// phospholipase A2, group IVB (cytosolic) | JMJD7-PLA2G4 | 219095_at | 2.564 |
| nicotinamide N-methyltransferase | NNMT | 202237_at | 2.558 |
| cholinergic receptor, nicotinic, alpha 6 | CHRNA6 | 207568_at | 2.558 |
| coiled-coil domain containing 69 | CCDC69 | 1553102_a_at | 2.551 |
| cysteine conjugate-beta lyase 2 /// similar to RNA binding motif protein, X-linked /// RNA b | CCBL2 /// LOC | 1556336_at | 2.545 |
| coiled-coil domain containing 69 | CCDC69 | 212886_at | 2.538 |
| Zinc finger protein 64 homolog (mouse) | ZFP64 | 229186_s_at | 2.538 |
| BCL2-like 11 (apoptosis facilitator) | BCL2L11 | 225606_at | 2.538 |
| ribonuclease H2, subunit B | RNASEH2B | 229210_at | 2.525 |
| chromosome 18 open reading frame 24 | C18orf24 | 217640_x_at | 2.525 |
| hypothetical protein LOC284898 | LOC284898 | 1562030_at | 2.513 |
| myelin basic protein | MBP | 210136_at | 2.506 |
| pyridine nucleotide-disulphide oxidoreductase domain 2 | PYROXD2 | 228384_s_at | 2.506 |
| SH3-domain GRB2-like 3 | SH3GL3 | 211565_at | 2.506 |
| ets variant 3 | ETV3 | 214480_at | 2.506 |
| frizzled homolog 7 (Drosophila) | FZD7 | 203706_s_at | 2.500 |
| ectonucleotide pyrophosphatase/phosphodiesterase 5 (putative function) | ENPP5 | 237054_at | 2.494 |
| hypothetical protein LOC100129444 | LOC100129444 | 236272_at | 2.488 |
| cation channel, sperm-associated, beta | CATSPERB | 1570470_at | 2.481 |
| hypothetical LOC653602 | LOC653602 | 229546_at | 2.475 |
| chromosome 9 open reading frame 126 | C9orf126 | 228174_at | 2.463 |
| ADAMTS-like 1 | ADAMTSL1 | 1552808_at | 2.463 |
| fin bud initiation factor homolog (zebrafish) | FIBIN | 231001_at | 2.457 |
| Rho GTPase activating protein 18 | ARHGAP18 | 225171_at | 2.445 |
| family with sequence similarity 65, member C | FAM65C | 227654_at | 2.439 |
| prostaglandin F2 receptor negative regulator | PTGFRN | 224937_at | 2.433 |
| MANSC domain containing 1 | MANSC1 | 220945_x_at | 2.427 |
| phospholipid scramblase 4 | PLSCR4 | 218901_at | 2.427 |
| chromosome 11 open reading frame 21 | C11orf21 | 220560_at | 2.421 |
| mitogen-activated protein kinase kinase 6 | MAP2K6 | 205698_s_at | 2.421 |
| arsenic (+3 oxidation state) methyltransferase | AS3MT | 223652_at | 2.415 |
| Parkinson disease (autosomal recessive, juvenile) 2, parkin | PARK2 | 207058_s_at | 2.415 |
| coiled-coil domain containing 138 | CCDC138 | 235644_at | 2.415 |
| glycosyltransferase 8 domain containing 2 | GLT8D2 | 221447_s_at | 2.415 |
| glycosyltransferase 8 domain containing 2 | GLT8D2 | 227070_at | 2.415 |
| integrin, beta 8 | ITGB8 | 226189_at | 2.410 |
| P antigen family, member 1 (prostate associated) | PAGE1 | 206897_at | 2.404 |
| hypothetical FLJ13197 | FLJ13197 | 219871_at | 2.392 |
| zinc finger protein 541 | ZNF541 | 232604_at | 2.392 |
| V-set and transmembrane domain containing 2A | VSTM2A | 230117_at | 2.392 |
| microtubule-associated protein 7 | MAP7 | 202890_at | 2.392 |
| Synaptotagmin XVII | SYT17 | 229053_at | 2.392 |
| aldehyde dehydrogenase 6 family, member A1 | ALDH6A1 | 221588_x_at | 2.387 |
| BRF1 homolog, subunit of RNA polymerase III transcription initiation factor IIIB (S. cerevis | BRF1 | 215676_at | 2.381 |
| paraneoplastic antigen MA2 | PNMA2 | 209598_at | 2.381 |
| GLE1 RNA export mediator homolog (yeast) | GLE1 | 206920_s_at | 2.381 |

Table S2.4 cont'd.

| | | | |
|--|-----------------------|--------------|-------|
| synaptotagmin XII | SYT12 | 228072_at | 2.375 |
| MOCO sulphurase C-terminal domain containing 2 | MOSC2 | 227417_at | 2.370 |
| ribosomal protein L13 | RPL13 | 229590_at | 2.364 |
| dehydrogenase/reductase (SDR family) member 2 | DHRS2 | 206463_s_at | 2.358 |
| chromosome 4 open reading frame 23 | C4orf23 | 220891_at | 2.358 |
| elongation of very long chain fatty acids (FEN1/Elo2, SUR4/Elo3, yeast)-like 3 | ELOVL3 | 234513_at | 2.358 |
| testis specific, 14 | TSGA14 | 215637_at | 2.353 |
| gap junction protein, alpha 3, 46kDa | GJA3 | 239572_at | 2.353 |
| hypothetical protein LOC100130506 | LOC100130506 | 236656_s_at | 2.353 |
| integrin, beta 4 | ITGB4 | 204990_s_at | 2.353 |
| phospholipase C, beta 4 | PLCB4 | 203895_at | 2.353 |
| hypothetical LOC401052 | LOC401052 | 232812_at | 2.353 |
| Fanconi anemia, complementation group D2 | FANCD2 | 242560_at | 2.353 |
| hypothetical LOC346547 | FLJ42291 | 238648_at | 2.347 |
| SEC31 homolog B (S. cerevisiae) | SEC31B | 209889_at | 2.347 |
| sphingomyelin synthase 2 | SGMS2 | 227038_at | 2.347 |
| chromosome 14 open reading frame 147 | C14orf147 | 213508_at | 2.342 |
| SEC16 homolog B (S. cerevisiae) | SEC16B | 228150_at | 2.342 |
| chromosome 11 open reading frame 54 | C11orf54 | 223268_at | 2.342 |
| transmembrane protein 190 | TMEM190 | 1552594_at | 2.342 |
| non-metastatic cells 5, protein expressed in (nucleoside-diphosphate kinase) | NME5 | 206197_at | 2.336 |
| chromosome 4 open reading frame 12 | C4orf12 | 241401_at | 2.331 |
| Spectrin, beta, non-erythrocytic 1 | SPTBN1 | 213914_s_at | 2.331 |
| 2,5-oligoadenylate synthetase 1, 40/46kDa | OAS1 | 205552_s_at | 2.331 |
| KIAA1652 protein | KIAA1652 | 1560671_at | 2.326 |
| toll-interleukin 1 receptor (TIR) domain containing adaptor protein | TIRAP | 1552804_a_at | 2.326 |
| chromosome 6 open reading frame 64 | C6orf64 | 218784_s_at | 2.326 |
| progesterone receptor membrane component 2 | PGRMC2 | 213227_at | 2.320 |
| 5-nucleotidase domain containing 1 | NT5DC1 | 223178_s_at | 2.315 |
| Protein kinase (cAMP-dependent, catalytic) inhibitor alpha | PKIA | 226864_at | 2.315 |
| aldehyde dehydrogenase 6 family, member A1 | ALDH6A1 | 204290_s_at | 2.309 |
| solute carrier family 25, member 27 | SLC25A27 | 230624_at | 2.304 |
| solute carrier family 39 (zinc transporter), member 8 | SLC39A8 | 209267_s_at | 2.304 |
| chromosome 10 open reading frame 11 | C10orf11 | 223703_at | 2.294 |
| phospholipase C, beta 1 (phosphoinositide-specific) | PLCB1 | 215687_x_at | 2.283 |
| EF-hand calcium binding domain 3 /// similar to hypoxia-inducible protein 2 | EFCAB3 /// LOC1553392 | 1553392_at | 2.283 |
| SLIT and NTRK-like family, member 4 | SLITRK4 | 232636_at | 2.283 |
| LIM and cysteine-rich domains 1 | LMCD1 | 218574_s_at | 2.283 |
| caspase 10, apoptosis-related cysteine peptidase | CASP10 | 205467_at | 2.278 |
| tensin like C1 domain containing phosphatase (tensin 2) | TENC1 | 212494_at | 2.278 |
| hypothetical LOC151162 /// mannosyl (alpha-1,6-)-glycoprotein beta-1,6-N-acetyl-glucosaminyl transferase 1 | LOC151162 /// | 212098_at | 2.278 |
| CAP, adenylate cyclase-associated protein, 2 (yeast) | CAP2 | 212551_at | 2.273 |
| ephrin-A5 | EFNA5 | 227955_s_at | 2.268 |
| phosphoinositide-3-kinase interacting protein 1 | PIK3IP1 | 221756_at | 2.262 |
| CD302 molecule | CD302 | 203799_at | 2.262 |
| coxsackie virus and adenovirus receptor pseudogene 1 | CXADRP1 | 239155_at | 2.262 |
| spermatogenesis associated 6 | SPATA6 | 238459_x_at | 2.252 |
| nucleoredoxin | NXN | 219489_s_at | 2.252 |
| mucin 1, cell surface associated | MUC1 | 213693_s_at | 2.252 |
| decorin | DCN | 211813_x_at | 2.252 |
| neuropeptide Y receptor Y5 | NPY5R | 207400_at | 2.252 |
| septin 8 | 08-Sep 226627_at | 226627_at | 2.252 |
| nicotinamide N-methyltransferase | NNMT | 202238_s_at | 2.247 |
| chromosome 1 open reading frame 53 | C1orf53 | 1558507_at | 2.247 |
| mucin 1, cell surface associated | MUC1 | 207847_s_at | 2.242 |
| carbohydrate (chondroitin 4) sulfotransferase 11 | CHST11 | 219634_at | 2.242 |
| dipeptidyl-peptidase 4 | DPP4 | 203716_s_at | 2.232 |
| ELL associated factor 2 | EAF2 | 219551_at | 2.232 |
| transducin (beta)-like 1X-linked | TBL1X | 201868_s_at | 2.232 |
| OMA1 homolog, zinc metallopeptidase (S. cerevisiae) | OMA1 | 226019_at | 2.232 |
| retinoic acid receptor responder (tazarotene induced) 2 | RARRES2 | 209496_at | 2.232 |

Table S2.4 cont'd.

| | | | |
|--|--------------|--------------|-------|
| NADH dehydrogenase (ubiquinone) 1 beta subcomplex, 6, 17kDa | NDUFB6 | 1559042_at | 2.227 |
| solute carrier family 46, member 3 | SLC46A3 | 214719_at | 2.222 |
| glycine C-acetyltransferase (2-amino-3-ketobutyrate coenzyme A ligase) | GCAT | 205164_at | 2.222 |
| similar to pM5 (3 partial) /// NODAL modulator 1 /// NODAL modulator 2 /// NODAL modulator 3 | LOC100133864 | 242922_at | 2.222 |
| sidekick homolog 1, cell adhesion molecule (chicken) | SDK1 | 229912_at | 2.217 |
| SIX homeobox 4 | SIX4 | 229796_at | 2.212 |
| cell cycle progression 1 | CCPG1 | 221511_x_at | 2.212 |
| metallothionein 1M | MT1M | 217546_at | 2.203 |
| potassium channel tetramerisation domain containing 12 | KCTD12 | 212188_at | 2.203 |
| basonuclin 1 | BNC1 | 1552487_a_at | 2.198 |
| basic helix-loop-helix family, member e41 | BHLHE41 | 221530_s_at | 2.193 |
| zinc finger (CCCH type), RNA-binding motif and serine/arginine rich 1 | ZRSR1 | 206512_at | 2.193 |
| nuclear factor (erythroid-derived 2)-like 3 | NFE2L3 | 204702_s_at | 2.193 |
| prostaglandin D2 synthase 21kDa (brain) | PTGDS | 211748_x_at | 2.188 |
| chromosome 12 open reading frame 35 | C12orf35 | 218614_at | 2.188 |
| sema domain, immunoglobulin domain (Ig), short basic domain, secreted, (semaphorin) 3 | SEMA3A | 206805_at | 2.174 |
| hypothetical protein LOC100131731 | LOC100131731 | 1557263_s_at | 2.169 |
| arachidonate 5-lipoxygenase-activating protein | ALOX5AP | 204174_at | 2.165 |
| Rho GTPase activating protein 18 | ARHGAP18 | 225173_at | 2.165 |
| methylcrotonoyl-Coenzyme A carboxylase 2 (beta) | MCCC2 | 1560033_at | 2.165 |
| bestrophin 4 | BEST4 | 1552296_at | 2.160 |
| ferritin, heavy polypeptide 1 | FTH1 | 214211_at | 2.160 |
| dipeptidyl-peptidase 4 | DPP4 | 211478_s_at | 2.160 |
| ATP synthase, H+ transporting, mitochondrial F1 complex, delta subunit | ATP5D | 203926_x_at | 2.155 |
| frizzled homolog 2 (Drosophila) | FZD2 | 210220_at | 2.151 |
| runt-related transcription factor 1 | RUNX1 | 209360_s_at | 2.151 |
| engulfment and cell motility 1 | ELMO1 | 204513_s_at | 2.151 |
| solute carrier family 27 (fatty acid transporter), member 1 | SLC27A1 | 226728_at | 2.151 |
| flavin containing monooxygenase 4 | FMO4 | 206263_at | 2.151 |
| RAB40B, member RAS oncogene family | RAB40B | 204547_at | 2.141 |
| similar to Six transmembrane epithelial antigen of prostate | MGC87042 | 217553_at | 2.141 |
| zinc finger, FYVE domain containing 16 | ZFYVE16 | 1555982_at | 2.141 |
| chromosome 12 open reading frame 72 | C12orf72 | 1563474_at | 2.137 |
| smoothened homolog (Drosophila) | SMO | 218629_at | 2.132 |
| V-set and immunoglobulin domain containing 1 | VSIG1 | 243764_at | 2.128 |
| cytochrome P450, family 39, subfamily A, polypeptide 1 | CYP39A1 | 1553977_a_at | 2.123 |
| hypothetical protein LOC283658 | LOC283658 | 239741_at | 2.123 |
| intraflagellar transport 122 homolog (Chlamydomonas) | IFT122 | 220744_s_at | 2.119 |
| cell cycle progression 1 | CCPG1 | 214151_s_at | 2.114 |
| transcription elongation factor A (SII), 3 | TCEA3 | 226388_at | 2.110 |
| polymerase (DNA directed), mu | POLM | 222238_s_at | 2.110 |
| Chromosome 12 open reading frame 32 | C12orf32 | 241074_at | 2.105 |
| LIM domains containing 1 | LIMD1 | 222762_x_at | 2.105 |
| von Willebrand factor A domain containing 5A | VWA5A | 205011_at | 2.105 |
| spermatogenesis associated 17 | SPATA17 | 230763_at | 2.101 |
| NHL repeat containing 3 | NHLRC3 | 227040_at | 2.096 |
| Hypothetical LOC645513 | LOC645513 | 1561761_x_at | 2.096 |
| C-type lectin domain family 7, member A | CLEC7A | 1555213_a_at | 2.096 |
| phospholipid scramblase 1 | PLSCR1 | 202430_s_at | 2.096 |
| syntrophin, beta 1 (dystrophin-associated protein A1, 59kDa, basic component 1) | SNTB1 | 226438_at | 2.092 |
| ubiquitin-like modifier activating enzyme 7 | UBA7 | 203281_s_at | 2.088 |
| phosphoribosyl pyrophosphate synthetase 2 | PRPS2 | 203401_at | 2.083 |
| SATB homeobox 1 | SATB1 | 203408_s_at | 2.083 |
| Carbohydrate (chondroitin 4) sulfotransferase 11 | CHST11 | 226368_at | 2.083 |
| formin binding protein 1 | FNBP1 | 230389_at | 2.083 |
| prostaglandin D2 synthase 21kDa (brain) | PTGDS | 212187_x_at | 2.079 |
| inhibin, alpha | INHAA | 210141_s_at | 2.079 |
| zinc finger protein 853 | ZNF853 | 232884_s_at | 2.079 |
| chromosome 5 open reading frame 4 | C5orf4 | 220751_s_at | 2.075 |
| nei endonuclease VIII-like 1 (E. coli) | NEIL1 | 219396_s_at | 2.075 |
| coiled-coil domain containing 82 | CCDC82 | 220693_at | 2.070 |

Table S2.4 cont'd.

| | | | |
|--|-----------------------|-------------|-------|
| zinc finger protein 658 | ZNF658 | 231950_at | 2.070 |
| coiled-coil domain containing 109B | CCDC109B | 218802_at | 2.066 |
| peroxisomal biogenesis factor 1 | PEX1 | 204873_at | 2.066 |
| ERO1-like beta (S. cerevisiae) | ERO1LB | 231944_at | 2.062 |
| fucosidase, alpha-L- 1, tissue | FUCA1 | 202838_at | 2.062 |
| cell division cycle associated 7-like | CDCA7L | 225081_s_at | 2.058 |
| cancer susceptibility candidate 5 | CASC5 | 228323_at | 2.053 |
| Hypothetical gene supported by BC043549; BX648102 | DKFZp686O13:216874_at | | 2.053 |
| transglutaminase 2 (C polypeptide, protein-glutamine-gamma-glutamyltransferase) | TGM2 | 201042_at | 2.053 |
| glutamate receptor, ionotropic, AMPA 3 | GRIA3 | 208032_s_at | 2.049 |
| RNA binding motif, single stranded interacting protein 2 | RBMS2 | 225778_at | 2.041 |
| LSM5 homolog, U6 small nuclear RNA associated (S. cerevisiae) | LSM5 | 202903_at | 2.041 |
| phytanoyl-CoA dioxygenase domain containing 1 | PHYHD1 | 226846_at | 2.037 |
| Nuclear autoantigenic sperm protein (histone-binding) | NASP | 242918_at | 2.037 |
| HBV preS1-transactivated protein 4 | PS1TP4 | 226381_at | 2.037 |
| hypothetical locus LOC401237 | FLJ22536 | 229280_s_at | 2.037 |
| CUG triplet repeat, RNA binding protein 2 | CUGBP2 | 227178_at | 2.033 |
| syndecan 3 | SDC3 | 202898_at | 2.033 |
| cold inducible RNA binding protein | CIRBP | 225191_at | 2.024 |
| elastin microfibril interfacier 1 | EMILIN1 | 204163_at | 2.020 |
| melanoma associated antigen (mutated) 1-like 1 | MUM1L1 | 229160_at | 2.020 |
| adaptor-related protein complex 2, alpha 1 subunit | AP2A1 | 223237_x_at | 2.016 |
| potassium inwardly-rectifying channel, subfamily J, member 12 | KCNJ12 | 207110_at | 2.008 |
| ribonuclease H2, subunit B | RNASEH2B | 219056_at | 2.008 |
| CTD (carboxy-terminal domain, RNA polymerase II, polypeptide A) small phosphatase-like | CTDSPL | 201906_s_at | 2.008 |
| myotubularin related protein 3 | MTMR3 | 202198_s_at | 2.008 |
| Rho guanine nucleotide exchange factor (GEF) 3 | ARHGEF3 | 218501_at | 2.008 |
| nuclear receptor subfamily 1, group H, member 3 | NR1H3 | 203920_at | 2.008 |
| ATP-binding cassette, sub-family A (ABC1), member 5 | ABCA5 | 213353_at | 2.008 |
| carbonic anhydrase XII | CA12 | 204509_at | 2.008 |
| cytochrome b5 type B (outer mitochondrial membrane) | CYB5B | 227382_at | 2.008 |
| potassium inwardly-rectifying channel, subfamily J, member 12 | KCNJ12 | 232289_at | 2.000 |

Chapter 3

3 LKB1 signalling protects dormant ovarian cancer spheroids from cell death in an AMPK-independent manner

3.1 Introduction

Ovarian cancer is the most lethal gynecologic malignancy in the western world, the overall survival of which has remained unchanged for more than 50 years^{1,2}. Models that can be used to uncover the molecular events important for disease dissemination are crucial since the majority of women with ovarian cancer (over 75%) are diagnosed at advanced stage³. Intraperitoneal implants identified in these patients with advanced-stage disease are the result of single cells and multicellular aggregates, or spheroids, that adhere to the mesothelial lining of various abdominal organs to establish secondary lesions⁴⁻⁶. In many cases, this is accompanied by accumulation of ascites fluid within the peritoneal cavity, where cells in suspension are exposed to a unique set of microenvironmental cues, allowing this population of cells to form secondary metastases^{3-5,7}. These non-adherent metastatic cells provide unique therapeutic challenges for treatment of ovarian cancer³.

The biological significance and clinical relevance of multicellular spheroids has been documented in many different tumour types⁸⁻¹⁴. It is well accepted that spheroids more closely mimic the cell-cell, cell-matrix interactions, metabolic gradients, cellular viability and differentiation of malignant cells within a solid tumour than do conventional monolayer cultures¹⁵. We have shown that ascites-derived ovarian cancer cells in suspension form dormant multicellular aggregates characterized by quiescence and decreased Akt activity¹⁶. These dormant cells are subsequently able to re-enter the cell cycle and grow when they reach an adherent substratum.¹⁶ Ovarian cancer cells that are able to resist anoikis and survive within ascitic fluid most likely have uniquely adapted key cell survival pathways to meet the nutrient and energy demands of this particular microenvironment.

A fundamental requirement of all cells is the ability to respond to various forms of metabolic stress and balance ATP consumption and generation in response. Under conditions where nutrients are low, AMPK acts as a metabolic checkpoint by activating catabolic processes and inhibiting anabolic metabolism^{17,18}. AMPK is a heterotrimeric complex containing a catalytic α -subunit and two regulatory subunits, β and γ . When intracellular ATP levels are low, AMP or ADP directly bind to the γ regulatory subunits. This causes a conformation change in the complex that allows AMPK to be phosphorylated at threonine 172 on the α subunit¹⁷. The primary kinase responsible for phosphorylation at this site is LKB1¹⁹⁻²¹.

It has been suggested that AMPK may function as a context-dependent tumour suppressor or oncogene²². Modest activation of AMPK may be cell protective, but prolonged or enhanced activation can be detrimental and result in growth arrest or cell death¹⁸. The most thoroughly characterized mechanism through which the LKB1/AMPK pathway regulates cell growth is by suppression of mTORC1 signalling. LKB1, on the other hand, is commonly regarded as a tumour suppressor, and is mutated in the rare hereditary autosomal dominant Peutz Jeghers Syndrome. These patients experience benign intestinal hamartomatous polyps and have an increased risk of developing malignant tumours²³. Despite this, LKB1 mutations have been identified in relatively few sporadic cancers.

Previous studies have shown that metabolic stress is induced when normal epithelial cells lose ECM attachment, resulting in a decreased ATP:ADP ratio and subsequent activation of AMPK²⁴⁻²⁶. However, this suspension-induced AMPK activation has yet to be examined in tumour spheroids. In our study, we use a disease-relevant spheroid model to interrogate the function of the LKB1/AMPK pathway in ovarian cancer cells. Our results indicate that LKB1 and AMPK serve distinct functions in ovarian cancer cells and spheroids to promote dormancy and anoikis-resistance.

3.2 Materials and Methods

3.2.1 Culture of cell lines, ascites-derived cells and isolation of native ascites spheroids

Ascites fluid from patients diagnosed with advanced stage (II-IV), high-grade serous epithelial ovarian cancer (Table S1) was used to establish primary cell cultures as previously described²⁷. The iOvCa147-E2 and iOvCa198 cell line were isolated from the EOC147 and EOC 198 ascites samples respectively. All work with patient materials has been approved by The University of Western Ontario Health Sciences Research Ethics Board (Protocol # 12668E and 16391E; Appendix B). Spheroids were isolated directly from ascites fluid by filtration through a 40 µm cell strainer (Becton Dickinson), washed with phosphate-buffered saline (PBS) into a collection tube with protein lysis buffer for immunoblot or embedded directly in OCT to obtain fresh frozen sections.

3.2.2 TCGA Analysis

Datasets from The Cancer Genome Atlas analysis of ovarian serous cystadenocarcinoma samples were downloaded from the University of California Santa Cruz Cancer Genomics Browser (<https://genome-cancer.ucsc.edu>)²⁸ and from the Memorial Sloan-Kettering Cancer Center's cBioPortal for Cancer Genomics (<http://www.cbioportal.org/>)²⁹. Array comparative genomic hybridization data was acquired at the Broad TCGA genome characterization center using the Affymetrix Genome-Wide Human SNP Array 6.0 platform. Raw data was analyzed using the GISTIC2 method to generate gene-level copy-number variation (CNV) estimates and downloaded as either thresholded copy-number calls or as log₂-transformed CNV values. Protein expression data was generated and processed at the MD Anderson Cancer Center TCGA proteome characterization center using reverse-phase protein array (RPPA) technology as described³⁰ and downloaded either natural log-transformed values or as z-scores.

3.2.3 Immunoblotting and Immunofluorescence

Whole cell protein lysates were generated from cell lines and ascites-derived cells in adherent and spheroid culture as previously described³¹. Antibodies used for immunoblot against p-AMPK α Thr172 (#2535), AMPK α (#5832), p-LKB1 Ser428 (#3482), LKB1 (#3050), p-p70S6K1 Thr 389 (#9234), p-ACC (#3661), ACC (#3676) and p70S6K1 (#2708) were obtained from Cell Signaling Technology (Danvers, MA). Anti-Tubulin antibody was obtained from Sigma. AICAR was purchased from Caymen Chemical Company (Ann Arbor, MI) and A-769662 from Tocris Bioscience (Bristol, UK). Immunofluorescent (IF) analysis was performed on fresh frozen sections that were fixed (4% formaldehyde), permeabilized (0.1% Triton X-100 in PBS), and blocked (5% BSA in 0.1% Triton X-100) before incubation with p-AMPK α antibody (#ab51110) from abcam® Inc. (Cambridge, MA). Following primary antibody incubation and PBS washes, sections were incubated for 1 hour with anti-rabbit FITC secondary antibody (1:250; Sigma-Aldrich). After further washing, sections were incubated with 4',6-diamidino-2-phenylindole (DAPI; 1:1000) and slides were mounted with Vectashield (Vector Laboratories, Burlingame CA, USA). Fluorescence images were captured using an Olympus AX70 upright microscope and ImagePro image capture software.

3.2.4 Cell Viability and ATP assays

Cells were seeded to either 24-well tissue culture plastic or ultra-low attachment (ULA) plates at a density of 1.0×10^4 to form adherent cultures or 5.0×10^4 per well to form spheroids, respectively.. Treatment was initiated at time of seeding for cells in suspension while cells under adherent conditions were given 12 hours to adhere prior to commencing treatment. CellTiter-Glo® reagent (Promega, Madison, WI) was prepared according to manufacturer's instructions. At 72h post-treatment, spheroids were collected, pelleted and left in a minimal volume of media (100 μ L), at which point CellTiter-Glo® reagent was added in a 1:1 volume ratio. Under adherent conditions, cells were harvested directly in CellTiter-Glo® reagent (1:1 reagent/media) after a 20 minute incubation period. All samples were subject to a freeze/thaw cycle prior to analysis. Approximately 200 μ L of the mixture was added to a white-walled 96-well micro-plate and luminescence signal was detected using a microplate spectrophotometer (Wallac 1420 Victor 2; Perkin-Elmer,

Waltham, MA). Treatments were conducted in at least duplicate wells and luminescence readings normalized to cells treated with vehicle control.

3.2.5 siRNA transfections

All siRNA transfections were performed in a 6-well format. The day prior to transfection, cells were plated at a density of approximately 1×10^5 cells per well in antibiotic-free media. The next day, DharmaFECT transfection reagent (DharmaFECT1 for OVCA429 and iOVCA147-E2 and DharmaFECT3 for SKOV3) was used to transfect cells, as per manufactures protocol. Briefly, 1 μ l of DharmaFECT1 or 4 μ l of DharmaFECT3 was combined with 10nM siRNA in a volume of 1mL of media (Wisent) and incubated for 20 min; the complexes of DharmaFECT and siRNAs were then added directly to each well. Media was removed 24 hours following transfection and replaced with fresh antibiotic-free growth media. At this point, the cells were incubated until nearly confluent, approximately 72 hours following transfection. *PRKAA1* and *STK11* siRNAs (M-005027-02 and M-005035-02 respectively) were obtained from Dharmacon (Thermo Fisher Scientific Inc., Waltham, MA). All siRNAs used were siGENOME SMARTpool predesigned pools of four oligos.

3.2.6 Graphing and Statistical Analysis

All graphs were generated using GraphPad Prism 5 (GraphPad Software, San Diego, CA). Data were expressed as Mean \pm SEM, as indicated. All statistical analysis (Student's *t*-test and Analysis of Variance (ANOVA) with Tukey's Multiple Comparison Test) was performed using GraphPad Prism 5. Tests of significance were set at $p < 0.05$.

3.3 Results

3.3.1 AMPK α 1 is expressed in metastatic ovarian tumour samples and is associated with a high frequency of copy-number gains and amplifications.

AMPK has been described in many instances to serve as a tumour suppressor despite the lack of genetic evidence to demonstrate a loss of AMPK function in cancer¹⁸. In order to assess AMPK activity in a large number of serous ovarian tumours, the majority of which (91.1%) are from metastatic, stage III-IV cases, we made use of level 3 array comparative genomic hybridization (aCGH) and reverse phase protein array (RPPA) data from The Cancer Genome Atlas (TCGA). This analysis revealed copy-number gain of the *PRKAA1* gene (encoding AMPK α 1) in 36% (111/311) of samples (Figure 3.1A). To determine whether *PRKAA1* copy-number correlated with protein expression, we plotted RPPA data against copy-number calls for both phosphorylated (T172) and total AMPK α 1. This demonstrated a significant increase in both phosphorylated (Figure 3.1B) and total AMPK α 1 (Figure 3.1C) in samples with copy-number gain. Using log₂-transformed copy-number data, we also performed regression analysis to measure the correlation between *PRKAA1* copy-number and protein expression. This revealed a positive correlation between copy-number and AMPK α 1 protein expression (both phosphorylated and total; Figure 3.1D&E). In addition, we also noted a positive correlation between AMPK α 1 protein expression and activity (Figure 3.1F). To verify AMPK α 1 expression and activity in fresh tumour specimens, we performed western blots on lysates harvested from metastatic tumour samples obtained by our lab (Figure 3.1G). Indeed, our direct results demonstrate that AMPK α 1 is expressed and active in metastatic ovarian tumours.

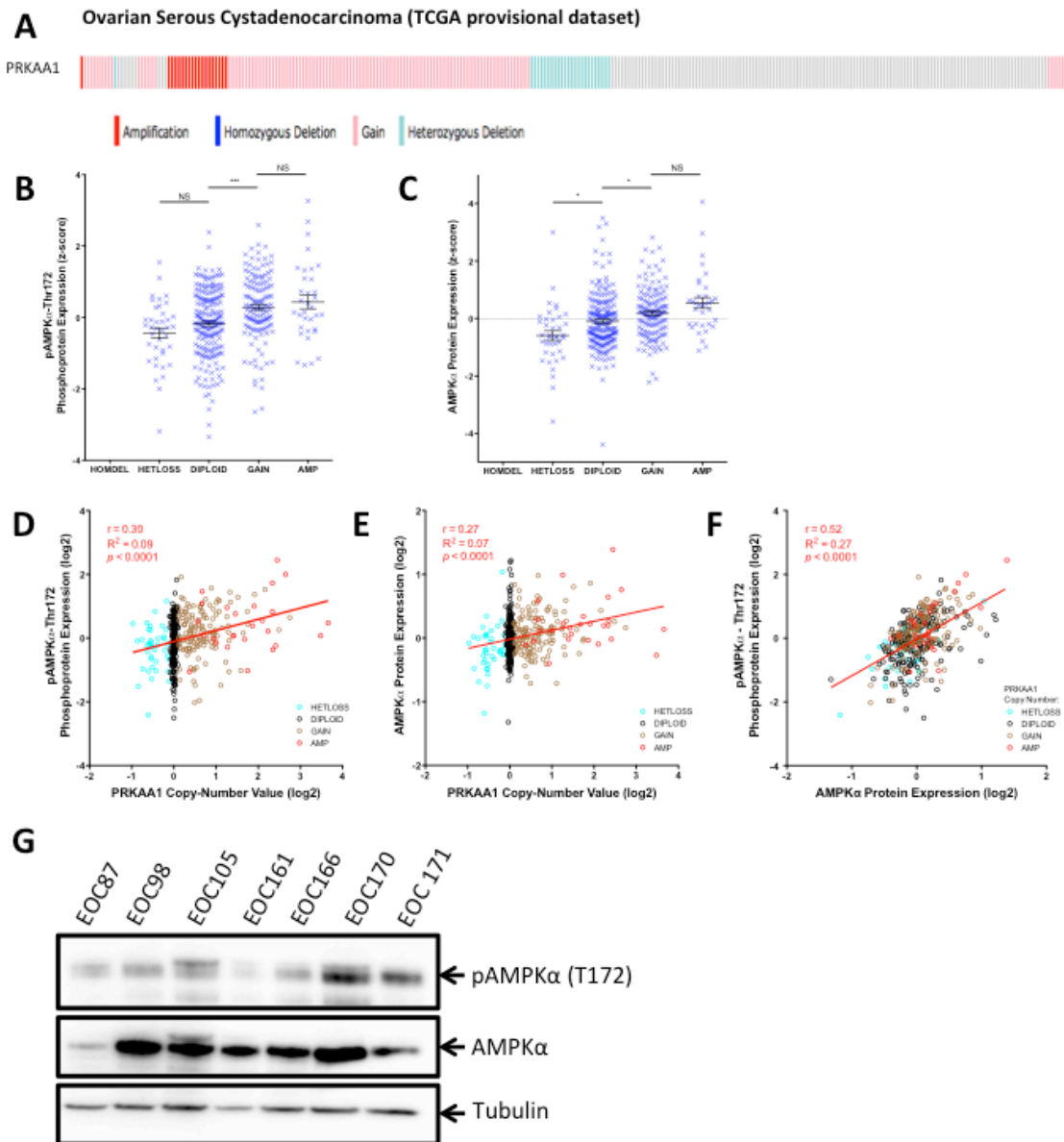


Figure 3.1: The AMPK pathway is active in metastatic ovarian tumour samples.

(A) Gene copy-number calls at the *PRKAA1* locus are depicted for 311 ovarian serous cystadenocarcinoma tumors (red & pink = high-level & low-level amplification, respectively; teal & blue = heterozygous & homozygous deletion, respectively). OncoPrint obtained from cBioPortal.org. (B,C) Phosphorylated and total AMPK α 1 protein (quantitative RPPA; n=398) expression data were transformed to z-scores and depicted as functions of copy-number. One-way ANOVA with Tukey's Test was performed (*p<0.05; ***p<0.001). (D,E) ln-transformed protein expression (n=397; re-transformed to log₂ values) data depicted as a function of log₂-transformed copy number values. (F) Phosphorylated AMPK α 1 protein expression depicted as a function of total protein. Correlation and linear regression analysis performed: line of best fit, Pearson's r, Goodness-of-fit R², and p values all reported. (G) Lysates were generated from metastatic tumour samples from seven ovarian cancer patients and immunoblot was performed to examine AMPK activity in these samples.

3.3.2 Multicellular aggregates filtered from patient ascites fluid exhibit enhanced AMPK activity.

Our lab has previously demonstrated that ovarian cancer cells which form multicellular aggregates *in vitro* enter a dormant state, a process which is aided by decreased AKT activity¹⁶. Herein, we postulate that the AMPK pathway is another pathway, that mediates spheroid formation-induced dormancy. due to its unique ability to respond to stresses, such as nutrient deprivation and hypoxia. In order to evaluate this, we analyzed AMPK activity in native ascites spheroids filtered directly from patient ascites fluid by western blot and immunofluorescence. Lysates generated from ascites spheroids filtered directly from a number of different patient ascites samples revealed a significant increase in AMPK activity in spheroids compared to matched adherent samples from the same patient (Figure 3.2A). Additionally, immunofluorescence on ascites-derived spheroids revealed intense expression of phosphorylated AMPK α 1 in the cytoplasm and along the cell membrane (Figure 3.2B). These data indicate that AMPK activity is enhanced in actively metastatic cells in spheroids within malignant ascites fluid.

3.3.3 Ovarian cancer cell lines and ascites-derived cells in suspension exhibit decreased levels of ATP and enhanced AMPK activity.

Following our observation that AMPK activity is enhanced in native ascites spheroids, we sought to investigate regulation of this phenomenon further using spheroids formed *in vitro*. We hypothesized that as a result of spheroid formation induced-dormancy, the metabolic state of cells within these multicellular aggregates is decreased. To assess this, we used Cell Titer Glo® luminescence-based ATP assay to determine levels of intracellular ATP in ovarian cancer cells in adherent and spheroid form. Indeed, ATP levels were significantly lower in spheroids compared to their adherent counterparts (Figure 3.3A). Correspondingly, western blot analysis of adherent and spheroid ovarian cancer cells revealed a significant increase in AMPK activity associated with spheroid formation (Figure 3.3B,C). Taken together, these data demonstrate decreased ATP levels that are associated with increased AMPK activity when ovarian cancer cells aggregate to form multicellular clusters or spheroids.

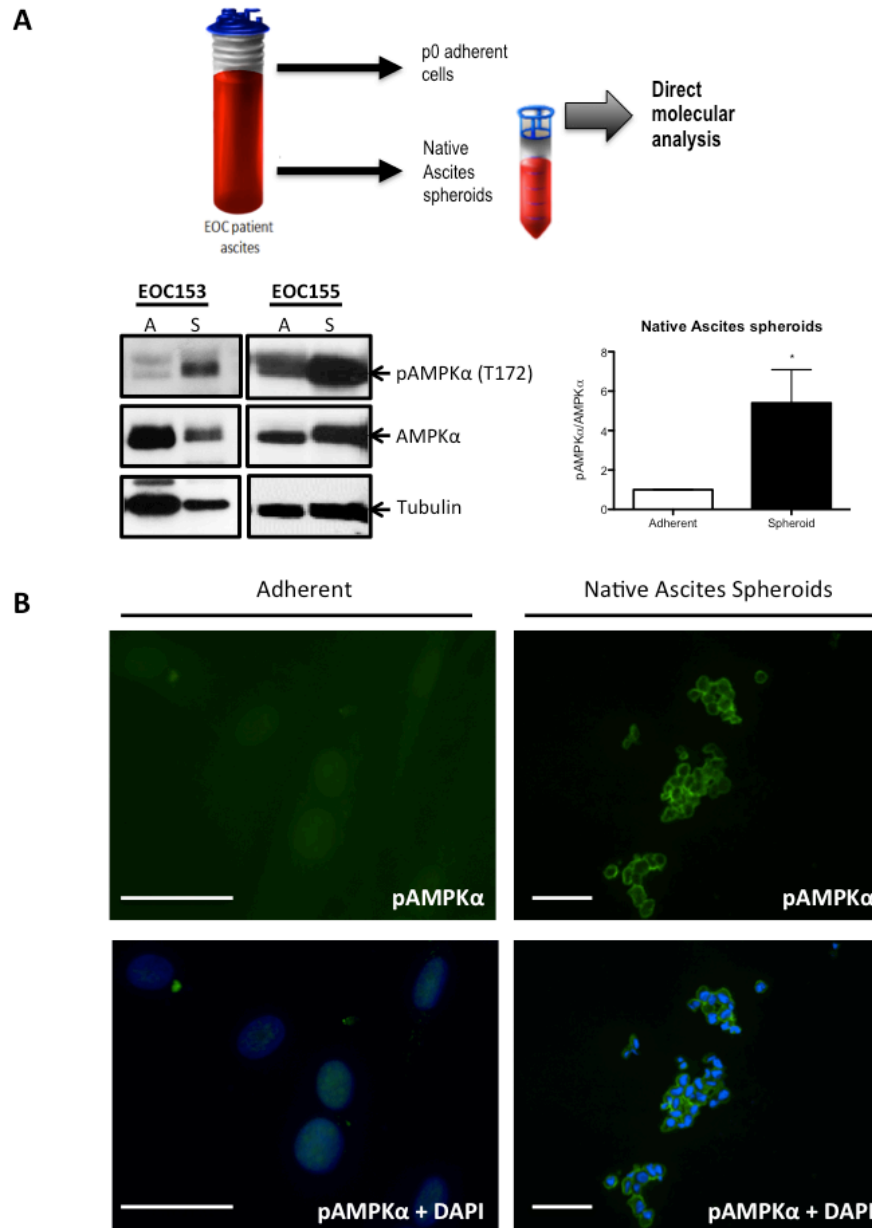


Figure 3.2: Native ascites spheroids have enhanced AMPK activity compared to adherent cells.

(A) Lysates were prepared from filtered spheroids [S] and passage 0 adherent cells [A] from 5 independent patient ascites samples. Immunoblot (shown representative image from two samples) and subsequent densitometry were performed to determine levels of phosphorylated AMPK α 1 compared to total protein. Bars: Mean \pm SEM. Levels of phosphorylated AMPK α 1 were compared using Student's t-test (* $p < 0.05$). (B) Spheroids filtered from patient ascites fluid for immunofluorescence analysis compared to early passage adherent cells from the same patient [EOC 169]. Nuclei (blue) and pAMPK α 1 (green) are visible. Scale bar: 100 μ m.

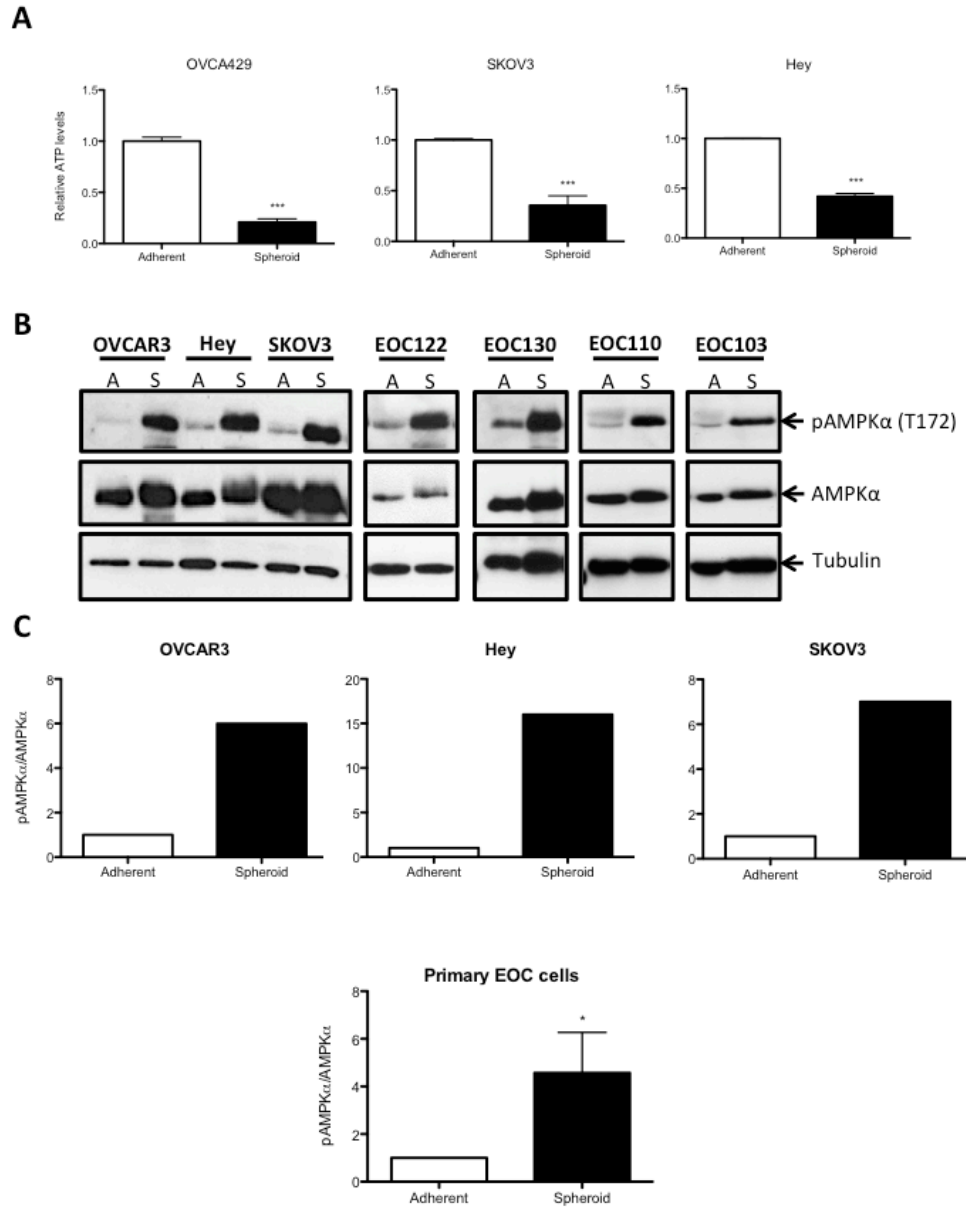


Figure 3.3: Spheroids formed from EOC cell lines and ascites-derived cells have decreased levels of ATP and corresponding increases in AMPK activity.

(A) Quantification of ATP levels in EOC cell lines cultured in both adherent and spheroid conditions using luminescence-based ATP assay CellTiter Glo®. Difference in viable cells between each culture condition was accounted for by normalizing results to total protein levels for each sample. Bars: Mean \pm SEM. Student's t-test was used to compare levels of ATP between culture conditions (** $p < 0.001$). (B) Immunoblot performed on EOC cell lines and ascites-derived EOC cells to determine levels of phosphorylated and total AMPK α 1 protein. (C) Densitometry was performed on cell lines and primary EOC cells ($n=14$) to compare levels of phosphorylated AMPK α 1 between adherent and spheroid cultured cells. Bars: Mean \pm SEM. Student's t-test was used to determine statistical significance ($*p < 0.05$).

3.3.4 LKB1 protein is expressed in metastatic ovarian tumour samples.

Activity of the key upstream AMPK kinase LKB1 is commonly thought to be tumour suppressive³². Multiple studies have suggested that single allelic inactivation of the *STK11* gene encoding LKB1 is sufficient to promote tumorigenesis, while other data suggests that biallelic loss may be required³³⁻³⁶. In order to examine status of LKB1 in serous ovarian tumours we again made use of data from the TCGA. Whereas copy-number gain was common for *PRKAA1*, heterozygous deletion of *STK11* was detected in 84% of samples (262/311; Figure 3.4A). This single allelic loss correlated with decreased protein expression compared to samples with normal copy-number (Figure 3.4B), and a positive correlation between *STK11* copy-number and LKB1 protein expression when we performed regression analysis on log2-transformed copy-number data (Figure 3.4C). When we sought to determine LKB1 expression in metastatic tumour samples obtained by our lab, however, we consistently observed expression of phosphorylated and total LKB1 (Figure 3.4D). Therefore, despite single allele loss of *STK11*, LKB1 protein expression is maintained in metastatic ovarian cancer cells and may in fact serve an important function in late-stage disease.

3.3.5 Suspension-induced activation of AMPK signalling is accompanied by enhanced LKB1 signalling and inhibition of mTORC1.

We next wanted to determine the specific components of the AMPK pathway that may also be altered when ovarian cancer cells are put in suspension. We first focused on LKB1 as a critical upstream activator of AMPK signalling. Immunoblot revealed increased phosphorylation of LKB1 at Serine 428 in spheroids formed from a number of ovarian cancer cell lines and ascites-derived cells compared to cells grown under adherent conditions (Figure 3.5A,B). Although its phosphorylation state does not affect its catalytic activity, phosphorylation at Ser428 has been shown to be important for the tumour suppressive functions of LKB1³⁷. LKB1 can be localized to the nucleus or cytoplasm, and the cytoplasmic pool of LKB1 has been shown to contribute to the tumour suppressive function of this kinase³². We determined by cellular fractionation and

immunoblotting that LKB1 protein in adherent and spheroid-cultured cells is located in the cytoplasm (Figure S3.1).

Since the LKB1/AMPK signalling pathway has been identified as a key negative regulator of mTORC1 signalling, we next focused on this pathway as a downstream readout for AMPK's ability to rewire cellular metabolism in these clusters of cells. Immunoblot performed on spheroids from cell lines and ascites-derived cells revealed a significant decrease in mTORC1 activity as determined by p70S6K1 phosphorylation (Figure 3.5C). Taken together, these results provide additional evidence for decreased anabolic metabolism that occurs when cells detach into suspension and form spheroids, indicating that the LKB1/AMPK/mTORC1 signalling axis may be a crucial mediator of cell survival in this context.

3.3.6 Spheroids are much less sensitive to further activation of the AMPK pathway than adherent ovarian cancer cells.

It has been previously demonstrated that treatment of ovarian cancer cells with AMP mimetic AICAR results in increased AMPK activity and decreased viability of adherent cells^{38,39}. Similarly, in our study, we demonstrate robust activation of AMPK after treatment of ovarian cancer cells with 1 mM AICAR, which corresponds with decreased mTORC1 activity (Figure 3.6A). In addition, AICAR treatment of various ovarian cancer cell lines and ascites-derived cells results in decreased viability in cells cultured under both adherent and suspension conditions. Importantly, the detrimental effects of AICAR treatment on spheroid cell viability are not observed until later time points compared to their adherent counterparts (Figure 3.6B). When spheroids are treated with AICAR during reattachment, however, a significant reduction in dispersion area was observed highlighting the detrimental effect that AMPK activation has on cell proliferation (Figure 3.6C).

To further explore mechanisms of AMPK activation, we also tested a more specific allosteric AMPK activator, A-769662, which stimulates AMPK directly without affecting the kinase domain⁴⁰. Treatment of ovarian cancer cells with A-769662 (100 μ M) results in activation of AMPK as indicated by enhanced phosphorylation of ACC (Figure

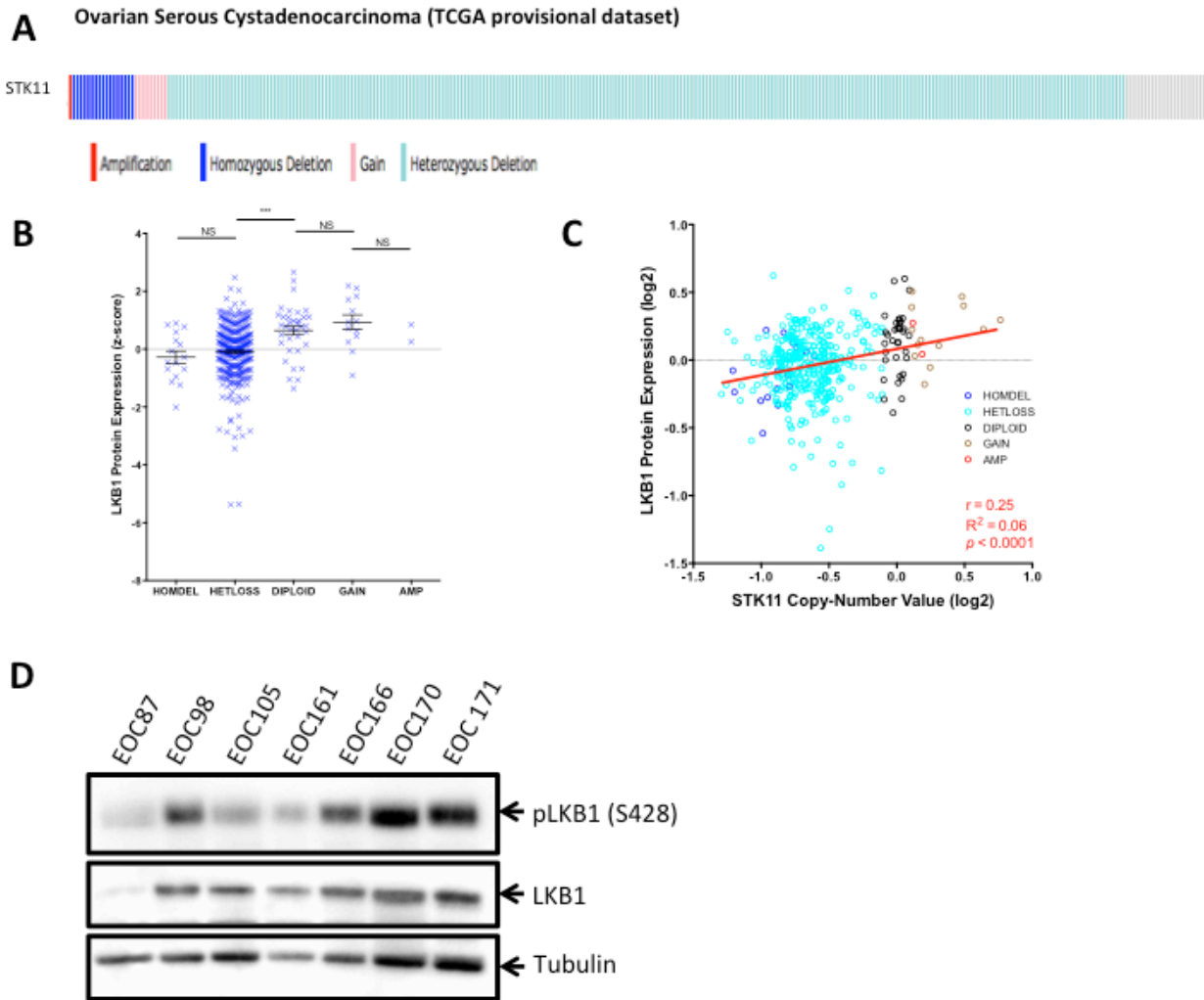


Figure 3.4: Despite heterozygous deletion, LKB1 protein is expressed in metastatic ovarian tumour samples.

(A) Gene copy-number calls at the *STK11* locus are depicted for 311 ovarian serous cystadenocarcinoma tumors (red & pink = high-level & low-level amplification, respectively; teal & blue = heterozygous & homozygous deletion, respectively). OncoPrint obtained from cBioPortal.org. (B) *STK11* protein (quantitative RPPA; n=398) expression data was transformed to z-scores and depicted as functions of copy-number. One-way ANOVA with Tukey's Test was performed (** $p < 0.001$). (C) ln-transformed protein expression (n=397; re-transformed to log₂ values) data depicted as a function of log₂-transformed copy number values. Correlation and linear regression analysis performed: line of best fit, Pearson's r, Goodness-of-fit R², and p values all reported. (D) Lysates were generated from metastatic tumour samples from seven ovarian cancer patients and immunoblot was performed to examine LKB1 expression in these samples.

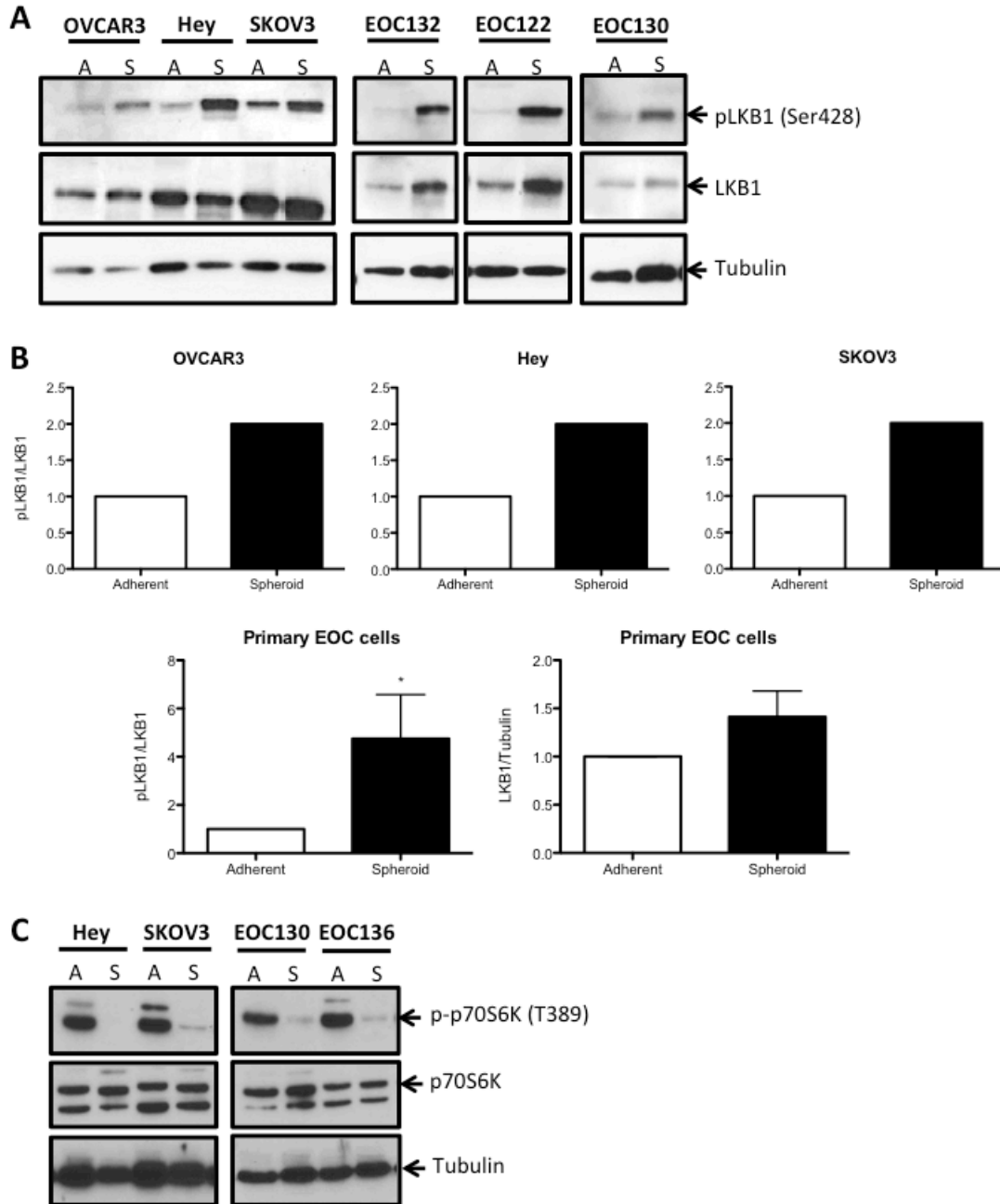


Figure 3.5: Spheroids formed from EOC cell lines and ascites-derived cells express LKB1 protein and have decreased levels of mTORC1 signalling.

(A) Immunoblot performed on EOC cell lines and ascites-derived EOC cells to determine levels of phosphorylated and total LKB1 protein. (B) Densitometry was performed on cell lines and primary EOC cells (n=16) to compare levels of phosphorylated and total LKB1 between adherent and spheroid cultured cells. Bars: Mean \pm SEM. Student's t-test was used to determine statistical significance (*p<0.05). (C) Immunoblot performed on EOC cell lines and ascites-derived EOC cells to determine levels of phosphorylated and total p70S6K1 protein as a read-out of mTORC1 activity.

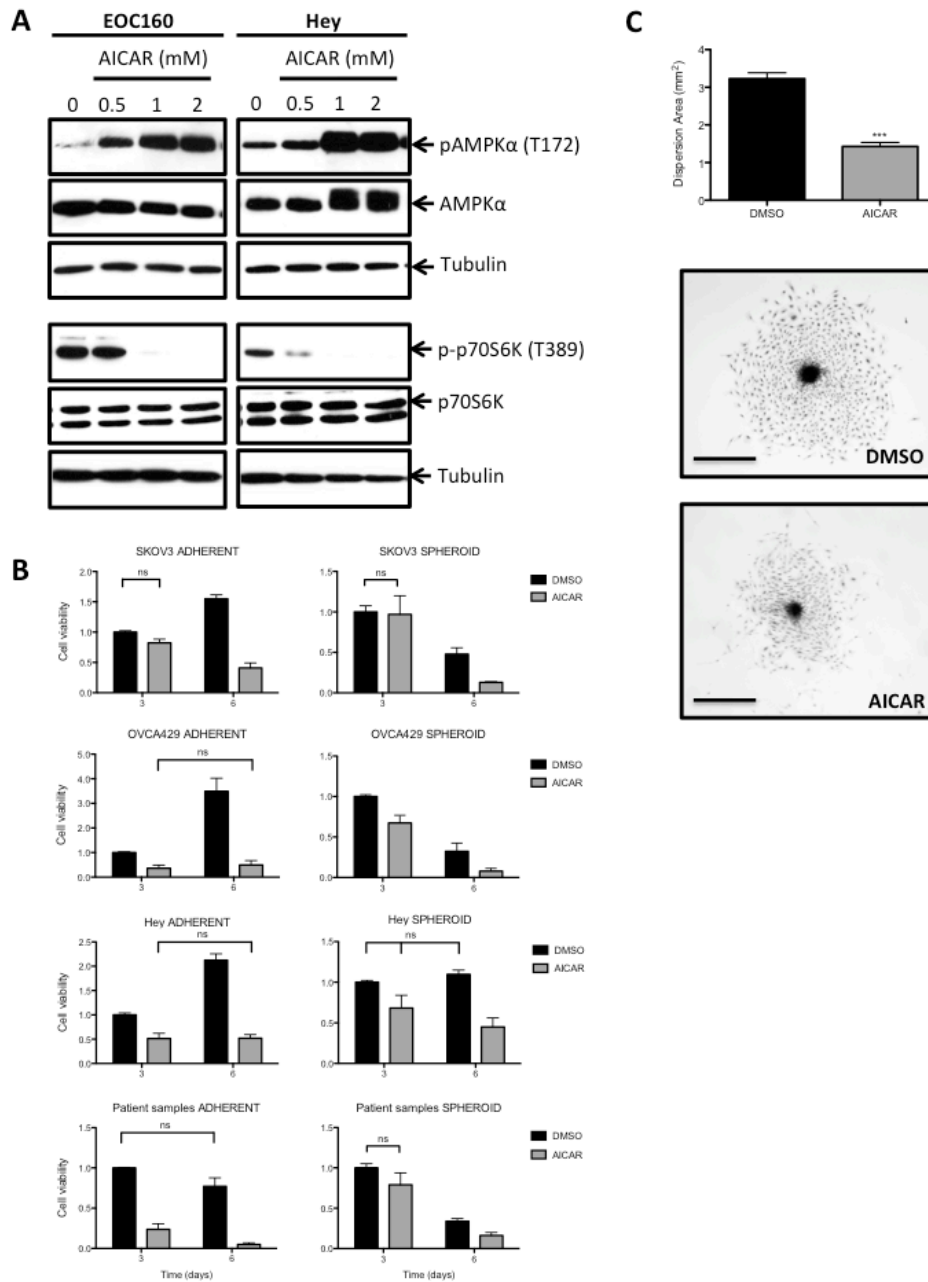


Figure 3.6: AICAR treatment of EOC cell lines and ascites-derived cells decreases cell viability in adherent and spheroid cells.

(A) Immunoblot performed on EOC cells treated for 24 hours with various doses of AICAR as indicated. (B) Viability of ovarian cancer cell lines and ascites-derived cells following 3 and 6 days of AICAR (1mM) treatment in adherent and spheroid culture conditions. Bars: Mean \pm SEM. Effect of treatment at each timepoint was determined using Student's t-test. Results are significant ($p < 0.05$) unless otherwise indicated. (C) Reattachment of spheroids (72h) formed from ascites-derived cells ($n=9$) treated with AICAR (1mM) at time of seeding to suspension culture. Quantifications performed using ImageJ and Student's t-test used to compare areas between groups (***) $p < 0.001$). Representative image of one patient sample (EOC154) depicted. Scale bar: 100 μ m.

3.7A). Similarly to AICAR treatment, this compound also reduces viability of ovarian cancer cells in adherent culture. However, there is no effect of A-769662 treatment on viability of cells in spheroids (Figure 3.7B). These results suggest that actively proliferating, adherent ovarian cancer cells are more sensitive to AMPK activation, but quiescent cells in multicellular spheroids are less impacted by a further increase in the activation state of this pathway.

Following the observation that both AICAR and A-769662 have detrimental effects on ovarian cancer cells in adherent culture, we further characterized this reduced viability by determining whether cells were undergoing apoptosis or arresting in a particular phase of the cell cycle. Both compounds result in a decreased proportion of cells in the S-phase of the cell cycle as early as 24 hours after treatment. The effect observed with AICAR treatment is more robust across different cell lines than that observed with A-769662 (Figure S3.2). We also used Caspase-Glo® luminescence-based assay which uses caspase 3/7 activity as a read-out for apoptosis. We found that 72 hours following treatment with AICAR (1mM), there was a significant induction of apoptosis, an effect which was not observed in A-769662-treated cells (Figure S3.2). These results suggest that these two compounds have different mechanisms of action in ovarian cancer cells: AICAR decreases ovarian cancer cell viability largely by apoptosis, whereas A-769662 elicits a cytostatic response thereby blocking ovarian cancer cell growth.

3.3.7 LKB1, but not AMPK, is required for ovarian cancer cell survival in suspension.

Given the relative insensitivity of ovarian cancer cells in suspension to further activation of AMPK, we assessed the functional impact of attenuation of the LKB1/AMPK pathway in spheroids. In order to do this we transfected ovarian cancer cell lines with siRNAs targeting either *PRKAA1* (AMPK α 1) or *STK11* (LKB1). A number of established ovarian cancer cell lines were screened for LKB1 and AMPK expression and activity in adherent culture (Figure S3.3) and those with the highest activity were used in knockdown experiments. Effective knockdown of *STK11* and *PRKAA1* was achieved in cells in both adherent (Figure 3.8A) and suspension (Figure 3.8B) cultures. Cells in adherent culture were not sensitive to knockdown of either AMPK α 1 or LKB1 with

respect to cell viability, most likely since these cells are proliferating and not under metabolic stress, therefore not requiring this pathway. Surprisingly, knockdown of AMPK α 1 had no impact on the survival of cells in suspension, while loss of LKB1 significantly reduced viability of cells in spheroids (Figure 3.8C). These results point to AMPK-independent LKB1 signalling as an important stress adaptation used by ovarian cancer cells in suspension in order to avoid anoikis.

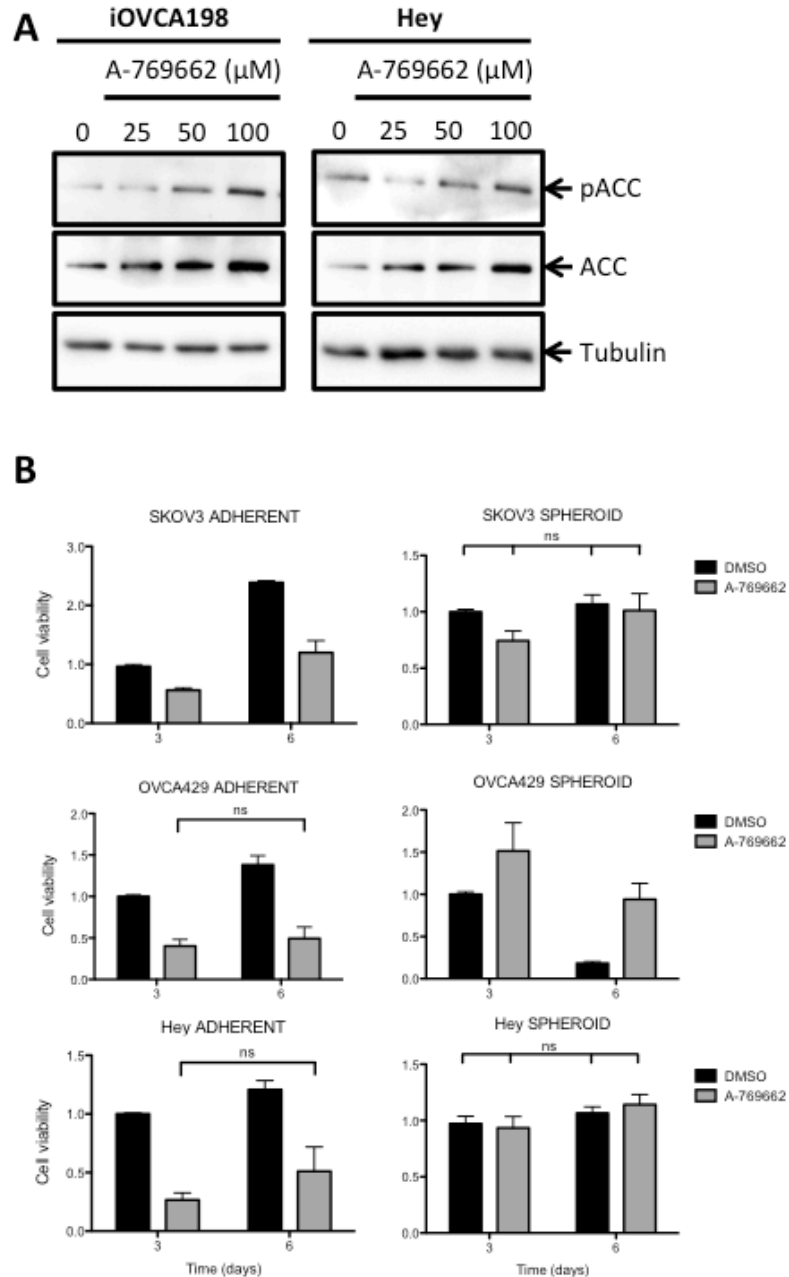


Figure 3.7: Allosteric AMPK activator A-769662 decreases viability of EOC cells in a context-dependent manner.

(A) Immunoblot performed on EOC cells treated for 24 hours with various doses of A-769662 as indicated. AMPK activation determined by levels of phosphorylated ACC. (B) Viability of ovarian cancer cell lines following 3 and 6 days of A-769662 (100 μM) treatment in adherent and spheroid culture conditions. Bars: Mean \pm SEM. Effect of treatment at each timepoint was determined using Student's t-test. Results are significant ($p < 0.05$) unless otherwise indicated.

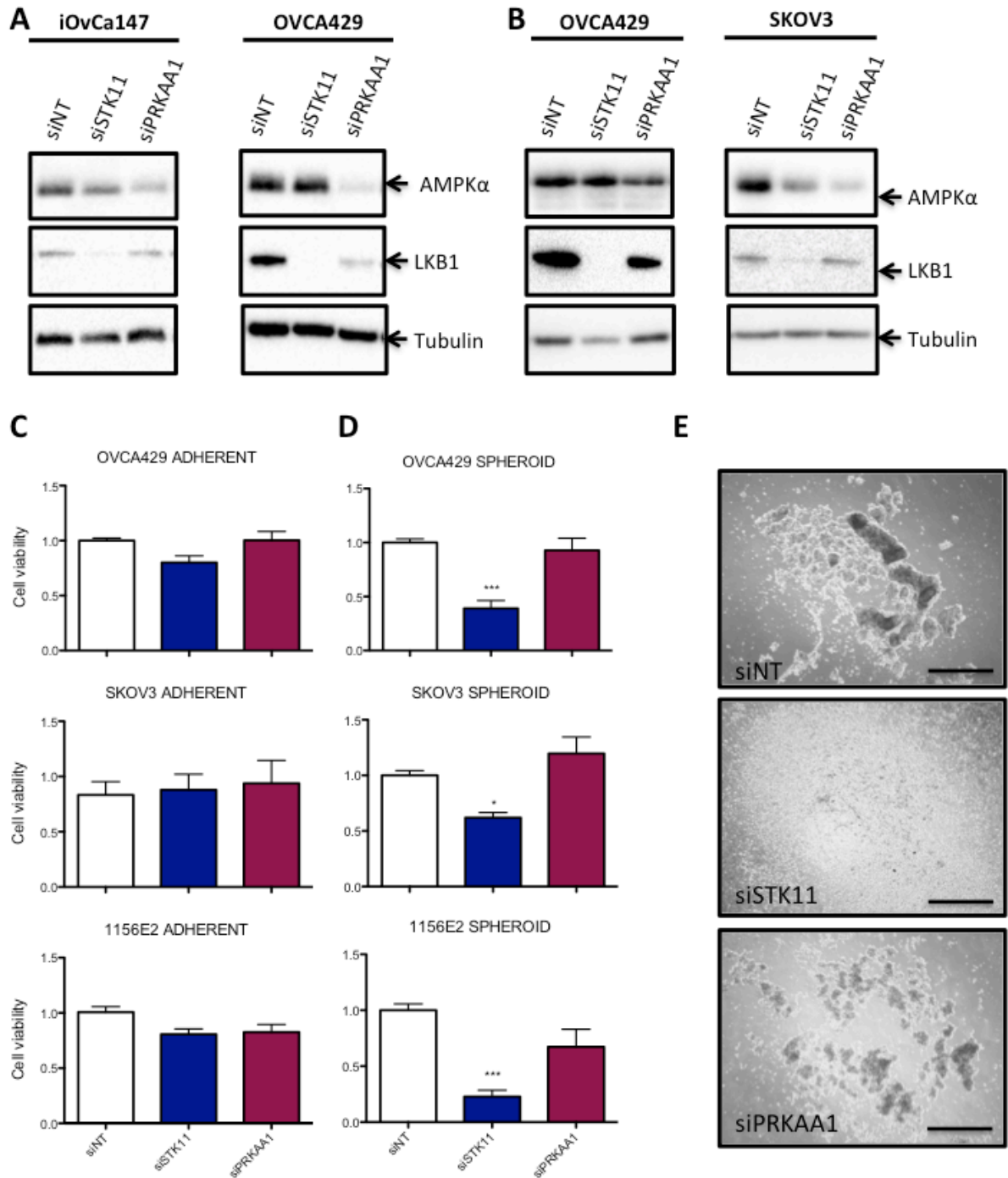


Figure 3.8: siRNA-mediated knockdown of *STK11* but not *PRKAA1* results in a decrease in viability of ovarian cancer spheroids.

(A,B) Immunoblot performed for proteins as indicated on adherent and spheroid ovarian cancer cells 72 hours after transfection or 3 days after spheroid formation respectively. (C,D) Cell viability as determined by Cell Titer Glo® assay on ovarian cancer cell lines in adherent or suspension culture respectively after three days (seeded to these conditions 72 hours after transfection). (E) Images of day 3 OVCA429 spheroids following siRNA knockdown as indicated. Scale Bar: 100 μ m.

3.4 Discussion

The distinct mode of metastatic spread whereby EOC cells transit the peritoneal cavity in suspension, presents unique therapeutic challenges for treatment of advanced-stage ovarian cancer. Characterization of this unique population of non-adherent cells will provide insights into novel targets for treatment of this deadly disease. Our laboratory has previously shown that ovarian cancer cells in suspension have a propensity to aggregate and form dormant multicellular clusters or spheroids. This dormancy is reversible upon reattachment to an adherent substratum, a process that is dependent upon AKT¹⁶. Following up on this observation, we show in this report that cells in dormant EOC spheroids have reduced metabolic activity and as such induce the LKB1/AMPK metabolic stress response pathway. Indeed, we demonstrate that AMPK activity is enhanced in quiescent ovarian cancer spheroids. Also, direct pharmacologic activation of AMPK in proliferating adherent ovarian cancer cells leads to cytostasis and ultimately a decrease in cell viability. Our surprising new result, however, is that where maintenance of LKB1 expression is required for ovarian cancer cell survival in suspension, AMPK is not necessary. This implies an AMPK-independent role for LKB1 in mediating anoikis-resistance in ovarian cancer cells. This is the first study to demonstrate a pro-survival function for LKB1, a kinase that has been traditionally considered to be a tumour suppressor.

Expansive tumour growth is typically dependent on over-proliferative malignant cells that lack the normal response to induce protective growth arrest. Under nutrient-rich conditions, proliferative cancer cells should have low to absent levels of active AMPK signalling. Indeed, we show that expression of phosphorylated AMPK α is marginal in the majority of cultured EOC cells assessed; however, AMPK activity is significantly elevated upon spheroid formation. Ectopic activation of this pathway in proliferating cells using the AMP mimetic AICAR or an allosteric AMPK α activator A-769662 result in decreased viability. These agents most likely produce this effect through different mechanisms. Although both compounds induce a potent cytostatic response, AICAR treatment eventually results in significant cell death due to induction of apoptosis whereas A-769662 does not. A recent report highlighted the difference between these two

compounds, demonstrating that the growth-suppressive effects of AICAR are actually independent of AMPK in a glioma model⁴¹. Thus, the decreased viability observed in ovarian cancer spheroids treated with AICAR may in fact occur via AMPK-independent mechanisms. Taken together, this indicates that suppressed AMPK signalling is required to sustain active tumour growth, and supports a general idea that this pathway possesses classical tumour suppressor function under these conditions. However, when cells are in suspension AMPK is activated to facilitate cellular quiescence, and further activation is of lesser consequence on viability. These results indicate that AMPK acts like a typical tumour suppressor, yet its function may be utilized to promote protection from apoptosis during later stages of ovarian cancer progression.

Along this same reasoning, it is not unreasonable to postulate that LKB1 function may be context-specific during ovarian cancer progression given its array of downstream targets. A recent report of a conditional mouse model for serous ovarian carcinoma determined that loss of one *Stk11* allele in the context of *Pten* loss within the OSE leads to the development of high-grade papillary serous ovarian carcinomas⁴². This is not the first study to demonstrate synergism between LKB1 and other tumour suppressors or oncogenes. In fact, LKB1 has been shown to accelerate tumorigenesis in conjunction with p53⁴³, *Kras*⁴⁴, and c-myc⁴⁵. This provides additional support for the complex function of this important kinase. Indeed, the molecular signature of a particular tumour is likely another factor that impacts the operational role of LKB1 in a particular type or stage of cancer¹⁸. Although the study by Tanwar and colleagues⁴² implicates loss of LKB1 function in the initiation of ovarian cancer, knockout is performed in the ovarian surface epithelium and not the secretory epithelium of oviduct; the secretory epithelial cells of the distal fallopian tube is now considered the site of origin for high-grade serous ovarian cancer⁴⁶⁻⁴⁸. Since loss of *STK11* in premalignant serous tubal intraepithelial carcinoma lesions in humans has not yet been documented, studies in this regard would provide additional insight into the role of LKB1 in ovarian cancer initiation.

In this report, we show that analysis of the serous ovarian cancer provisional dataset from cBioPortal indicated that 84% of tumours exhibit heterozygous loss of *STK11* the gene encoding LKB1²⁹. Despite this, we show that numerous EOC solid tumour

specimens, as well as established ovarian cancer cell lines, express LKB1 protein. Interestingly, we also show copy number gains or amplifications in *PRKAA1*, which encodes AMPK α 1, in 36% of samples. This suggests that there may be compensatory mechanisms to upregulate AMPK activity in late-stage ovarian tumours which harbour reduced LKB1 in order to maintain a functional pathway for tumour cell survival during metastasis. It is also possible that this discordance in LKB1 and AMPK copy number variations indicates that these kinases may not necessarily be acting in concert in advanced-stage ovarian cancer. Our data imply that although *STK11* haploinsufficiency may occur and predispose to ovarian cancer initiation, maintenance of functional LKB1 signalling pathway is likely essential during metastatic progression particularly to fuel recurrence of chemoresistant ovarian cancer.

The LKB1/AMPK signalling pathway represents an immediate response to metabolic stress and reduced energy supply to downregulate anabolic metabolism and shunt pathways to utilize alternative energy substrates¹⁸. Previous data from our laboratory has shown a decrease in AKT activity upon spheroid formation and an accompanying induction of dormancy¹⁶ and autophagy (Correa, Shepherd, DiMattia, unpublished). We now show that the LKB1/AMPK pathway is induced in EOC spheroids, which has opposing regulatory effects on mTORC1 compared with what would be observed by AKT. Indeed, we show that mTORC1 activity is reduced in spheroids. This result indicates that the LKB1/AMPK signalling cascade acts to reduce protein translation and induce autophagy, likely in concert with downregulated AKT activity.

It has been shown in other cell systems that LKB1/AMPK is an important mediator of protecting detached epithelial cells from anoikis^{24,26}. Interestingly, targeted knockdown of *STK11* (LKB1) in our study demonstrated a significant reduction in spheroid cell viability yet there was no effect when AMPK α 1 activity was reduced. We confirmed that there was no compensatory effect of AMPK α 2 expression in *PRKAA1*-knockdown spheroid cells that could explain this lack of effect (Appendix A). This implies that LKB1 plays an important role in mediating anoikis-resistance and dormancy in EOC spheroids independent of AMPK. AMPK is the most studied downstream target of LKB1. However, LKB1 has been called a “master kinase” given its ability to phosphorylate at

least 12 other downstream proteins, referred to as AMPK-related kinases (ARKs: MARK1, MARK2, MARK3, MARK4, SIK1, SIK2, SIK3, BRSK1, BRSK2, SNRK, NUAK1, NUAK2)⁴⁹. The ARKs have been shown to play roles in many important aspects of cell function including cell polarity (MARK, BRSK)^{50,51}, cell proliferation (NUAKs)^{52,53} and CREB-regulated gene transcription (SIKs)⁵⁴⁻⁵⁶. It seems likely that one or more of these ARKs are important downstream mediators of the LKB1-dependent decrease in cell viability we observe in ovarian cancer spheroids. One likely candidate, microtubule affinity-regulating kinase 4 (MARK4), is able to phosphorylate Raptor on the same residue as AMPK, resulting in inhibition of mTORC1 signalling⁵⁷. Another of these kinases, NUAK1 may also be an interesting target to investigate in our system, as it is able to promote cell survival during periods of nutrient deprivation⁵⁸. Further studies are needed to determine which of the numerous substrates downstream from LKB1 are mediating this requirement to maintain cell viability in ovarian cancer spheroids.

Although literature supports the idea that *STK11* acts as a tumour suppressor during early steps of tumorigenesis, our *STK11* knockdown results provide yet another example of a protein, in this case LKB1, exhibiting an important reciprocal metastasis-promoting function during late-stage disease. EOC spheroids have the capacity to harbour a niche of chemotherapy-resistant cells. Our data supports this idea, and importantly we provide the first evidence that AMPK-independent LKB1 signalling may play a significant role in adaptive resistance mechanisms in these metastasis-promoting structures.

3.5 References

1. Statistics, C.C.S.s.A.C.o.C. Canadian Cancer Statistics 2013. *Canadian Cancer Society* (2013).
2. Nik, N.N., Vang, R., Shih, I.M. & Kurman, R.J. Origin and Pathogenesis of Pelvic (Ovarian, Tubal, and Primary Peritoneal) Serous Carcinoma. *Annu Rev Pathol* (2013).
3. Lengyel, E., *et al.* Epithelial ovarian cancer experimental models. *Oncogene* (2013).
4. Burleson, K.M., *et al.* Ovarian carcinoma ascites spheroids adhere to extracellular matrix components and mesothelial cell monolayers. *Gynecol Oncol* **93**, 170-181 (2004).
5. Burleson, K.M., Hansen, L.K. & Skubitz, A.P. Ovarian carcinoma spheroids disaggregate on type I collagen and invade live human mesothelial cell monolayers. *Clinical & experimental metastasis* **21**, 685-697 (2004).
6. Kenny, H.A., Nieman, K.M., Mitra, A.K. & Lengyel, E. The first line of intra-abdominal metastatic attack: breaching the mesothelial cell layer. *Cancer Discov* **1**, 100-102 (2011).
7. Landen, C.N., Jr., Birrer, M.J. & Sood, A.K. Early events in the pathogenesis of epithelial ovarian cancer. *Journal of clinical oncology : official journal of the American Society of Clinical Oncology* **26**, 995-1005 (2008).
8. Barbone, D., *et al.* The Bcl-2 repertoire of mesothelioma spheroids underlies acquired apoptotic multicellular resistance. *Cell death & disease* **2**, e174.
9. Bertuzzi, A., Fasano, A., Gandolfi, A. & Sinisgalli, C. Necrotic core in EMT6/Ro tumour spheroids: Is it caused by an ATP deficit? *Journal of theoretical biology* **262**, 142-150.
10. Dolznig, H., *et al.* Modeling Colon Adenocarcinomas in Vitro A 3D Co-Culture System Induces Cancer-Relevant Pathways upon Tumor Cell and Stromal Fibroblast Interaction. *Am J Pathol* **179**, 487-501.
11. Grun, B., *et al.* Three-dimensional in vitro cell biology models of ovarian and endometrial cancer. *Cell Prolif* **42**, 219-228 (2009).
12. Sodek, K.L., Ringuette, M.J. & Brown, T.J. Compact spheroid formation by ovarian cancer cells is associated with contractile behavior and an invasive phenotype. *International journal of cancer* **124**, 2060-2070 (2009).
13. Valcarcel, M., *et al.* Three-dimensional growth as multicellular spheroid activates the proangiogenic phenotype of colorectal carcinoma cells via LFA-1-dependent VEGF: implications on hepatic micrometastasis. *Journal of translational medicine* **6**, 57 (2008).
14. Waite, C.L. & Roth, C.M. PAMAM-RGD conjugates enhance siRNA delivery through a multicellular spheroid model of malignant glioma. *Bioconjug Chem* **20**, 1908-1916 (2009).
15. Kunz-Schughart, L.A., Doetsch, J., Mueller-Klieser, W. & Groebe, K. Proliferative activity and tumorigenic conversion: impact on cellular metabolism in 3-D culture. *American journal of physiology* **278**, C765-780 (2000).

16. Correa, R.J., Peart, T., Valdes, Y.R., Dimattia, G.E. & Shepherd, T.G. Modulation of AKT activity is associated with reversible dormancy in ascites-derived epithelial ovarian cancer spheroids. *Carcinogenesis* **33**, 49-58 (2012).
17. Mihaylova, M.M. & Shaw, R.J. The AMPK signalling pathway coordinates cell growth, autophagy and metabolism. *Nat Cell Biol* **13**, 1016-1023 (2011).
18. Liang, J. & Mills, G.B. AMPK: a contextual oncogene or tumor suppressor? *Cancer Res* **73**, 2929-2935 (2013).
19. Hawley, S.A., *et al.* Complexes between the LKB1 tumor suppressor, STRAD alpha/beta and MO25 alpha/beta are upstream kinases in the AMP-activated protein kinase cascade. *J Biol* **2**, 28 (2003).
20. Shaw, T.J., Senterman, M.K., Dawson, K., Crane, C.A. & Vanderhyden, B.C. Characterization of intraperitoneal, orthotopic, and metastatic xenograft models of human ovarian cancer. *Mol Ther* **10**, 1032-1042 (2004).
21. Woods, A., *et al.* LKB1 is the upstream kinase in the AMP-activated protein kinase cascade. *Current biology : CB* **13**, 2004-2008 (2003).
22. Mandal, S., Guptan, P., Owusu-Ansah, E. & Banerjee, U. Mitochondrial regulation of cell cycle progression during development as revealed by the tenured mutation in *Drosophila*. *Developmental cell* **9**, 843-854 (2005).
23. Hemminki, A., *et al.* A serine/threonine kinase gene defective in Peutz-Jeghers syndrome. *Nature* **391**, 184-187 (1998).
24. Ng, T.L., *et al.* The AMPK stress response pathway mediates anoikis resistance through inhibition of mTOR and suppression of protein synthesis. *Cell Death Differ* **19**, 501-510 (2012).
25. Schafer, Z.T., *et al.* Antioxidant and oncogene rescue of metabolic defects caused by loss of matrix attachment. *Nature* **461**, 109-113 (2009).
26. Avivar-Valderas, A., *et al.* Regulation of autophagy during ECM detachment is linked to a selective inhibition of mTORC1 by PERK. *Oncogene* **32**, 4932-4940 (2013).
27. Shepherd, T.G., Theriault, B.L., Campbell, E.J. & Nachtigal, M.W. Primary culture of ovarian surface epithelial cells and ascites-derived ovarian cancer cells from patients. *Nat Protoc* **1**, 2643-2649 (2006).
28. Goldman, M., *et al.* The UCSC Cancer Genomics Browser: update 2013. *Nucleic Acids Res* **41**, D949-954 (2013).
29. Gao, J., *et al.* Integrative analysis of complex cancer genomics and clinical profiles using the cBioPortal. *Science signaling* **6**, p11 (2013).
30. Tibes, R., *et al.* Reverse phase protein array: validation of a novel proteomic technology and utility for analysis of primary leukemia specimens and hematopoietic stem cells. *Molecular cancer therapeutics* **5**, 2512-2521 (2006).
31. Peart, T.M., Correa, R.J., Valdes, Y.R., Dimattia, G.E. & Shepherd, T.G. BMP signalling controls the malignant potential of ascites-derived human epithelial ovarian cancer spheroids via AKT kinase activation. *Clinical & experimental metastasis* **29**, 293-313 (2012).
32. Alessi, D.R., Sakamoto, K. & Bayascas, J.R. LKB1-dependent signaling pathways. *Annu Rev Biochem* **75**, 137-163 (2006).
33. Bardeesy, N., *et al.* Loss of the *Lkb1* tumour suppressor provokes intestinal polyposis but resistance to transformation. *Nature* **419**, 162-167 (2002).

34. Hernan, I., *et al.* De novo germline mutation in the serine-threonine kinase STK11/LKB1 gene associated with Peutz-Jeghers syndrome. *Clin Genet* **66**, 58-62 (2004).
35. Jishage, K., *et al.* Role of Lkb1, the causative gene of Peutz-Jegher's syndrome, in embryogenesis and polyposis. *Proceedings of the National Academy of Sciences of the United States of America* **99**, 8903-8908 (2002).
36. Miyoshi, H., *et al.* Gastrointestinal hamartomatous polyposis in Lkb1 heterozygous knockout mice. *Cancer Res* **62**, 2261-2266 (2002).
37. Sapkota, G.P., *et al.* Phosphorylation of the protein kinase mutated in Peutz-Jeghers cancer syndrome, LKB1/STK11, at Ser431 by p90(RSK) and cAMP-dependent protein kinase, but not its farnesylation at Cys(433), is essential for LKB1 to suppress cell growth. *J Biol Chem* **276**, 19469-19482 (2001).
38. Cheong, J.H., *et al.* Dual inhibition of tumor energy pathway by 2-deoxyglucose and metformin is effective against a broad spectrum of preclinical cancer models. *Molecular cancer therapeutics* **10**, 2350-2362 (2011).
39. Priebe, A., *et al.* Glucose deprivation activates AMPK and induces cell death through modulation of Akt in ovarian cancer cells. *Gynecol Oncol* **122**, 389-395 (2011).
40. Goransson, O., *et al.* Mechanism of action of A-769662, a valuable tool for activation of AMP-activated protein kinase. *J Biol Chem* **282**, 32549-32560 (2007).
41. Liu, X., *et al.* Discrete mechanisms of mTOR and cell cycle regulation by AMPK agonists independent of AMPK. *Proceedings of the National Academy of Sciences* (2014).
42. Tanwar, P.S., *et al.* Loss of LKB1 and PTEN tumor suppressor genes in the ovarian surface epithelium induces papillary serous ovarian cancer. *Carcinogenesis* (2013).
43. Wei, C., *et al.* Mutation of Lkb1 and p53 genes exert a cooperative effect on tumorigenesis. *Cancer Res* **65**, 11297-11303 (2005).
44. Ji, H., *et al.* LKB1 modulates lung cancer differentiation and metastasis. *Nature* **448**, 807-810 (2007).
45. Partanen, J.I., Nieminen, A.I. & Klefstrom, J. 3D view to tumor suppression: Lkb1, polarity and the arrest of oncogenic c-Myc. *Cell cycle (Georgetown, Tex)* **8**, 716-724 (2009).
46. Erickson, B.K., Conner, M.G. & Landen, C.N., Jr. The role of the fallopian tube in the origin of ovarian cancer. *Am J Obstet Gynecol* (2013).
47. Kessler, M., Fotopoulou, C. & Meyer, T. The molecular fingerprint of high grade serous ovarian cancer reflects its fallopian tube origin. *Int J Mol Sci* **14**, 6571-6596 (2013).
48. Piek, J.M., *et al.* BRCA1/2-related ovarian cancers are of tubal origin: a hypothesis. *Gynecologic oncology* **90**, 491 (2003).
49. Lizcano, J.M., *et al.* LKB1 is a master kinase that activates 13 kinases of the AMPK subfamily, including MARK/PAR-1. *The EMBO journal* **23**, 833-843 (2004).

50. Hayashi, K., Suzuki, A. & Ohno, S. A novel function of the cell polarity-regulating kinase PAR-1/MARK in dendritic spines. *Bioarchitecture* **1**, 261-266 (2011).
51. Saadat, I., *et al.* Helicobacter pylori CagA targets PAR1/MARK kinase to disrupt epithelial cell polarity. *Nature* **447**, 330-333 (2007).
52. Hou, X., *et al.* A new role of NUA1: directly phosphorylating p53 and regulating cell proliferation. *Oncogene* **30**, 2933-2942 (2011).
53. Sun, X., Gao, L., Chien, H.Y., Li, W.C. & Zhao, J. The regulation and function of the NUA1 family. *J Mol Endocrinol* **51**, R15-22 (2013).
54. Katoh, Y., *et al.* Silencing the constitutive active transcription factor CREB by the LKB1-SIK signaling cascade. *Febs J* **273**, 2730-2748 (2006).
55. Katoh, Y., *et al.* Salt-inducible kinase-1 represses cAMP response element-binding protein activity both in the nucleus and in the cytoplasm. *Eur J Biochem* **271**, 4307-4319 (2004).
56. Takemori, H., Kajimura, J. & Okamoto, M. TORC-SIK cascade regulates CREB activity through the basic leucine zipper domain. *Febs J* **274**, 3202-3209 (2007).
57. Li, L. & Guan, K.L. Microtubule-associated protein/microtubule affinity-regulating kinase 4 (MARK4) is a negative regulator of the mammalian target of rapamycin complex 1 (mTORC1). *J Biol Chem* **288**, 703-708 (2013).
58. Suzuki, A., *et al.* ARK5 suppresses the cell death induced by nutrient starvation and death receptors via inhibition of caspase 8 activation, but not by chemotherapeutic agents or UV irradiation. *Oncogene* **22**, 6177-6182 (2003).

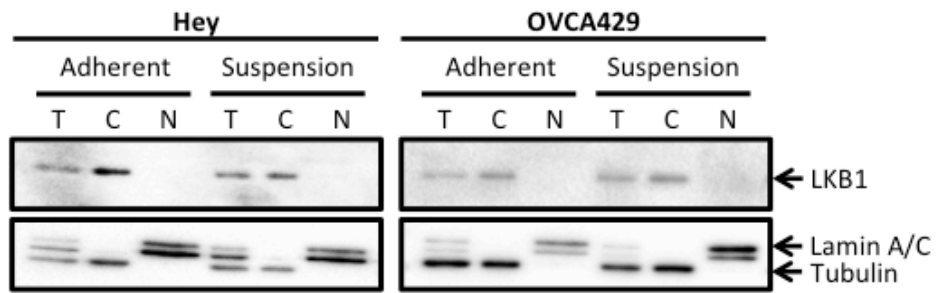


Figure S3.1: LKB1 is located in the cytoplasm in adherent and spheroid EOC cells. Immunoblot performed on whole-cell (T), cytoplasmic (C), and nuclear (N) protein extracts isolated from ovarian cancer cell lines to determine subcellular localization of LKB1 protein. Lamin A/C and tubulin used as nuclear and cytoplasmic loading controls, respectively.

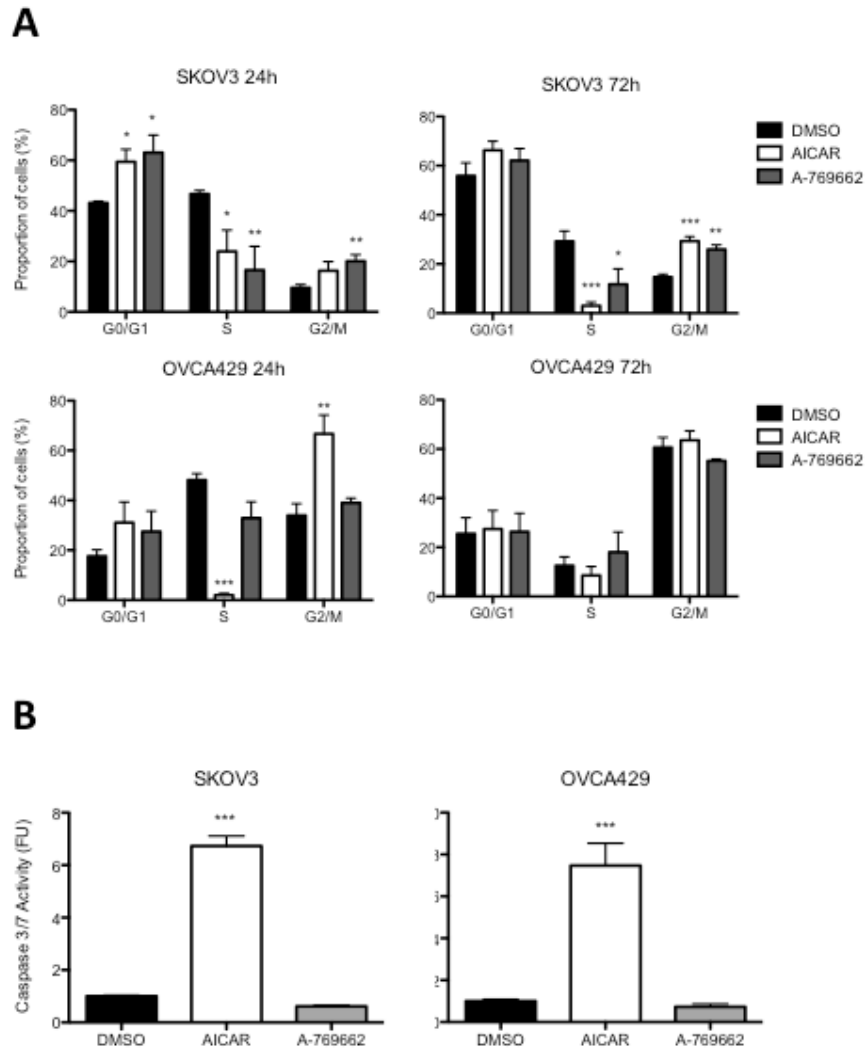


Figure S3.2: AICAR and A-769662 have different effects on cell cycle progression and apoptosis in adherent ovarian cancer cells.

(A) Cell cycle analysis (BrdU and PI) by flow cytometry on ovarian cancer cells following 24 and 72 hours of treatment with either AICAR or A-769662 ($n=2$ for each cell line). (B) Caspase 3/7 activity 72 hours following treatment with either AICAR or A-769662 as determined by Caspase-Glo®. Bars: Mean \pm SEM. Effect of treatment determined by One-way ANOVA (* $p<0.05$; ** $p<0.01$; *** $p<0.001$).

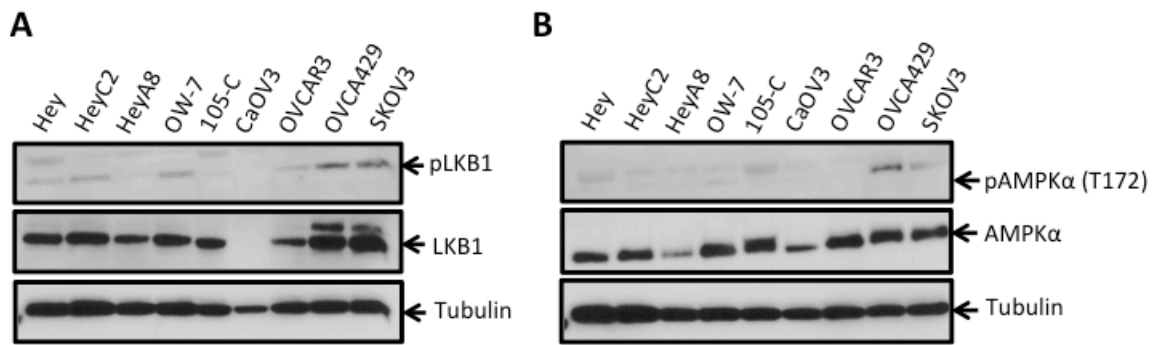


Figure S3.3: LKB1 and AMPK are expressed in EOC cell lines under adherent conditions but activity is low.

(A, B) Immunoblot performed on a number of ovarian cancer cell lines cultured under adherent conditions in order to determine levels of phosphorylated and total LKB1 and AMPK as indicated.

Chapter 4

4 Discussion

4.1 Summary of findings

The high level of a mortality associated with high-grade serous ovarian cancer has been directly attributed to intra-abdominal metastases, which recur despite aggressive surgical and chemotherapeutic interventions. The presence of microscopic disease and dormant, chemotherapy-resistant cancer cells is likely the cause of these recurrences. Therefore, experimental models that allow us to better understand the biology and pathogenesis of dormant high-grade ovarian cancer cells are crucial to uncover more effective treatment options for patients with advanced-stage disease. Our studies use a highly-relevant, tractable, non-adherent culture system to examine the molecular underpinnings of multicellular spheroid formation and subsequent reattachment to an adherent substratum. These structures induce dormancy and mimic the spheroid state of ovarian cancer cells in ascites, which facilitates the spread of this cancer.

I focused on two distinct cellular signalling systems and discovered in the first instance that BMP signalling is decreased upon spheroid formation, a process that is reversed when these clusters reattach to an adherent substratum (Chapter 2). To examine the functional implications of this dynamic regulation, I constitutively activated BMP signalling and discovered a detrimental effect on spheroid formation, resulting in smaller, more loosely aggregated clusters. Activation of this pathway during spheroid reattachment on the other hand, resulted in increased cellular dispersion. These phenotypic alterations in spheroid formation and reattachment observed in response to BMP signalling, were shown to be mediated, in part, by interaction with the PI3K/AKT signalling pathway. Specifically, constitutive activation of BMP signalling resulted in enhanced AKT activity, which was shown to contribute to increased spheroid reattachment observed as a result of overactive BMP signalling.

Given the ability of the PI3K/AKT and BMP signalling pathways to act together to alter spheroid formation and reattachment, I chose to examine other key cell survival pathways, which might act in concert with AKT in EOC cells. The objective was to

identify signalling pathways that may interact to maintain the viability of ovarian cancer cells and allow seeding of recurrent disease. In doing so, we expect to identify new potential therapeutic targets for which drugs may already exist or lay the ground work for use of specific combinatorial treatments. Additional rationale for this route of investigation was provided by other work in our laboratory demonstrating an AKT-dependent induction of dormancy and autophagy in EOC spheroids¹. Investigating this area of research revealed number of studies that reported AMPK-dependent induction of autophagy under conditions of stress such as glucose deprivation and hypoxia^{2,3}. Therefore, I hypothesized that, in addition to the AKT pathway, the LKB1/AMPK signalling cascade would be an important contributor to spheroid-formation induced dormancy.

AMPK has a unique ability integrate extracellular nutrient and energy signals in order to control the metabolic function of cells. I discovered that AMPK activity is greatly enhanced in ovarian cancer spheroids and this is associated with enhanced phosphorylation of its upstream kinase, LKB1 (Chapter 3). Activation of AMPK is detrimental in adherent, proliferating cells but has little effect on dormant, multicellular spheroids. On the other hand, targeted knockdown experiments highlight an AMPK-independent role for LKB1 in survival of cells in suspension. This is the first demonstration of a pro-survival function for LKB1, a kinase that has been primarily considered to be a tumour suppressor.

The data presented in this thesis discusses two signalling pathways that play distinct roles in EOC spheroid formation and survival. Both pathways however, present potential therapeutic targets for the unique population of non-adherent ovarian cancer cells within ascites fluid.

4.2 BMP signalling plays context-specific roles during ovarian cancer spheroid formation and reattachment

Although a dichotomous role for TGF- β in carcinogenesis is well-established, this is not the case for BMP signalling. More *in vitro* and *in vivo* evidence is required to determine whether this pathway is indeed oncogenic or tumour suppressive and in which

types and stages of cancers this is true. BMP signalling is generally considered a critical pathway during development controlling cell differentiation. Therefore, it is reasonable to suppose that induction of BMP signalling in cancer cells might be anti-oncogenic causing a differentiation-related program to force cancer cells out of the cell cycle. It is also possible that BMP signalling has been co-opted by cancer cells in a pro-oncogenic manner to facilitate maintenance of the cancer cell phenotype.

Our study focused on dissecting the contribution of the BMP signalling cascade during the various phases of ovarian cancer progression using a biologically-relevant, tractable *in vitro* model system. This model takes into account the unique mode of ovarian cancer metastasis, whereby multicellular spheroids represent an important conduit through which cells are able to survive until they reach a mesothelial surface where re-implantation and invasion are possible. It has been suggested that ovarian cancer cells within multicellular aggregates or spheroids undergo EMT, acquiring more mesenchymal characteristics, preparing them to reattach and invade, forming secondary metastases when conditions are favourable^{4,5}.

The data presented in Chapter 2 confirms that spheroids formed from primary ovarian cancer cells undergo EMT, characterized by decreased expression of the E-cadherin gene. This is supported by previous evidence that E-cadherin expression is reduced in cells isolated from ascites compared to their solid tumour counterparts⁶ as well as other studies demonstrating that ovarian cancer cell lines with more mesenchymal characteristics have an increased propensity for compact spheroid formation⁵. The autonomous down-regulation of BMP signalling during spheroid formation and the decreased propensity for compact spheroid formation when this pathway is activated suggests that BMP signalling may in fact be opposing the natural EMT response of EOC spheroids. This is concordance with a study published in 2011 by the Weinberg lab in which they documented that the BMP pathway had the ability to antagonize TGF- β -induced EMT in mammary epithelial cells⁷. Indeed, activation of BMP signalling within EOC spheroids results in increased E-cadherin expression when compared to controls, suggesting that inhibition of EMT could be a potential mechanism through which BMP signalling decreases spheroid compaction.

Although activated BMP signalling in spheroids results in smaller, more loosely aggregated clusters this does not result in an overall decrease in cell viability. Therefore, it should not be assumed that activation of this pathway is detrimental. Rather, it may 'prime' cells within these aggregates to more readily attach and disperse. Indeed, when spheroids with constitutively active BMP signalling are exposed to an adherent substratum, they have an increased propensity for reattachment and dispersion. This is supported by previous work demonstrating that BMP4 has the ability to enhance motility and invasion of adherent primary ovarian cancer cells^{8,9}.

Taken together, these findings suggest that inhibition of BMP signalling may in fact be a viable therapeutic target through which to prevent EOC spheroid reattachment and formation of secondary metastatic lesions. We show that inhibition of the BMP pathway using a small molecule inhibitor as well as BMP antagonist, noggin, does in fact decrease the ability of cells to disperse from a spheroid following re-introduction to an adherent substratum. Since this does not completely prevent spheroids from reattaching, it is likely that the BMP signalling pathway acts in conjunction with other pathways during this process.

Our studies uncovered an interaction between the BMP and AKT signalling cascades and demonstrated that these two pathways act in concert to promote EOC spheroid reattachment. This finding is supported by other reports demonstrating that the PI3K/AKT pathway is required for BMP-induced migration and invasion in gastric, colon and pancreatic cancer cells^{10,11}. This highlights the potential for targeting these pathways in combination for treatment of metastatic ovarian cancer. Xenograft models will be important to determine whether this interaction is translatable in an *in vivo* setting. Weroha and colleagues recently published elegant work validating the use of a novel 'tumourgraft' model whereby ovarian cancer patient tumour material is minced and intraperitoneally injected into immune-compromised mice¹². The tumours formed in mice recapitulate the clinical and molecular characteristics of the patient tumour but also mimic the patient's clinical response to chemotherapeutic treatment. This is an extremely exciting, highly translatable *in vivo* model with which to test the potential response of an patient's tumour to a targeted therapeutic. Using this model, we would be able to test the

therapeutic response of a number of ovarian cancer tumour specimens to treatment with the small molecule inhibitors of BMP and AKT signalling that I have in the studies described in this thesis. Molecular analysis of these ‘tumourgrafts’ would allow us to determine patient-specific responses to modulation of these two signalling pathways prior to and following treatment.

This work highlights the fact that the BMP signalling pathway exerts the majority of its effects during spheroid reattachment and dispersion. Therefore, it would be interest to examine the contribution of tumour-stroma interactions in this process and the role that the BMP signalling pathway plays in mediating these interactions. Carcinoma-associated fibroblasts (CAFs) have become increasingly recognized as important components of the tumour microenvironment that can aid in the initiation and progression of a number of different cancers including breast, prostate and ovarian¹³⁻¹⁶. Interestingly, normal fibroblasts co-cultured with carcinoma cells results in an irreversible conversion to a CAF phenotype, suggesting that fibroblasts exposed to cancer cells exhibit permanent, heritable changes^{13,14,16}. Recent studies in ovarian cancer have demonstrated that the presence of CAFs can contribute to tumour progression, omental and lymph node metastases, in addition to being associated with poor patient prognosis^{17,18}. Fu and colleagues were able to obtain primary cultures of CAFs from ovarian cancer patients and co-culture these with EOC cells¹⁹. Analysis of conditioned medium from this co-culture system revealed the presence of number of soluble factors including TGF- β and a number of BMPs. Using our *in vitro* system, it would be of interest to determine the effects of this co-culture media on spheroid reattachment both under ambient conditions as well in spheroids with constitutively activated BMP signalling and those treated with noggin. These studies would provide an additional layer of complexity to our model system, allowing us to not only determine the contribution of CAFs to spheroid reattachment and dispersion but also allow us to determine the interaction between the BMP signalling pathway and this population of cells (Figure 4.1).

The results presented in this thesis have uncovered an important role for BMP signalling in cellular cohesion and EMT during spheroid formation and cellular motility

during reattachment. This has laid the groundwork for preclinical models to investigate the utility of targeting this pathway for treatment of advanced-stage ovarian cancer.

4.3 LKB1 has AMPK-independent effects on cellular viability in ovarian cancer spheroids

Given the important roles that the AKT signalling pathway plays in EOC spheroids both in mediating responses to BMP signalling but also in contributing to spheroid formation-induced dormancy, I wanted to identify other candidate pathways known to interact with the PI3K/AKT pathway. Taking into account the dormant state of the cells within spheroids and their decreased metabolism an obvious candidate for investigation was the AMPK signalling cascade given its unique ability to respond to changes in extracellular energy and nutrient supply. The AMPK and PI3K/AKT signalling pathways converge on mTORC1 and have opposing regulatory effects on this complex²⁰. We have demonstrated that in ovarian cancer spheroids decreased AKT activity and induction of cellular dormancy is associated with enhanced and sustained AMPK activity (Figure 4.1).

Other studies in our laboratory have linked cellular dormancy and quiescence within multicellular spheroids with induction of autophagy (Correa, DiMattia, and Shepherd, unpublished data). AMPK has the ability to directly induce autophagy by phosphorylating and positively regulating ULK1, a critical protein for autophagy initiation²¹⁻²³. AMPK can also indirectly induce autophagy through its ability to inhibit mTORC1 by phosphorylation of TSC2 and Raptor. A study by Avivar-Valderas and colleagues in 2012 highlighted the potential for interaction between mTORC1, AMPK and a member of the unfolded protein response (UPR) pathway, protein kinase (PKR)-like endoplasmic reticulum kinase (PERK) in autophagy induction and anoikis-resistance in mammary epithelial cells²⁴. It was noted that in response to loss of ECM attachment PERK was able to activate AMPK through its upstream kinase, LKB1 although the precise mechanism through which this occurs remains unclear. This suspension-induced AMPK activity was required for inhibition of mTORC1 and induction of autophagy. This was the first study to implicate the LKB1/AMPK/mTORC1 signalling cascade as a key regulator of anoikis in epithelial cells.

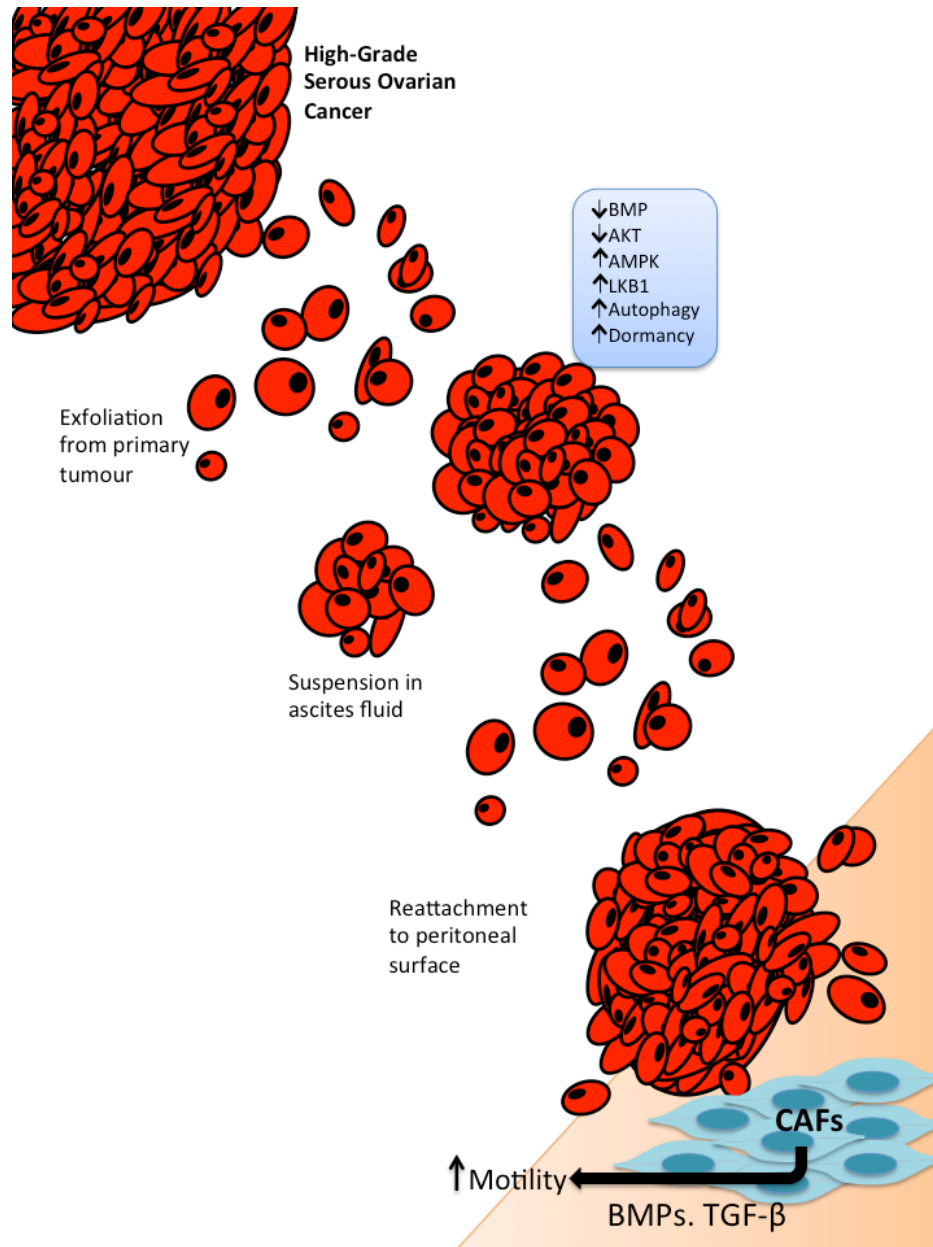


Figure 4.1: Contribution of BMP and LKB1/AMPK signalling pathways to ovarian cancer metastasis.

A number of pathways and processes are uniquely altered in ovarian cancer spheroids, aiding in cellular aggregation and induction of dormancy. Specifically, the BMP signalling pathway is down-regulated during ovarian cancer spheroid formation and aids in cellular aggregation and cohesion. Alternatively, the LKB1/AMPK signalling cascade is up-regulated during spheroid formation and contributes to spheroid formation-induced dormancy. Many of these signalling aberrations are reversed during spheroid reattachment. We propose that upon spheroid reattachment to serosal surfaces of various peritoneal organs (omentum, appendix, intestine), carcinoma-associated fibroblasts (CAFs) secrete a number of cytokines, such as BMPs and TGF- β s, to enhance proliferation, motility and invasion.

Applying these findings to our system, I chose to focus on LKB1 and mTORC1 as critical upstream and downstream mediators of AMPK signalling in EOC spheroids. As discussed in this thesis, suspension-induced AMPK activation in ovarian cancer cells is in fact associated with enhanced phosphorylation of its upstream kinase LKB1 and decreased activity of mTORC1. Surprisingly, targeted knockdown of AMPK did not have any effect on viability of cells within ovarian cancer spheroids. This was unexpected given the important role AMPK is known to play in cell survival under nutrient replete conditions. However, targeted knockdown of LKB1 results in significant reduction in viability of cells within multicellular aggregates, indicating an important role for this kinase in anoikis-resistance of ovarian cancer cells independent of AMPK.

As described in the introduction to this thesis, LKB1 phosphorylates 12 other kinases in addition to AMPK, termed the AMPK-related kinases (ARKs). Interestingly, one of these kinases, microtubule affinity-regulating kinase 4 (MARK4) has very recently been shown to phosphorylate Raptor on the same residue as AMPK, resulting in inhibition of mTORC1 signalling²⁵ (Figure 4.2). Another of these kinases, NUA1 may also be an interesting target to investigate in our system as it has been shown to be a target of AKT in addition to LKB1²⁶. Similar to AMPK, NUA1 is able to promote cell survival during times of nutrient deprivation²⁷. Although their functions are not as well characterized as AMPK, it is likely that one or more of the ARKs may be important mediators of the pro-survival functions of LKB1 in our system. Targeted knockdown of each of these ARKs (MARK1-4, NUA1, NUA2, SIK 1-3, SNRK, BRSK1, BRSK2) and assessment of cell viability in suspension would be the most effective method through which to determine our target(s) of interest.

These studies are the first to identify a pro-survival function for the tumour suppressor LKB1 in a metastatic cancer setting. Further studies will focus on examining the effect that LKB1 loss has on cellular quiescence and autophagy induction in ovarian cancer spheroids, as well as determining downstream mediators of LKB1 in our system. Perhaps we have uncovered a unique LKB1 signalling axis crucial in mediating anoikis-resistance in ovarian cancer cells.

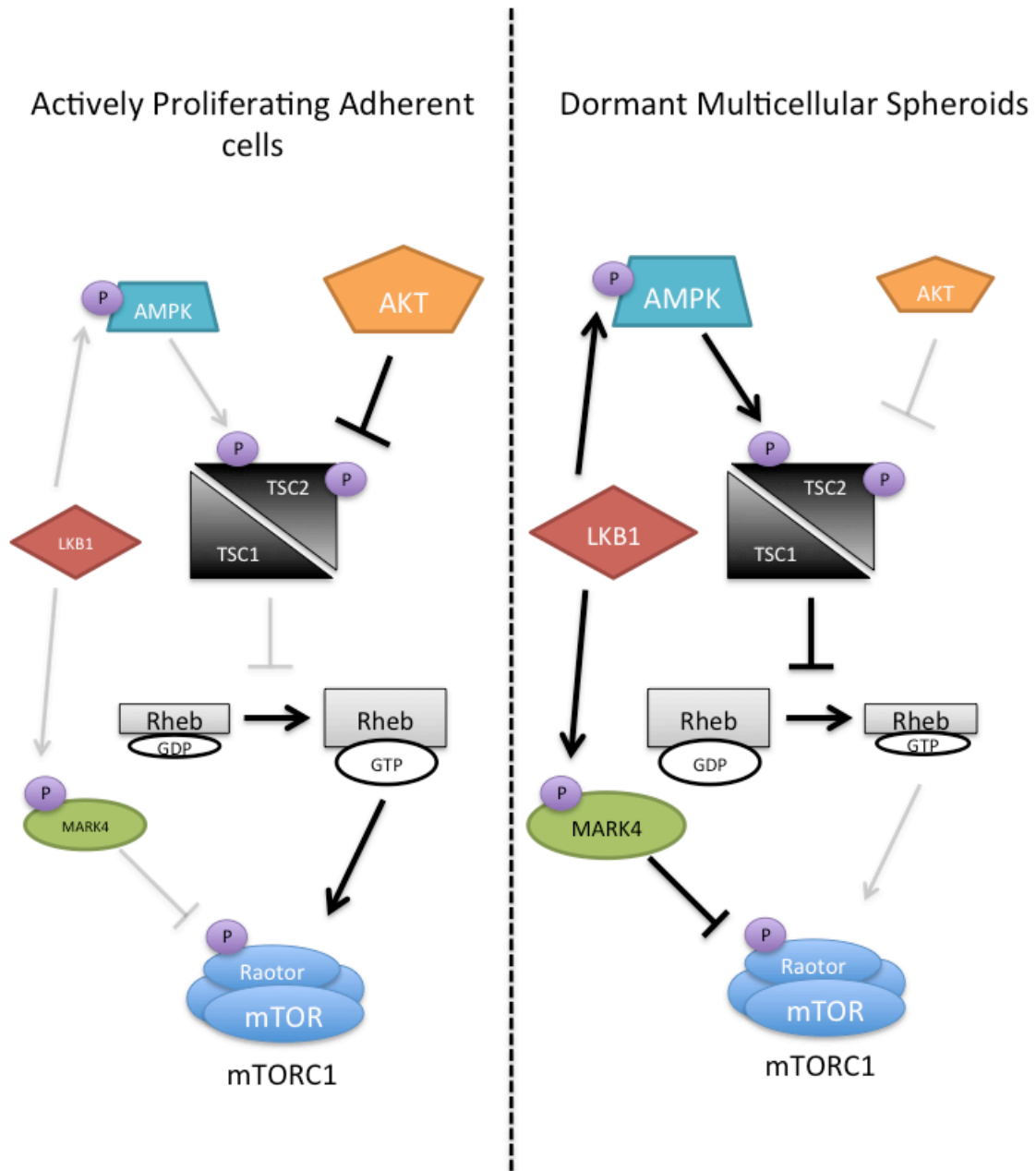


Figure 4.2: Proposed mechanisms of dormancy induction in ovarian cancer spheroids.

AMPK and AKT have opposing regulatory effects on mTORC1 via phosphorylation of TSC2. mTORC1 activity is decreased in multicellular spheroids and this corresponds with decreased AKT activity and enhanced AMPK activation. LKB1 not only functions as an upstream kinase for AMPK but also for a number of AMPK-related kinases (ARKs). One of these ARKs, MARK4, phosphorylates Raptor leading to inhibition of mTORC1. This is another potential kinase with elevated activity in dormant ovarian cancer spheroids. We propose that LKB1 is an important mediator of spheroid-formation induced dormancy independent of AMPK.

4.4 BMP and LKB1 signalling: Is there a connection?

The ability to avoid anoikis is an adaptation that is afforded to all metastatic ovarian cancer cells. In fact this biologic phenomenon is probably important in a variety of cancers that induce ascites formation or pleural effusions including mesothelioma²⁸, gastric cancer²⁹ and pancreatic cancer³⁰. We have shown that under non-adherent conditions these cells have a propensity to aggregate and form multicellular clusters or spheroids, conferring them with a survival advantage. Therapeutic targeting of this population of cells while they are suspended within the peritoneal cavity or at the point of reattachment to form secondary metastatic lesions would be beneficial since the majority of ovarian cancer patients succumb to recurrent, metastatic disease. In this thesis I have specifically focused on two signalling pathways with diverse functions in ovarian cancer spheroid biology.

One of the few studies linking LKB1 to the TGF- β /BMP signalling pathway demonstrated that LKB1 is able to phosphorylate Smad4, preventing it from binding DNA, resulting in inhibition of both TGF- β and BMP signalling cascades³¹. Future studies could focus on examining potential interaction between these two signalling cascades through Smad4 or other transcriptional targets. It would also be important to determine whether there may be a functional link between these pathways. Perhaps decreased cellular cohesion that occurs as a result of activated BMP signalling will render cells in suspension even more susceptible to knockdown of LKB1. It would also be interesting to determine the activity of the TGF- β /BMP pathways in cells that have LKB1 knocked down. This may provide additional mechanistic evidence for the AMPK-independent effects of LKB1 in our system.

Both studies discussed in Chapter 2 and 3 of this thesis could be expanded with the use of the recent Pax8-Cre p53^{mut}/PTEN^{-/-}/BRCA1/2^{-/-} mouse model of high grade serous cancer (HGSC)³². In this model, disease begins in the fallopian tube secretory epithelium with the development of STIC lesions which progress to HGSC, which metastasizes throughout the peritoneum, similar to the human disease. This is an extremely relevant model, as it highly resembles the progression of human ovarian cancer and provides opportunities to study the earliest events in initiation of HGSC.

The majority of studies to date have focused on BMPs in the ovary and OSE. However, now that it is clear the OSE is not the origin of high-grade serous ovarian cancer, it would be of interest to determine the role that the BMP signalling pathway plays in the fallopian tube. To set the stage it will be relevant to determine the expression of various BMPs and their receptors by IHC in STIC lesions from human and mouse fallopian tube. Based on the expression levels, knockout of these specific components of the pathway using the aforementioned mouse model would provide insight into the role of this pathway in initiation and early pathogenesis of high-grade serous ovarian cancer. This would nicely complement the studies presented in this thesis where we demonstrate a role for this pathway in advanced-stage HGSC.

Very little is known about the role of LKB1 in ovarian cancer pathogenesis. However, recent studies from the Teixeira lab demonstrate that loss of *Pten* and *STK11* in the OSE results in formation of high-grade papillary serous carcinomas³³. This suggests that loss of LKB1 may be important in tumour establishment, but based on the findings presented in this thesis, LKB1 also aids in cell survival during later metastatic stages. However, the transgenic mouse model of high-grade serous ovarian cancer discussed above is a more relevant model with which to test this hypothesis since it provides a more accurate representation of disease initiation. Knockout of *STK11* in addition to *Pten* *Tp53* and *Brcal/2* specifically in the secretory epithelium of the fallopian tube may in fact result in more rapid disease progression in this model. Ideally, all combinations of this knockouts focusing on this gene set would provide the most relevant information regarding the importance of LKB1 in the initiation and progression of HGSC. These mouse models would indicate which genes, in combination with homozygous or heterozygous loss of LKB1 activity might predispose secretory epithelial cells to transformation and metastasis to the ovary and peritoneal cavity. These studies would help to determine at which stage of disease progression LKB1 activity is important for either disease progression or inhibition, providing additional support for the findings discussed in Chapter 3.

4.5 Synthesis

The goal of this thesis was to contribute to our knowledge of ovarian cancer metastasis, particularly focusing on multicellular spheroids as major contributors to formation of secondary metastatic lesions. The data presented in Chapters 2 and 3 characterizes two signalling pathways that are dysregulated in EOC spheroids and discusses the potential for targeting these pathways therapeutically. Overall, this body of work has contributed to the field of ovarian cancer metastasis by uncovering unique and complex interactions between a number of signalling cascades and provided rationale for investigating these pathways further in preclinical models. Understanding the unique characteristics afforded to non-adherent ovarian cancer cells is critical for the identification of more effective treatment regimes particularly for late-stage recurrent disease.

4.6 References

1. Correa, R.J., Peart, T., Valdes, Y.R., Dimattia, G.E. & Shepherd, T.G. Modulation of AKT activity is associated with reversible dormancy in ascites-derived epithelial ovarian cancer spheroids. *Carcinogenesis* **33**, 49-58 (2012).
2. Meijer, A.J. & Codogno, P. AMP-activated protein kinase and autophagy. *Autophagy* **3**, 238-240 (2007).
3. Papandreou, I., Lim, A.L., Laderoute, K. & Denko, N.C. Hypoxia signals autophagy in tumor cells via AMPK activity, independent of HIF-1, BNIP3, and BNIP3L. *Cell Death Differ* **15**, 1572-1581 (2008).
4. Shield, K., Ackland, M.L., Ahmed, N. & Rice, G.E. Multicellular spheroids in ovarian cancer metastases: Biology and pathology. *Gynecol Oncol* **113**, 143-148 (2009).
5. Sodek, K.L., Ringuette, M.J. & Brown, T.J. Compact spheroid formation by ovarian cancer cells is associated with contractile behavior and an invasive phenotype. *International journal of cancer* **124**, 2060-2070 (2009).
6. Veatch, A.L., Carson, L.F. & Ramakrishnan, S. Differential expression of the cell-cell adhesion molecule E-cadherin in ascites and solid human ovarian tumor cells. *International journal of cancer. Journal international du cancer* **58**, 393-399 (1994).
7. Scheel, C., *et al.* Paracrine and autocrine signals induce and maintain mesenchymal and stem cell states in the breast. *Cell* **145**, 926-940 (2011).
8. Shepherd, T.G. & Nachtigal, M.W. Identification of a putative autocrine bone morphogenetic protein-signaling pathway in human ovarian surface epithelium and ovarian cancer cells. *Endocrinology* **144**, 3306-3314 (2003).

9. Theriault, B.L., Shepherd, T.G., Mujoomdar, M.L. & Nachtigal, M.W. BMP4 induces EMT and Rho GTPase activation in human ovarian cancer cells. *Carcinogenesis* **28**, 1153-1162 (2007).
10. Chen, X., Liao, J., Lu, Y., Duan, X. & Sun, W. Activation of the PI3K/Akt Pathway Mediates Bone Morphogenetic Protein 2-Induced Invasion of Pancreatic Cancer Cells Panc-1. *Pathol Oncol Res*.
11. Kang, M.H., *et al.* Inhibition of PI3 kinase/Akt pathway is required for BMP2-induced EMT and invasion. *Oncol Rep* **22**, 525-534 (2009).
12. Weroha, S.J., *et al.* Tumorgrafts as in vivo surrogates for women with ovarian cancer. *Clinical cancer research : an official journal of the American Association for Cancer Research* (2014).
13. Bhowmick, N.A., Neilson, E.G. & Moses, H.L. Stromal fibroblasts in cancer initiation and progression. *Nature* **432**, 332-337 (2004).
14. Hayward, S.W., *et al.* Malignant transformation in a nontumorigenic human prostatic epithelial cell line. *Cancer Res* **61**, 8135-8142 (2001).
15. Kuperwasser, C., *et al.* Reconstruction of functionally normal and malignant human breast tissues in mice. *Proceedings of the National Academy of Sciences of the United States of America* **101**, 4966-4971 (2004).
16. Olumi, A.F., *et al.* Carcinoma-associated fibroblasts direct tumor progression of initiated human prostatic epithelium. *Cancer Res* **59**, 5002-5011 (1999).
17. Cai, J., *et al.* Fibroblasts in omentum activated by tumor cells promote ovarian cancer growth, adhesion and invasiveness. *Carcinogenesis* **33**, 20-29 (2012).
18. Zhang, Y., *et al.* Ovarian cancer-associated fibroblasts contribute to epithelial ovarian carcinoma metastasis by promoting angiogenesis, lymphangiogenesis and tumor cell invasion. *Cancer Lett* **303**, 47-55 (2011).
19. Fu, S., *et al.* Stromal-epithelial crosstalk provides a suitable microenvironment for the progression of ovarian cancer cells in vitro. *Cancer Invest* **31**, 616-624 (2013).
20. Liang, J. & Mills, G.B. AMPK: a contextual oncogene or tumor suppressor? *Cancer Res* **73**, 2929-2935 (2013).
21. Egan, D.F., *et al.* Phosphorylation of ULK1 (hATG1) by AMP-activated protein kinase connects energy sensing to mitophagy. *Science* **331**, 456-461 (2011).
22. Kim, J., Kundu, M., Viollet, B. & Guan, K.L. AMPK and mTOR regulate autophagy through direct phosphorylation of Ulk1. *Nat Cell Biol* **13**, 132-141 (2011).
23. Lee, J.W., Park, S., Takahashi, Y. & Wang, H.G. The association of AMPK with ULK1 regulates autophagy. *PLoS One* **5**, e15394 (2010).
24. Avivar-Valderas, A., *et al.* Regulation of autophagy during ECM detachment is linked to a selective inhibition of mTORC1 by PERK. *Oncogene* **32**, 4932-4940 (2013).
25. Li, L. & Guan, K.L. Microtubule-associated protein/microtubule affinity-regulating kinase 4 (MARK4) is a negative regulator of the mammalian target of rapamycin complex 1 (mTORC1). *J Biol Chem* **288**, 703-708 (2013).
26. Suzuki, A., *et al.* Identification of a novel protein kinase mediating Akt survival signaling to the ATM protein. *J Biol Chem* **278**, 48-53 (2003).

27. Suzuki, A., *et al.* ARK5 suppresses the cell death induced by nutrient starvation and death receptors via inhibition of caspase 8 activation, but not by chemotherapeutic agents or UV irradiation. *Oncogene* **22**, 6177-6182 (2003).
28. Barbone, D., *et al.* The Bcl-2 repertoire of mesothelioma spheroids underlies acquired apoptotic multicellular resistance. *Cell death & disease* **2**, e174.
29. Mayer, B., *et al.* Multicellular gastric cancer spheroids recapitulate growth pattern and differentiation phenotype of human gastric carcinomas. *Gastroenterology* **121**, 839-852 (2001).
30. Tai, J., Cheung, S.S., Ou, D., Warnock, G.L. & Hasman, D. Antiproliferation activity of Devil's club (*Oplopanax horridus*) and anticancer agents on human pancreatic cancer multicellular spheroids. *Phytomedicine* (2013).
31. Moren, A., Raja, E., Heldin, C.H. & Moustakas, A. Negative regulation of TGFbeta signaling by the kinase LKB1 and the scaffolding protein LIP1. *J Biol Chem* **286**, 341-353 (2011).
32. Perets, R., *et al.* Transformation of the fallopian tube secretory epithelium leads to high-grade serous ovarian cancer in brca;tp53;pten models. *Cancer cell* **24**, 751-765 (2013).
33. Tanwar, P.S., *et al.* Loss of LKB1 and PTEN tumor suppressor genes in the ovarian surface epithelium induces papillary serous ovarian cancer. *Carcinogenesis* (2013).

Appendix A: Additional Figures

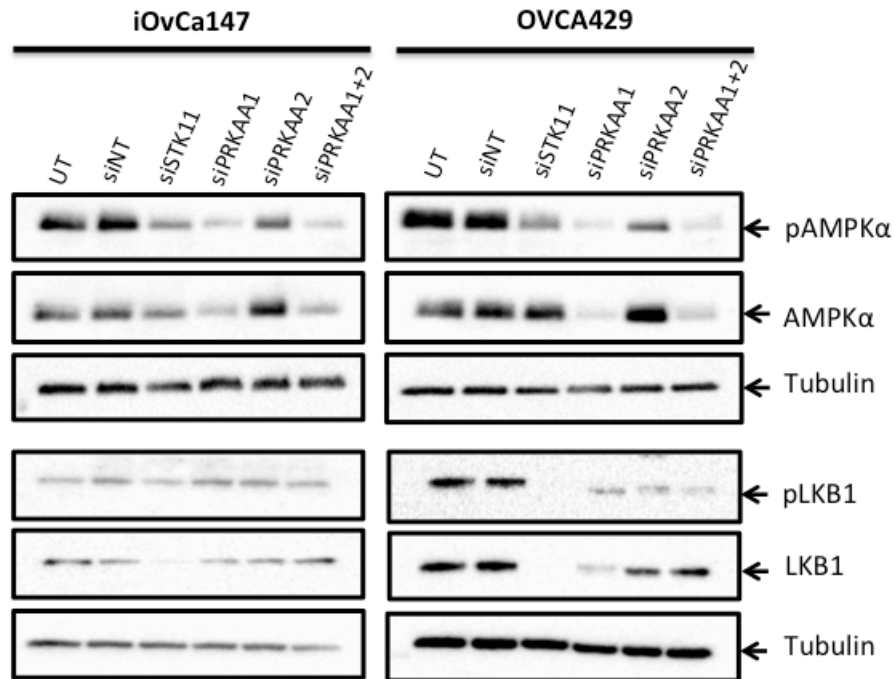


Figure 1: siRNA-mediated knockdown of *PRKAA2* does not affect levels of AMPK α . Immunoblot performed on proteins as indicated 72 hours after transfection of adherent EOC cells with siRNA. AMPK α expression and activity is decreased by *PRKAA1* knockdown but not *PRKAA2*.

Appendix B: Ethics Approval



Use of Human Participants - Ethics Approval Notice

Principal Investigator: Dr. Gabriel DiMattia
Review Number: 12668E
Review Level: Delegated
Approved Local Adult Participants: 90
Approved Local Minor Participants: 0
Protocol Title: Development of Biological Models for the translation ovarian cancer research initiative.
Department & Institution: Biochemistry, University of Western Ontario
Sponsor:
Ethics Approval Date: December 09, 2011 **Expiry Date:** December 31, 2015
Documents Reviewed & Approved & Documents Received for Information:

| Document Name | Comments | Version Date |
|------------------------|--|--------------|
| Revised Study End Date | The study end date has been extended to December 31, 2015 to allow for project completion. | |

This is to notify you that The University of Western Ontario Research Ethics Board for Health Sciences Research Involving Human Subjects (HSREB) which is organized and operates according to the Tri-Council Policy Statement: Ethical Conduct of Research Involving Humans and the Health Canada/ICH Good Clinical Practice Practices: Consolidated Guidelines; and the applicable laws and regulations of Ontario has reviewed and granted approval to the above referenced revision(s) or amendment(s) on the approval date noted above. The membership of this REB also complies with the membership requirements for REB's as defined in Division 5 of the Food and Drug Regulations.

The ethics approval for this study shall remain valid until the expiry date noted above assuming timely and acceptable responses to the HSREB's periodic requests for surveillance and monitoring information. If you require an updated approval notice prior to that time you must request it using the UWO Updated Approval Request Form.

Members of the HSREB who are named as investigators in research studies, or declare a conflict of interest, do not participate in discussion related to, nor vote on, such studies when they are presented to the HSREB.

The Chair of the HSREB is Dr. Joseph Gilbert. The UWO HSREB is registered with the U.S. Department of Health & Human Services under the IRB registration number IRB 00000940.



Office of Research Ethics

The University of Western Ontario
 Room 4180 Support Services Building, London, ON, Canada N6A 5C1
 Telephone: (519) 661-3036 Fax: (519) 850-2466 Email: ethics@uwo.ca
 Website: www.uwo.ca/research/ethics

Use of Human Subjects - Ethics Approval Notice

Principal Investigator: Dr. T.G. Shepherd

Review Number: 16391E

Review Level: Expedited

Review Date: August 12, 2009

Protocol Title: Investigating key signalling pathways in secondary tumour implants formed during ovarian cancer metastasis

Department and Institution: Oncology, London Health Sciences Centre

Sponsor: CIHR-CANADIAN INSTITUTE OF HEALTH RESEARCH

Ethics Approval Date: August 28, 2009

Expiry Date: September 30, 2014

Documents Reviewed and Approved: UWO Protocol, Letter of Information and Consent.

Documents Received for Information:

This is to notify you that The University of Western Ontario Research Ethics Board for Health Sciences Research Involving Human Subjects (HSREB) which is organized and operates according to the Tri-Council Policy Statement: Ethical Conduct of Research Involving Humans and the Health Canada/ICH Good Clinical Practice Practices: Consolidated Guidelines; and the applicable laws and regulations of Ontario has reviewed and granted approval to the above referenced study on the approval date noted above. The membership of this REB also complies with the membership requirements for REB's as defined in Division 5 of the Food and Drug Regulations.

The ethics approval for this study shall remain valid until the expiry date noted above assuming timely and acceptable responses to the HSREB's periodic requests for surveillance and monitoring information. If you require an updated approval notice prior to that time you must request it using the UWO Updated Approval Request Form.

During the course of the research, no deviations from, or changes to, the protocol or consent form may be initiated without prior written approval from the HSREB except when necessary to eliminate immediate hazards to the subject or when the change(s) involve only logistical or administrative aspects of the study (e.g. change of monitor, telephone number). Expedited review of minor change(s) in ongoing studies will be considered. Subjects must receive a copy of the signed information/consent documentation.

Investigators must promptly also report to the HSREB:

- a) changes increasing the risk to the participant(s) and/or affecting significantly the conduct of the study;
- b) all adverse and unexpected experiences or events that are both serious and unexpected;
- c) new information that may adversely affect the safety of the subjects or the conduct of the study.

If these changes/adverse events require a change to the information/consent documentation, and/or recruitment advertisement, the newly revised information/consent documentation, and/or advertisement, must be submitted to this office for approval.

Members of the HSREB who are named as investigators in research studies, or declare a conflict of interest, do not participate in discussion related to, nor vote on, such studies when they are presented to the HSREB.

Appendix C: Summary of Clinical Data for EOCs

| Sample | Age | Histological Subtype | Grade | Stage |
|-------------|-----|--|----------|-------|
| EOC57 | 46 | Serous adenocarcinoma | 3 | IIIC |
| EOC61 | 78 | Serous adenocarcinoma | 3 | IIIC |
| EOC63 | 70 | Carcinosarcoma | 3 (High) | IIIC |
| EOC116 | 64 | Papillary serous | 2 | IIIC |
| EOC120 | 70 | Goblet cell carcinoma | n.a. | n.a. |
| EOC122 | 56 | Serous carcinoma | High | IIIC |
| EOC129 | 74 | Serous carcinoma | High | IIIC |
| EOC132 | 59 | Serous Adenocarcinoma | High | IIIC |
| EOC136 | 42 | Serous ovarian carcinoma | High | IV |
| EOC137 | 77 | Serous Carcinoma | High | IIIC |
| EOC140 | 76 | poorly differentiated carcinoma | High | IIIC |
| EOC148 | 67 | Bilateral ovarian serous carcinoma | High | IC* |
| EOC149 | 69 | Serous adenocarcinoma | High | IIIC |
| EOC153 | 48 | Serous (60%) and endometrioid (40%) | High | IIA |
| EOC154 | 66 | Serous intra-abdominal carcinomatosis | High | IIIC |
| EOC155 | 66 | Serous adenocarcinoma (poorly-differentiated) | High | IIIC |
| EOC156 | 67 | Serous | High | IIIC |
| EOC158 | 45 | Papillary serous | 2/3 | IIIC |
| EOC159 | 57 | Serous adenocarcinoma | High | n.a. |
| EOC160 | 47 | Cystadenofibroma (benign) | n.a. | n.a. |
| EOC171 | 65 | Serous carcinoma | High | IIIC |
| iOVCA130 | 59 | Serous Carcinoma | High | IIIC |
| iOVCA147-E2 | 43 | Serous (70%) and clear cell (30%) adenocarcinoma | 2 | IIC |
| iOVCA198 | 65 | serous adenocarcinoma | High | n.a. |

*, stage was defined as at least IC for this patient.

n.a., not available

Appendix D: Copyright Permissions

1/28/2014

Rightslink Printable License

SPRINGER LICENSE TERMS AND CONDITIONS

Jan 28, 2014

This is a License Agreement between Teresa M Peart ("You") and Springer ("Springer") provided by Copyright Clearance Center ("CCC"). The license consists of your order details, the terms and conditions provided by Springer, and the payment terms and conditions.

All payments must be made in full to CCC. For payment instructions, please see information listed at the bottom of this form.

| | |
|-------------------------------------|--|
| License Number | 3317810075785 |
| License date | Jan 28, 2014 |
| Licensed content publisher | Springer |
| Licensed content publication | Clinical & Experimental Metastasis |
| Licensed content title | BMP signalling controls the malignant potential of ascites-derived human epithelial ovarian cancer spheroids via AKT kinase activation |
| Licensed content author | Teresa M. Peart |
| Licensed content date | Jan 1, 2012 |
| Volume number | 29 |
| Issue number | 4 |
| Type of Use | Thesis/Dissertation |
| Portion | Full text |
| Number of copies | 5 |
| Author of this Springer article | Yes and you are the sole author of the new work |
| Order reference number | |
| Title of your thesis / dissertation | Mechanisms of ovarian cancer spheroid formation and reattachment |
| Expected completion date | Apr 2014 |
| Estimated size(pages) | 150 |
| Total | 0.00 CAD |

Terms and Conditions

Introduction

The publisher for this copyrighted material is Springer Science + Business Media. By clicking "accept" in connection with completing this licensing transaction, you agree that the following terms and conditions apply to this transaction (along with the Billing and Payment terms and conditions established by Copyright Clearance Center, Inc. ("CCC"), at the time that you opened your Rightslink account and that are available at any time at <http://myaccount.copyright.com>).

Curriculum Vitae

Teresa Marie Peart

EDUCATION

University of Western Ontario, London, Ontario
PhD, Anatomy and Cell Biology Sept 2008-March 2014

University of Western Ontario, London, Ontario
Bachelor of Science, Honours Cell and Developmental Biology 2007

McKinnon Park Secondary School, Caledonia, Ontario
OSSD and Ontario Scholar Award 2003

RESEARCH-RELATED EXPERIENCE

University of Western Ontario, London, Ontario
Translational Ovarian Cancer Research Program Sept. 2008-March 2014

- My research examines the role of key signalling pathways and their relation to ovarian cancer pathogenesis
- Using novel cell culture methods to examine hypotheses
- Presented findings at a number of local and National conferences
- Author on several peer-reviewed publications

Fourth year thesis project Sept. 2006-May 2007

- Studied the muscle physiology of exercising grass carp
- Responsible for developing and carrying out methods for exercising grass carp as well as accurately sampling blood and muscle
- Performed various in-vitro tests
- Responsible for keeping accurate laboratory records
- Presented findings in two conferences

TEACHING EXPERIENCE

Undergraduate Teaching assistant, Medical Science 4461, University of Western Ontario

Jan 2012-April 2012

Undergraduate Teaching assistant, Medical Science 4900, University of Western Ontario

Sept 2011-present

Honours Student Mentorship

Arlan Walsh, Department of Biochemistry, University of Western Ontario

Sept 2010-April 2011

- Responsible for training student in proper laboratory techniques, overseeing daily experiments as well as providing expertise crucial for project completion

Anton Shimanovsky, Department of Biology, McMaster University

Sept 2009-Aug 2010

- Responsible for training student in proper laboratory techniques as well as overseeing daily experiments

Dominik Dobransky, Department of Biochemistry, University of Western Ontario

Sept 2009-April 2010

- Responsible for training student in proper laboratory techniques, overseeing daily experiments as well as providing expertise crucial for project completion

Undergraduate Teaching assistant, Anatomy and Cell Biology 3319, University of Western Ontario

Sept 2008-April 2009

SCHOLARSHIPS

Ontario Graduate Scholarship

Sept. 2012-Sept. 2013

CIHR student training program in Cancer Research

Sept. 2009-Sept. 2013

PUBLICATIONS**Peer-Reviewed Publications**

Correa RJ, Ramos Valdes Y, **Peart TM**, Fazio EN, Bertrand M, McGee J, Préfontaine M, Sugimoto A, DiMattia GE, Shepherd TG (2014). Combination of AKT inhibition with autophagy blockade effectively reduces ascites-derived ovarian cancer cell viability. *Carcinogenesis*.

Peart T, Correa R, DiMattia GE, Shepherd TG (2012). BMP signalling controls the malignant potential of ascites-derived human epithelial ovarian cancer cells via Akt kinase activation in an *in vitro* metastasis model. *Clinical and Experimental Metastasis*

Correa R, **Peart T**, Ramos-Valdes Y, DiMattia GE, Shepherd TG (2011). Modulation of AKT activity is associated with reversible dormancy in ascites-derived epithelial ovarian cancer spheroids. *Carcinogenesis*.

Abstracts

Peart T., Ramos-Valdés Y, Bertrand M, Sugimoto AK, Préfontaine M, DiMattia GE, and Shepherd TG (2010) Activated BMP signalling differentially modulates cellular adhesion and motility in epithelial ovarian cancer spheroids. *UWO department of Oncology Research and Education Day; awarded poster prize*

Peart T., Ramos-Valdés Y, Bertrand M, Sugimoto AK, Préfontaine M, DiMattia GE, and Shepherd TG (2010) Activated BMP signalling differentially modulates cell adhesion and motility during ovarian cancer spheroid formation and attachment. *5th Annual Canadian Conference on Ovarian Cancer Research; Toronto, Ontario.*

Peart T., Bertrand M, Sugimoto AK, Prefontaine M, DiMattia GE and Shepherd TG (2011) Activated BMP signalling modulates multicellular spheroid formation and reattachment of ascites-derived human epithelial ovarian cancer cells in an *in vitro* model of metastasis. *Published in AACR 102nd Annual Meeting Program; Denver, CO.*

Peart T., Bertrand M, Sugimoto AK, Prefontaine M, DiMattia GE and Shepherd TG (2011) Activated BMP signalling modulates multicellular spheroid formation and reattachment of ascites-derived human epithelial ovarian cancer cells in an *in vitro* model of metastasis. *Paul Harding Research Day; London, Ontario.*

Peart T., Bertrand M, Sugimoto AK, Prefontaine M, DiMattia GE and Shepherd TG (2011) Activated BMP signalling modulates multicellular spheroid formation and reattachment of ascites-derived human epithelial ovarian cancer cells in an *in vitro* model of metastasis. *Canadian Cancer Research Conference; Toronto, Ontario.*

Peart T., Bertrand M, Sugimoto AK, Prefontaine M, DiMattia GE and Shepherd TG (2012) The 5'-AMP-activated protein kinase (AMPK) pathway is upregulated in ovarian cancer spheroids to promote the dormant phenotype. *Paul Harding Research Day; London, Ontario; awarded poster prize.*

Peart T., Bertrand M, Sugimoto AK, Prefontaine M, DiMattia GE and Shepherd TG (2012) The 5'-AMP-activated protein kinase (AMPK) pathway is upregulated in ovarian cancer spheroids to promote the dormant phenotype. *Canadian Conference on Ovarian Cancer Research; Quebec City, Quebec; awarded prize for oral presentation.*

Peart T., Bertrand M, Sugimoto AK, Prefontaine M, DiMattia GE and Shepherd TG (2012) The 5'-AMP-activated protein kinase (AMPK) pathway is upregulated in ovarian cancer spheroids to promote the dormant phenotype. *UWO Oncology Research and Education Day.*